

AN ABSTRACT OF THE THESIS OF

Benjamin J. Figard for the degree of Doctor of Philosophy in Biochemistry and Biophysics presented on February 14, 2007.

Title: Electron Molecule Interactions of Amino Acids and Peptides.

Abstract approved: _____

Max L. Deinzer

Electron-biomolecule interactions are a biologically relevant field of study because there are several ion fragmentation techniques that have come to the forefront in mass spectrometric analysis that involve the interaction of charged peptides and free electrons. By studying the electron energies that cause fragmentation in neutral amino acids, amino acid derivatives, and peptides, new insights into the mechanisms of biomolecule damage and ion fragmentation have been gained.

Low energy electron capture experiments performed on a standard mass spectrometer using a specifically designed probe for non-volatile compounds provided proof of principle for low energy electron capture leading to peptide fragments. The largest assigned ion from a peptide was the z_7-1 ion from the peptide substance P. For peptides with carboxylic acids on the C-terminus, $z-1$ ions were observed along with $(M-H)^-$ ions for peptides smaller than a hexamer. The assignment of the ions produced by low energy electron capture to c and $z-1$ ions was supported by high resolution low electron energy negative ion mass spectrometry with the alanine dimer.

Using resonance electron capture – mass spectrometry, the amino acid esters, i.e. ethyl, isopropyl, and t-butyl esters of glycine, alanine, and phenylalanine were studied and these showed effective yield peaks at 3.5-3.7 eV and 8.8–9.5 eV for the carboxylate negative ions that were not observed for the underivatized amino acids or their methyl esters. The effective yield peaks in the carboxylate negative ions are attributed to electronically excited Feshbach resonances.

N-Acetyl amino acids and peptides show strong ions with effective yield maxima at 1-2 eV electron energy that are due to shape resonances of the π^* orbital. The dominant ions are either the $(M-H)^-$ or z-1 ions for the compounds with c-terminal carboxylic acids. Their methyl esters show c ions as the dominant fragments. The cleavage of the peptide backbone involves $\pi^* - \sigma^*$ orbital mixing because capture occurs by the π orbitals but sigma bonds are ultimately cleaved. The general conclusion of this thesis is that electrons with energy between 1-2 eV are captured by shape resonances of the π^* orbital at the amide bond leading to formation of z-1 and c type ions.

©Copyright by Benjamin J. Figard
February 14, 2007
All Rights Reserved

Electron Molecule Interactions of Amino Acids and Peptides

by

Benjamin J. Figard

A THESIS

submitted to

Oregon State University

In partial fulfillment of
the requirements of the
degree of

Doctor of Philosophy

Presented February 14, 2007
Commencement June 2007

Doctor of Philosophy thesis of Benjamin J. Figard presented on February 14, 2007.

APPROVED:

Major Professor, representing Biochemistry and Biophysics

Chair of the Department of Biochemistry and Biophysics

Dean of the Graduate School

I understand that my thesis will become a part of the permanent collection of Oregon State University libraries. My signature below authorizes release of my thesis to any reader upon request.

Benjamin J. Figard, Author

ACKNOWLEDGEMENTS

The author would like to acknowledgement the help and support of the members of the Mass Spectrometry and specifically Dr. Yuri Vasil'ev and Jeff Morr  who were invaluable during this work. I would also like to thank my friends, family, and the OSURFC for the support and at times, distraction. Lastly, I would like to thank Dr. Max Deinzer for giving me the opportunity to learn under his mentoring.

TABLE OF CONTENTS

	<u>Page</u>
Introduction.....	1
Introduction.....	1
Electron / Molecule Interactions.....	3
Methods for Studying Negative Ions.....	8
REC-MS Sample Introduction.....	13
Relevant Ionization Techniques for Biomolecules.....	14
Recent Developments in Electron – Molecule Interactions in Biomolecules	17
Methods.....	46
Introduction.....	46
JEOL Sector.....	46
In-Beam and Flash Volatilization probes.....	48
High-Resolution Negative Ion Mass Spectrometry.....	51
Electron Monochromator.....	52
Electron Monochromator Time of Flight Mass Spectrometer.....	53
Chemical modification of amino acids and peptides.....	55
Computational studies.....	60
Results.....	69
Negative Ion Energy Calibrated Mass Spectrometry.....	69
Flash Volatilization Mass Spectrometry.....	73
Negative Ion High Resolution Energy Calibrated Mass Spectrometry	73

TABLE OF CONTENTS (Continued)

	<u>Page</u>
Resonance Electron Capture.....	74
Esters of Amino Acids.....	74
N-Acetyl Amino Acids.....	84
Peptides.....	91
Potential Energy Scans.....	101
Discussion.....	202
In Beam 2D Mass Spectroscopy.....	202
Negative Ion High Resolution Energy Calibrated Mass Spectrometry.....	202
Resonance Electron Capture – Mass Spectrometry	204
Amino Acid Esters.....	204
N-Acetyl Amino Acids.....	206
Peptides.....	207
Combined REC-MS Discussion.....	209
Potential Energy Scans.....	210
Conclusions.....	212
Bibliography.....	218

LIST OF FIGURES

<u>Figure</u>		<u>Page</u>
1	Schematic of a shape resonance as a function of energy versus distance between the electron and electron capturing molecule with the curves for the attractive forces, repulsive forces, and an illustration of the trapping potential well for the shape resonance.....	26
2	Energy versus internuclear distance for a model electron-capturing molecule with relative potential surfaces for Feshbach resonance to parent neutral excited state.....	27
3	Comparison of the electron configuration of a hypothetical molecule that forms an anion by shape or Feshbach resonances.....	28
4	Comparison of the parent singlet (S_1) and triplet (T_1) electronic states for the Feshbach resonances of a hypothetical molecule.....	29
5	Comparison of the parent states Feshbach resonances of a hypothetical molecule the singlet (S_1) and triplet (T_1) electronic states.....	30
6	Comparison of the resonance maxima E_1 and E_2 and the parent singlet (S_1) and triplet (T_1) electronic states for the Feshbach resonances of a hypothetical molecule.....	31
7	The vertical transition range for a model hypothetical molecule and thermodynamic quantities $D(AB)$, $EA(A \cdot)$, $EA(B \cdot)$, and ΔH_1	32
8	The vertical transition of a hypothetical molecule to form a molecular anion at A on the M^-_1 energy surface.....	33
9	The theoretical electron attachment spectrum from the hypothetical molecule using the “reflection” of the Gaussian distribution through the anion curves.....	34
10	Theoretical electron attachment spectrum from (A) Franck-Condon transitions and (B) a more typical representation, i.e. effective yield curves.	35
11	Schematic diagram of a trochoidal electron monochromator – electron transmission spectrometer.....	36
12	Schematic diagram of a trochoidal electron monochromator – electron energy loss spectrometer.....	37

LIST OF FIGURES (Continued)

<u>Figure</u>		<u>Page</u>
13	Schematic diagram of a trochoidal electron monochromator - mass spectrometer.....	38
14	The ETS experimental data (A) and the derivative of the ETS data (B) of a hypothetical molecule.....	39
15	The theoretical electron attachment spectrum (A) and the ETS data (B) of a hypothetical molecule.	40
16	The theoretical electron attachment spectrum (A) and the total effective yield curve from a REC-MS experiment (B) of a hypothetical molecule.....	41
17	The total effective yield curve (A) and the effective yield curve for an individual m/z from a REC-MS experiment (B) of a hypothetical molecule.....	42
18	The nomenclature for ions formed by cleavage of the peptide backbone bonds.....	43
19	The structure formed after the addition of an electron to the positively charged amine group is a high energy Rydberg state.....	44
20	The ECD mechanism for the fragmentation of the peptide backbone to form c and z ions by capture of an electron at a generic amide group in the peptide backbone.....	45
21	Schematic of the parts of the wire in beam probe where (a) is the wire to pin connector , (b) is the point where the wire to pin connector is cut off, (c) is the portion of the wire to pin connector not used and (d) is the filament wire twisted around itself to form a loop.....	63
22	Original schematic of the Flash volatilization probe with (a) the tip, (b) the electrical contact post, (c) the filament wire, (d) second electrical contact rod, (e) a ceramic insulator, (f) the ceramic ring with set screw, (g) ceramic support ring, (h) Teflon rods, (i) copper wires, (j) barrel electrical connectors, (k) a nylon spacer, and (k) an electrical feed though.....	64
23	Schematic of the final probe tip used as the flash volatilization probe. (a) Ceramic tube, (b) probe tip, and (c) the “barrel” of the probe tip.....	65

LIST OF FIGURES (Continued)

<u>Figure</u>		<u>Page</u>
24	Mechanism of Fmoc deprotection from an amino acid or peptide with a generic base as the catalyst.....	66
25	Mechanism of solid phase peptide synthesis (SPPS) for making a dimer of glycine with a methyl ester on the C-terminus using HMBA resin from Nova Biochem.....	67
26	Resonant electron capture spectrum produced from alanine dimer with electron energy of ~1 eV.....	120
27	Resonant electron capture spectrum produced from alanine dimer with electron energy of ~6 eV.....	121
28	The resonance electron capture mass spectrum from methionine enkephalin shows all four possible z-1 type and (M-H)- ions.....	122
29	The resonance electron capture mass spectrum of YFF amide shows peaks for c ₁ , c ₂ , z ₁ -1, z ₂ -1, and (M-H)- ions at electron energies between ~0.5- 1.5 eV.....	123
30	The resonance electron capture mass spectrum of substance p shows prominent peaks for the z _n -1 series (n = 2-7) with the most abundant peaks of z ₄ -1 and z ₅ -1.....	124
31	The resonance electron capture mass spectrum of cystine dimethyl ester diHCl shows the M• ion and other ions from the interaction of electrons with energies ~1 – 1.5 eV.....	125
32	High resolution negative ion mass spectrum of the alanine dimer fragment ion m/z 72, C ₃ H ₄ O ₂ , or (z-1) ion at ~1 eV electron energy with the ³⁵ Cl ³⁷ Cl ⁻ and ³⁷ Cl ₂ ⁻ ions as internal reference ions.....	126
33	Effective yield curves of the carboxylate anion, (M-X)-, from the amino acid glycine (blue) and its esters, methyl (red), ethyl (purple), isopropyl (green), and t-butyl (aqua).....	127
34	Effective yield curves of the carboxylate anion, (M-X)-, from the amino acid esters of glycine, methyl (red), ethyl (purple), isopropyl (green), and t-butyl (aqua).....	128
35	Effective yield curves of the -OX anion from the amino acid glycine (blue) and its esters, methyl (red), ethyl (purple), isopropyl (green), and t-butyl (aqua).	129

LIST OF FIGURES (Continued)

<u>Figure</u>		<u>Page</u>
36	Effective yield curves of the -OX anion from the amino acid esters of glycine, methyl (red), ethyl (purple), isopropyl (green), and t-butyl (aqua).....	130
37	Effective yield curves of the carboxylate anion, (M-X)-, from the amino acid alanine (blue) and its esters, methyl (red), ethyl (purple), and t-butyl (aqua).....	131
38	Effective yield curves of the carboxylate anion, (M-X)-, from the amino acid esters of alanine, methyl (red), ethyl (purple), and t-butyl (aqua).....	132
39	Effective yield curves of the carboxylate anion, (M-H)-, from the amino acids for glycine (blue), alanine (red), and phenylalanine (purple).....	133
40	Effective yield curves of the carboxylate anion, (M-Me)-, from the amino acid methyl esters for glycine (blue), alanine (red), and phenylalanine (purple).....	134
41	Effective yield curves of the carboxylate anion, (M-Et)-, from the amino acid ethyl esters for glycine (blue), alanine (red), and phenylalanine (purple).....	135
42	Effective yield curves of the carboxylate anion, (M-iPr)-, from the amino acid isopropyl esters for glycine (blue) and phenylalanine (purple).....	136
43	Effective yield curves of the carboxylate anion, (M-tBu)-, from the amino acid t-butyl esters for glycine (blue), alanine (red), and phenylalanine (purple).....	137
44	Effective yield curves of the -OX anion from the amino acid glycine (blue) and its esters, methyl (red), ethyl (purple), and t-butyl (aqua).....	138
45	Effective yield curves of the -OX anion from the amino acid esters of alanine, methyl (red), ethyl (purple), and t-butyl (aqua).....	139
46	Effective yield curves of the hydroxyl anion, -OH, from the amino acids for glycine (blue), alanine (red), and phenylalanine (purple)....	140

LIST OF FIGURES (Continued)

<u>Figure</u>		<u>Page</u>
47	Effective yield curves of the methoxy anion, -OMe, from the amino acid methyl esters of glycine (blue), alanine (red), and phenylalanine (purple).....	141
48	Effective yield curves of the ethoxy anion, -OEt, from the amino acid ethyl esters of glycine (blue), alanine (red), and phenylalanine (purple).....	142
49	Effective yield curves of the iso-propyl anion, -OiPr, from the amino acid isopropyl esters of glycine (blue) and phenylalanine (purple).....	143
50	Effective yield curves of the t-butoxy anion, -OtBu, from the amino acid t-butyl esters of glycine (blue), alanine (red), and phenylalanine (purple).....	144
51	Effective yield curves of the carboxylate anion, (M-X)-, from the amino acid phenylalanine (blue) and its esters; methyl (red), ethyl (purple), isopropyl (green), and t-butyl (aqua).....	145
52	Effective yield curves of the carboxylate anion, (M-X)-, from the amino acid esters of phenylalanine; methyl (red), ethyl (purple), isopropyl (green), and t-butyl (aqua).....	146
53	Effective yield curves of the -OX anion from the amino acid phenylalanine (blue) and its esters, methyl (red), ethyl (purple), isopropyl (green), and t-butyl (aqua).....	147
54	Effective yield curves for the formation of the -R anion from phenylalanine (blue) and its esters; methyl (red), ethyl (purple), isopropyl (green), and t-butyl (aqua).....	148
55	The REC-MS of N-Acetyl Alanine for ions generated by scanning electron energies from 0 - ~10 eV.....	149
56	The REC-MS of N-Acetyl Alanine for ions generated by scanning electron energies from 0 - ~10 eV.....	150
57	Effective yield curve for the (M-H) ⁻ ion with m/z 130 from N-Acetyl Alanine.....	151
58	Effective yield curve for pseudo z-1 ion with m/z 72 from N-Acetyl Alanine.....	152

LIST OF FIGURES (Continued)

<u>Figure</u>		<u>Page</u>
59	The REC-MS of N-Acetyl Phenylalanine for ions generated by scanning electron energies from 0 - ~10 eV	153
60	Effective yield curve for the (M-H) ⁻ ion with m/z 206 from N-Acetyl Phenylalanine	154
61	Effective yield curve for the (M-R) ⁻ ion with m/z 116 from N-Acetyl Phenylalanine.....	155
62	Effective yield curve for the R ⁻ ion with m/z 91 from N-Acetyl Phenylalanine.....	156
63	The REC-MS of N-Acetyl Tyrosine for ions generated by scanning electron energies from 0 - ~10 eV.....	157
64	Effective yield curve for the (M-H) ⁻ ion with m/z 222 from N-Acetyl Tyrosine.....	158
65	Effective yield curve for the (M-R) ⁻ ion with m/z 116 from N-Acetyl Tyrosine.....	159
66	Effective yield curve for the pseudo z-1 ion with m/z 164 from N-Acetyl Tyrosine.....	160
67	The REC-MS of N-Acetyl Tryptophan for ions generated by scanning electron energies from 0 - ~10 eV.	161
68	Effective yield curve for the (M-H) ⁻ ion with m/z 245 from N-Acetyl Tyrosine.....	162
69	Effective yield curve for the (M-R-H) ⁻ ion with m/z 115 from N-Acetyl Tyrosine.....	163
70	Effective yield curve for the pseudo z-1 ion with m/z 187 from N-Acetyl Tyrosine.....	164
71	The REC-MS of Ala ₂ for ions generated by scanning electron energies from 0 - ~10 eV.....	165
72	Effective yield curves for the formation of the four most intense ions from the REC-MS of Ala ₂ ; (M-H) ⁻ (blue), z ₁ -1 (pink), c ₁ (red), and b ₁ (aqua).....	166

LIST OF FIGURES (Continued)

<u>Figure</u>		<u>Page</u>
73	The effective yield curves for the (M-H) ⁻ ions from N-acetyl alanine (blue) and the alanine dimer (pink).....	167
74	The effective yield curves for the pseudo z-1 ion from N-acetyl alanine (blue) and z ₁ -1 ion from the alanine dimer (pink).....	168
75	The effective yield curves for the pseudo c ion from N-acetyl alanine (blue) and c ₁ ion from the alanine dimer (pink).....	169
76	(A) The raw REC-MS of N-Acetyl Ala ₂ generated by scanning electron energies from 0 - ~10 eV.....	170
77	Effective yield curves for the formation of the four most intense ions from the REC-MS of Acetyl-Ala ₂ ; (M-H) ⁻ (red), z ₁ -1 (blue), pseudo z ₂ -1 (pink), and c ₁ (aqua).....	171
78	Effective yield curves for pseudo z-1 (blue) from the N-Acetyl Ala, z ₁ -1 (red) ion from Ala-Ala, and the z ₁ -1 (red) ion and pseudo z ₂ -1 (aqua) from N-Acetyl Ala-Ala.....	172
79	Effective yield curves of the (M-H) ⁻ ions for N-acetyl Ala (blue), Ala-Ala (pink), and N-acetyl Ala-Ala (red).....	173
80	Effective yield curves for the pseudo c ₀ ion (blue) and c ₁ ion (pink) from the N-Acetyl Ala-Ala, pseudo c ₀ ion (red) from the N-Acetyl Ala, and the c ₁ ion (aqua) from the Ala-Ala.....	174
81	The effective yield curves of (M-H) ⁻ (red), pseudo z ₂ -1 (pink), z ₁ -1 (blue), and c ₁ (aqua) ions from N-Acetyl Ala-Ala.....	175
82	The REC-MS of Ala ₃ with Cl ⁻ removed with z-1 series, c ₂ , and (M-H) ⁻ ions generated by scanning electron energies from 0 - ~10 eV.....	176
83	Effective yield curves for the formation of the four intense ions from the REC-MS of Ala ₃ ; (M-H) ⁻ (red), z ₁ -1 (blue), pseudo z ₂ -1 (pink), and c ₂ (aqua).....	177
84	The REC-MS of N-Acetyl Ala ₃ with Cl ⁻ removed with the c series, z-1 series, and (M-H) ⁻ ions generated by scanning electron energies from 0 - ~10 eV.....	178

LIST OF FIGURES (Continued)

<u>Figure</u>		<u>Page</u>
85	Effective yield curves for the formation of the three z- 1 ions from the REC-MS of N-acetyl Ala ₃	179
86	Effective yield curves for the formation of the four intense ions from the REC-MS of N-acetyl Ala ₃ ; pseudo z ₃ -1 (blue), z ₂ -1 scaled by 1/10 (pink), z ₁ -1 (red), and (M-H) ⁻ (aqua).....	180
87	Effective yield curves of three intense ions from the REC-MS of N-acetyl Ala ₃ ; pseudo c ₀ (blue), c ₁ (pink), and c ₂ (red).....	181
88	The effective yield curves of the z-1 ion series (pseudo z ₃ -1, blue, z ₁ -1, pink, and 1/10 z ₂ -1, green), c ion series (pseudo-c ₀ , red, c ₁ , aqua, and c ₂ , purple), and the (M-H) ⁻ ion (brown) from N-Acetyl Ala-Ala-Ala.....	182
89	The effective yield curves for the z-1 ions (z ₁ -1, blue, pseudo z ₂ -1, pink), c ions (c ₁ , aqua), and (M-H) ⁻ (red) ions from N-acetyl Ala-Ala and for the z-1 ions (z ₁ -1, green, 1/10 z ₂ -1, brown, pseudo z ₃ -1, purple), c ions (pseudo c ₀ , light blue, c ₁ , light aqua, c ₂ , neon green), and (M-H) ⁻ (grey) ions from N-acetyl Ala-Ala-Ala.....	183
90	The effective yield curves for the z-1 ions (z ₁ -1, blue, pseudo z ₂ -1, pink), c ions (c ₁ , aqua), and (M-H) ⁻ (red) ions from N-acetyl Ala-Ala and for the z-1 ions (z ₁ -1, green, 1/10 z ₂ -1, brown, pseudo z ₃ -1, purple), c ions (pseudo c ₀ , light blue, c ₁ , light aqua, c ₂ , neon green), and (M-H) ⁻ (grey) ions from N-acetyl Ala-Ala-Ala.....	184
91	The REC-MS of Ala ₃ -OMe with Cl ⁻ from CCl ₄ removed with ions generated by scanning electron energies from 0 - ~10 eV.....	185
92	Effective yield curves for the formation of the ions c ₁ with m/z 87 and c ₂ with 158 from the REC-MS of Ala ₃ -OMe.....	186
93	The m/z for the c and z ion series of alanine trimer compounds....	187
94	Effective yield curves for c ₁ (blue) and c ₂ (pink) ions from Ala-Ala-Ala-OMe	188
95	Effective yield curves for z ₁ -1 and z ₂ -1 ions from Ala-Ala-Ala-OMe...	189
96	REC-MS of a less purified Ala-Ala-Ala-OMe product with the Cl ⁻ ion removed.....	190

LIST OF FIGURES (Continued)

<u>Figure</u>		<u>Page</u>
97	Effective yield curves from c_1 (m/z 87), c_2 (m/z 158), and z_2-1 (m/z 157) ions from A_3 -OMe.....	191
98	Effective yield curve for m/z 193 for the ion of the Fmoc side product from Ala-Ala-Ala-OMe.....	192
99	The REC-MS of N-Acetyl Ala_3 -OMe with the c_1 , c_2 , (M-H) ⁻ ions labeled and with ions generated by scanning electron energies from 0 - ~10 eV.....	193
100	Effective yield curves for the formation of the ions c_1 , c_2 , and (M-H)- with m/z's 129, 200, and 286 from the REC-MS of N-acetyl Ala_3 -OMe.....	194
101	Effective yield curves for the formation of the ion ⁻ OMe with m/z 31 and z_1 with m/z 87 from the REC-MS of N-acetyl Ala_3 -OMe.....	195
102	Scheme for capture of an electron at the amide group and peptide backbone cleavage to form c and z-1 ions.....	196
103	Scheme for capture of an electron at the carboxylic acid group and peptide backbone cleavage to form z-1 ions.....	197
104	Effective yield curves from z-1 ion series: z_1-1 (blue), z_2-1 (pink), and pseudo z_3-1 (red), for N-acetyl- A_3 and z-1 ion series: z_1-1 (aqua), z_2-1 (purple), and pseudo z_3-1 (brown), for N-acetyl- A_3 -OMe.....	198
105	Effective yield curves from the c ion series: pseudo c_0 (red), c_1 (pink), and c_2 (blue), for N-acetyl- A_3 and c ion series: pseudo c_0 (aqua), c_1 (purple), and c_2 (brown), for N-acetyl- A_3 -OMe.....	199
106	Potential energy surface in relation to the phi-psi angles for alanine dimer using the UHF/6-31 **G++ method to calculate the vertical electron attachment energy.....	200
107	Potential energy surface in relation to the phi-psi angles for alanine dimer using the UHF/aug-cc-pVDZ method to calculate the vertical electron attachment energy.....	201

LIST OF TABLES

<u>Table</u>		<u>Page</u>
1	Comparison of electron correlation and basis set on vertical electron attachment energy (VEAE or VT) and time to complete the calculation. “geo” indicates that a optimum geometry was calculated using the described method to determine the VEAE. The UMP4 calculations used the UMP2 because it was impossible to calculate the geometry at the UMP4 level. All calculations were performed using Gaussian 03 on a dual processor 1.0 GHz computer with 1.5 gB of RAM and a Windows 2000 operating system.....	68
2	Relative intensities (RI) and effective yield maxima (E_m) for the specific ion types listed for amino acids and their esters.....	104
3	Relative intensities (RI) calculated from a resonance electron capture ion and effective yield maxima (E_m) for the specific ion types listed for amino acids and their esters.....	106
4	The effective yield (EY) maxima for each m/z from N-acetyl Ala, the associated intensities for each maximum, and the relative intensity (RI) as calculated compared to the most intense effective yield maximum. M/z’s without EY maxima listed denote that no clear EY maxima or range that lead to the m/z were present in the effective yield curve.....	108
5	The effective yield (EY) maxima for each m/z from N-acetyl Phe, the associated intensities for each maximum, and the relative intensity (RI) as calculated compared to the most intense effective yield maximum. M/z’s without EY maxima listed denote that no clear EY maxima or range that lead to the m/z were present in the effective yield curve.....	109
6	The effective yield (EY) maxima for each m/z from N-acetyl Try, the associated intensities for each maximum, and the relative intensity (RI) as calculated compared to the most intense effective yield maximum. M/z’s without EY maxima listed denote that no clear EY maxima or range that lead to the m/z were present in the effective yield curve.....	110

LIST OF TABLES (Continued)

<u>Table</u>		<u>Page</u>
7	The effective yield (EY) maxima for each m/z from N-acetyl Trp, the associated intensities for each maximum, and the relative intensity (RI) as calculated compared to the most intense effective yield maximum. M/z's without EY maxima listed denote that no clear EY maxima or range that lead to the m/z were present in the effective yield curve.....	111
8	The effective yield (EY) maxima for each m/z from Ala-Ala, the associated intensities for each maximum, and the relative intensity (RI) as calculated compared to the most intense effective yield maximum. M/z's without EY maxima listed denote that no clear EY maxima or range that lead to the m/z were present in the effective yield curve.....	112
9	The effective yield (EY) maxima for each m/z from N-acetyl Ala-Ala, the associated intensities for each maximum, and the relative intensity (RI) as calculated compared to the most intense effective yield maximum. M/z's without EY maxima listed denote that no clear EY maxima or range that lead to the m/z were present in the effective yield curve.....	113
10	The effective yield (EY) maxima for each m/z from Ala-Ala-Ala, the associated intensities for each maximum, and the relative intensity (RI) as calculated compared to the most intense effective yield maximum. M/z's without EY maxima listed denote that no clear EY maxima or range that lead to the m/z were present in the effective yield curve.....	114
11	The effective yield (EY) maxima for each m/z from N-acetyl Ala-Ala-Ala, the associated intensities for each maximum, and the relative intensity (RI) as calculated compared to the most intense effective yield maximum. M/z's without EY maxima listed denote that no clear EY maxima or range that lead to the m/z were present in the effective yield curve.....	115
12	The effective yield (EY) maxima for each m/z from Ala-Ala-Ala-OMe, the associated intensities for each maximum, and the relative intensity (RI) as calculated compared to the most intense effective yield maximum. M/z's without EY maxima listed denote that no clear EY maxima or range that lead to the m/z were present in the effective yield curve.....	117

LIST OF TABLES (Continued)

<u>Table</u>		<u>Page</u>
13	The effective yield (EY) maxima for each m/z from N-acetyl Ala-Ala-Ala-OMe, the associated intensities for each maximum, and the relative intensity (RI) as calculated compared to the most intense effective yield maximum. M/z's without EY maxima listed denote that no clear EY maxima or range that lead to the m/z were present in the effective yield curve.....	118
14	Comparison of the “corners” of the Φ and Ψ potential energy surfaces for the L- and D-stereoisomers of the N-methyl alanine dimer. The VEAЕ values are given in eV for each Φ and Ψ combination where Φ and Ψ are given in degrees. The VEAЕ values are compared between the inverse Φ and Ψ angles for the stereoisomers so that $\Phi = -180$ and $\Psi = 180$ of the L-stereoisomer is compared with the $\Phi = 180$ and $\Psi = -180$ of the D- stereoisomer. All other comparisons are made in the same manner.....	119

Interactions of Low Energy Electrons with Amino Acids and Peptides

Introduction

Research on low energy electron/biomolecule interactions is a relevant subject in biology because of the relatively recent development of electron capture dissociation (ECD) and related techniques in mass spectrometry[1-3]. These mass spectrometric techniques are expanding the analytical capabilities for studying peptides, proteins, and post-translational modifications. While the practical use of these techniques is increasing, there remain questions about the mechanisms for fragmentation of the analytes in these experiments. The mechanism for the fragmentation of a multiply charged peptide by capture of a free electron has remained a matter of considerable debate. [1, 4-9] The interaction between low energy electrons, < 10 eV, and multiply charged positive ions in ECD is related to a technique known as resonance electron capture (REC) where low energy electrons interact with neutral molecules in the gas phase producing negative ions. From studying electron/molecule interactions using REC, where electron energies can be controlled precisely, it is hoped that insights into the mechanism of ECD can be gleaned.

Very little work has been done on electron interactions with neutral amino acids and none on peptides and proteins. [10-12] Several reports have been released on resonance electron capture (REC) of nucleic acid bases and model compounds for nucleotides and nucleosides [13-16] but they are of limited utility for adding insight into the mechanism of ECD. Thus basic studies for gaining insight into the ECD mechanism need to be done. The limited volatility of peptides must be addressed and therefore it is

important to study the effects of derivatization that are known to improve volatility of certain compounds [17]. In addition the peptides themselves need to be studied by REC using methods appropriate for non-volatile compounds. A brief experimental outline is informative for explaining the scope of this thesis.

The purpose of this thesis is to study the effects of low energy electrons on peptides as a model for other electron-induced molecule fragmentations used in mass spectrometry. The overall goal is to determine the energy required for forming fragment ions using REC-MS. Initial studies using a JEOL 600 MS for in-beam experiments served to determine whether negative fragment ions can be observed for non-volatile peptides, what types of fragment ions are produced, and an idea of the maximum sizes of peptides that can be studied. The high resolution experiments were used to unambiguously determine the empirical formula of the fragment negative ions observed using the in-beam sample introduction technique. In practice this was only possible when the observed signal was very intense and therefore was only done using one compound. The REC-MS studies were performed to study the effects on resonance electron capture by modifying the C and N termini of amino acids and peptides. Furthermore, by studying the fragment ions produced and the associated electron energies it was hoped that mechanistic insight into the formation of fragment ions, specifically peptide backbone cleavages, for related techniques could be gathered. The introduction will cover the basics of electron / molecule interactions, negative molecular ion fragmentations, related ionization techniques, sample introduction, and the relevant research to the study of REC by amino acids and peptides.

Electron / Molecule Interactions

Electrons with energies below ~ 10 eV can interact resonantly to form transient negative ions (TNI) with biomolecules to yield molecular anions or dissociate to produce fragment ions and radicals[18]. REC involves trapping of electrons by molecules to form transient negative ions. TNIs or resonances have lifetimes that vary from only slightly longer than the time it would take the electron to travel past the molecule, i.e. $\sim 10^{-14}$ s, to $\sim 10^{-3}$ s. Resonances have traditionally been classified into three types, based on trapping interactions: they are referred to as shape resonances, nuclear excited Feshbach resonances, and electronically excited Feshbach resonances. [19] Nuclear excited Feshbach resonances have been divided into the sub-classes of vibrationally and rotationally excited Feshbach resonances to prevent confusion between excitation of the atomic movement modes and excitation of the nuclear sub-atomic particles.

A shape resonance is formed by the attractive polarization potential due to the attractive forces (coulombic, polarization, dipole, and others) (Eq. 1) between the electron and the neutral molecule, and the repulsive centrifugal potential (Eq. 2) arising from the relative motion of the interacting bodies as the electron approaches the molecule (Fig. 1)[20]. The trapping potential well is an illustration of the shape resonance and is not intended to include all of the interactions that exist in the molecule but enough to explain the principle of shape resonance. The attractive potential, V_A , is defined by α , the polarizability of the molecule, r , the distance between the electron and the neutral molecule, and q , the charge. The repulsive potential, V_R is defined by r , the distance between the electron and the neutral molecule, μ , the reduced mass of the electron and

molecule, and ℓ , the angular momentum quantum number of the electron. Examination of Eq. 2 shows why the angular momentum of electrons in shape resonances must be non-zero, or non s-wave, because if $\ell = 0$, $V_R = 0$ and there is no trapping. Therefore s-wave capture, $\ell = 0$, does not lead to shape resonances but it is possible for certain classes of compounds to undergo s-wave capture, leading to shape resonances, but these are outside the scope of this work. The assignment of wave type or ℓ can be done using electron transmission spectroscopy (ETS) and will be discussed later under the techniques section. The name “shape resonance” comes from the shape of the trapping barrier that determines the lifetime of the resonance.

$$V_A = -\alpha q^2 / 2r^4 \quad (1)$$

$$V_R = \hbar^2 \ell (\ell + 1) / 2r^2 \mu \quad (2)$$

Feshbach resonances all derive from a parent excited state, vibrational, rotational, or electronic. When described in terms of molecular orbitals, the electronically excited Feshbach resonance can be explained with a model where there is a neutral ground state and any number of neutral excited states that exist energetically above the neutral state (Fig. 2). If the addition of the electron to a neutral excited state produces a positive electron affinity for the negative excited state relative to the neutral excited state, then the neutral excited state is termed the “parent state” of the negative excited state that is the Feshbach resonance. Put another way, the Feshbach resonance is lower in energy than the parent neutral state because capture of an electron and excitation of another electron into an excited state requires less energy than excitation of a lone electron into the same excited state. The same concept applies to vibrational and rotational Feshbach resonances in which the parent states are now vibrationally and/or rotationally excited.

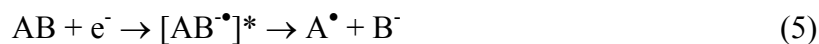
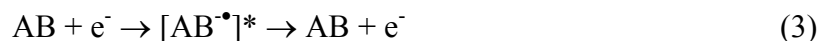
There are specific names for some types Feshbach resonances, one of which should be mentioned here. A “core excited resonance” is another name for an electronically excited Feshbach where the parent state is the ionization potential of the molecule and this term is common in literature.

A more simplistic explanation of the difference between Shape and Feshbach resonance can be made using molecular orbital theory (Fig. 3). The neutral molecule has filled bonding orbitals and any number of unoccupied orbitals energetically above zero including π^* , σ^* , and the singlet (S_1) and triplet (T_1) states. If an electron is captured into the unoccupied π orbital and the trapping interaction is a shape resonance then this is a π^* shape resonance. The example of the π^* shape resonance illustrates an additional important point, that is that the trapping interaction, the shape or Feshbach resonance, is separate from the orbital type. In theory any trapping interaction can occur with any orbital but in reality there are limits based upon the specific molecule and what interactions are possible for that molecule.

Feshbach resonances involve some reorganization of the electronic structures. Using the examples of singlet and triplet neutral states (Fig. 4), the parent state for the resulting Feshbach resonance can be easily understood. The excitation of an electron requires a reorganization of the electronic energy levels because it occurs simultaneously with resonance capture (Fig. 5). In the case where E_1 is less than either of the possible parent states, there is the possibility of a Feshbach resonance but not to the total exclusion of a possible shape resonance (Fig. 6). In practice Feshbach resonances are typically within 0.2 - 0.5 eV of the parent state but they can be further apart energetically for larger molecules[21]. In the second case when E_2 is greater than the parent states, the

probability is that the resonance is a shape resonance. It could be a Feshbach resonance of another higher energy parent state but it is not a Feshbach resonance of either parent state shown, S_1 and T_1 (Fig. 6).

Whatever the origin of the resonance, there are three reactions that the TNI can undergo. [22, 23] First, the TNI can re-emit or autodetach an electron to produce a neutral molecule and an electron (Eq. 3). Autodetachment can occur in as little time as an electronic transition, 10^{-16} s. If the TNI can stabilize the ion by transfer of the energy into vibrational and rotational modes (Eq. 4) it is possible for the ion to survive as long as 10^{-3} s. TNIs that survive for longer than 10^{-6} s are described as long-lived molecular ions. The last possible reaction the TNI can undergo is a breakdown into a neutral radical and an anion (Eq. 5). The breakdown of the TNI can occur on the same time scale as vibrational movements (10^{-14} s) up to the lifetime of the TNI.



The relationship of the processes, in energy vs distance between A and B in a diatomic model molecule, AB, follows the Franck-Condon Principle (Fig. 7). The curve labeled “M” is the potential energy surface for A-B as a function of internuclear distance between A and B [20, 24, 25]. The other two curves are surfaces for the M^{\bullet} species consisting of the radical and anion, A^- and B^{\bullet} for the lower curve (M^{\bullet}_1) and A^{\bullet} and B^- for the upper curve (M^{\bullet}_2). The neutral and anionic curves can be compared because of the presence of an electron at infinite distance which can be added to the M curve without

changing the energy of the curve and will therefore allow for direct comparison of the curves.

Energies that appear above the parent state potential energy surface lead to negative electron affinities (EA's) and those below lead to positive EA's[24]. Specifically for the model molecule AB, the electron affinities of the radicals are positive for B• or negative for A• (Fig. 7). The energy for homolytic dissociation of AB is the change in energy from the ground state of M to the curve M at infinity and is labeled D(AB). The heat of formation for A• and B• from AB is shown as ΔH_1 and is the change in energy between the molecule's ground state and the curve M•₁ at infinity[25]. From the figure the relationship between D(AB) and the heat of formation and the electron affinity can be extracted (Eq. 6) and will be discussed further below. ΔH_2 is not shown but would be calculated the same way as ΔH_1 and is the energy difference between the AB ground state and the A• + B• at infinity[26].

$$D(AB) = EA(A\bullet) + \Delta H_1 = EA(B\bullet) + \Delta H_2 \quad (6)$$

The electron capture process involves a vertical transition in a standard potential energy diagram because of the large mass difference between the nucleus and electron that causes the electron to move 10^3 times faster than the nucleus. In other words the electron is captured long before the nucleus has time to adjust to the optimum internuclear distance in the radical anion. The Born-Oppenheimer approximation is a simplifying device that allows the massive nucleus to be treated as stationary so that the internuclear repulsion can be dealt with separately from the electrostatics of the electron when calculating molecular orbitals. The capture of an electron must then be limited to the space constrained within the two outer dashed vertical lines and equal or above the

initial ground state (Fig. 7). Once an electron is captured the possibility of nuclear relative position change is possible so that if the capture of an electron leads to an ion at “A”, the atoms A and B move apart (Fig. 8). Once the distance between A and B passes the line labeled “B”, autodetachment is no longer possible unless the nuclei move back together again. The intermediary ion $AB^{*\cdot}$ (Eq. 3) formed by the capture of the electron can be stabilized by collisions or radiative loss (Fig. 8 “C”) of energy into a lower bounded energy state that generates a long-lived molecular ion (Eq. 5). In the case of an ion that is not stabilized it may proceed to dissociate or move to a distance so that A^- and B^\cdot cannot interact. The ground state has a Gaussian distribution of A-B distances and can be correlated with the energy of the electron captured by reflection through the anion curve to give a theoretical electron absorption spectrum where electron energy is equal to zero at the ground state of AB (Fig. 9). From the electron absorption spectrum the appearance energies (ε_1 and ε_2), electron energy capture maxima ($\varepsilon(\max)_1$ and $\varepsilon(\max)_2$) and information about the slope of the anion curve above the ground state that captures the electron, can be determined. The slope of the anion curve is determined by the deformation of the peak from a Gaussian shape. The typical way to view the intensity vs electron energy correlation is to place electron energy on the x-axis (Fig. 10). The comparison of how the theoretical electron absorption spectrum compares to experimental data will be left until these methods have been introduced.

Methods for Studying Negative Ions

Resonances have been studied by techniques including ETS, REC-MS, and electron energy loss spectroscopy (EELS). ETS and REC-MS are complementary techniques. ETS gives information on the electron energies associated with formation of the resonance, but provides no information regarding the fate of the resonance. [27] REC-MS gives the resulting fate of the resonance, the ions, and the electron energies that result in ion formation, but not all the electron energies that form the resonances because [28, 29] some resonance states formed from capture of electrons autodetach before detection can occur in the MS, and are therefore not observed. Comparison of schematics of the two instruments and EELS serves to illustrate the differences (Fig. 11-13).

All instrument schematics start with a filament, collimating lens, a dispersion region, additional collimating lens, and a reaction chamber. The most popular means to select and control electron energies is to use the trochoidal electron monochromator (EM) design of Stamatovic and Schultz[30, 31] that has remained basically the same since its invention. The EM or dispersion region utilizes crossed magnetic and electrical fields to filter the electron energy. The electron energy can be scanned rapidly by changing the electrical field or the filament potential. Tuning of the electron monochromator can be done to achieve an energy resolution of 50 meV at the cost of electron beam current. Typically working conditions for REC-MS are more likely to be 100-200 meV for improved signal intensity due to a stronger electron beam current

The ETS is the simplest of the instruments (Fig. 11). In the reaction chamber (Fig. 11 e) the mono-energetic electron beam can interact with gas phase molecules. If the electron beam does interact with molecules there is a drop in the electron current that is recorded by the detector (Fig. 11 g). The electron energy is scanned with the EM and the

electron current is recorded and displayed as the derivative of current intensity vs electron energy (Fig. 14). The ETS data should correlate directly to the theoretical electron absorption spectra described by the reflection through the anion curve or more correctly the theoretical data should match the ETS data. However, because ETS data are reported as the derivative of the intensity absorption vs electron energy, and this must be kept in mind when comparing the theoretical electron attachment spectrum and the ETS data.

The derivative of the experimentally determined values is used because it makes the interpretation of the data easier due to the more obvious peaks and inflections (Fig. 15). When ETS data is compared to the theoretical electron absorption spectrum it can be seen that the appearance energy should correlate with the start of change in the ETS curve and that $\epsilon(\text{max})$ should correlate to the crossing point from negative to positive (Fig. 14). In reality there are electron transmission effects that are unrelated to the electron capture by the molecule or overlapping resonances that may shift the overall ETS curve away from the x-axis. Therefore, the assignment of the lower limit of the appearance energy is often taken from the “dip” or the local minimum preceding the rise in the ETS spectrum. Furthermore, the mid point between the “dip” and the “peak,” or the local maximum following the rise in the ETS curve, is taken as the maximum intensity or $\epsilon(\text{max})$ (Fig. 15). The energy difference between the “dip” and the “peak,” or the “dip to peak” measurement as termed by Burrow et al, has been used to calculate the angular momentum of the captured electron [32]. The calculation of the angular momentum can only be done using a class of related compounds.

EELS is used to understand the energy of neutral transitions of electrons by the energy lost from scattered electrons. EELS experiments utilize two monochromators with the first providing a fixed mono-energetic electron beam that interacts with the gas phase molecules (Fig. 12). In ETS the detector is in-line with the electron beam but in EELS the detector is off the axis of the electron beam to detect the scattered electrons. The second monochromator is scanned to determine the energy of the electrons after the inelastic collisions with the molecules. Most EELS experiments are done using initial electron energies well above the range for resonant interaction (~ 200 eV) and the results reflect the difference between the initial energy of the electrons and the energy of the electrons after collisions. There are some related experiments that have been used to study the energy of the autodetached electrons from resonant electron capture processes, but these experiments are even rarer than the EELS experiments. The use of EELS to study biomolecules has been limited due to the difficulty of generating gas phase molecules.

In both ETS and EELS the energies of the electrons interacting with the molecule were determined but there was no correlation with the resulting fragment ions from the electron / molecule interactions. REC-MS allows for correlation of negative fragment ion formation with electron energy by extraction of the negative ions produced in the reaction chamber into a mass analyzer (Fig. 13). The key difference between the reaction chamber of the REC-MS and ETS is the repeller with a negative potential that pushes the ions into the mass analyzer. By scanning the electron energy produced by the monochromator, effective yield curves or correlations between electron energy and the resulting fragment negative ions can be recorded.

The data recorded from REC-MS using an EM-rToF-MS are 3-dimensional, i.e. m/z vs intensity vs electron energy. The 3-D data can be broken down to be more easily visualized into a total effective yield curve that is the sum of all effective yield curves for each m/z , and effective yield curves for each m/z . An effective yield curve is the curve of ion intensity vs electron energy and is so named because it is a composite of electron attachment, electron autodetachment, and partitioning between possible fragmentation channels that results in the ion versus the electron energy.

When comparing the total effective yield curve and the theoretical electron capture spectrum for a compound there are two obvious differences (Fig. 16). First, the overall shape of the total effective yield curve may not be Gaussian. The reason that the effective yield curve peak is non-Gaussian is that only a portion of the molecular anions have sufficient lifetime to survive and be detected before autodetachment occurs. Second, the observed effective yield maximum is different from the theoretical electron attachment spectrum, $\epsilon(\max)$. Again, the difference is related to the lifetime of the ions before autodetachment. By mentally reflecting the electrons back through the anion curve (Fig. 7) it can be seen that in the example, where the A-B lengths are closest to the point where autodetachment become impossible, the ions are more likely to survive and be detected. The trend of lower electron energies that correlates with longer A-B bond lengths typically improves detectability in REC-MS. The appearance energy determined by REC-MS is very close to the appearance energy observed in ETS and predicted by the theoretical electron attachment spectrum. The observed appearance energy can be taken as an upper limit of the actual lowest energy to produce a vertical transition.

The total effective yield curve can be separated into the individual effective yield curves of ion intensity vs electron energy for each ion of a given mass (Fig 17). The individual effective yield curves can be relatively complex in shape due to thermodynamics, orbital mixing, and multiple resonances leading to the same fragment ion. The example maxima of $\varepsilon(x)_2$ and $\varepsilon(x)_3$ show the importance of using ETS and REC-MS, to study a single compound (Fig 15). With REC-MS, $\varepsilon(x)_2$ and $\varepsilon(x)_3$ could be mistaken for being two overlapping resonances. When the ETS data is included in the analysis, the conclusion is that there are two effective yield maxima from one resonance.

When assigning the origin of a resonance as a shape or Feshbach resonance, additional information beyond ETS or REC-MS data are required. Simply put, the location and peak shape of an electron energy curve do not in and of themselves provide enough information to assign a resonance as either a shape or Feshbach resonance. As mentioned before, Feshbach resonances must be correlated with a parent excited state that is usually within 0.5 eV of and energetically above the Feshbach resonance. Parent excited states are often determined by absorption spectroscopy techniques such as IR and UV-VIS, for vibrationally and electronically excited Feshbach resonances, respectively, and EELS for vibrationally excited Feshbach resonances.

REC-MS Sample Introduction

The EM-rToF-MS has one clear limitation regarding the compounds that can be analyzed; the analytes must be in the ion source to resonantly interact with the electrons. The problem of getting the analyte molecules to the ion source to be ionized is not new.

One of the easiest solutions to this problem has been the application of heat to the sample causing it to go into the gaseous phase. However, heating is not a universal solution and many compounds, including peptides and proteins, can break down or pyrolyze instead of volatilizing. In-beam (IB) - chemical ionization (CI) was developed as an alternative to conventional heating and is achieved by using a probe tip or loop coated with sample that is inserted into the ion source either in or near the ion plasma. The first reported use of the IB-CI technique with peptides showed that molecular ions could be observed for peptides with two to six residues at temperatures 150° C below that required by conventional heating. [33] Early work also showed that IB-electron impact (EI) could be used to provide structural information in addition to generating a molecular ion. [34]

In the determination of the experimental parameters for the IB technique it was determined that rapid heating leads to increased formation of the molecular ion over fragmentation or pyrolysis. [35-37] Rapid heating or flash volatilization (FV) prevents pyrolysis by overcoming the energy bonding the molecule to the surface before the energy equilibrates through all degrees of freedom. Early experiments utilized varied materials including metal wires, polyimide coated wire, Teflon, Vespel, glass, and ceramic. Experimentation on IB and FV came to a sudden end with the development of techniques such as fast atom bombardment (FAB) in 1980 and later matrix assisted laser desorption ionization (MALDI) (1989) and electrospray ionization (ESI) (1989).

Relevant Ionization Techniques for Biomolecules

Since its discovery, ESI has become a very powerful technique for volatilizing and ionizing aqueous molecules into the gas phase. It has only been fairly recently that ESI, when coupled to a FT-ICR-MS mass analyzer and detector, has had electrons introduced to produce fragment ions from a charge neutralization reaction on multiply charged positive peptide ions. [2] The fragmentation of multiply charged positive ions by electrons is known as electron capture dissociation (ECD) a technique that has several unique characteristics. First, ECD produces c and z ions in contrast to other MS/MS fragmentation techniques for peptides like collision assisted dissociation (CAD), blackbody infrared radiative dissociation (BIRD), infrared multiphoton dissociation (IRMPD), and others that produce predominantly b and y ions (Fig. 18). [1, 38] Second, post-translational modifications, such as phosphorylation and glycosylation, are more resistant to cleavage and loss by ECD and are in direct contrast to many of the aforementioned techniques that favor fragmentation and β -elimination of post-translational modifications. Marshall and coworkers showed the complementary nature of ECD and techniques that fragment post-translational modifications by sequencing the peptide of a glycopeptide with ECD and the glycan structure by IRMPD. [39] ECD was used to unambiguously determine the location of the post-translation modification of the glycan structure that was not possible by IRMPD, even though IRMPD cleaved the peptide backbone to produce sequencable ions as well. In contrast, IRMPD cleaved all of the sugar bonds present to completely “sequence” the glycan structure while ECD did not break any bonds contained in the glycan structure. Third, ECD shows a strong preference for cleaving disulfide bonds thereby eliminating additional preparative steps before sample analysis. Last, ECD has been shown to reduce or eliminate scrambling in H/D

measurements from exchange in experiments on proteins. Furthermore, ECD has been used to identify relative abundances of stereoisomeric peptides, peptides with one amino acid's stereochemistry changed, by the fragmentation patterns to 1% accuracy compared to 3-5% with CAD [40, 41].

While ECD is increasingly used to answer practical biological questions, an understanding of the mechanism of ECD has remained obscure; it has been addressed mainly by computational methods. The rf potentials used to trap ions in the ICR cell are incompatible with monoenergetic electrons thereby preventing any correlation between electron energy and fragmentation. The initial mechanism proposed for ECD was a non-ergodic fragmentation, or a fragmentation that occurs before there is redistribution of the internal energy of the molecule. The principle idea behind the earlier proposed mechanism is that the electron is captured by a positively charged side chain quaternary amine. The captured electron would release an H atom that was hydrogen bonded to the carbonyl oxygen of a nearby amide leading to cleavage of the C $_{\alpha}$ -N bond adjacent to the amide (Fig. 19). [2] Recently the non-ergodic hypothesis of the ECD mechanism has come into question. The initial model based on density functional theory (DFT) calculations, had inherent limitations and could not explain many of the experimental observations [6]. High level calculations using small model compounds (formaldehyde and N-methylacetamide) and amino acid-sized models suggested that the N-C bond dissociation would be more facile than originally predicted. Presently, the claim of non-ergodic fragmentation remains tenuous at best. Further computational studies have led to a revised mechanism where the amide bond is the site of electron capture forming a super base that can abstract a nearby proton (Fig. 20). [5] The experimental evidence cited in

support of this mechanism is the observation that all α -amide bonds are cleaved, with the exception of proline, and are not limited to amide bonds proximate to positive charge sites in the peptide or protein.

Recent Developments in Electron – Molecule Interactions in Biomolecules

The breadth of work involving electron / molecule interactions is too broad to be effectively reviewed here. However, the specific areas of interest to REC for peptides and amino acids will be examined. The specific topics that will be included are theoretical calculations, limited to calculations addressing the ECD mechanism or REC, and REC and ETS data reported for peptides, amino acids, and their related derivatives. Disulfide bonded compounds will be discussed because of the relevance to ECD and to provide a review for future work that may be done in this field upon REC of disulfide bonded peptides. The reason that information on disulfide linkage electron capture is important is that disulfide bridges in proteins are ubiquitous. Top down proteomics by ECD will depend on being able to cleave the disulfide linkages, and the electron energies may be different than that needed for backbone fragmentation. Bottom-up proteomics depends on first cleaving disulfide bonds for effective proteolytic digestion which is usually conducted under basic conditions. If disulfides have to be mapped out, proteolysis becomes difficult if not impossible without cleaving the disulfides, and if disulfides are first reduced the information of where they are is lost. Finally, H/D exchange studies in proteins, disulfides are always a nuisance, because under the acid conditions necessary to preserve the deuterium content, the disulfides are hard to cleave and digestion by pepsin

is hindered. A direct mass spectrometric approach by electron reduction would alleviate all of these problems. Any further correlation with other experimental techniques or compound classes will be left for the discussion as required.

Recent computational studies by Simons and co-workers[42] on electron capture has focused on a model system, i.e. the alanine dimer. The authors calculated the vertical electron attachment energies (VEAEs) for fragmentation by capture of an electron into a σ^* orbital. The results showed that the σ^* state that allowed for fragmentation of all bonds was approximately 6 eV and that the presence of nearby positive charges resulted in lowering of the energies for electron capture. Furthermore, the authors studied the possibility of capture of the electron into unoccupied low lying π orbital and coupling of the π^* state with the σ^* state to produce σ bond cleavage. The computational results showed capture of an electron by the neutral molecule into a π orbital to be 2.5 - 2.8 eV. The possibility of coupling with a σ^* state was also explored and it was found that the most energetically favorable option was the cleavage of the C_{α} -N bond (Fig. 16). The computational experiments in this report show the possibility of π orbital electron capture, leading to indirect-DEA as the mechanism for electron capture dissociation. Indirect-DEA is the capture of an electron into a bound anion state followed by transfer into another bond cleaving state (Fig. 17). This is an example of π^* - σ^* state mixing where the electron is captured by the π orbital but results in σ -bond cleavage through electron coupling to the σ^* state [43]. π^* - σ^* state mixing is important in explaining the cleavage of σ bonds at energies below the direct σ^* state capture.

Another important model compound for ECD and REC that has been studied by computational methods is $H_3C-S-S-CH_2-CH_2-NH_3^+$. Such disulfide bonds are prominent

in protein and peptide structures. As mentioned before it was discovered early on that electron capture in ECD results in cleavage of disulfide bonds. Due to its importance, as the only mass spectrometric technique known presently to cleave disulfide bonds, there have been several attempts to elucidate the mechanistic features. The mechanism of disulfide cleavage involves two possibilities as shown in the model compound. Electron capture can occur directly into the σ orbital of the disulfide bond or the electron can be captured by the positively charged primary amine group and then transferred to the σ orbital associated with the disulfide bond. In related work it was shown that the presence of two positive charges within 30 Å from the midpoint of the disulfide bond results in lowering of the VEAE to the unoccupied σ orbital from its value of 0.9 eV[44]. The model compound tested here was designed to allow for exothermic attachment to the virtual σ orbital in order to test the energy requirements of each fragmentation pathway. The authors concluded that both fragmentation pathways resulted in the same fragment ions (Fig. 18) and the electron attachment cross section for $-\text{NH}_3^+$ capture at $4 \times 10^{-17} \text{ cm}^2$ to $2 \times 10^{-16} \text{ cm}^2$ and the electron attachment to the σ orbital of the disulfide bond at $2 \times 10^{-18} \text{ cm}^2$ to $7 \times 10^{-17} \text{ cm}^2$ for low energy electrons ($\sim 0.1 \text{ eV}$). At this distance between the disulfide bond and positive charge, the authors expected similar branching ratios, or approximately equal fragmentation through each channel. The effect of increasing distances changes the cross section for the $-\text{NH}_3^+$ channel by r^{-2} and the σ^* by $14.4 \text{ eV \AA} / r (\text{\AA})$ leading to the conclusion that for a distance of 5-15 Å attachment to the σ orbital will be more favored until, capture by a σ orbital becomes endothermic at $\sim 15 \text{ \AA}$. The most important conclusion from this work is that the nearby presence of a positive charge should lower the VEAE of a disulfide containing compound and that the fragmentation of

the disulfide bond should be enhanced. The overarching conclusion for disulfide bond fragmentation is that neither mechanism has been disproved and in fact each is plausible.

There is a limited amount of work detailing the REC-MS data for amino acids including glycine[45, 46], alanine[47], cysteine[10], proline[48], and N-acetyl tryptophan[49]. More recently data were published on glycine, alanine, phenylalanine, tyrosine, tryptophan, and their respective methyl esters[50]. The earliest of electron capture by amino acids is the appearance energy of the carboxylate anion of glycine at 1.01 ± 0.06 eV reported by Muftakhov et al[26]. Several related compounds were also studied and the appearance energies for $(M-H)^-$ were reported for acetic acid, acetamide, and ethyl acetate at 1.29 ± 0.03 eV, 1.95 ± 0.05 eV, and 2.40 ± 0.05 eV respectively. Acetic acid had an additional appearance energy for the formation of a negative ion formed by the loss of a hydrogen atom from the C_α carbon at 2.35 ± 0.20 eV. The bond dissociation energy of the bonds are 4.58 eV for the carboxylate oxygen-hydrogen bond and the 4.22 eV for the C_α carbon-hydrogen bond. The electron affinity of the radicals are, 3.29 eV for the carboxylate radical and 1.87 eV for the C_α carbon radical which can be calculated from the bond dissociation energy and the appearance energy. The conclusion that can be drawn from these results is that fragmentation into either ion is determined energetically by the electron affinity of the fragment radicals.

The first report on fragmentation channels for an amino acid from attachment of electrons with energies between 0 -15 eV was on glycine in 2002 [45]. The most intense ion observed was the $(M-H)^-$ ion formed at the carboxyl group with an energy maximum at 1.4 eV. The formation of this ion occurs through the precursor ion attributed to the π^* orbital by correlation with electron transmission spectroscopy and calculations. The π^*

resonance forms one other fragment ion with m/z 58 that is attributed to the elemental composition of either $\text{H}_2\text{C}_2\text{O}_2^-$ or $\text{H}_4\text{C}_2\text{NO}^-$. Including these two fragment ions, a total of nine negative ions were reported. The production of an H^- ion has a maximum at an electron energy near to zero eV, but the mechanism of formation of the ion at this energy remains unexplained because the reaction is endothermic. The remaining fragment negative ions, with m/z 16 (O^-/NH_2^-), 17 (OH^-), 26 (CN^-), 28 (H_2CN^-), 45 (HCO_2^-), and 56 ($\text{H}_2\text{C}_2\text{NO}^-$), have electron energy maxima at ~ 6 eV. The fragments formed at electron energy ~ 6 eV are attributed to a core excited resonance. The second report on glycine served to confirm the results of the original report, but with substantive deviations that included a maximum effective yield for the $(\text{M}-\text{H})^-$ ion at 1.25 eV and no apparent hydrogen anion [46].

More recently experimental results for dissociative electron attachment of alanine were published[47]. The similarity with glycine was clear, since the most prominent fragment ion was $(\text{M}-\text{H})^-$ at 1.27 eV and the origin of the ion was attributed to the π^* state of the carboxylic acid group. Furthermore, eight other fragment ions observed at electron energies ~ 5.5 eV and 9.0 eV were attributed to core excited resonances.

Dissociative electron attachment to proline is similar to that for glycine and alanine[48]. First, the $(\text{M}-\text{H})^-$ ion is dominant with an effective yield peak at 1.2 eV. There were six fragmentation channels including the $(\text{M}-\text{H})^-$ ion. Three other ions were observed with effective yield maxima in the energy range of the π^* orbital. The “glycyl-yl” ion, as termed by the authors, has m/z 74 and an effective yield maximum of 1.1 eV. The ion with m/z 26, i.e. CN^- , showed two effective yield maxima at 1.6 eV and at 8.2 eV. All of the low energy fragment ions plus the ions with m/z 45 (HCO_2^-) and 17 (OH^-)

are all attributed to shape resonances involving the π^* orbital. The π^* orbital was assigned by electron transmission spectroscopy at 1.91 eV. The higher energy electron effective yield maxima, ≥ 4.9 eV, are attributed to core excited resonances.

Dissociative electron attachment to cysteine showed seven fragmentation channels[10]. In contrast to the amino acids with aliphatic side chains only one fragmentation channel does not have an effective yield curve maximum below 2 eV. The fragmentation channel with only a higher electron energy effective yield maximum produced the ion with m/z 16 which is either O^- or NH_2^- . The five ions have electron energy maxima lower than the electron energy of the $(M-H)^-$ effective yield maximum. The authors assign the effective yield maxima at 0.4 eV (S^- , SH^-) and 0.6 eV ($(Cys-H)^-$) to electron capture associated with the sulfur atom on the side chain. The shape resonances resulting from the π^* states were assigned to the fragmentation channels producing SH^- (1.6 eV), S^- (1.1 eV), and $(M-H)^-$ (1.1 eV). The energy of the π^* state was determined by correlation with ETS data that showed a maximum at 1.98 eV which is sufficiently above the lowest effective yield peaks at electron energies, 0.4 eV and 0.6 eV. Along with the ion with m/z 16, two of the previously mentioned ions, those with m/z 32 (S^-) and 33 (SH^-), have additional effective yield maxima > 5 eV that are assigned to core excited resonances.

The first analysis of REC for an amino acid with an aromatic side chain was reported for the derivatized N-Acetyl Tryptophan (NAT)[49]. The aromatic side chain on an amino acid led to formation of a fragment ion type that has not previously been observed, $(M-R)^-$, where R is the side chain. The $(M-R)^-$ ion is dominant with effective yield maxima at 0.1 eV and the dominant resonance at 1.6 eV. Furthermore, as observed

for the (M-H)⁻ ion of glycine there are effective yield maxima at ~5 eV and 4.9 eV for the (M-R)⁻ ion of NAT. Of the ten fragmentation channels reported, six have effective yield maxima at ≥ 4.9 eV that are attributed to core-excited resonances. Eight of the fragmentation channels have low energy effective yield maxima (< 2 eV) that are attributed to shape resonances of the π^* states but no attempt has been made to differentiate between the orbitals associated with the side chain aromatic ring, the amide of the N-acetyl, or carboxylic acid groups. The authors either did not observe or do not report the formation of a R⁻ species or any fragmentation channels associated with the side chain other than its loss, i.e. the (M-R)⁻ ion and the ion with m/z 96 ion that they assign to an empirical formula of H₆C₅NO. Furthermore, the ion with m/z 58 is attributed to cleavage of the peptide backbone, used loosely in this case, in a manner consistent with an ECD type cleavage of the amide bond to form a C- type cleavage although these fragments are not mentioned as such by the authors.

Aflatooni et al studied the formation of negative ions for glycine, alanine, phenylalanine, tryptophan, proline, and cystiene by ETS [51]. Using model compounds and computational studies the authors were able to assign the π^* orbitals of the aforementioned amino acids. Formic acid is used as a model for the carboxylic acid group and it has a VEAE of 1.73 eV. From the assignment of 1.73 eV from formic acid as being the π^* state, assignment can now be made for the π^* states associated with the carboxylic acid groups, 1.93 eV for glycine, 1.80 eV for alanine, 1.85 eV for phenylalanine, 1.60 eV for tryptophan, 1.91 eV for proline, and 1.98 eV for cystiene. Toluene with VEAE's of 1.21 eV and 4.80 eV can be used as a model for the side chain of phenylalanine $\pi^*_{1,2}$ and π^*_3 states. Therefore the VEAE from phenylalanine at 0.87 eV

is the energy for the $\pi^*_{1,2}$ orbital. The side chain of tryptophan was modeled by indole which has VEAE of 0.90 eV for π^*_1 , 1.85 eV for π^*_2 , and 2.71 eV for π^*_3 thereby leading to the assignment of the resonance at 0.68 eV as the π^*_1 state of tryptophan.

Vasil'ev et al studied five amino acids, glycine, alanine, phenylalanine, tyrosine, and tryptophan, and their methyl esters by REC-MS [50]. The data from this report can be summarized collectively because in many cases the results are analogous. In the simplest amino acids with aliphatic side chains the dominant fragmentation occurs via a resonance on the carboxyl group that generates a resonance stabilized carboxylate anion in the energy range 1-1.5 eV depending on the exact compound and experimental conditions. The resonances at 1.0 - 1.5 eV are assigned to π^* orbitals associated with the carboxylic acid group and the aromatic side chains. A second set of higher resonances at 5eV and higher, lead to fragment ions resulting from cleavage of C-H, C-C, and C-N bonds. The resonances 5 eV and higher are attributed to Feshbach resonances of the $n \rightarrow \pi^*$ (5.64 - 5.9 eV), $p \rightarrow p^*$ (6.5 eV) types, and other singlet states. The methyl esterification of the carboxylic acid group results in limited or no change in the electronic configuration with the exception of the diminished production of the carboxylate anion upon resonance electron capture which can be attributed to the much stronger O-C bond of the ester. The presence of aromatic side chains in the amino acids, phenylalanine, tyrosine, and tryptophan adds additional sites for REC. The data for these compounds show that there are resonances associated with the side chains that lead to their cleavage from the backbone at electron energies lower than that of the resonance associated with the carboxylic acid group. Further discussion of the experimental results of this report on

amino acids and methyl esters will be left to correlation to with the experimental results presented in this thesis.

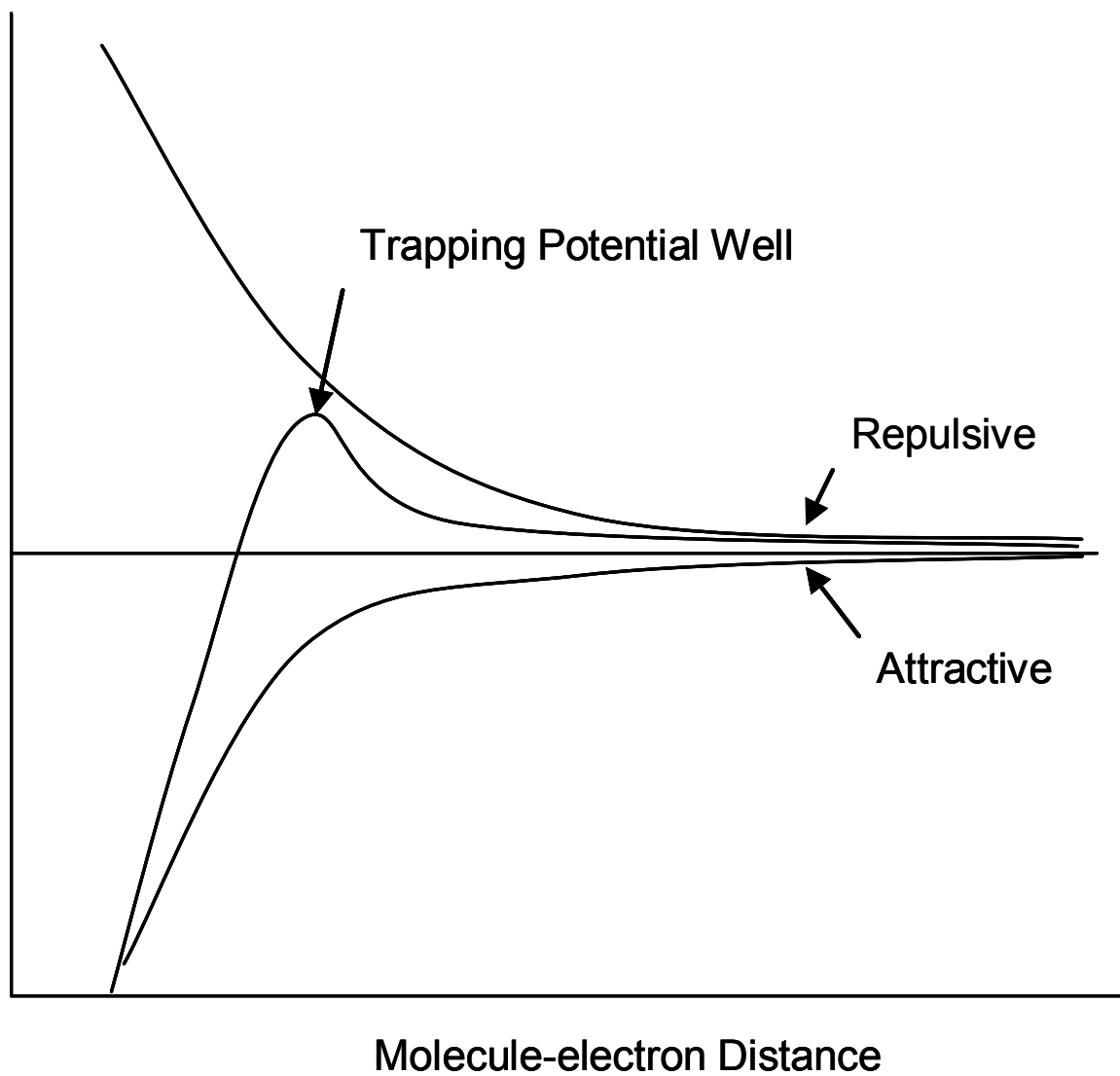


Figure 1. Schematic of a shape resonance as a function of energy versus distance between the electron and electron capturing molecule with the curves for the attractive potentials, repulsive potentials, and an illustration of the trapping potential well for the shape resonance.

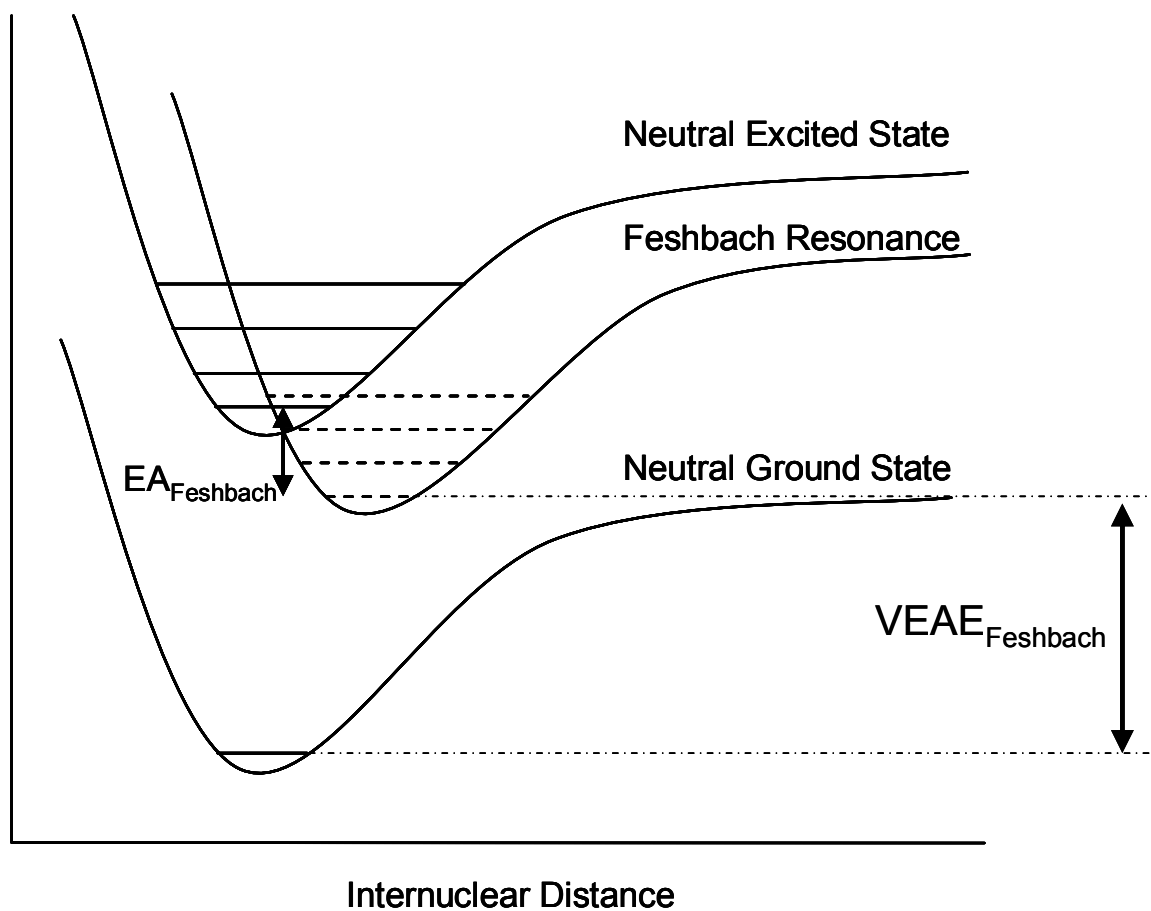


Figure 2. Energy versus internuclear distance for a model electron-capturing molecule with relative potential surfaces for Feshbach resonance to parent neutral excited state. EA_{Feshbach} is the electron affinity of the excited state. $VEAE_{\text{Feshbach}}$ is the minimum vertical electron attachment energy for the Feshbach resonance and is lower in energy than the associated neutral excited state that is the parent state of the Feshbach resonance.

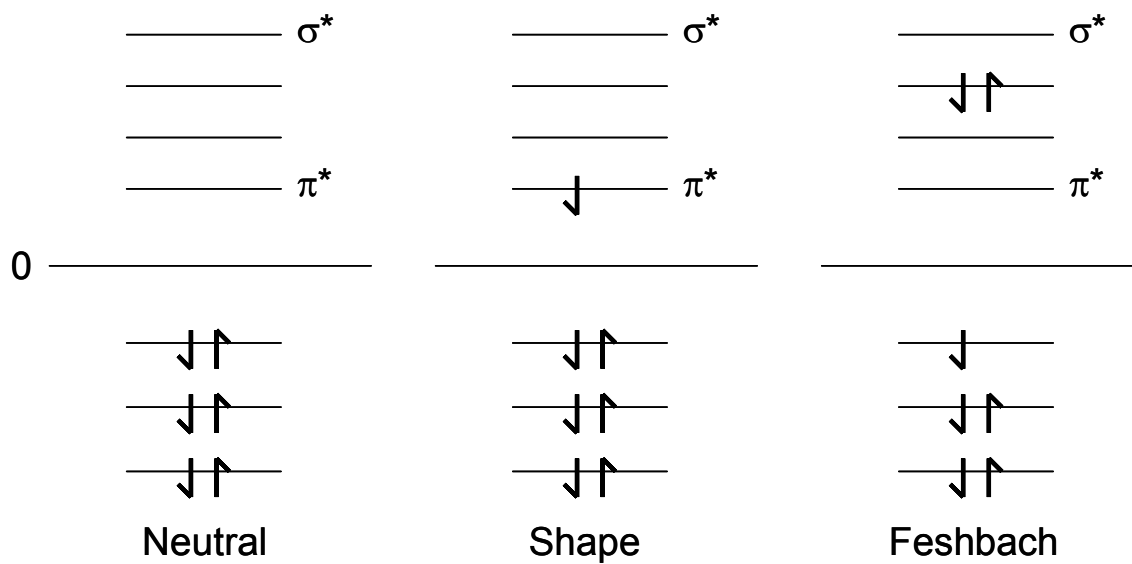


Figure 3. Comparison of the electron configuration of a hypothetical molecule that forms an anion by shape or Feshbach resonances. The change in energy of the orbitals by the addition of an extra electron is ignored for the purpose of this example.

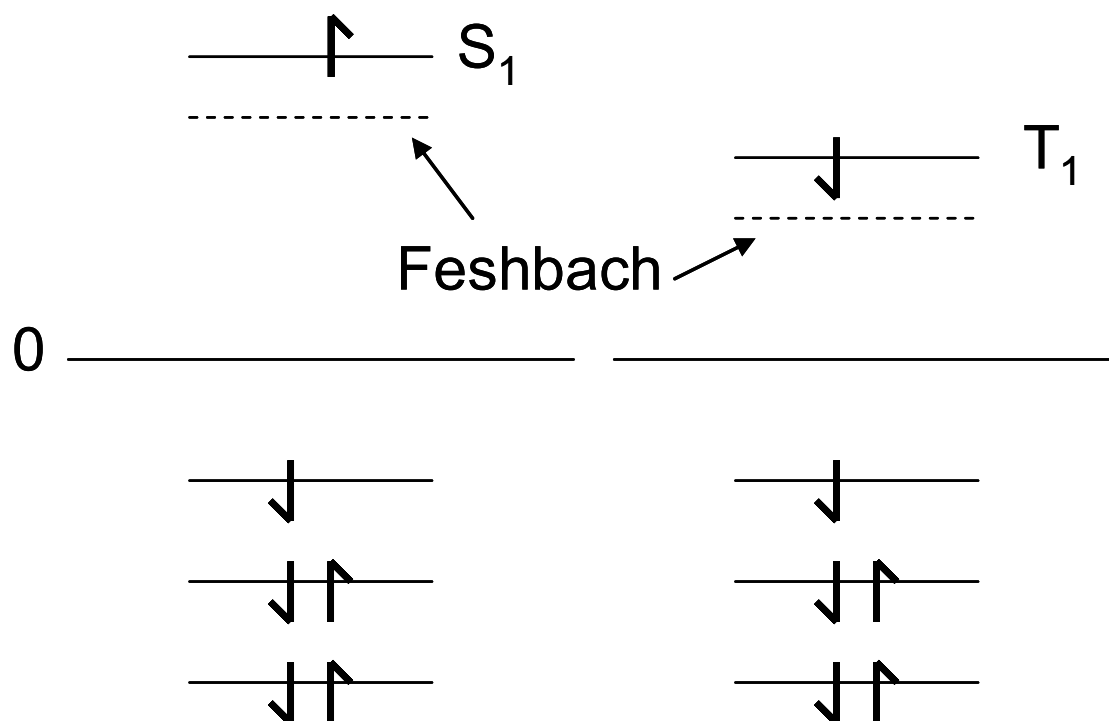


Figure 4. Comparison of the parent singlet (S_1) and triplet (T_1) electronic states for the Feshbach resonances of a hypothetical molecule. The change in energy of the orbitals by promotion of a bonding electron to the excited state is ignored in this example.

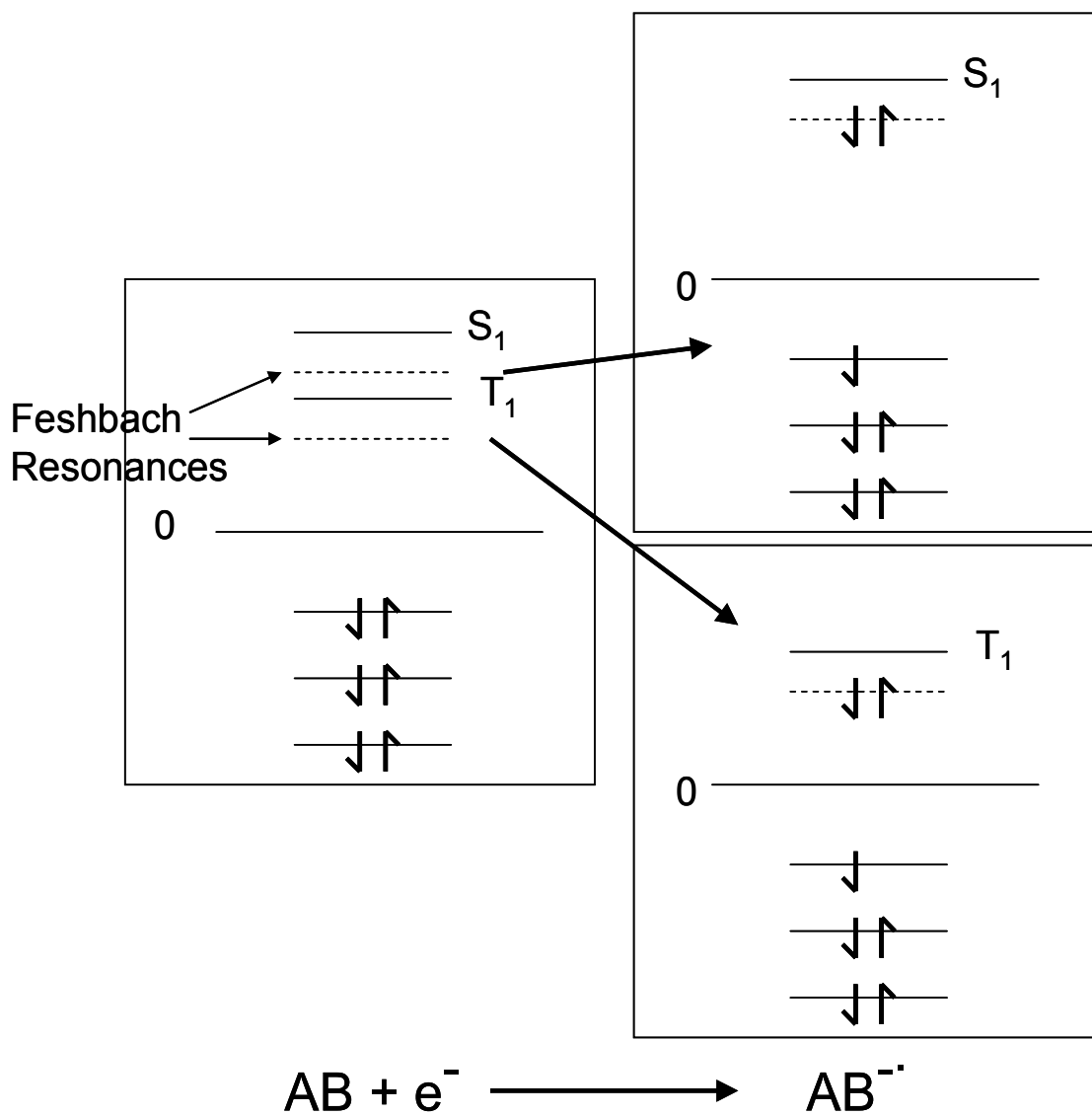


Figure 5. Comparison of the parent states Feshbach resonances of a hypothetical molecule the singlet (S_1) and triplet (T_1) electronic states. Both Feshbach resonances involve excitation of one electron from the occupied orbitals of the neutral hypothetical molecule to pair with the captured electron. The parent states of the Feshbach resonances can be inferred from the energy of the Feshbach resonance because the Feshbach resonances are lower in energy than the parent state and within ~ 0.5 eV. The change in energy of the orbitals by the addition of an extra electron is ignored for the purpose of this example.

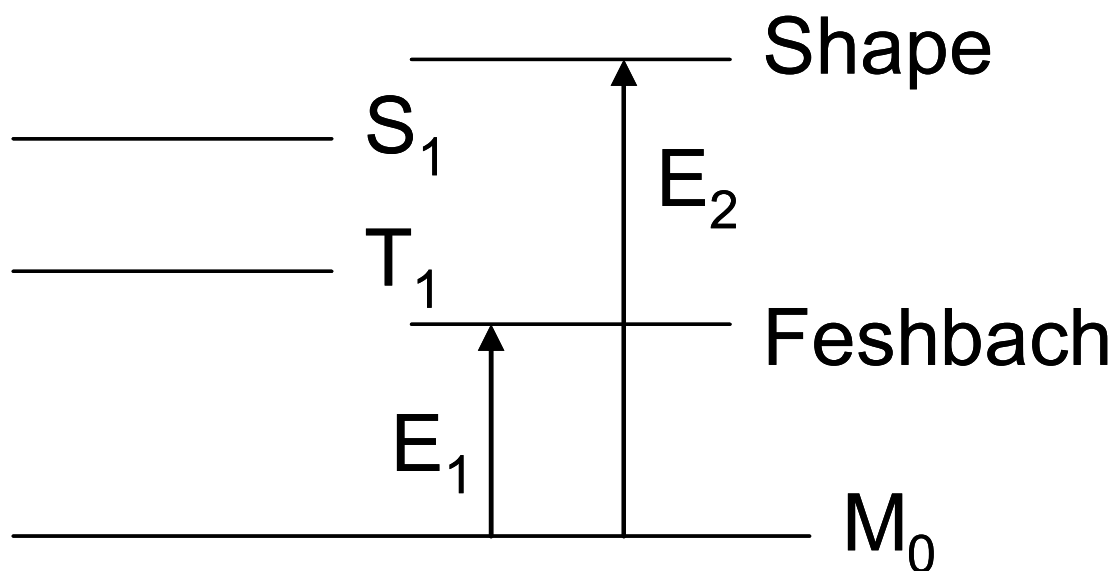


Figure 6. Comparison of the resonance maxima E_1 and E_2 and the parent singlet (S_1) and triplet (T_1) electronic states for the Feshbach resonances of a hypothetical molecule. The assignments of Feshbach and Shape resonances to E_1 and E_2 , respectively, is based upon the relative energy of the neutral electronic transitions.

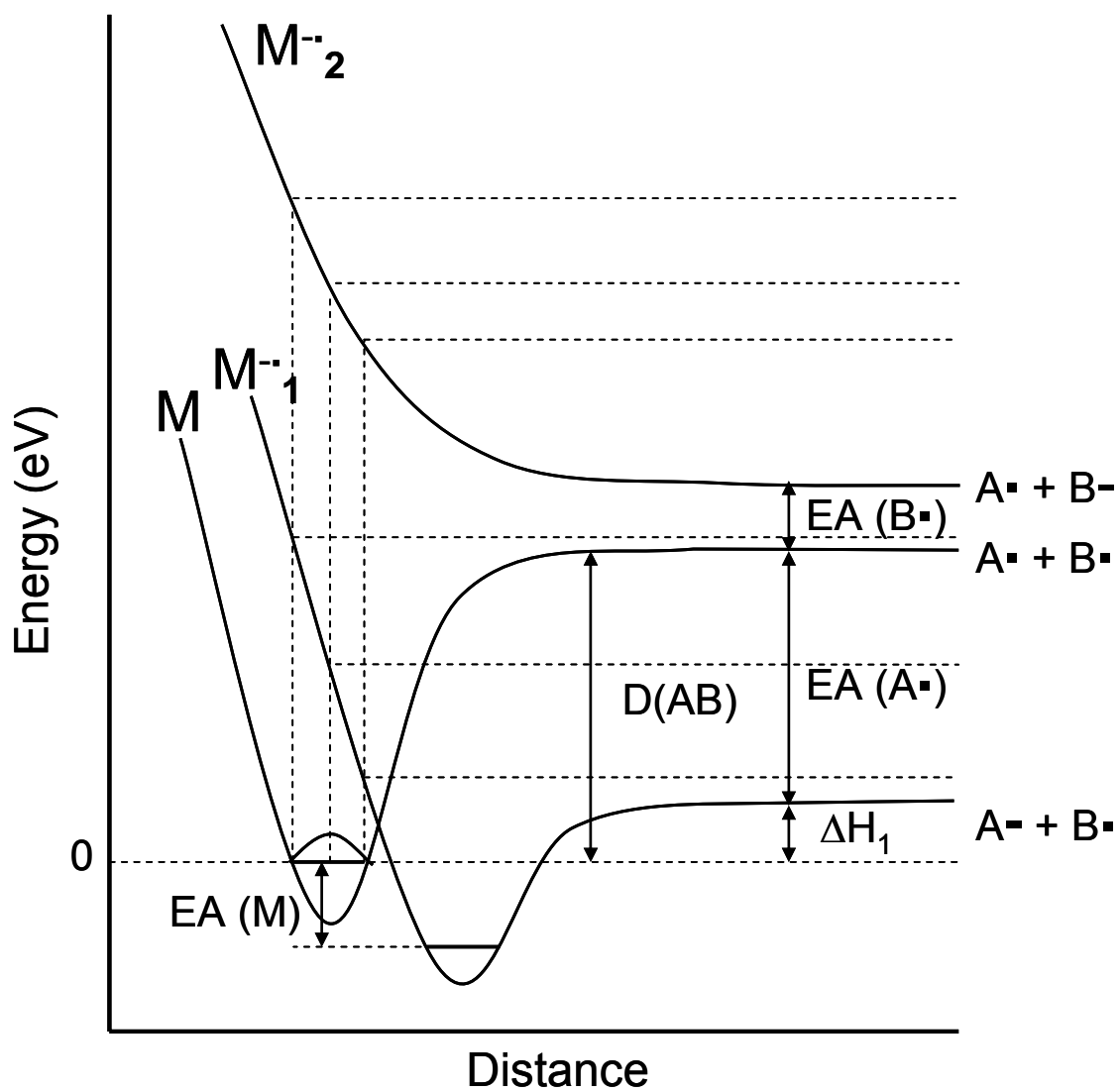


Figure 7. The vertical transition range for a model hypothetical molecule and thermodynamic quantities $D(AB)$, $EA(A^{\bullet})$, $EA(B^{\bullet})$, and ΔH_1 . [24, 25]

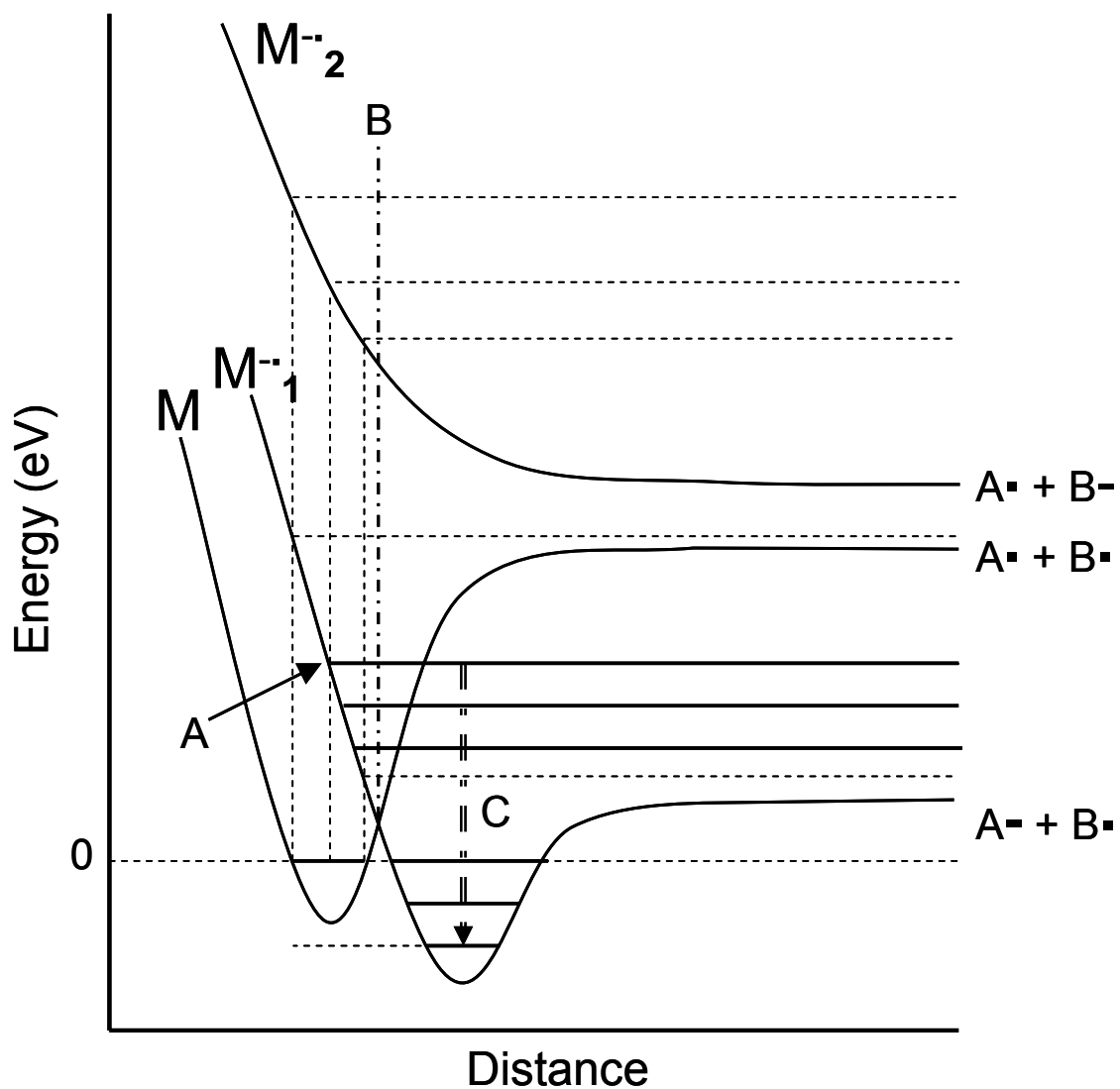


Figure 8. The vertical transition of a hypothetical molecule to form a molecular anion at A on the M^{-1} energy surface. The molecular anion is able to change geometry, thereby lengthening the A-B bond, passing the line B where autodetachment becomes impossible and the molecule can be stabilized into a lower energy bounded state, C, to form a long-lived molecular ion. [24, 25]

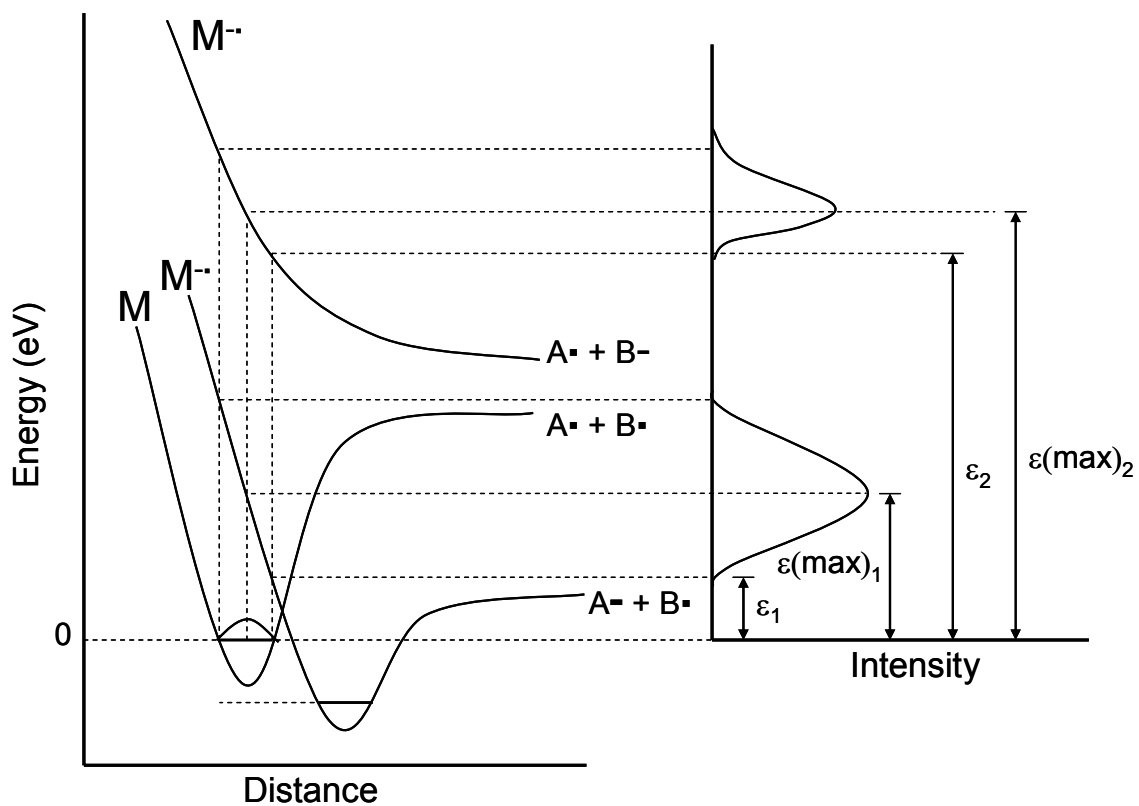


Figure 9. The theoretical electron attachment spectrum from the hypothetical molecule using “reflection” of the Gaussian distribution through the anion curves. [20, 25, 52]

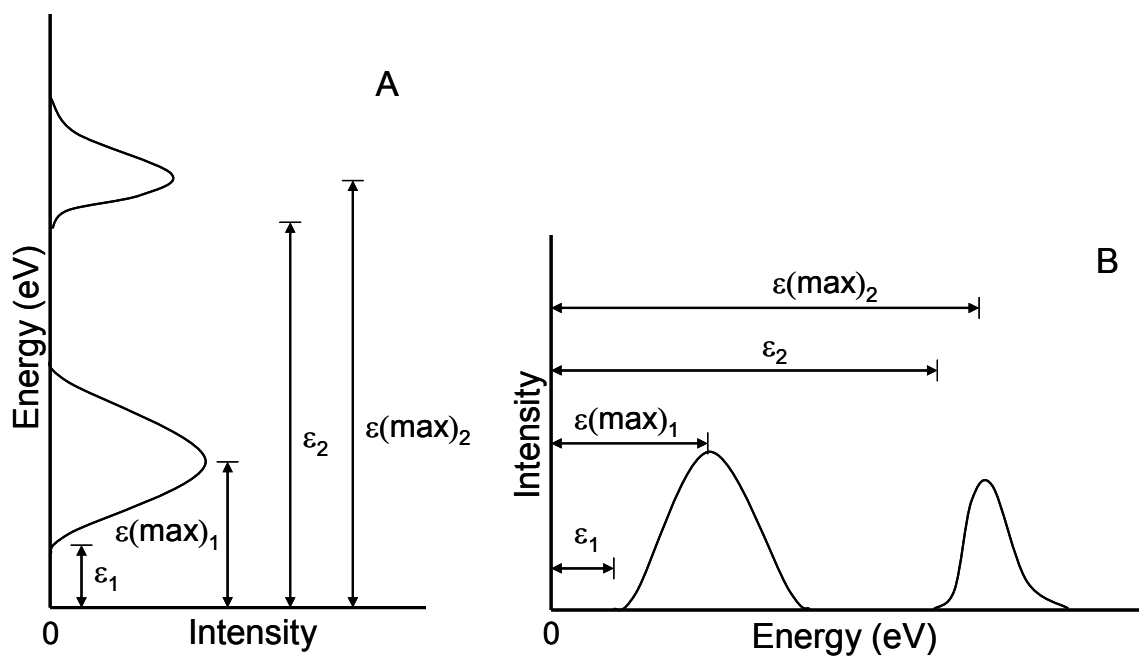


Figure 10. Theoretical electron attachment spectrum from (A) Franck-Condon transitions and (B) a more typical representation, i.e. effective yield curves. The two representations present the same information but are rotated 90° relative to each other.

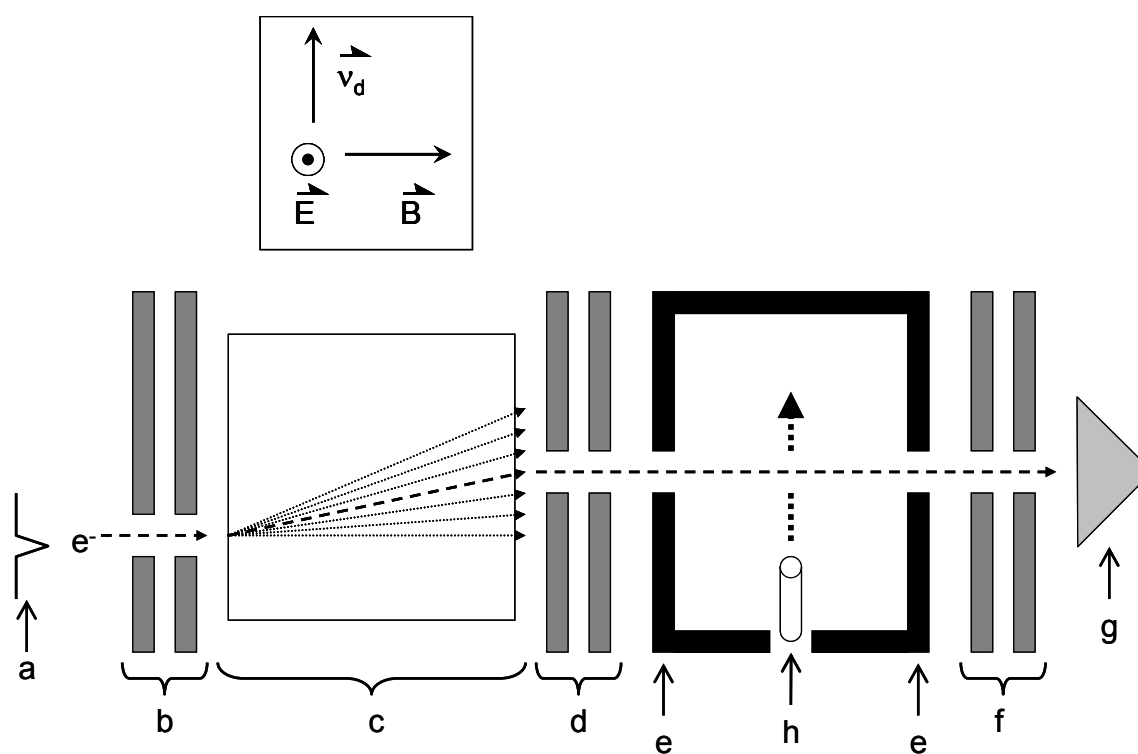


Figure 11. Schematic diagram of a trochoidal electron monochromator – electron transmission spectrometer (ETS) with (a) filament, (b) collimating lenses, (c) deflection region, (d) exit lenses, (e) reaction chamber, (f) electron collector lenses or retarding potentials, (g) electron collector detector, and (h) the source of molecular beam. [53]

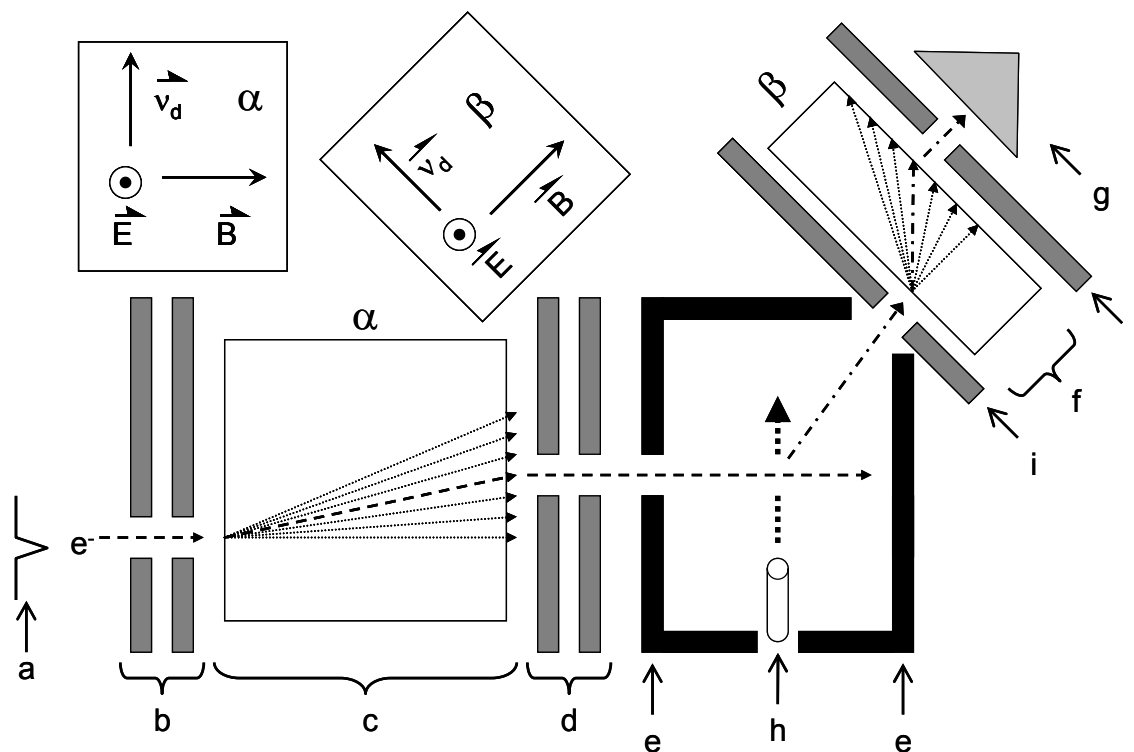


Figure 12. Schematic diagram of a trochoidal electron monochromator – electron energy loss spectrometer (EELS) with (a) filament, (b) collimating lenses, (c) a electron deflection region, (d) exit lenses, (e) reaction chamber, (f) b electron deflection region, (g) electron collector detector, (h) the source of molecular beam, and (i) collimating lenses.

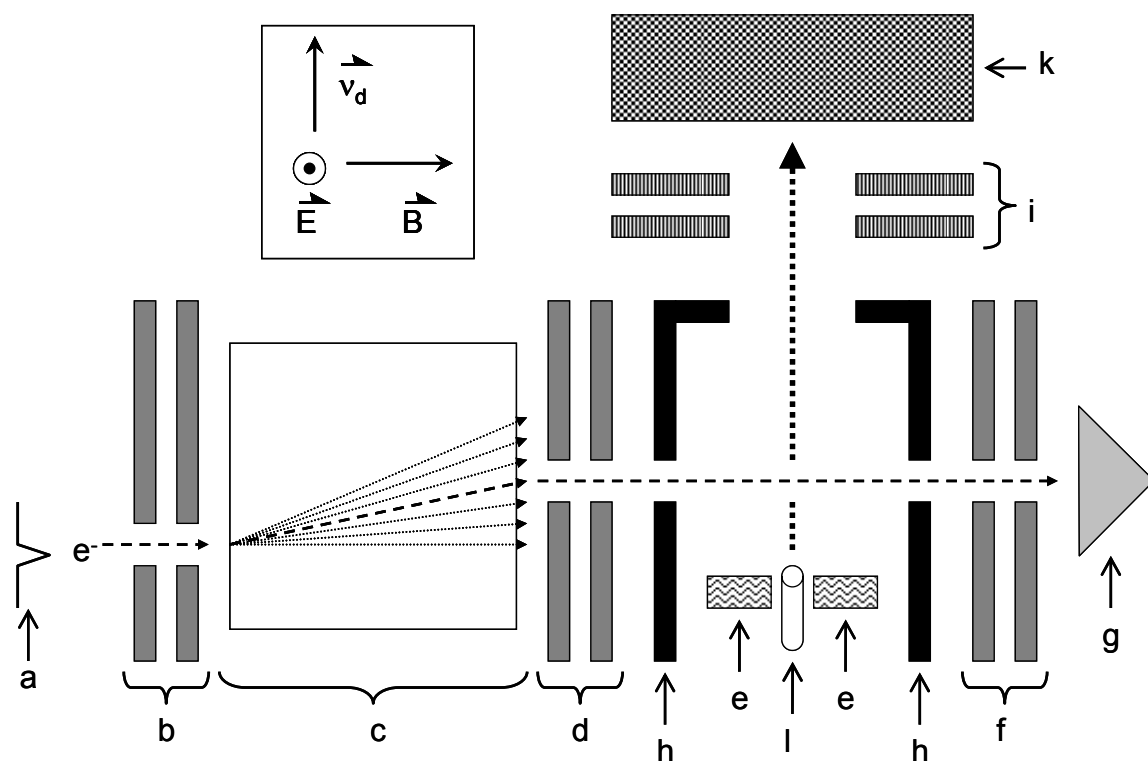


Figure 13. Schematic diagram of a trochoidal electron monochromator - mass spectrometer with (a) filament, (b) collimating lenses, (c) deflection region, (d) exit lenses, (e) anion repeller, (f) electron collector lenses, (g) electron collector detector, (h) reaction chamber, (i) ion extraction optics, (k) mass analyzer and detector, and the (l) source of the molecular beam. [50, 54-56]

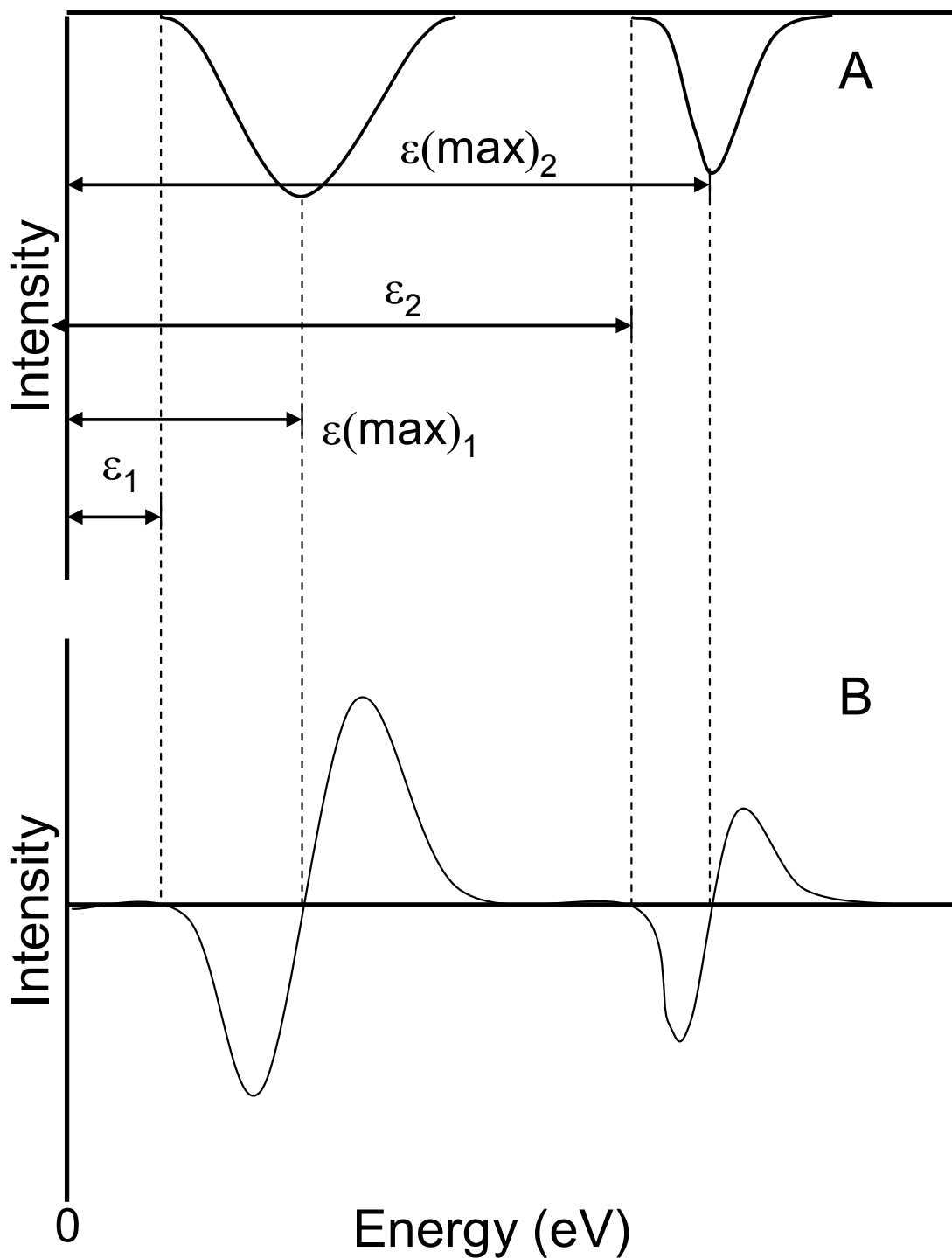


Figure 14. The ETS experimental data (A) and the derivative of the ETS data (B) of a hypothetical molecule. The associated appearance energies (ϵ_1 and ϵ_2) and resonance maxima ($\epsilon(\max)_1$ and $\epsilon(\max)_2$) are shown.

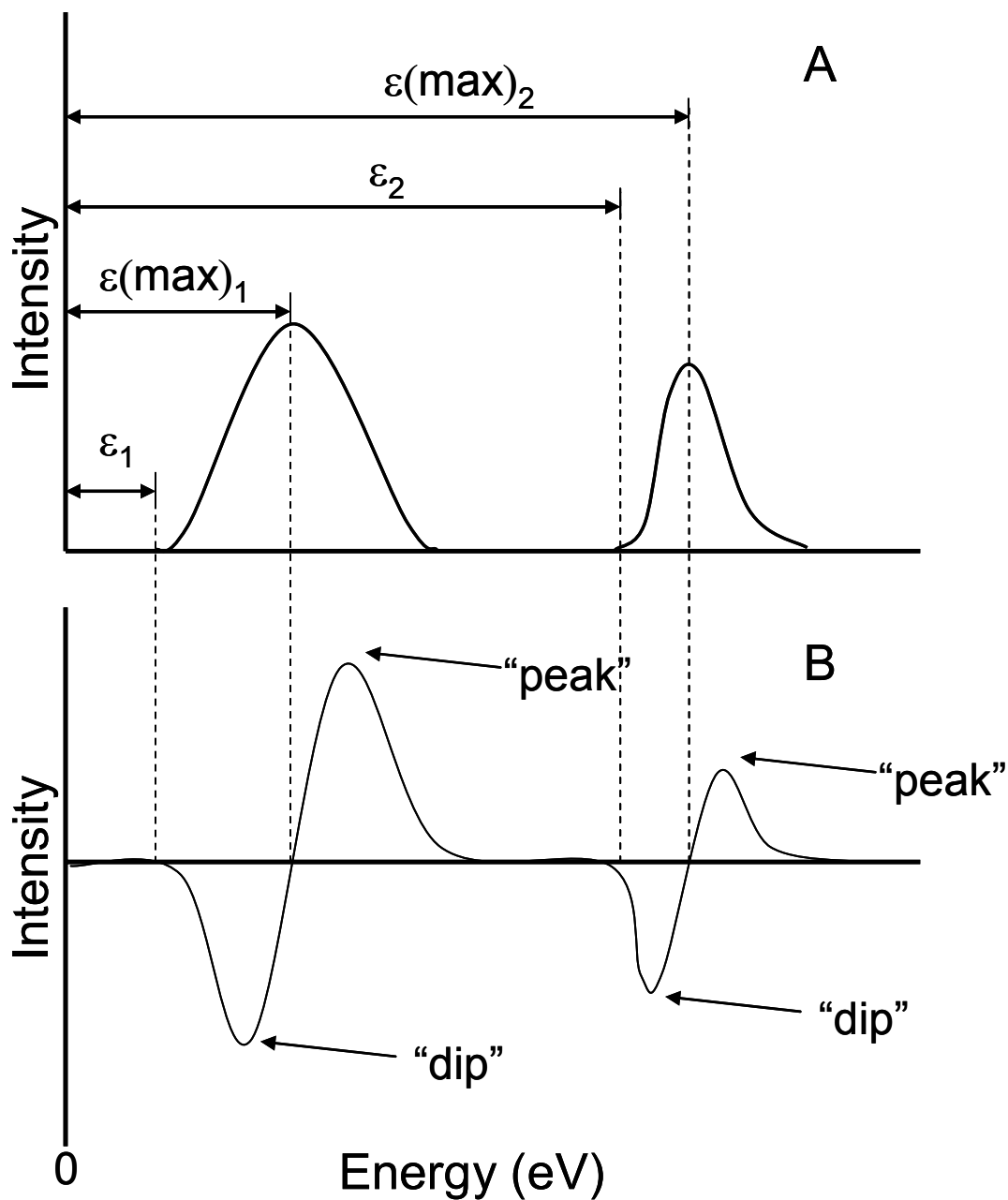


Figure 15. The theoretical electron attachment spectrum (A) and the ETS data (B) of a hypothetical molecule. The associated appearance energies (ϵ_1 and ϵ_2) and resonance maxima ($\epsilon(\max)_1$ and $\epsilon(\max)_2$) are shown.

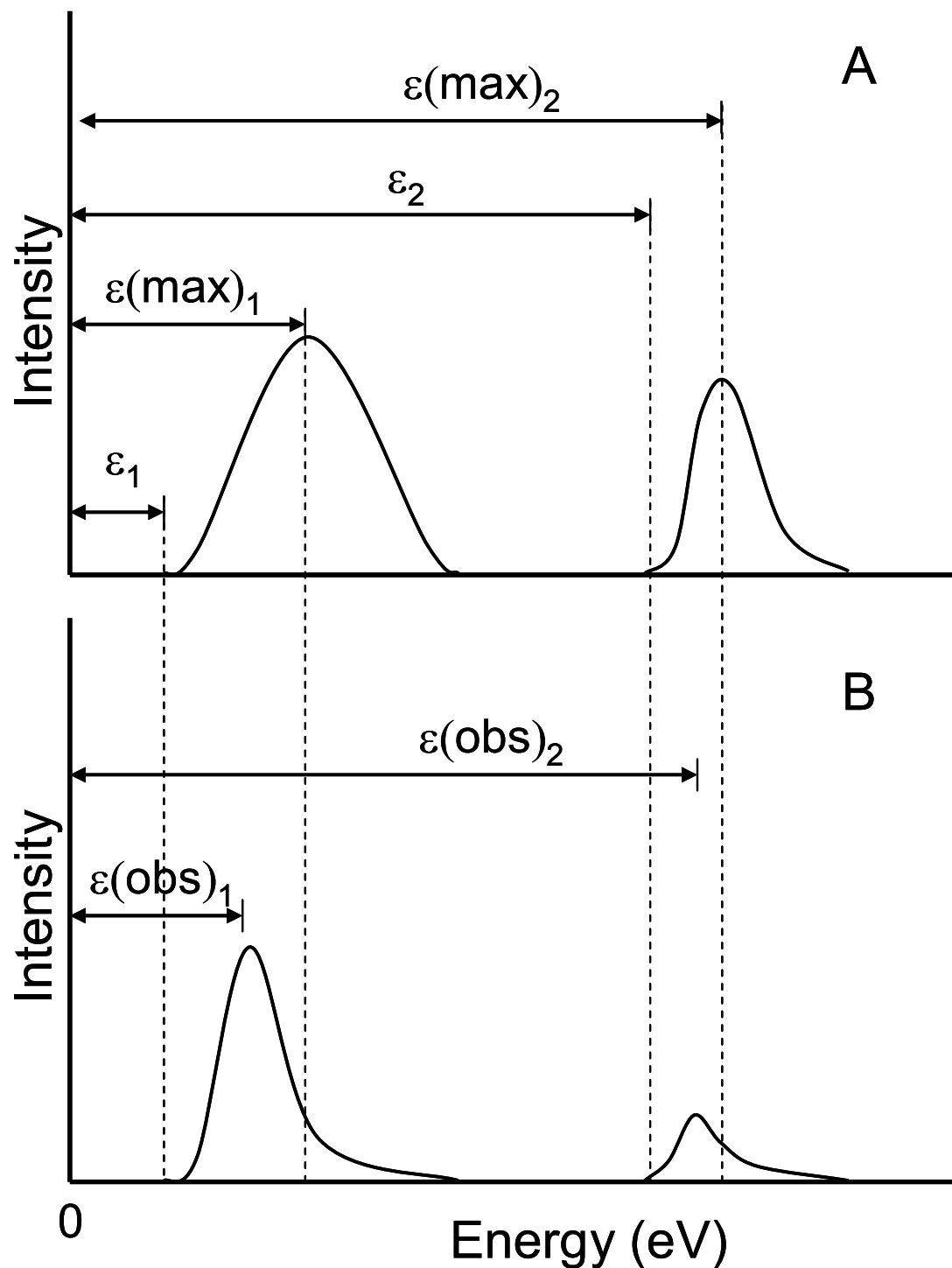


Figure 16. The theoretical electron attachment spectrum (A) and the total effective yield curve from a REC-MS experiment (B) of a hypothetical molecule. The appearance energies (ϵ_1 and ϵ_2), resonance maxima ($\epsilon(\max)_1$ and $\epsilon(\max)_2$), and effective yield maxima ($\epsilon(\text{obs})_1$ and $\epsilon(\text{obs})_2$) are shown.

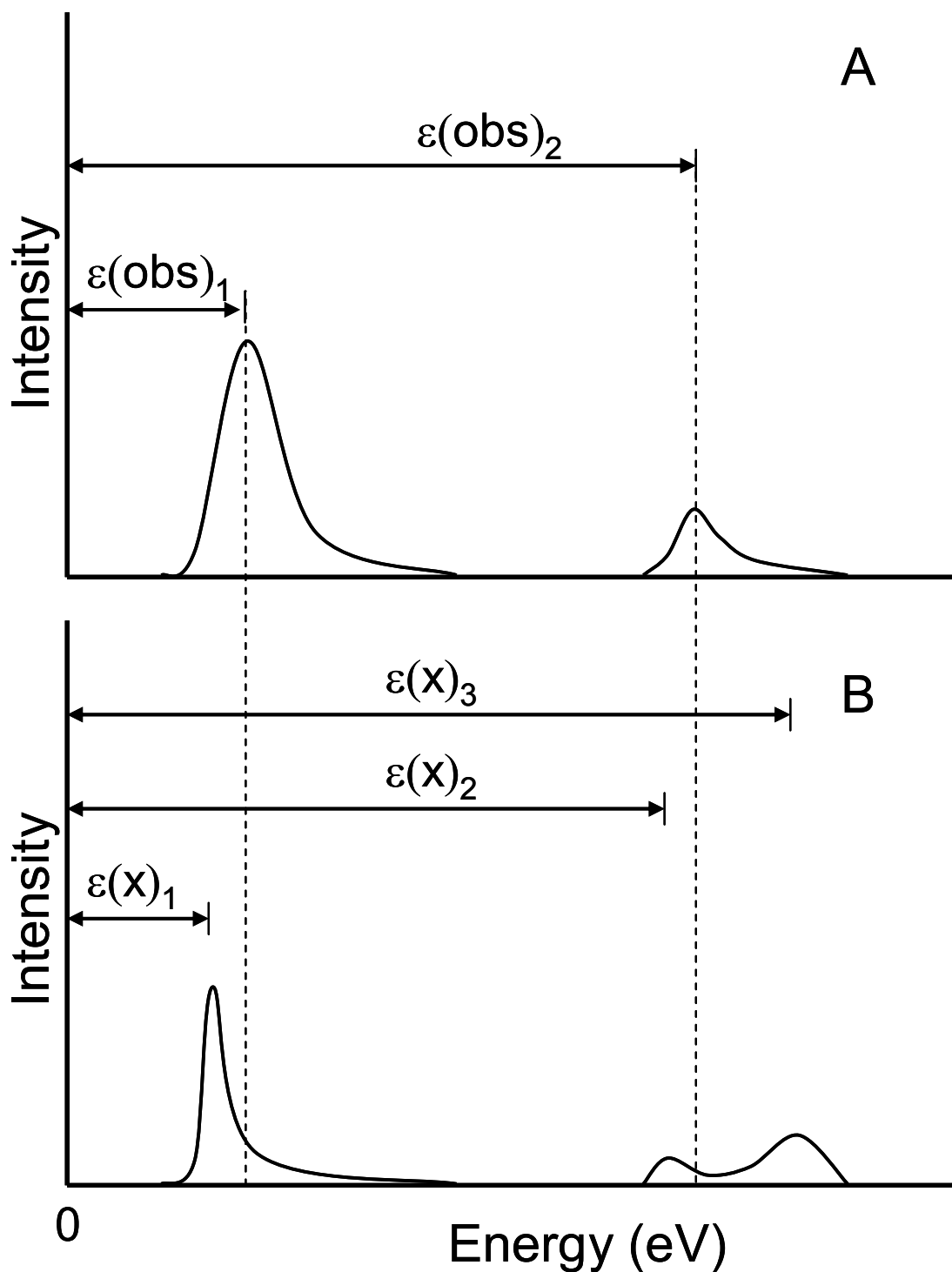


Figure 17. The total effective yield curve (A) and the effective yield curve for an individual m/z from a REC-MS experiment (B) of a hypothetical molecule. The total effective yield maxima ($\epsilon(\text{obs})_1$ and $\epsilon(\text{obs})_2$) and the individual m/z effective yield maxima ($\epsilon(x)_1$, $\epsilon(x)_2$, and $\epsilon(x)_3$) are shown.

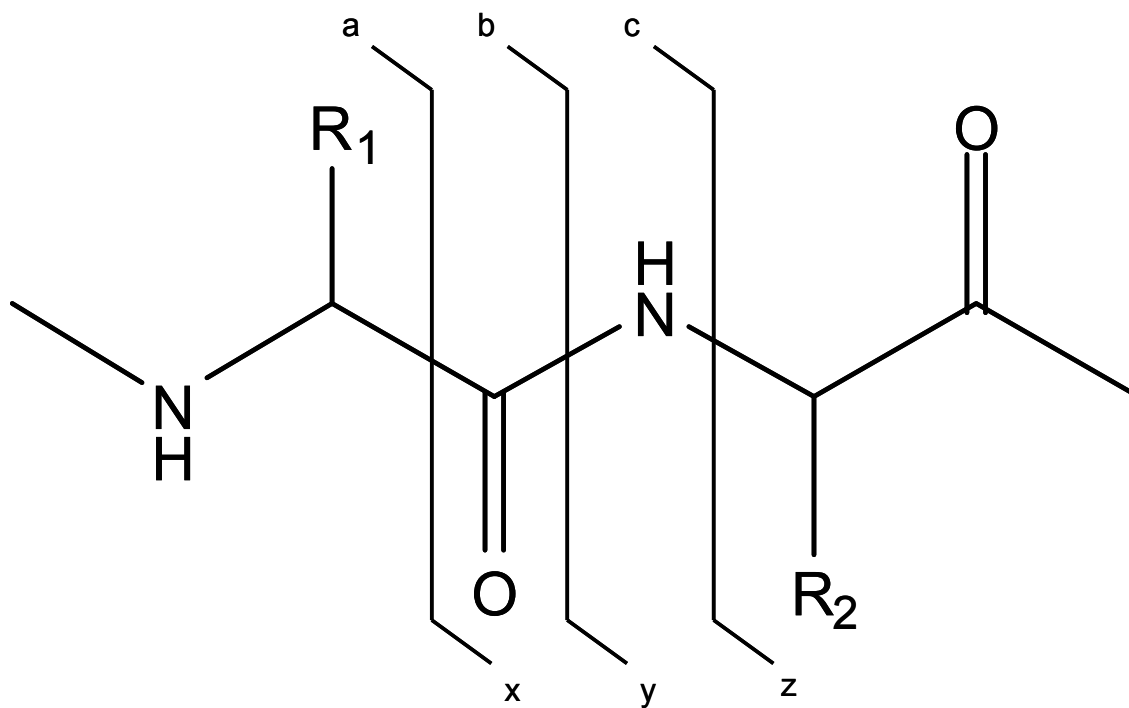


Figure 18. The nomenclature for ions formed by cleavage of the peptide backbone bonds.
[1]

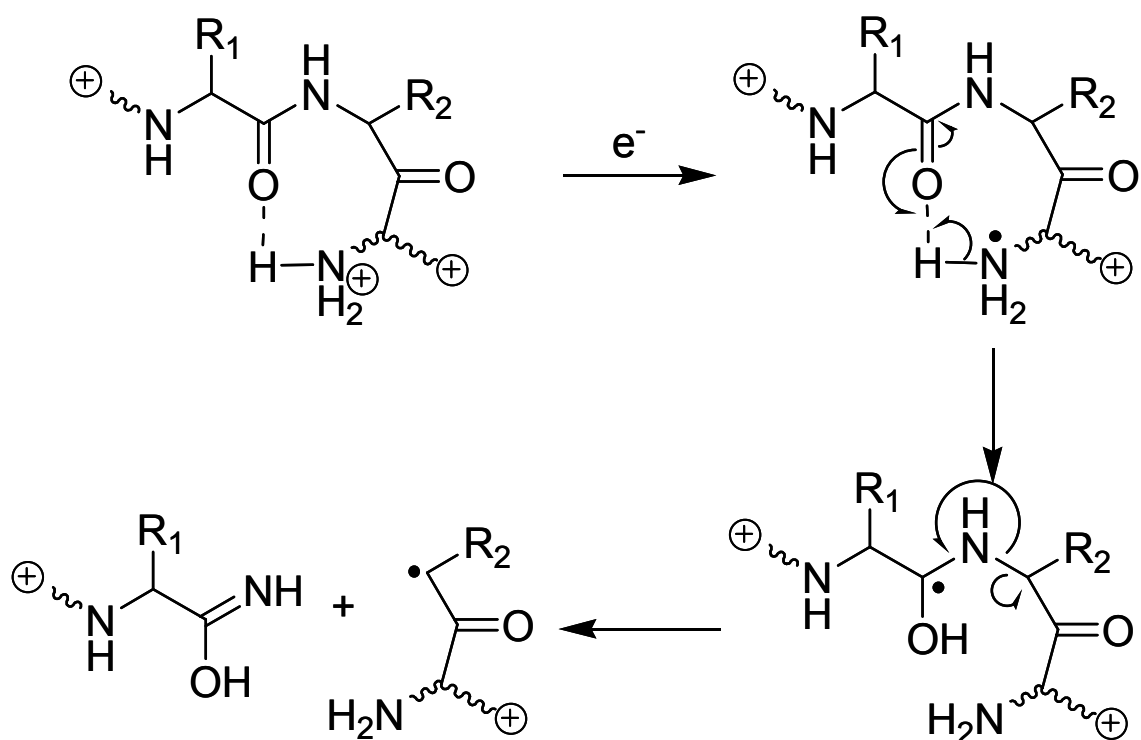


Figure 19. The structure formed after the addition of an electron to the positively charged amine group is a high energy Rydberg state. [2]

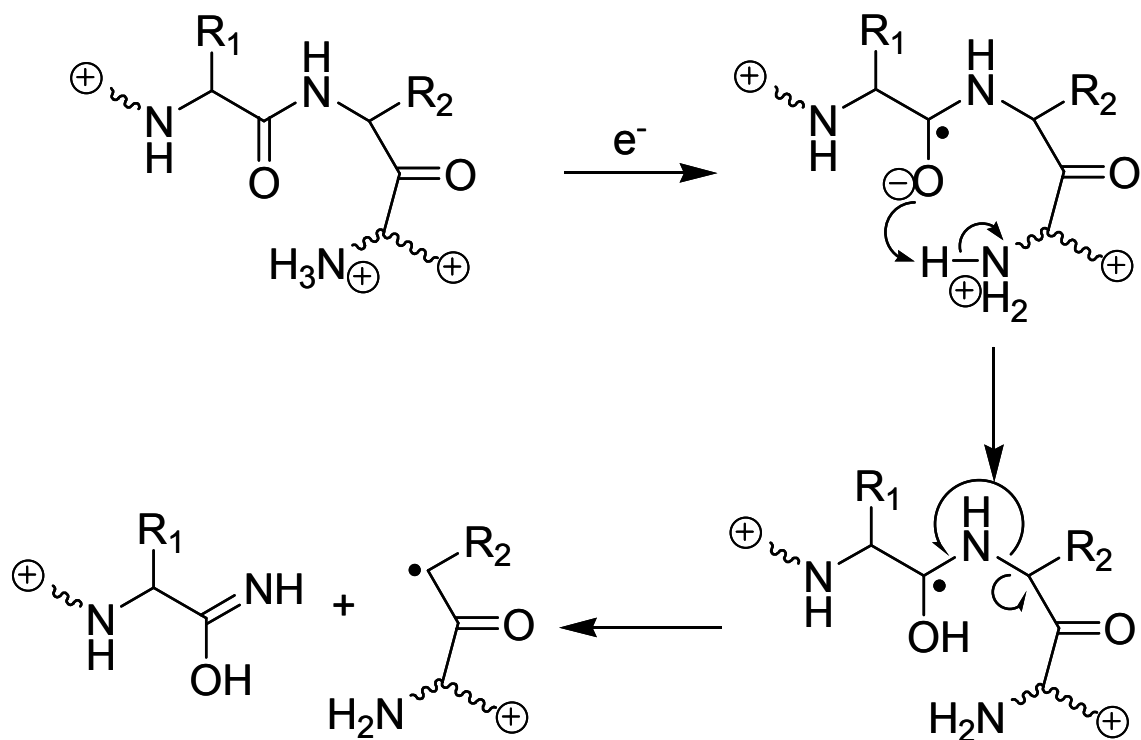


Figure 20. The ECD mechanism for the fragmentation of the peptide backbone to form c and z ions by capture of an electron at a generic amide group in the peptide backbone. [5]

Methods

Introduction

The purpose of this section of the thesis is to introduce and explain the instrumentation, experimental conditions, the organic methods used for the derivatization of amino acids and peptides, and the computational methods used to calculate the vertical electron attachment energy for a potential energy surface of phi and psi angles.

JEOL Sector

The JEOL 600H - MS allows for the ionization and mass analysis of a wide variety of compounds [57]. While the JEOL 600 allows for ionization by many different techniques including Electron Impact (EI), Chemical Ionization (CI), and Fast Atom Bombardment (FAB), only the negative ion mode will be discussed due its direct applicability to electron capture. The JEOL 600 allows for rough control of the energy of the electrons that interact with the analytes. The electron energy can be calibrated using CCl_4 introduced through the calibrant reservoir in place of PFK. The electron energy was manually scanned from 0-10 V on the electron energy dial in ~ 1 V increments to produce rough electron energy calibration curves. Electron energy calibration curves were constructed every time the instrument settings were changed. Ion intensity was recorded for individual ions with m/z 35 for Cl^- , m/z 70 for Cl_2^- , and m/z 82 for CCl_2^- . The electron

energy for the effective yield curves for m/z 35, 70, and 82 are known and are 0 eV, 1 eV and 6 eV respectively.

The analytes can be introduced by either a direct insertion probe or by gas chromatography but only the direct insertion probe was used in this research. The direct insertion probe was modified to hold a homemade in-beam probe that will be discussed below.

The data were recorded in profile mode because of the increased sensitivity in detection of low intensity ions. The ion source was heated to between 200 - 250 °C but varied to some degree due to the heating of the ion source by the filament.

The JEOL 600H MS is a dual sector instrument, with an electrostatic sector to correct for a Gaussian energy distribution of the ions and a scanning magnetic sector which allows for any instant in time to record an ion of a given m/z [57]. The magnetic sector works by using a magnetic field perpendicular to the direction that a charged particle is traveling for focusing an ion of a given mass. From basic physics it is known that the velocity will remain constant but that the direction the particle travels in changes. The velocity of the particle is given by (Eq. 7 -8):

$$q * V = (m * v^2) / 2 \quad (\text{Eq. 7})$$

$$v = ((2 q * V) / m)^{1/2} \quad (\text{Eq. 8})$$

where q is the charge of the particle, V , is the voltage of the accelerating potential, m , is the mass and, v , is the velocity. By substituting Eq. 8 into the magnetic term of the Lorentz force law field strength, B , Eq. 9 is obtained (Eq. 9) where r , is the radius of the arc of the magnetic sector, and all other variables are as defined previously. Thus the m/q

or mass to charge ratio, m/z , is dependent upon the magnetic field squared for a fixed voltage and radius (Eq. 10).

$$q * v * B = (m * v^2) / r \quad (\text{Eq. 9})$$

$$m / q = (B^2 * r^2) / 2 V \quad (\text{Eq. 10})$$

By rapidly scanning the magnetic field it is possible to scan a mass to charge ratio range and thereby acquire a mass spectrum. An alternative is scanning the electric field which leads to a linear relation between V and m/q , but this scanning mode suffers from a limitation in sensitivity. Scanning the magnetic field generates a mass spectrum where the sensitivity is basically independent of the mass to charge ratio but mass to charge does not show an exponential relationship to the magnetic field strength (Eq. 10) because of magnet hysteresis. For the experiments described in this thesis, the JEOL 600 MS was operated in the magnet scanning mode.

In-Beam and Flash Volatilization Probes

The In-Beam probe tips were constructed in house. The probe tips (Fig. 21) that proved most effective were constructed from wire that was mounted in a wire to female pin connector (a). The wire to female pin connector was modified (e) to fit into the capillary slot in the standard JEOL EI/CI probe (f). Filament wire was twisted around itself to form a semi-rigid support and loop (d). The twisted filament wire was threaded through the center of the modified wire to pin connector and bent back over and fed back into the modified wire to pin connector to secure the wire loop. The length of the loop and wire was limited by the length of the vacuum connector of the probe. It was

empirically refined through repeated experimentation. The results of the experiments with probe length were that the end of the loop is approximately flush with the end of the vacuum connector of the probe.

Other probe tip designs were constructed and tested including glass capillaries and Vespel tips, both in a variety of configurations. However, these tips were abandoned because of the success of the filament wire probe which was found to be reusable, easily cleaned or replaced, and which yielded high quality data that were readily interpretable.

An in-beam flash volatilization probe (Fig. 22) was constructed so that the tip of the probe would be near the low energy electron beam. The tip (a) was made from a 3.81 mm stainless steel rod that fit into the port on a stock JEOL Inc. FAB ion source probe. A 5mm electrical contact post (b) was machined directly on the steel rod to allow attachment of one end of the flash volatilization sample wire (c). A 1.27mm offset hole was drilled into the rod to accommodate a second electrical contact post for the other end of the sample wire. This post (d) was made of a 1.02 mm tungsten rod inserted into a ceramic tube (e). To enable control over the distance between the sample wire and the electron beam filament, a ceramic ring (f) with a set screw was machined to fit the steel rod. The entire tip assembly was held in place by a ceramic ring (g) attached to three Teflon rods (h) for insertion into the probe shaft. These rods provided electrical isolation because the potential of the probe tip was that of the source block. The open three rod design allowed for simplicity in evacuating the probe when inserted into the mass spectrometer's vacuum system and for allowing space to make the connections from the probe tip to the wires (i) leading to the feedthrough. The connecting wires were isolated from the stainless steel shaft by a two-hole ceramic rod wrapped with Teflon tape. At the

back end of the shaft, the electrical connections from the wire to the feedthrough, rated for 16 amps at 6 kV, were made with barrel-type in-vacuum connectors (j). A nylon spacer (k) was made to create a large space for electrical isolation in order to prevent arcing to the probe shaft. The connections between the nylon spacer and probe shaft and the nylon spacer and the feedthrough were made with KW-16 fittings (l).

The initial design of the probe was constructed and had to be further modified because the nylon rods that provided electronic isolation were not rigid enough to prevent the wire used to transfer the current from misaligning the tip of the probe from the source opening. The majority of the probe was reused with modifications to the probe tip and replacement of the three Teflon rods to a support structure that consisted of a single solid tube of machinable ceramic (Fig. 23). The ceramic tube (a) was held in place by set screws and fit over the steel shaft of the probe. The probe tip (b) was modified to have two different diameters. The section of the tip that entered the mass spectrometer's ion source was the same diameter as before, 3.81mm, with the same length. A "barrel" (c) of the tip was created that was the same diameter as the steel shaft of the probe and a set-screw mark was cut into the barrel to facilitate alignment. As in the original probe tip, a hole was drilled through the length of the tip to allow the second electrode to enter the source and was again isolated by a ceramic tube. The copper wire was attached to the tungsten rod was done by a barrel type connector. The wire was connected to the barrel of the probe tip by drilling a hole into the "barrel" of the tip and securing it to the tip with a set-screw. The modifications can be viewed as a simplification of the design and as a result it is now easier to disassemble, repair, and re-assemble.

The electronics are designed with a voltage limiter to prevent the sample wire from melting at high temperatures (≥ 1000 °C), which itself was tested by the yellow white light emitted from the sample wire. A second voltage limiter was built into the controls to allow the user to control the upper limit of heating. Finally, the electronics were constructed to allow heating rates of the sample wire to be varied from ~ 100 °C/s to ≥ 1000 °C/s. Control of the heating rate is critical because very fast heating may not allow sufficient time to produce mass spectra and very slow heating may result in sample pyrolysis rather than desorption.

High-Resolution Negative Ion Mass Spectrometry

High resolution spectra of the fragment ions were recorded using the stock JEOL EI probe and recorded in the negative mode on the JEOL 600-MS. The instrument was initially tuned using PFK and then further refined using specific calibrants for each experiment. The model compound, the alanine dimer (AA), was used because the ion intensity was strong enough to produce observable ions at higher resolution. The resolving power (R) required to determine ion elemental composition was calculated from (Eq. 11):

$$R = m / (\Delta m) \quad (\text{Eq. 11})$$

where m is the mass of the ion and Δm is the difference in mass to be resolved. A resolving power of $R = 3000$ was necessary to determine the elemental composition of amino acids and peptides studied here. High resolution settings could not be used for all

ions studied because the intensity of some ions in the negative mode were not sufficiently strong to provide an observable signal at the higher resolution.

High resolution mass spectral measurements require internal standards. PFK is typically used but there are some others whose masses are well known. Because the ions in question were of low mass and the experimental conditions were performed with low energy electrons, PFK was not used. Instead other halogen containing compounds were used to calibrate electron energy roughly and m/z for ions precisely. For fragment ion with m/z 72 from the alanine dimer the Cl_2^- ions from CCl_4 were used with nominal m/z 70, 72, and 74 that form at energy ~ 1 eV. For the ions with m/z 87 and 88 for alanine dimers, different calibration compounds were required. Several fragment ions from compounds were tested but eventually the Br^- ion, with m/z 79 and 81, from tribromoethylene and the I^- ion, m/z 127, from iodomethane were used. Both of these ions form at energies near to zero eV and require a balancing of ion signal at electron energy 1-2 eV and internal calibrant ion formation at ~ 0 eV.

Electron Monochromator

An electron-monochromator (EM) is a device designed to produce mono-energetic or near mono-energetic electron beams. The electron beam can then be focused and directed to interact with an ion beam. The process of producing mono-energetic electrons has remained basically the same since Stamatovic and Schultz made their monochromator [30, 31]. The initial electrons are generated from a heated filament and collimated. The collimated electrons enter crossed electric and magnetic fields that cause

the electrons to deflect in a plane based upon the energy of the electrons. If the magnetic and electric fields remains fixed, the potential of the filament can be scanned changing the energy of the electrons reaching the aperture in the exit collimating lenses. The collimated electrons then enter the ion source where they can interact with atoms and molecules. A schematic of the EM (Fig. 11- 13) and a more detailed description of its general characteristics were described previously[55, 56].

Electron Monochromator Time of Flight Mass Spectrometer

An electron monochromator time of flight mass spectrometer (EM-ToF-MS) employs an analyzer with which the m/z ratio is measured as a result of the time it takes the ion to travel the length of a flight tube. The EM in the EM-ToF-MS system produces negative ions as a result of the interactions of the mono-energetic electrons and the neutral molecules in the ion source. The negative ions are extracted from the ion source into the time of flight (ToF) mass analyzer, by pulsing at 80 kHz [55, 56].

A ToF operates because ions exiting the ion source have been given kinetic energy, E_k that is the product of the charge, q , and the accelerating potential, V (Eq. 12).

$$E_k = q * V \quad (\text{Eq. 12})$$

Given that kinetic energy is also the mass of the ion, m , times velocity of the ion, v , squared divided by two (Eq. 13) it is possible to solve for the mass to charge ratio (Eq. 14).

$$E_k = m * v^2 / 2 \quad (\text{Eq. 13})$$

$$m / q = 2 V / v^2 \quad (\text{Eq. 14})$$

Since velocity, v , is related to the length of the flight path, L , divided by the time it takes to travel the length of the flight path, t , (Eq. 15) it is possible to relate the mass to charge ratio to flight time (Eq. 16).

$$v = L / t \quad (\text{Eq. 15})$$

$$m / q = 2 V * t^2 / L^2 \quad (\text{Eq. 16})$$

If the accelerating potential and length of the flight path are fixed, then the mass to charge ($m/q = m/z$) ratio is directly proportional to the square of the flight time.

The EM-ToF-MS for resonance electron capture experiments has an orthogonal reflectron ToF. The orthogonal geometry improves the signal to noise (S/N) of the mass analyzer by performing the mass analysis perpendicular to the axis of ion extraction from the ion source. The orthogonal instrument geometry prevents interference, or dark current, from neutral species traveling in a straight line that have entered the field free region or in the case of electron capture, ions that have undergone autodetachment or were generated as neutral loss species.

The reflectron serves to improve mass resolution during the analysis by ToF by focusing ions with a Gaussian distribution of energies but a single mass to charge. The exact workings of the reflectron are beyond the scope of this work but a simple explanation of the necessity for the reflectron is useful. Ions exit the ion source and enter the accelerating region of the ToF with a spread of energies which must be corrected in order to be able to distinguish ions of very small mass difference. In the EM-ToF-MS, possible sources of ion energy spread are the spread of energy in the electron beam and the internal energy transferred to the neutral molecule from heating to volatilize the sample.

The combined characteristics of a recently described EM-ToF-MS [55, 56] allow for very rapid scanning of the electron energy and simultaneous acquisition of mass spectra according to their m/z at each electron energy. The individual electron energy mass spectra are combined to generate a 3-D REC-MS. The electron energy for effective yield peaks are assigned based on the intensity maxima for all peaks for each ion.

Chemical Modification of Amino Acids and Peptides

Methyl Esters

Diazomethane

The use of diazomethane is advantageous as it provides for the cleanest methyl esterification reaction due to the reagent being able to literally be blown off after completion of the reaction [58]. The drawbacks of diazomethane are its toxicity, explosive potential and its indiscriminate reactivity. The indiscriminate reactivity of diazomethane was the reason that it was not used to make the final products.

Fischer Esterification

The Fischer esterification method can be either acid or base catalyzed [58, 59]. The reaction conditions involve refluxing the peptide or amino acid in the alcohol to be used to esterify the carboxylic acid in the presence of an acid catalyst, usually HCl. The

resulting product is the ester hydrochloride salt of the peptide or amino acid. The advantage of HCl catalyzed Fischer esterification in REC-MS is that the HCl provides an internal energy calibrant because the effective yield curve of Cl^- from the capture of electrons by HCl is well established. The drawback of Fischer esterification is that the conditions for catalysis of the carboxylic acid also activate the amide bond of the peptide leading to cleavage of the peptide. In the case of homopolymers, like peptides containing only one amino acid, the purification of truncated products is difficult because of their similarity in polarity and pKa and therefore is why Fischer esterification was not able to be used. If the peptides being derivatized were not homopolymers the possibility of using this method would be viable.

Iodomethane

Iodomethane is a methylation reagent that undergoes nucleophilic displacement of the iodine. Iodomethane has the advantages of being easy to clean up which is achieved simply by adding a quenching reagent and removing the quenching agent at reduced pressure. The drawback of iodomethane is that it is susceptible to nucleophilic attack by the N-terminal amine group under basic conditions. N-terminal nucleophilic attack can result in formation of a quaternary amine which is positively charged. The reaction is favored under basic conditions and can be catalyzed by sodium cyanide. Iodomethane was not used because the side product containing a quaternary amine could not be minimized enough to produce the amount of sample needed. Iodomethane could be used if the N-terminus of a peptide was protected, for example by an N-Acetyl group.

Carbodiimide

Carbodiimide reagents are standard for the activation of carboxylic acids to nucleophilic attack [59]. The most important usage of carbodiimides is to form amides in peptide chemistry. The primary advantage of carbodiimide reagents is the specificity for carboxylic acids in the presence of amides. A second advantage of carbodiimide reagents is the susceptibility of the carboxylic acid/carbodiimide intermediate to nucleophilic attack allowing for a variety of possible final products. The reaction can be catalyzed by nucleophilic compounds such as 4-dimethyl amino pyridine (DMAP).

The most prominent drawback of using carbodiimides is the production of urea as a byproduct. Urea is notorious for being very difficult to remove from the reaction mixture. Because of the difficulty of removing the urea byproduct, two solutions have been developed. First, an immobilization procedure can be used on the substrate or peptide so that the urea can be washed away [59]. A resin to immobilize the peptide being synthesized is an example of this strategy. Alternately, the carbodiimide can be immobilized on either a resin [60] or on silica gel [61]. The immobilized carbodiimide reagent can be washed and filtered in order to isolate the product. The reactions that were used in this study were using SiliaBond Carbodiimide from Silicycle (Quebec City, Quebec, Canada) and will be described below.

N-terminus Derivatization

Fmoc

9-Fluorenyl methoxy carbonyl (Fmoc) is a standard protecting group for amines and the most favored for the N-terminus in peptide synthesis [59]. The popularity of the Fmoc protecting group is due to the ease of introduction onto the N-terminus, the simplicity of the procedure, and the overall yield of product obtained upon cleavage. Fmoc can be introduced by a variety of reagents with two of the most popular being Fmoc-succinimide (Fmoc-OSu) and Fmoc chloride (Fmoc-Cl). Fmoc-OSu is popular because it prevents dimerization of the compound being protected. Fmoc-Cl has the advantage of providing a simpler clean up procedure. Whichever reagent is used, basic reaction conditions are used in order to allow for nucleophilic attack of the Fmoc carbonyl by the amine to occur.

Fmoc deprotection is carried out under basic conditions. The typical reagents are 20% piperidine in DMF because most peptides are soluble in DMF. The base deprotects by removing a proton at the 9 position of the fluorene ring which leads to the formation of a double bond with the methoxy carbon and releases the tricyclic aromatic ring compound, CO₂, and a free amine with simultaneous regeneration of the neutral piperidine base (Fig. 24).

Peptide Synthesis

Solid phase peptide synthesis (SPPS) is a technique for making pure synthetic peptides by immobilizing the peptides on a resin [59]. SPPS works by using C-terminal

bound peptides and a repeated sequence of N-terminal peptide deprotection and N-terminally protected amino acid coupling (Fig. 25). The coupling of amino acids is accomplished using carbodiimides or other carboxylic acid activating reagents. The protection of the N-terminus can be achieved by either Fmoc, as described above, or by t-butyl carbamate (Boc) chemistry but Fmoc is more prominently used. In either case following deprotection, the side product is washed away with solvent. In the case of Fmoc chemistry, the solvent is usually DMF.

Cleavage of the peptide from the resin is typically carried out to produce the free carboxylic acid. The most common procedure is to use orthogonal protection schemes so that cleavage from the resin occurs under different conditions than that involved in N-terminal deprotection. In the case of Fmoc, the cleavage condition from the resin is mildly acidic.

However some resins can be used to cleave and produce different C-terminal modifications which involves amidation or methyl ester formation. By coupling the initial amino acid to a 4-hydroxymethyl benzoic acid (HMBA) resin [60] the final product can be cleaved to produce a variety of products including the methyl esters.

Compounds

All peptides, amino acids, and amino acid derivatives were purchased from Sigma/Aldrich (Milwaukee, WI) with purity of 99% unless otherwise stated. N-acetyl alanine and N-acetyl Ala-Ala were purchased from Research Plus (NJ). The immobilized carbodiimide was purchased from Silicycle (Quebec City, Quebec, Canada) under the

trade name SiliaBond Carbodiimide with a minimum loading of 0.88 mmol/g. All other chemicals were purchased from VWR except for Fmoc-Cl and piperidine which were purchased from Sigma/Aldrich.

Ala-Ala-Ala-OMe Synthesis

Ala-Ala-Ala (1 eq, 49.4 mg) was suspended in 4 mL of DMF and 4 mL of double distilled (dd) H₂O to form a clear solution. Fmoc-Cl (4 eq, 0.2303 g) was added and stirred. After 10 minutes the solution was clear and a small amount of Na₂CO₃ was added and the pH tested which was pH ~10. The reaction was stirred overnight and analyzed by LC-MS for product. The crude product was lyophilized. The dried product was resuspended in DCM (2.2 mL) and MeOH (0.4 mL) per the requirement for 1 g / 5 mL liquid for using immobilized carbodiimide. The immobilized carbodiimide (4 eq, 0.4928 g) was added to the mixture and stirred for 2 hrs. The reaction was monitored by LC-MS. Immobilized carbodiimide was removed by filtration and washed with DCM which in turn was removed under reduced pressure. The Fmoc protecting group was removed by 4 mL of 20% piperidine in DMF for 30 minutes. The mixture was freeze dried again and the product removed by aqueous wash of the solid which was then analyzed by LC-MS. The aqueous product was freeze dried and washed with hexane and used for REC-MS experiments.

Computational Studies

Computations were carried out on the alanine dimer with a C-terminal methyl amide to determine the possible effects of the conformation of a model compound on the vertical electron attachment energy (VEAE) [62]. The model was constructed using Chem Draw 3D, the geometry optimized, and the coordinate system redefined to allow for variation of the phi and psi angles by scanning two dihedral angles and fixing all other bond angles and lengths. The calculations on phi and psi angles were performed to test the possible effects of peptide conformation on VEAE.

The VEAE was calculated as the energy difference between the neutral singlet of the model compound and the anion doublet[28]. All calculations were performed using unrestricted methods because the unpaired electron for the radical anion doublet requires unrestricted methods when using the Gaussian 2003 computational suite. Calculations were performed on personal computers with Windows operating systems. Test calculations were performed on the effects of electron correlation on the energies and on the time required for the various computational methods (Table 1). Two potential energy scans or surfaces based on phi and psi angles were calculated using UHF/6-31++G** and UHF/aug-cc-pVDZ.

The basis sets were selected for fairly high level calculations with diffuse and polarization functions. The basis set, 6-31++G** is a split valence type where six primitive Gaussians are used to calculate the atomic orbital basis function. The numbers 3 and 1 refer to the number of primitive Gaussians used to calculate the valence orbitals for the heavy atoms and hydrogen atoms respectively. The “++” indicates that diffuse functions will be added to both heavy atoms and hydrogen atoms and “**” indicates that polarization functions are added to both heavy and hydrogen atoms. Aug-cc-pVDZ is a

double zeta basis set which means that each atomic orbital is defined by two functions. The “aug” means “augmented” and that this basis set includes diffuse functions. The “cc-p” stands for “correlation consistent polarized” and denotes the inclusion of polarization functions in the basis set.

A further reason that these basis sets were used is that it was computationally feasible to compute the large number of structures necessary for a PES on phi and psi angles. Aug-ccp-VDZ was specifically used to allow correlation with the computational results of the Simons group that used a similar alanine dimer as a model for calculations[42]. The 6-31++G** calculations were performed as a test case and to assure that the phi psi potential energy surface was calculated if the aug-ccp-VDZ calculations were to time intensive.

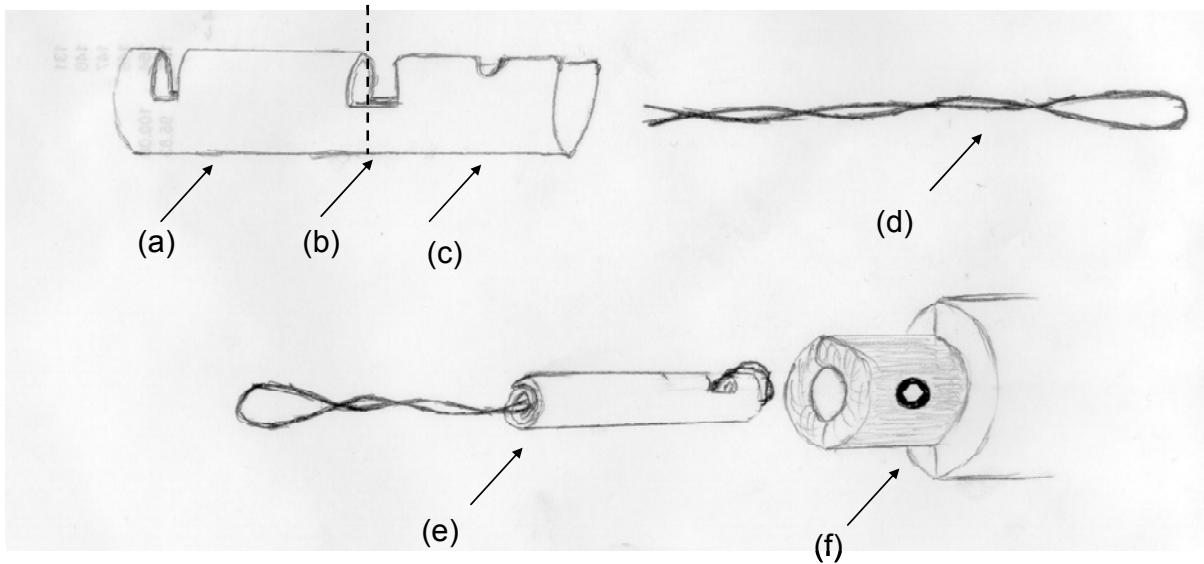


Figure 21. Schematic of the parts of the wire in-beam probe where (a) is the wire to pin connector , (b) is the point where the wire to pin connector is cut off, (c) is the portion of the wire to pin connector not used and (d) is the filament wire twisted around itself to form a loop. The wire to pin connector is compressed into a support for the filament wire loop (e) that fits into the capillary holder of the stock JEOL probe (f).

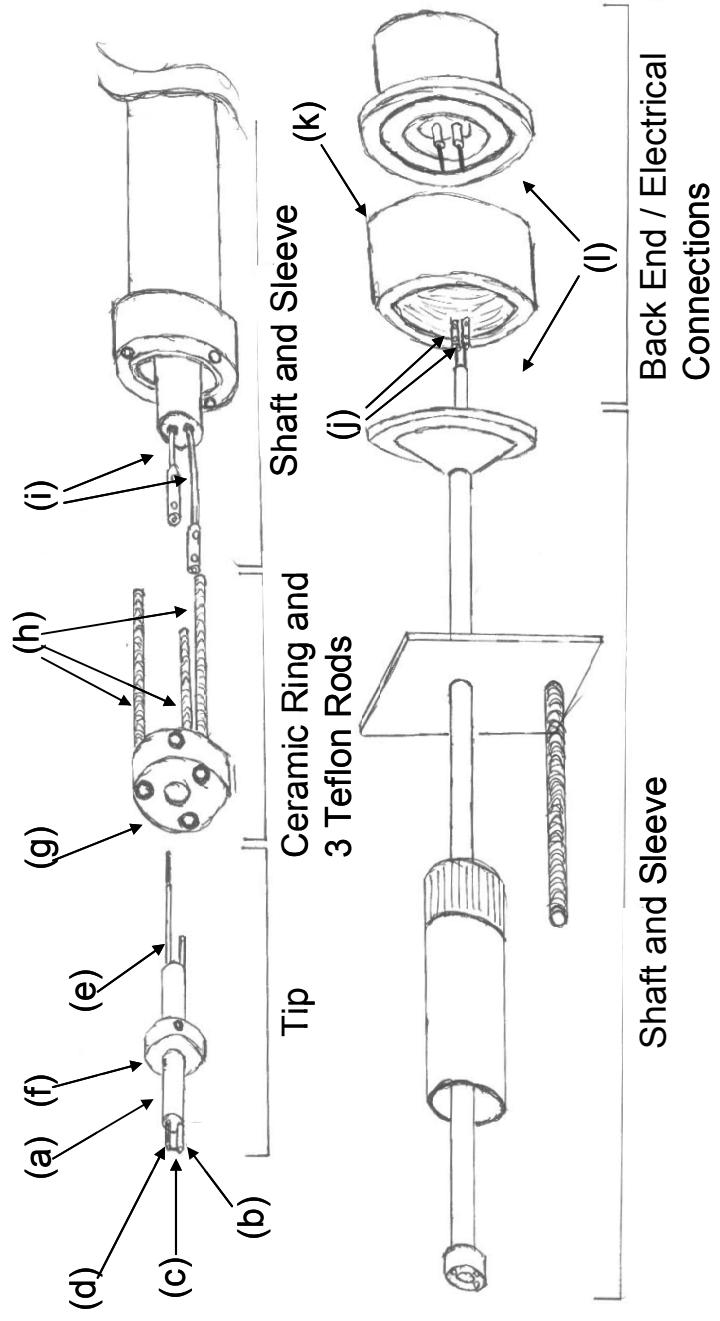


Figure 22. Original schematic of the Flash volatilization probe with (a) the tip, (b) the electrical contact post, (c) the filament wire, (d) second electrical contact rod, (e) a ceramic insulator, (f) the ceramic ring with set screw, (g) ceramic support ring, (h) Teflon rods, (i) copper wires, (j) barrel electrical connectors, (k) a nylon spacer, and (l) an electrical feed through.

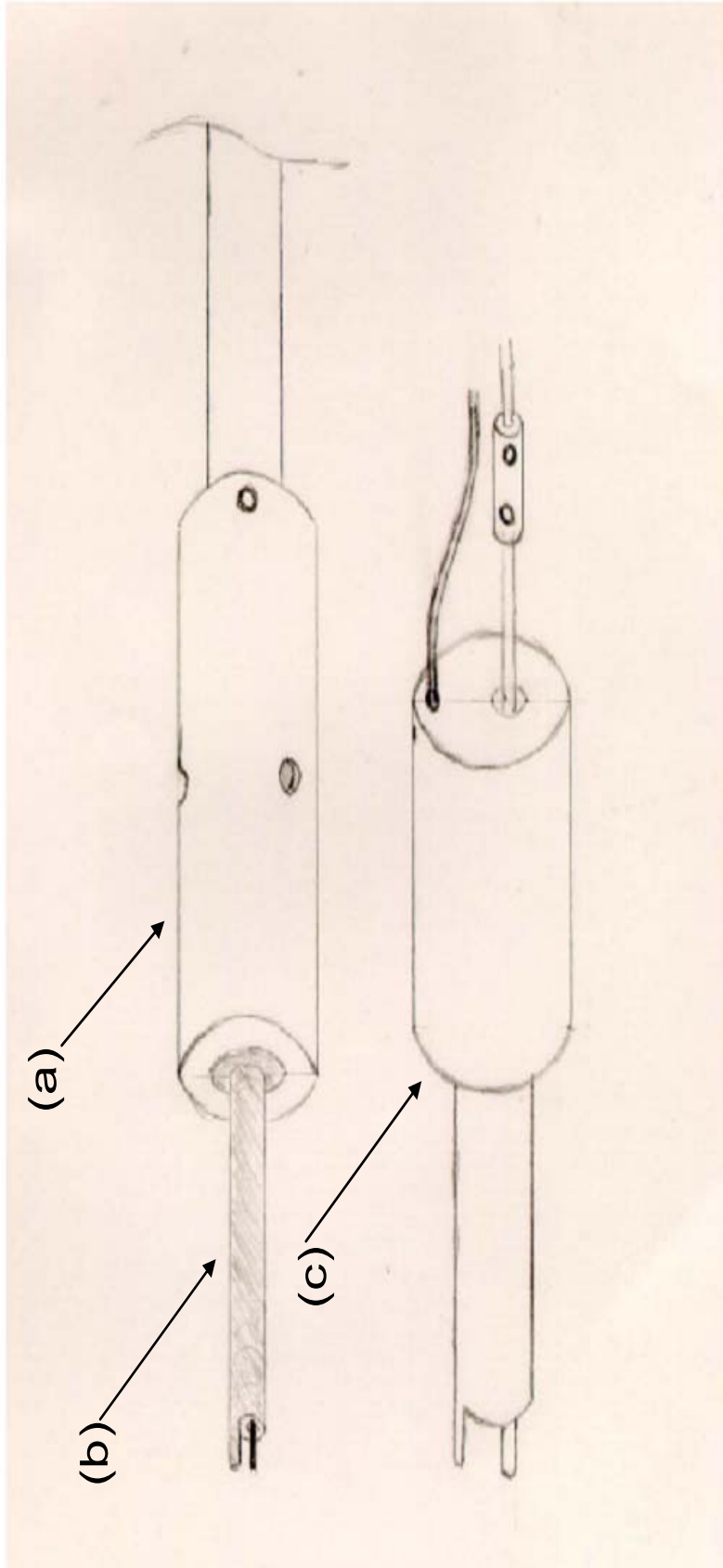


Figure 23. Schematic of the final probe tip used as the flash volatilization probe. (a) Ceramic tube, (b) probe tip, and (c) the "barrel" of the probe tip.

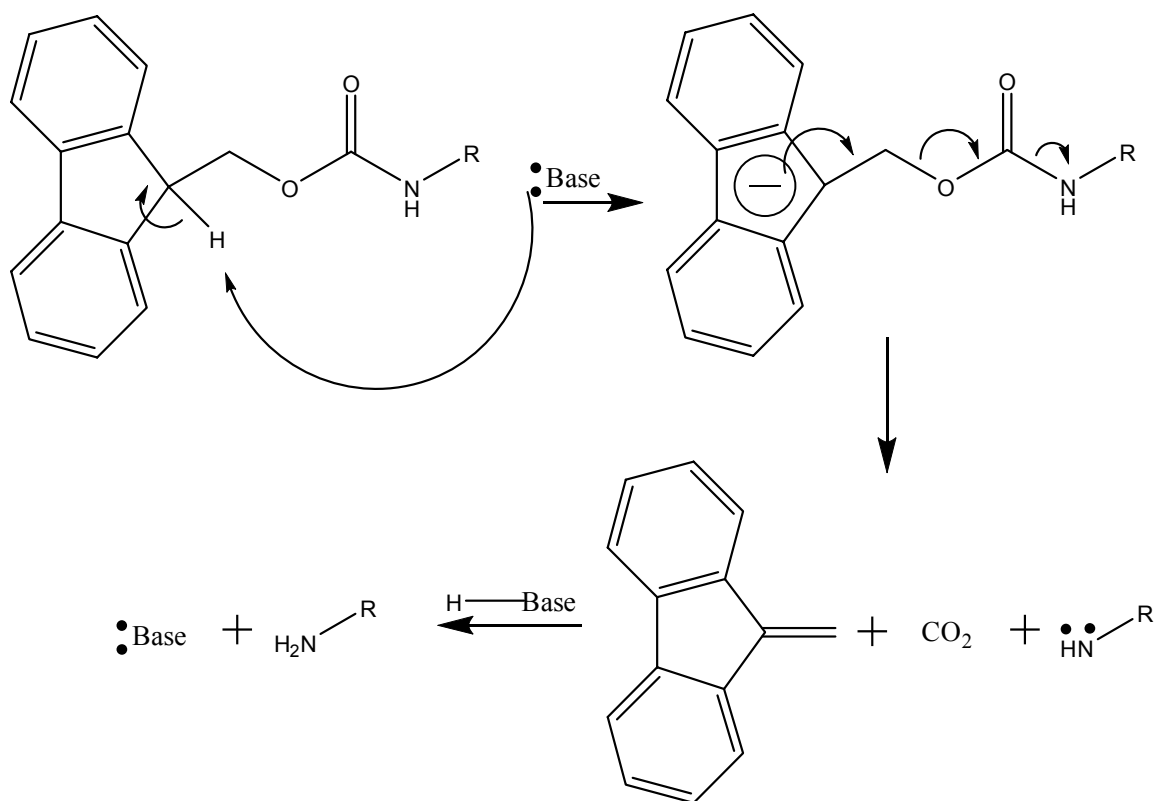


Figure 24. Mechanism of Fmoc deprotection from an amino acid or peptide with a generic base as the catalyst.

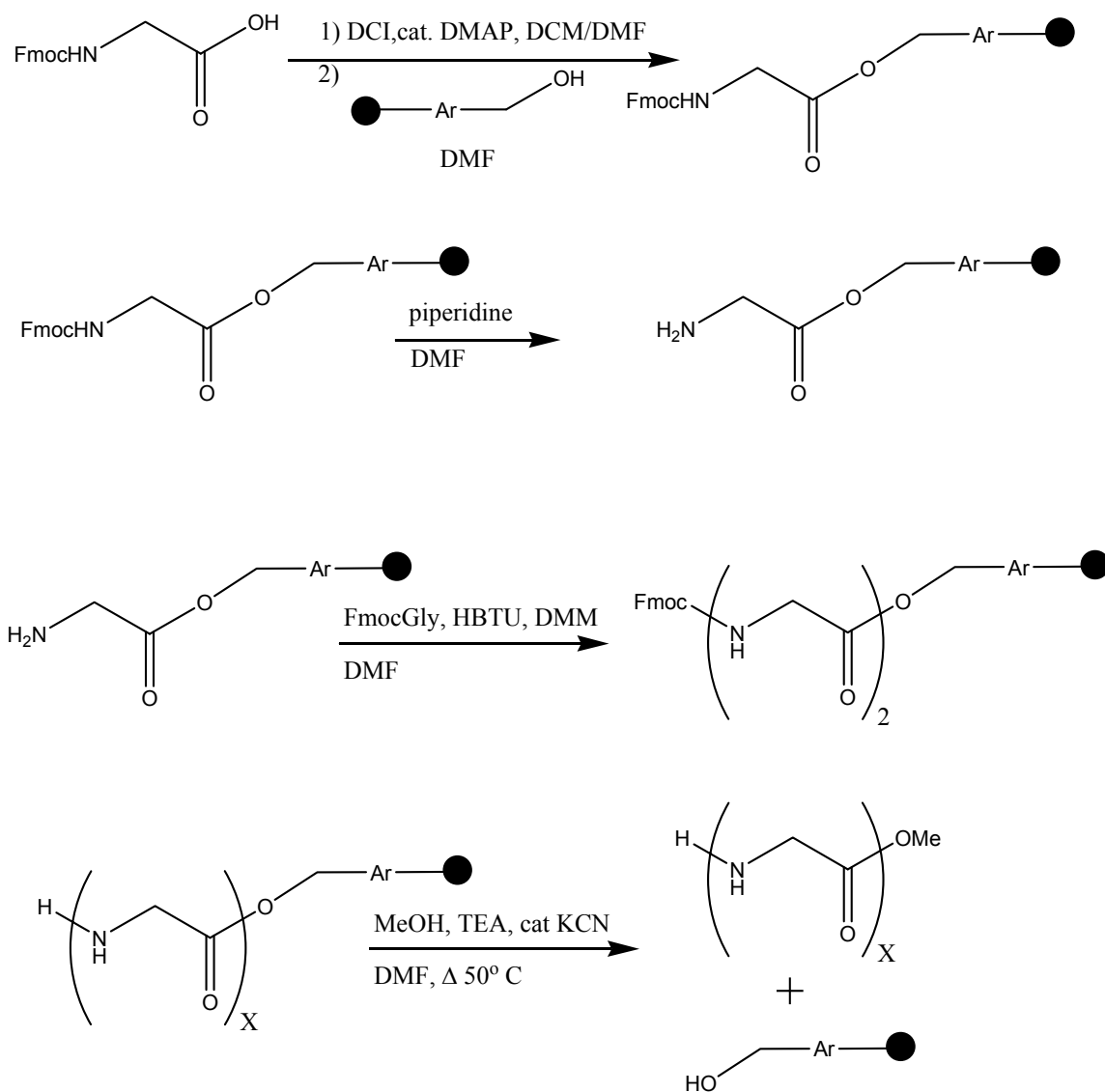


Figure 25. Mechanism of solid phase peptide synthesis (SPPS) for making a dimer of glycine with a methyl ester on the C-terminus using HMBA resin from Nova Biochem.

Table 1. Comparison of electron correlation and basis set on vertical electron attachment energy (VEAE or VT) and time to complete the calculation. “geo” indicates that a optimum geometry was calculated using the described method to determine the VEAE. The UMP4 calculations used the UMP2 because it was impossible to calculate the geometry at the UMP4 level. All calculations were performed using Gaussian 03 on a dual processor 1.0 GHz computer with 1.5 GB of RAM and a Windows 2000 operating system.

Electron Correlation and Basis Set	Energy diff (eV)	Total time for Calculation (min)
UHF 6-31 ** G ++ VT	0.863	9.03
UHF 6-31 ** G ++ geo VT	0.877	318.67
UB3LYP 6-31 ** G ++ VT	0.408	23.57
UB3LYP 6-31 ** G ++ geo VT	0.411	119.83
UMP2 6-31 ** G ++ VT	0.682	29.60
UMP2 6-31 ** G ++ geo VT	0.681	229.87
UMP4 6-31 ** G ++ (MP2 geo) VT	0.858	1020.60

Electron Correlation and Basis Set	Energy (hartrees)	Time for cal
HF 6-31 G	-246.8906371	0:00:15
UHF 6-31 ** G ++ (neu)	-247.0222381	0:03:11
UHF 6-31 ** G ++ (anion)	-246.9905098	0:08:51
UHF 6-31 ** G ++ (neu) geo	-247.0273031	5:09:43
UHF 6-31 ** G ++ (anion) geo	-246.9950797	0:08:57
UB3LYP 6-31 ** G ++ (neu)	-248.5457238	0:07:14
UB3LYP 6-31 ** G ++ (anion)	-248.530747	0:16:20
UB3LYP 6-31 ** G ++ (neu) geo	-248.5488348	1:44:23
UB3LYP 6-31 ** G ++ (anion) geo	-248.5337226	0:15:27
UMP2 6-31 ** G ++ (neu)	-247.8004713	0:10:43
UMP2 6-31 ** G ++ (anion)	-247.7754102	0:18:53
UMP2 6-31 ** G ++ (neu) geo	-247.8049605	3:29:59
UMP2 6-31 ** G ++ (anion) geo	-247.7799184	0:19:53
UMP4 6-31 ** G ++ (neu) MP2 geo	-247.0247762	7:41:25
UMP4 6-31 ** G ++ (anion)	-246.9932628	9:19:11

Results

Introduction

The data presented here show that low energy electrons and neutral amino acids and peptides interact to form negative fragment ions that can be observed by mass spectrometry. The high resolution experiments determine the exact empirical formula of the negative fragment ions from the alanine dimer to assign the ions formed. The RECM-MS experiments provide effective yield curves for formation of negative fragment ions thereby comparing electron energy and formation of negative ions. The calculation of potential energy surfaces attempts to determine the effect of peptide conformation on vertical electron attachment energy.

Negative Ion Energy Calibrated Mass Spectrometry

In-Beam 2D Mass Spectrometry

Energy calibrated in-beam resonance electron capture mass spectra were recorded for the following compounds: alanine dimer, methionine enkephalin, YFF amide, substance P, and cystine dimethyl ester diHCl. These compounds were chosen because they were available in relatively large amounts commercially (> 25 mg) for reasonable prices and representative of all the compounds tested. Furthermore, substance P is a well known mass spectrometric standard and has been extensively studied by desorption techniques.

The low energy calibrated mass spectrum, ~ 1 eV, for alanine dimer shows four main fragmentation channels (Fig. 26). The most intense ion observed was the $(M-H)^-$ ion followed by the ion with m/z 72 that could be either a b or z-1 ion. The ions with m/z 87 and 88 were also observed along with several weaker fragment ions and can be c or y ions respectively. The relatively “high” energy mass spectrum (~ 6 eV) shows a number of different fragment ions (Fig. 27) with m/z 87 as the base peak. The $(M-H)^-$, m/z 72, and m/z 115 ions were also observed along with other weaker fragments at “high” energy.

The peptide, methionine enkephalin (MW = 573, YGGFM) shows many fragmentation channels including one that produces a base peak with m/z 352 (Fig. 28). All possible y ions with m/z 148, 295, 352, and 409 and z-1 ions with m/z 132, 279, 336, and 393 are also observed. Finally, a weak $(M-H)^-$ ion is observed.

Methionine enkephalin is a typical example whose z-1 ion series is observed for all possible cleavages (Fig. 28). However, the base peak for methionine enkephalin is formed at m/z 352 which is the same mass as that for the y_3 ion. In fact, the entire y series is also observed, but the reason that they are observed as the y ions and not the y-1 ions, as in the case of the z ions that are observed as z-1 ions, is not readily apparent. There exists the possibility of forming a stable negative ion by rearrangement of the y ion. However, the presence of the y ion series suggests that the peptides may be breaking down due to heating which is necessary for volatilizing them. If y ions are due to thermal breakdown, then it is not clear why the b ions are not observed. The thermal fragmentation of the peptides may lead to formation of a positive N-terminal fragment and a negative C-terminal fragment. The C- termini are able to form carboxylate negative

ions which would explain why the y ions are observed. Since the b ions are associated with the N-termini and do not have the carboxylate group to form a stable negative ion, they are not observed. The smaller peptides like YFF amide (Fig. 29) show lower intensity y ions which gives some credence to the possible source of these y ions as products from pyrolysis. Smaller peptides need less heat to volatilize and therefore are less likely to undergo pyrolysis.

The peptide, YFF amide (MW = 474, YFF-NH₂) is unique in this study because it is one of two peptides without a carboxylic acid or ester functionality on the C-terminus. The inclusion of other C-terminal amide groups is important because it expands the types of compounds studied in order to understand the effects of different functional groups on REC processes. The other C terminal amide compound studied is substance P. The base peak is the c₂ ion with m/z 336 (Fig. 29). In the case of the in-beam experiments, this is the exception to the rule of seeing z-1 fragment ions as intense fragments which may be due to the fact that the C-terminus is an amide group. However, this was not the case for substance P which also has a C-terminal amide and has z-1 ions. Furthermore, all of the peptides studied had additional fragment ions that were not explained by backbone cleavages. The other ions that are observed for YFF amide are (M-H)⁻ and c₁ and weak z₁-1 and z₂-1 ions.

Substance P (MW = 1347, RPKPQQFFGLM-NH₂) shows the fragmentation channels associated with z_n-1 ions for n= 2 to 7 with the base peak of z₅-1 ion (Fig. 30). The z-1 series for substance P is the most complete z-1 series in larger peptides (> 8 residues) and includes the largest assigned fragment ion in these studies for z₇-1 with m/z

851. There are other fragmentation channels not identified with peptide backbone cleavages.

Another type of amino acid compound was analyzed by electron energy controlled negative ion mass spectrometry to explore the possibility of studying other compounds that undergo electron capture dissociation. Cystine dimethyl ester diHCl is a small disulfide bonded dimer. The base peak in the mass spectrum results from the cleavage of the disulfide bond to form an $(M/2)^-$ ion (Fig. 31). Another unique feature was the observation of the M^- ion at m/z 268 and a strong signal at m/z 116.

The cystine dimethyl ester has a disulfide bond as apposed to the peptide bonds in their structures. There are two important differences observed in the negative ion mass spectrum (Fig. 31). First, there is a peak for the molecular ion, M^- , which is not observed in any other peptide or amino acid. Second, the formation of a $(M/2)^-$ ion occurs by cleavage of the disulfide bond. The cleavage of the disulfide bond is an expected result because cleavage of the disulfide bonds have been observed previously in ECD experiments in proteins and peptides. The observation of the $(M/2)^-$ ion is proof of principle that disulfide bond cleavage can be studied by REC-MS and gives a preliminary estimate of the electron energy for cleavage of the disulfide bond of ~ 1 eV.

The experimental results from the energy calibrated, low energy electron IB experiments provide proof of principle that negative ions can be observed from the interaction of low energy electrons and neutral peptides. The ions types observed are tentatively z-1, c and y series ions and $(M-H)^-$ ions for smaller peptides. The results will be discussed in more detail below.

Flash Volatilization Mass Spectrometry

The flash volatilization probe was tested with several compounds including methionine enkephalin but the results observed were limited. Unfortunately the high voltage in the ion source caused electrical shocks to the operators and these experiments on flash volatilization had to be terminated.

On the basis of what has been learned, with the in-beam methods discussed above, the flash volatilization probe should be ideal for REC studies on peptides once the problems with electroshocks have been solved. There are two solutions to this problem that could be utilized given more resources. First, purchase a probe from the instrument manufacturer that has characteristics needed for flash volatilization. Second, redesign the probe to use a smaller diameter of shaft rod that will in turn allow for a smaller ceramic tube. Having a smaller ceramic tube would prevent the electroshocks because the electrical contact is made within the vacuum lock system and the ceramic tube is nearly the maximum diameter that can be inserted via the vacuum lock.

Negative Ion High Resolution Energy Calibrated Mass Spectrometry

Ala-Ala

The negative ions from high resolution MS experiments were recorded for ions with m/z 72 and 87 from the alanine dimer at low electron energy. The exact mass 72.02100 Th was recorded with an error of -1.8 ppm for the empirical formula of $C_3O_2H_4$

whose calculated mass is 72.02113. This is the exact mass for the z-1 ion (Fig. 32). The m/z 87 ion was observed with an exact mass of 87.05613 Th which amounts to an error of 3.3 ppm for the empirical formula $C_3N_2OH_7$ whose calculated mass is 87.05585. $C_3N_2OH_7$ is the empirical formula of the c ion. Ppm error is calculated by the difference in mass between the measured mass and the mass calculated for the empirical formula divided by the measured mass and this quantity multiplied by 10^6 (Eq. 17).

$$\text{ppm} = 10^6 * ((\text{Mass}_{\text{Measured}} - \text{Mass}_{\text{Calculated}})/\text{Mass}_{\text{Measured}}) \quad (\text{Eq. 17})$$

The high resolution experimental data demonstrate unambiguously that the fragment negative ions are z-1 and c ions. Observations of z-1 and c ions by resonance electron capture of low energy electrons means that capture of an electron by a neutral peptide produces fragment ions that come from the cleavage of the same peptide backbone bond as ECD. Furthermore these fragments occur at electron energies of approximately 1 eV.

Resonance Electron Capture – Mass Spectrometry

Esters of Amino Acids

Glycine

The effective yield curves of glycine show a change in the maxima for the formation of the carboxylate anion (Fig. 33). The formation of the carboxylate anion from underivatized glycine is the dominant ion formed and has an effective yield

maximum at 1.28 eV[50]. The glycine methyl ester has also been reported by Vasil'ev et al and it has a slightly higher effective yield maximum in the low energy range for the carboxylate anion at 1.3 eV [50]. For both glycine and its methyl ester there are effective yield peaks at 5.15 eV and 5 eV respectively. The remaining ions reported were concluded to be fairly similar with the exception of the relative intensity of the O^- ion, OH^- for glycine and OMe^- for glycine methyl ester. However, even with the difference in relative intensities for these ions, the effective yield maxima are quite close, viz 6 eV for glycine OH^- ion and 5.45 for the glycine methyl ester OMe^- ion.

Dramatic differences in the number of resonance states, in relative intensity and resonance energies are observed for glycine, and the methyl, ethyl, isopropyl, and t-butyl esters of glycine for the production of the carboxylate anion $(\text{M-X})^-$, the O^- ions, $(\text{M-R})^-$ ions, and NH_2/O^- ions (Table 2) [50]. Comparison of the effective yields curves (Fig. 33 - 34) indicates that replacement of hydrogens on the esterifying alkyl groups with a carbon atom, results in a shift in the effective yield maxima. In the case of glycine and its methyl ester the global maxima in the effective yield curve are at 1.2 - 1.5 eV whereas for ethyl, isopropyl, and t-butyl esters the lowest effective yield maxima are higher in energy at 3.6 - 3.7 eV. For the ethyl and t-butyl esters the global maxima of the carboxylate anion effective yield curves are at 9.5 eV and 9.6 eV respectively. The three highest maxima for the ethyl and t-butyl esters show good overall agreement within experimental error. The agreement can be attributed largely to the width of the electron beam of ~ 200 meV. However, the isopropyl ester carboxylate anion has a global effective yield maximum at 3.6 eV and does not have a maximum at ~ 5.5 eV. The final two maxima at 8.4 eV and 9.3 eV are near in energy to the ~ 9.5 eV maximum for the ethyl and t-butyl

esters. The final variation of the glycine ethyl ester carboxylate anion is the presence of a maximum at 1.2 eV.

In contrast to the formation of the carboxylate anion from glycine and its esters, the cleavage of the adjacent carbon-oxygen bond between the carbonyl carbon and the ester oxygen is fairly similar in energy from one compound to another (Fig. 35 - 36). The effective yield maxima for these ions, i.e. $-OX$ ions, are within 0.55 eV for all those studied suggesting a similar origin for these ions.

Alanine

The effective yield curves for alanine and the methyl ester of alanine have been previously reported and are included here for comparison [50]. Only the ethyl and t-butyl esters were available for study at the time the spectra reported here were recorded and therefore there is no data for the isopropyl ester of alanine. The formation of the carboxylate anion (Fig. 37 - 38) is similar to glycine and the glycine esters (Fig. 39 - 43). Alanine and the alanine methyl ester both have global, or the most intense, effective yield maximum at 1.2 eV for the carboxylate anion. The ethyl ester and t-butyl ester of alanine have global maxima at 9.4 eV for the carboxylate anion but then also have a second maximum at 3.5 and 3.7 eV respectively. There is a shoulder in both the ethyl and t-butyl effective yield curves between 5 and 6 eV but it is not sufficiently resolved to be called a maximum. Neither the ethyl nor t-butyl esters of alanine have a maximum at or near the energy of the effective yield maximum of alanine, at 1.2 eV, or the methyl ester of alanine, at 1.2 eV, for the carboxylate ion.

The adjacent cleavage, forming the $-OX$ ion, again shows insensitivity to esterification as there is only a difference of 0.3 eV between their effective yield maxima (Fig. 44 - 45). The alanine and alanine esters' effective yield maxima for the $-OX$ ion are all close in energy to those of glycine and its esters (Fig. 46 - 50). There are two other maxima that have been reported previously for production of the $-OX$ ion; at 10 eV from alanine and 3.1 eV for alanine methyl ester. There are no comparable effective yield maxima in either of the other esters studied.

The m/z 16 ion has an effective yield maximum at 6.6 eV for alanine and alanine methyl ester and in addition there is an effective yield curve from 7 - 11 eV for alanine methyl ester. The alanine ethyl ester has maxima at 6.6 eV and 9.5 eV but the alanine *t*-butyl ester has a single maximum at 0.8 eV. A broad hump over the range 5 eV to 11 eV appears to be noise although it could be a resonance, too.

Phenylalanine

The formation of the carboxylate anion results from a resonance with maxima of 1.16 eV and 1.2 eV for phenylalanine and the phenylalanine methyl ester respectively. There is an additional effective yield maximum in the range 9 - 11 eV (Fig. 51 - 52). The ethyl ester of phenylalanine has a global effective yield maximum at 3.3 eV and another peak at 9.2 eV for formation of the carboxylate anion. The carboxylate anion arising from the isopropyl ester appears from a global maximum at 3.3 eV and two more maxima at 1.3 eV and 8.2 eV. The *t*-butyl ester of phenylalanine has maxima at 0.8, 3.5, and 9.2 eV.

The OX^- anions were formed with maxima at 6 eV for phenylalanine, 6.65 eV for the methyl ester, 6 eV for the ethyl ester, and 6 eV for the isopropyl ester (Fig. 53). However, the t-butyl has anomalous maxima. These are at 0.7 eV, 7.9 eV and 8.8 eV.

Complementary ions $(\text{M-R})^-$ and R^- were generally observed with the one exception of the $(\text{M-R})^-$ ion for the isopropyl ester of phenylalanine. Phenylalanine has an effective yield maximum for the $(\text{M-R})^-$ at 1.45 eV. The esters show a small energy spread with $(\text{M-R})^-$ ion effective yield maxima for the methyl ester at 1.7 eV, the ethyl ester at 1.5 eV, and the t-butyl ester at 1.9 eV. The methyl ester of phenylalanine has an additional peak at 6.8 eV but it has a lower relative intensity of 6% compared to the peak at 1.7 eV with a relative intensity of 20%. In the case of R^- all phenylalanine compounds have effective yield peaks between 6 and 6.5 eV (Fig. 54). Both phenylalanine and the phenylalanine methyl ester have an additional peak at lower energy that is 1.4 eV and 1.55 eV respectively with relative intensities of 1.8% and 4 % respectively. The t-butyl ester of phenylalanine has an additional effective yield peak at 8.4 eV.

Finally, the ion with m/z 16 which could be due to O^- or NH_2^- , generally has effective yield maxima for phenylalanine compounds between 6 and 6.6 eV; although the t-butyl ester has two additional peaks at 0.7 eV and 9.4 eV (Fig. 49 - 50). The source of the peak with a maximum at 0.7 eV will be discussed below.

Combined Ester Results

The carboxylate anion is the most readily apparent stable negative ion for the underivatized amino acids. The ubiquity and intensities of these ions are experimentally

born out by the results presented here and those reported previously[45-48, 50]. If one momentarily ignores the resonances associated with methyl esters, the other esters show a consistent series of effective yield maxima in two ranges, 3.3 - 3.7 eV and 8.2 - 9.6 eV. The formation of effective yield maxima in the range 1.2 - 1.5 eV observed for the glycine ethyl ester and phenylalanine isopropyl ester (Fig. 41), seem to be a contribution from the underivatized amino acids. Therefore it is surprising that the maximum is not present in the spectra of other esters because complete derivatization is unlikely to have occurred even though all compounds have a stated purity of 99%. The reason these ions were not observed in all compounds, is that the rate of heating for the compounds may allow for more selective volatilization of the ester and not for the underivatized amino acid. Furthermore, the peak observed at 0.7 - 0.8 eV for several fragment ion effective yield curves such as the t-butyl ester of phenylalanine, is most likely an artifact of background noise due to the intense signal of Cl⁻ from HCl which has a well know maximum at 0.8 eV. HCl is in the sample because the compounds tested were the HCl salts of the amino acid esters as these commercially obtained esters were likely produced by Fischer esterification. By subtracting background spectra it is possible to minimize the presence of these effective yield peaks and conclusively assign them to Cl⁻ background noise.

The origin of the resonance leading to the effective yield maxima 3.3 - 3.7 eV for the carboxylate anions from the ethyl, isopropyl, and t-butyl esters have not been assigned previously. There are two possible explanations for the aforementioned peaks. First, the peaks arise from the π^* orbitals of the carboxylate group but have a higher energy requirement for cleavage to form the carboxylate anion than the underivatized

amino acids and the methyl esters and therefore are not observed at lower electron energies. The ETS spectra reported by Aflatooni and co-workers suggests that this would be on the extreme high energy edge of the π^* orbital [12]. The possibility of the high energy edge leading to fragmentation would be in contrast to typical effective yield maxima that are generally on the low energy side of resonances because of competition with autodetachment[19]. A second possibility is that these peaks arise as Feshbach resonances from singlet-triplet state transitions. Singlet-triplet transitions are typically lower in energy than singlet-singlet excited state transitions and would be likely candidates as the parent states for the peaks 3.3 - 3.7 eV.

The relative intensity data show that (Table 2) five compounds have as the dominant ion, i.e. the ion with the strongest intensity other than Cl^- , the one with m/z 46. The ion with m/z 46 is a decomposition product that has been observed in all of the amino acids and esters studied [50]. Correction of the relative intensity data to a non-decomposition product leads to a base peak assignment of one of the effective yield maxima in one of the five ions reported except for the t-butyl ester of phenylalanine where the ion with m/z 45 is the maximum ion (Table 3). In the case of t-butyl phenylalanine the effective yield peak at 9.2 eV has relative intensity of 94% and is comparable to the effective yield peaks at 9.6 eV for t-butyl glycine and 9.4 eV for t-butyl alanine, both of which are the base peak for these compounds.

The most obvious difference between the underivatized amino acids and their esters is that the effective yield maxima for the underivatized compounds are 1.16 - 1.28 eV and all base peaks from esters are produced with effective yield peaks at higher electron energies, ≥ 3 eV. In the case of the carboxylate anion for glycine t-butyl esters,

alanine t-butyl esters, and alanine ethyl ester, the base peaks have resonances 9.2 - 9.6 eV. The phenylalanine t-butyl ester also has its second strongest peak at 9.2 eV with a relative intensity of 94% as described above and is therefore very similar to the other esters. The remaining base peaks are either due to the OX^- ion or the m/z 16 ion and have effective yield maxima 5.45 - 6.6 eV. The high abundance ion peak with m/z 16 that looks like the base peak may be a result of leakage of O_2 into the mass spectrometer.

The change in effective yield maxima and relative intensities between the methyl ester and the larger esters remains unexplained. The isopropyl and t-butyl esters show constant effective yield maxima and relative intensities among the esters but the ethyl esters have three different base peak ions among the different esterified amino acids. Leaving aside the ethyl esters for the moment, the aromatic ring in phenylalanine has a limited effect on fragmentation of the esters in either the maxima or their relative intensities. The only exception is that there is a complementary ion to $(\text{M}-\text{R})^-$ i.e. R^- , and the reason that R^- is observed in phenylalanine has been described previously. But briefly, it is because the shape resonance at 4.51 eV associated with the benzene ring survives better because of the larger number of degrees of freedom within R^- which lowers the potential for electron autodetachment[50].

However, there are three inconsistencies within the t-butyl esters. First, there is the presence of an effective yield peak at 5.5 eV in the carboxylate anion for the glycine t-butyl ester. The presence of this peak is most likely due to the ^{13}C isotopic contribution of the $-\text{OX}$ ion, which has m/z 73 compared to the m/z of 74 for the carboxylate anion of glycine, and an effective yield peak at 5.7 eV. The intensity of the peak at 5.7 eV for m/z 73 (Fig. 50) should have $\sim 4.4\%$ contribution to the effective yield curve of m/z 74 (Fig.

43). The similarity of the overall effective yield curves for the t-butyl esters shows that the peak at 5.7 eV is not observed in the other two carboxylate anion effective yield curves. The presence of the ^{13}C isotopes in REC was observed by Laramée et al[63] for atrazine and CCl_4 . However, its presence does not change the effective yield curve of the compound compared to ^{12}C . Second, five ions from the t-butyl esters have peaks at 0.7 eV or 0.8 eV and while no other compound class shows these ions, it is likely that they are due to noise from the Cl^- ion which arises from HCl . Third, the $-\text{OtBu}$ ion from the t-butyl ester phenylalanine does not have an effective yield peak at ~ 5.5 eV but does have two peaks at 7.9 eV and 8.8 eV. There is no explanation for this variation because the effective yield peaks for the other ions are in overall good agreement with the ions from glycine and alanine t-butyl esters.

The isopropyl esters also show two variations but they are contained within the effective yield curves of the carboxylate anions. First, there are two higher energy peaks for the carboxylate anion from the glycine isopropyl ester at 8.4 eV and 9.3 eV that may be due to the lower intensity of the high energy effective yield peak and therefore are an artifact of the less apparent peak shape and maxima in the effective yield curve. Second, there is the presence of an effective yield maximum at 1.3 eV in the carboxylate anion of the isopropyl ester of phenylalanine. The origin of this peak may be due to contamination from the underivatized amino acid but is not observed in the other isopropyl esters studied. The reason for the lower contribution from the underivatized amino acid is that more controlled heating was used in the other experiments but it was not possible to control the heating rate for the isopropyl ester of phenylalanine.

The ethyl esters are considerably more complex in the number of effective yield peaks compared to the other esters. The glycine ethyl ester has four effective yield maxima two of which are consistent with the isopropyl and t-butyl esters i.e. 3.6 eV and 9.5 eV, and two of which are consistent with the underivatized amino acid i.e. 1.2 eV and 5.6 eV. The relative intensities of the effective yields at 1.2 eV and 5.6 eV at 9% for both, does not match the relative intensities for the underivatized amino acids, i.e. 100% for the 1.28 eV peak and 5.6% for that at 5.15 eV. The underivatized compound may contribute to the effective yield peak at 1.28 eV for the isopropyl ester of phenylalanine. However, there are dramatically different relative intensities which would be caused by the small amount of underivatized amino acid < 1%. The effective yield peaks for the methyl esters have counterparts in peaks and intensities at 13% (glycine), 51% (alanine), and 15% (phenylalanine) but they have no peak at ~6 eV. The two other oddities of the glycine ethyl ester are the lack of a peak at 16 and the presence of a peak at 2.7 eV for the (M-R)⁻ ion.

Alanine ethyl ester has effective yield maxima consistent with the overall trends of the ethyl, isopropyl, and t-butyl esters but one additional effective yield maximum appears at 9.5 eV for the ion with m/z 16 with a relative intensity of 46.4%. The reason for this fragmentation channel appearing at this electron energy is somewhat obscure but not totally surprising given that other fragment ions occur at this energy. The ion may be due to the presence of water or O₂ in the chamber, as effective yield maxima for such species are known to appear at electron energies > 6 eV. In contrast, the phenylalanine ethyl ester has basically the expected effective yield peaks observed for esters.

The most intense fragment ions changes from the $(M-H)^-$ ions in underivatized amino acids to other fragment ions. The effective yield maxima from the underivatized amino acids for the formation of the carboxylate anion changes from ~ 1 to 1.5 eV to the ranges of $3 - 4$ eV, $5 - 6$ eV, and ≥ 8 eV. The effective yield maxima for all other mass peaks remain basically unchanged but there are some variations in the relative intensities.

N-Acetyl Amino Acids

At present only one N-acetyl amino acid has been reported, i.e. N-acetyl tryptophan, but this amino acid derivative serves as a simple model for peptides.

N-Acetyl Alanine

Alanine is one of the simplest amino acids and the acetylation of the compound adds 43 amu to the mass. The REC-MS shows two prominent peaks at m/z 130 for the $(M-H)^-$ ion and at m/z 72 for the cleavage of the $C_\alpha - N$ bond minus a hydrogen atom (Fig. 55 and 56). The cleavage of the $C_\alpha - N$ bond is equivalent to the cleavage of the peptide backbone to form the z ion minus a hydrogen atom or a $(z-1)^-$ ion. In this case, two complete amino acids are not present and this cleavage is not a true z ion. The product will be thus referred to as a pseudo z ion. The formation of both of these ions appears in the energy range of 1 - 2 eV; more specifically 1.1 eV for $(M-H)^-$ (Fig. 57) and 1.8 eV for the pseudo z-1 ion (Fig. 58). A total of 15 fragmentation channels were apparent in the mass spectrum, but the effective yield maxima could not be determined in

all cases (Table 4). The fragmentations produce ions with m/z 58 which is the complementary ion of the pseudo z ion, the c ion, or more correctly a pseudo c ion since two complete amino acids are not present, and the effective yield maxima are at 2.0 eV and 9.5 eV.

N-Acetyl alanine is the simplest of the N-acetylated amino acids studied and mimics a peptide backbone with limited interaction of side chains during the resonance electron capture process. The formation of the carboxylate anion as the dominant ion with electron energy maximum at 1.1 eV is in fairly good agreement with the effective yield maximum of the underivatized amino acid at 1.2 eV. The agreement of the carboxylate anion effective yield maxima suggests that acetylation has a limited effect on the primary means of fragmentation and on the capture at the carboxylate functionality.

In the case of the second most intense peak at m/z 72 there remains the question of how this ion is formed. From the high resolution data for alanine dimer species it can be inferred that this ion is a $z-1$ type given that the electron energy is in a range similar for the fragmentation observed in the high resolution experiments. There cannot be other fragment ions that would generate this ion with the same m/z without complex rearrangement processes. Therefore the ion with m/z 72 will be labeled a pseudo $z-1$ ion because to be a true $z-1$ ion two linked amino acids in the peptide would be required.

The question immediately arises what is the mechanism of such a cleavage? Since it occurs with an effective yield maximum at 1.8 eV, it seems logical to surmise that this fragment must be associated with a π^* orbital but determining whether this orbital is associated with the amide or carboxylate group is impossible with these data. Therefore, the capture of an electron at either the amide or the carboxylic acid group could result in

a valid mechanism for the fragmentation to form the pseudo z-1 ion. The effective yield maximum of 1.8 eV is higher than the effective yield maximum for the loss of a hydrogen atom and the formation of the carboxylate anion at 1.1 eV suggesting that there is an additional energy requirement beyond the formation of a free hydrogen atom. The difference of 0.7 eV is sufficiently greater than the error due to the energy spread of the electron beam, ~ 0.2 eV, and the requirement of additional energy for forming this ion cannot be written off even if its' exact magnitude may not be as precisely defined as one would like.

One other ion from N-acetyl alanine that deserves in depth attention is m/z 58, the complementary ion of the pseudo z-type ion forming a pseudo c-type ion. The intensity of this ion at m/z 58 is considerably lower than the intensity of the pseudo z-1 ion but it has effective yield maxima at 2.0 eV and 9.6 eV. The ion with m/z 58 was observed previously in N-acetyl tryptophan but it was not realized to be a model of c -type ion formation by the authors despite having similar effective yield maxima at 1.6 eV and 8.3 eV. Discussion about this ion will be left until later once the data for N-acetyl tryptophan is presented.

N-Acetyl Phenylalanine

N-acetyl phenylalanine has two dominant peaks in the REC mass spectrum (Fig. 59). The dominant peaks are at m/z 206, that is the (M-H)⁻ ion, and at m/z 116 which is equivalent to (M-R)⁻ or loss of the side chain. The formation of the (M-H)⁻ has an effective yield maximum at 0.8 eV (Fig. 60) and the (M-R)⁻ has a maximum at 1.0 eV

(Fig. 61). Weak peaks for the pseudo z-1 (m/z 148) and pseudo c (m/z 58) ions were observed in the mass spectrum at 1.0 eV and 6.9 eV respectively. Among the 23 total fragment ions, the formation of the R^- ion maximum occurs at 6.9 eV (Fig. 62) (Table 5).

The N-acetyl phenylalanine is the simplest of the aromatic amino acids and the underivatized amino acid has been shown to form fragment ions after interacting with resonant electrons. Again the $(M-H)^-$ ion is the most intense in the mass spectrum and has an effective yield maximum at 0.8 eV which is lower than the peak of 1.16 eV reported for the underivatized phenylalanine. A surprising change in the mass spectrum peak intensity is that for the formation of the $(M-R)^-$ ion which has an intense peak at 1.4 eV. The energy of the $(M-R)^-$ peak for N-acetyl phenylalanine is not dramatically different from the peak for the corresponding $(M-R)^-$ ion from phenylalanine at 1.45 eV. The change in intensity suggests that the presence of the acetyl group on the amine provides additional stabilization by delocalizing the charge over the pseudo peptide backbone.

In contrast to the formation of the pseudo z-1 ion observed in the N-acetyl alanine spectrum at 1.8 eV the formation of a pseudo z-1 ion at m/z 147, is observed as a weak ion with a resonance peak of 6.4 eV. The formation of the ion with m/z 148 is much stronger and has an effective yield peak at 1.0 eV and is equivalent to the formation of a z ion. In either case, these ions are very small contributors to the total ion current observed. However, the pseudo c ion with m/z 58 is observed at a maximum of 6.9 eV, which is not in good agreement with the ion from N-acetyl alanine (m/z 58) where the effective yield maxima were 2.0 eV and 9.6 eV.

One further ion that is important to examine is the formation of the R^- ion with m/z 91. The effective yield peak at 6.9 eV for the N-acetyl phenylalanine is a good match

for the maximum observed for the same ion from phenylalanine at 6.4 eV. The second maximum observed in phenylalanine, at 1.4 eV i.e. the effective yield curve for R^- is not observed for N-acetyl phenylalanine. The delocalization of the charge over the pseudo-peptide backbone in the $(M-R)^-$ ion may lead to this ion being more favored. It remains to be seen whether this is borne out in peptides with aromatic side chains.

N-Acetyl Tyrosine

N-acetyl tyrosine has two dominant peaks one for the $(M-H)^-$ ion with m/z 222 and one for the $(M-R)^-$ ion with m/z 116 in the REC-MS (Fig. 63). The effective yield maxima are at 0.9 eV for $(M-H)^-$ (Fig. 64) and at 1.4 eV and 5.8 eV for $(M-R)^-$ with the former being the more intense (Fig. 65). The pseudo $z - 1$ ion was observed with an effective yield maximum at 1.3 eV (Fig. 66) with m/z 164 and the pseudo c ion at 7.6 eV with m/z 58. A total of 27 fragmentation channels were observed but no effective yield maximum was observed for the R^- ion with m/z 107. However, an effective yield peak was observed for the ion with m/z 106 at 0.7 eV (Table 6).

N-acetyl tyrosine is very near in structure to N-acetyl phenylalanine with the addition of a hydroxyl group on the aromatic ring in tyrosine distinguishing them. As in the other N-acetyl amino acids, N-acetyl tyrosine has a dominant $(M-H)^-$ ion with an effective yield maximum of 0.9 eV which is slightly lower than the peak observed for the underivatized amino acid at 1.12 eV. The second most intense peak is due to the $(M-R)^-$ ion with effective yield maxima at 1.4 eV and 5.7 eV which match the effective yield maxima of the underivatized amino acid at 1.55 eV and 6.3 eV.

The ion with m/z 164 is a pseudo $z-1$ ion and it is observed with a peak at 1.2 eV. Unlike the N-acetyl phenylalanine spectrum that showed a mass peak which matched the pseudo z ion and not the pseudo $z-1$ ion. Like N-acetyl alanine the pseudo $z-1$ ion has slightly higher energy than the $(M-H)^-$ ion for N-acetyl tyrosine. Also the pseudo c ion with m/z 58 has an effective yield maximum at 7.6 eV that matches the 6.9 eV resonance from N-acetyl phenylalanine.

In contrast to N-acetyl phenylalanine, the R^- ion is not observed but the $(R-H)^-$ is observed with an effective yield peak at 0.8 eV. The R^- ion was observed at 1.35 eV and 5 eV for underivatized tyrosine. The $(R-H)^-$ is not observed in any other spectrum reported for tyrosine and remains an anomaly. It may be due to the loss of a hydrogen atom that produces a more stable ion but there is no obvious mechanism to form this ion.

N-Acetyl Tryptophan

N-Acetyl Tryptophan is the only N-acetyl compound that has previously been reported [49]. It has three main peaks in the REC-MS (Fig. 67), with the dominant one being the $(M-H)^-$ ion with m/z 245 and an effective yield maximum at 0.7 eV (Fig. 68). The $(M-R)^-$ ion with m/z 116 has a weak signal ≥ 4.5 eV. The third most intense peak is at m/z 115 and it is produced with peaks at ~ 0 eV and 1.3 eV (Fig. 69). The effective yield maximum at ~ 0 eV is the more intense of the two producing the ion with m/z 115. The third, strong peak in the mass spectrum is at m/z 71 and it has an effective yield maximum at 1.5 eV. Like the previous two aromatic N-acetylated amino acids the R^- ion, with m/z 130 was observed in the REC-MS but there was a no apparent effective yield

maximum (Table 7). Ions with m/z 129 and 131 were observed with weak effective yield maxima at 0.5 eV and 0 eV respectively. Weak pseudo $z - 1$, m/z 188, (Fig. 70) and pseudo c ions, m/z 58, were observed at 1.1 eV and ≥ 5 eV, respectively among the 21 total fragmentations in the MS.

N-acetyl tryptophan is the only N-acetylated amino acid that has been previously reported[49]. The strongest ion in the mass spectrum recorded is the $(M-H)^-$ ion with an effective yield maximum at 0.7 eV which is in contrast to the previously reported data where $(M-H)^-$ is a weak ion with effective yield maxima at 0.4 eV and 1.1 eV. The second and third most intense ions, at m/z 71 and m/z 115, respectively were not observed in the previous report. The ion with m/z 115 has a global effective yield maximum at 0.2 eV and a second peak at 1.3 eV which may be related to the $(M-R)^-$ ion observed in N-acetyl phenylalanine, N-acetyl tyrosine, and the previously reported N-acetyl tryptophan data. Formation of this ion at near to zero electron energy is unexplained.

There is no peak in the mass spectrum for the R^- ion with m/z 130 and its absence is in agreement with the report by Abdoul-Carime et al[49]. The data reported for the amino acid and the methyl ester indicates there are R^- ions formed at 1.2 eV and 9 eV for the amino acid and 5 – 12 eV for the methyl ester. There are also weak mass spectral peaks for ions with m/z 129 at 0.5 eV and m/z 131 at 0 eV.

The pseudo $z-1$ ion for N-acetyl tryptophan at m/z 187 is observed with an effective yield maximum of 1.1 eV but the ion was not observed in the previous report for this compound. The effective yield maximum is in reasonable agreement with the $z-1$ ion of N-acetyl alanine at 1.8 eV and N-acetyl tyrosine at 1.2 eV. Also this ion is higher

in energy than the effective yield maximum of the $(M-H)^-$ at 0.7 eV. The pseudo c ion with m/z 58 is an unresolved peak with energy ≥ 5 eV and is in contrast to that reported with a more intense maximum at 1.6 eV and the weaker effective yield peak at 8.3 eV reported previously [49].

Combined N-Acetyl Results

The N-acetyl amino acids show fragment ions similar to the cleavage of the peptide back bone by ECD but because there are not two complete peptides these are not true c and z ions. Hence they are termed “pseudo” c and z ions. In N-acetyl alanine the pseudo z-1 ion is the second most intense ion, after the $(M-H)^-$ ion, suggesting that the fragmentation of the C_α -N bond is favored even without the amine that would be in a alanine dimer. The N-acetyl aromatic amino acids also show the z-1 ion but the $(M-R)^-$ ion is more intense. This suggests that the presence of aromatic amino acids may change the fragmentation of peptides containing aromatic amino acids compared to aliphatic amino acids. The N-acetylated amino acids show compared to similar effective yield maxima compared to the underivatized amino acids and are therefore N-Acetylation is a good means to improve volatility without dramatically changing the fragmentation of the amino acid.

Peptides

The REC-MS studies carried to this point have served as models for peptides. Until now there have been no reports on the interactions of this class of compounds with slow electrons. The data here are from studies designed to determine the effects of increasing peptide size and derivatization in a systematic manner based upon the alanine dimer and trimer peptides.

Ala-Ala

The REC-MS for the alanine dimer has a total of 16 fragmentation channels (Table 8) with formation of the $(M-H)^-$ ion being the most intense, followed by the ion with m/z 72 (Fig. 71). The effective yield maxima for the $(M-H)^-$ ions occur at 1.0 eV and at 1.6 eV for the ion with m/z 72 (Fig. 72). The formation of an ion with m/z 72 corresponds directly to a b type peptide backbone cleavage but it is also one mass unit lower than the expected mass for a z type ion cleavage. Two other ions with lower intensities correspond to the expected masses for peptide backbone cleavages to form y ions at 5.4 eV and 8.3 eV, and c ions at 1.4 eV and 8.9 eV. Unfortunately these ions have m/z 87 and 88 for the c and y ions respectively. Due to the low mass resolving power of the instrument, these cannot be unambiguously assigned to an empirical formula. Also observed is an ion with m/z 16 with effective yield maxima 6.1 eV and 9.3 eV.

The alanine dimer (A_2) has two main ions; $(M-R)^-$ and z-1 ions with effective yield maxima at 1.0 eV for $(M-R)^-$ and 1.4 eV and 8.9 eV z-1 ions. The difference in effective yields for the resonance at 0.4 eV is in line with the difference observed between the acetylated amino acid $(M-R)^-$ ions and the pseudo z-1 ions. Comparison of

the effective yield curves between N-acetyl alanine and A_2 are almost identical for the $(M-H)^-$ ions (Fig. 73) and pseudo $z-1$ and $z-1$ ions respectively (Fig. 74). The comparison of the pseudo c and c ions from N-acetyl alanine and A_2 lead to similar effective yield curves (Fig. 75). In contrast, the comparison of the intensities of the pseudo $z-1$ and z ions from N-acetyl alanine and A_2 , respectively, the intensities of the effective yield maxima for the pseudo c and c ions from the respective compounds are dramatically different. While the effective yield maxima from pseudo c and c ions from N-acetyl alanine and A_2 are very near each other, the reason for the dramatically lower intensity for the N-acetyl alanine pseudo c ion is not immediately apparent.

The other mass peak of particular interest is that at m/z 88 which corresponds to the y ion or cleavage of the amide bond. The two effective yield maxima for this compound at 5.4 eV and 8.9 eV suggest that this is not a ^{13}C isotopic contribution from the ion with m/z 87 and that it is a more energetically demanding process than the cleavage of the C_α -N bond. This is predicted by the computational work of Simons et al on the alanine dimer ECD fragmentation[44]. The authors report that the most energetically favorable bond for cleavage of this dimer is the C_α -N bond and that the other bonds would have a higher thermodynamic requirement for cleavage. The observation of this ion leads to validation of their prediction.

N-Acetyl Ala-Ala

The REC-MS for N-Acetyl Ala-Ala has strong ions with m/z 72 and m/z 201 and the $(M-H)^-$ ion with m/z 201 being the most intense ion (Fig. 76). Again, the ion with m/z

72 corresponds directly to a cleavage of the peptide backbone to form an ion which is one mass unit less than that for the expected z ion. The effective yield maximum for the ion with m/z 72 appears at 1.4 eV (Fig. 77) and at 0.7 eV for the $(M-H)^-$. The third most intense ion has m/z 143, but it is one mass unit less than the cleavage between the acetylated nitrogen and the C_α carbon of the first amino acid or a pseudo z_2-1 ion. The effective yield maximum appears at 1.1 eV for the ion with m/z 143 (Fig. 77). The formation of a c type ion with m/z 129 is observed with an effective yield maximum at 1.4 eV (Table 9).

The REC-MS for N-acetyl Ala-Ala is the first REC-MS where the $(M-H)^-$ ion is not the dominant fragmentation pathway arising from resonant electron capture. In this case, fragmentation to form the z_1-1 ion with m/z 72, at 1.4 eV, is the most intense ion but it has an effective yield maximum 0.7 eV higher than the $(M-H)^-$ ion at 0.7 eV and the $(M-H)^-$ ion is 0.4 eV lower than that for the pseudo z_2-1 ion with m/z 143 (Fig. 78 - 79). Similarly, the effective yield maxima are lower than the $(M-H)^-$ ions effective yield maxima by 0.7 eV for the pseudo $z-1$ ion from N-acetyl alanine and 0.7 eV for z_1-1 for A_2 . The z_1-1 and pseudo z_2-1 ions from N-acetyl Ala-Ala have similar effective yield maxima, i.e. 1.4 eV and 1.1 eV, respectively (Fig. 77).

A comparison of the pseudo c and c ions is not possible because the ion with m/z 58, i.e. the pseudo c ion, is too weak to display a useful effective yield curve. However, a comparison of the c_1 ions from A_2 and N-acetyl A_2 , shows almost identical effective yield curves, intensities, and maxima (Fig. 80). The comparison of the most intense ions from N-acetyl Ala-Ala (Fig. 81) shows a tight grouping of effective yield maxima that must all be associated with the π^* states of the amides or carboxylic acid.

Ala-Ala-Ala

The trimer of alanine has a REC-MS with 36 fragmentation channels (Table 10) (Fig. 82). The most intense fragmentation channel produces the ion with m/z 16. A strong $(M-H)^-$ and an ion with m/z 143 also are observed. The ion with m/z 16 has effective yield maxima at 6.2 eV and 9.2 eV and the effective yield maximum of the $(M-H)^-$ ion is 0.9 eV (Fig. 83). The ion with m/z 143 is the third most intense peak and it appears at one mass unit less than that for the z_2 ion. However it is also consistent with the mass for a b_2 type cleavage of the peptide backbone and it has effective yield maxima at 0.1 eV and 1.0 eV. The peak at m/z 72 corresponds to both a b_1 ion and a z_1-1 ion and it has an effective yield maximum at 2.0 eV. The ion with m/z 158 has an effective yield maximum at 1.6 eV and corresponds by mass to a c_2 ion.

The REC-MS for Ala-Ala-Ala is the first mass spectrum for a peptide in which the most intense ion is not a low energy effective yield maximum. Rather the ion with m/z 16 that has an effective yield maximum at 6.3 eV and a second maximum at 9.2 eV is the most intense. The effective yield curve matches that that would have been expected from water and therefore the ion with this m/z is most likely a contamination of either the sample or the source. The third most intense peak appears at m/z 46 which is a pyrolytic ion; it appears near to 0 eV. The ion with m/z 46 is not due to resonance electron capture by the compound and these two ions with m/z 16 and m/z 46 will not be discussed further.

The most intense peak resulting from resonance electron capture is the one at m/z 143 and it is due to the z_2-1 ion with effective yield maxima 0.1 eV and 1.0 eV (Fig. 83). The z_1-1 ion with m/z 72 has an effective yield maximum at 2.0 eV. A comparison of the z_1-1 , z_2-1 , c_2 (m/z 158) ions, and the $(M-H)^-$ ion again shows a set of fragmentations that are related to π^* states. The effective yield peak at 0 eV is most likely a “hot band” or the capture of a low energy electron by an energetically excited state caused by heating to volatilize the analyte.

N-Acetyl Ala-Ala-Ala

The REC-MS for N-acetyl alanine has 51 fragmentation channels (Table 11) with the most intense ion, i.e. that with m/z 143, being one mass unit less than the z_2 ion that would arise from backbone cleavage (Fig. 84). The effective yield curve for the ion with m/z 143 has two maxima; 0 eV and 0.9 eV (Fig. 85). In addition, two other ions are one mass unit less than the z_n-1 series ions, specifically the z_1-1 ion with m/z 72 and the pseudo z_3-1 ion with m/z 214. The z_1-1 ion has a peak at 1.3 eV and the pseudo z_3-1 ion has peaks at 0 eV and 0.9 eV. The $(M-H)^-$ ion was observed with effective yield peaks at 0 eV and 1.1 eV (Fig. 86). Also ions with m/z 's 58, 129, and 200 were observed that correspond with the mass expected for the pseudo c_0 , c_1 , and c_2 ions (Fig. 87). For m/z 129 there were two effective yield maxima at 0 eV and 1.3 eV and m/z 200 had almost identical maxima at 0 eV and 1.4 eV while the ion with m/z 58 had maxima at 1.5 eV and 7.1 eV.

The REC-MS for N-acetyl Ala-Ala-Ala has a dominant peak at m/z 143; it is the z_2-1 ion with effective yield maxima at 0 eV and 0.9 eV. The comparison of the ion with m/z 214, the pseudo z_3-1 , the z_2-1 ion, and z_1-1 ion with m/z 72 show effective yield maxima at 1.0 eV, 0.9 eV, and 1.3 eV, respectively (Fig. 86). The pseudo z_3-1 ion and z_2-1 ion also have very intense maxima at 0 eV that are “hot bands” due to the excited states. The ions with m/z 58, m/z 129, and m/z 200 belong to the c series and are the pseudo c_0 , c_1 , and c_2 ions showing similar effective yield maxima (Fig. 87). When the effective yield data are compared from the two ion series and the $(M-H)^-$ ion, and the curve from z_2-1 is scaled by a factor of 1/10, the curves show very close effective yield maxima (Fig. 88). Unlike the alanine dimer and N-acetyl alanine dimer compounds the N-acetyl Ala-Ala-Ala does not show a $z-1$ ion with an effective yield maximum higher in energy than that for the $(M-H)^-$ ion. The dominant effective yield maxima at 0 eV are likely caused by “hot bands” or excited states that capture near to zero energy electrons. The effective yield maxima at ~ 0 eV obscure the weaker maxima at $\sim 1-2$ eV.

A comparison of the c, $z-1$, $(M-H)^-$ ions from N-acetyl Ala-Ala and N-acetyl Ala-Ala-Ala shows a very tight group of effective yield maxima (Fig. 89 - 90). The exceptions are the “hot bands” at 0 eV that are not observed for N-acetyl Ala-Ala. The “hot bands” fragment ions are the most intense ions observed for the trimers and specifically the z_2-1 ions. The importance of this will be discussed later.

Ala-Ala-Ala-OMe

The REC-MS for Ala-Ala-Ala-OMe shows at least 23 fragmentation channels (Table 12) although not all of them can be assigned to fragmentations for Ala-Ala-Ala-OMe (Fig. 91). The side products from synthesis of the methyl ester, including small amounts of piperidine and the side product of Fmoc deprotection with m/z 193 showed peaks in the spectra. There is no observed negative ion for the carboxylate anion $(M-Me)^-$ but there is a weak $(M-H)^-$ ion for which the effective yield maximum cannot be determined. The ions with m/z 87 and 158 are observed and have almost the same effective yield maxima at ~ 1.6 eV and 1.4 eV, respectively (Fig. 92). The ions with m/z 87 and 158 can be either c or z ions based on the expected masses of peptide backbone fragmentation (Fig. 93).

The REC-MS from the Ala-Ala-Ala-OMe is confusing because the c and z ion series have the same masses. The ions c_1 with m/z 87 and c_2 with m/z 158 have weak effective yield ranges 0-3 eV and 6+ eV (Fig. 94). In contrast, the z_1-1 ion with m/z 86 and z_2-1 ion with m/z 157 have different effective yield curves (Fig. 95). The z_1-1 has an effective yield maximum at 0.1 eV, but the z_2-1 ion has 1.6 eV as an effective yield maximum which is in the range of other similar fragment ions. These ions do not have easily rationalized structures. Effective yield peaks were not observed for either the z_1 -Me ion with m/z 72 or the z_2 -Me ion with m/z 143. The z_1 -Me and z_2 -Me ions from Ala-Ala-Ala-OMe would be the equivalent of the z-1 ions observed from the Ala-Ala-Ala and other compounds. Only the peak at m/z 72 was observed but as mentioned before no effective yield could be determined.

The intensity of the signal for Ala-Ala-Ala-OMe was weaker because there was less sample available and therefore less introduced into the mass spectrometer. A less

pure sample (Fig. 96) has stronger effective yield peaks for the c ions and the z_2-1 ion (Fig. 97) due to more sample being introduced into the mass spectrometer. It is not clear whether the peaks are due to the Ala-Ala-Ala-OMe or to the Fmoc cleavage product. In the case of the ions with m/z 87, 157, and 158 it is unlikely that these ions are due to the Fmoc cleavage product because the effective yields match well with the other ions for the alanine trimer peptides. The peak at m/z 193 is likely due to the Fmoc cleavage product because the effective yield of this ion is near to 0 eV (Fig. 98).

N-Acetyl Ala-Ala-Ala-OMe

The N-acetyl alanine trimer methyl ester has 26 fragmentation channels (Table 13) with the most intense ion appearing with m/z 129. i.e the c_1 ion and the x_2 ion minus one mass unit (Fig. 99). The effective yield maxima for the ion with m/z 129 are at 1.6 eV and 9.3 eV (Fig. 100). The second most intense ion with m/z 200 is either the mass of the c_2 ion or a pseudo x_3 ion minus one with effective yield maximum at 1.2 eV. The ion forming $(M-H)^-$ with m/z 286 is observed at an effective yield maximum of 1.7 eV. An ion with m/z 87 was observed with an effective yield maximum at 6.7 eV and one with m/z 31 was observed with an effective yield range at ≥ 6 eV (Fig. 101). The $(M-Me)^-$ ion with m/z 272, was observed at an effective yield peak in the range of 1 to 2 eV.

The REC-MS for N-acetyl Ala-Ala-Ala-OMe has the most intense peak at m/z 129 which reflects the expected mass for the formation of the c ion with an effective yield maximum at 1.6 eV. The second most intense peak is also a c-type ion with m/z of 200 and an effective yield maximum at 1.2 eV. The $z-1$ ions that were observed for the

unesterified compounds with carboxylic acids are not observed here. Ions with m/z 157 and 228 are due to z_2-1 and pseudo z_3-1 series but these could also be the a_2 and pseudo a_3 ions, respectively. It is possible that the ions with m/z 157 and 228 are $z-1$ type ions but the formation of a stable anion structure due to loss of a hydrogen atom from a methyl ester seems improbable especially because the formation of the carboxylate anion by loss of a methyl group, in an identical manner to the parent carboxylic acid i.e. a $(z\text{-Me})^-$ ion, is not observed. Therefore the peaks at m/z 157 and 228 are tentatively assigned to the a_2 and pseudo a_3 ions, respectively with effective yield maxima at 1.5 eV for the a_2 ion and 1.2 eV for the pseudo a_3 ion.

In addition, there is the $(M-H)^-$ ion formed at 1.7 eV that results from π^* states with fragmentation channels in the 1-2 eV energy range. The presence of an $(M-H)^-$ ion at this electron energy is unexpected because in the methyl ester of alanine, the $(M-H)^-$ ion appears at 3.3 eV and 6 eV. The $(M-H)^-$ ion from the methyl ester does not show a rationalized structure for the anion that would be available at this energy. In contrast the $(M\text{-Me})^-$ ion forms the carboxylate anion at a similar effective yield maximum of 1.5 eV but with a weaker intensity than that resulting from the $(M-H)^-$ ion of the amino acid.

The most important difference between the N-acetyl Ala-Ala-Ala and N-acetyl Ala-Ala-Ala-OMe is a change in fragmentations. In the case where there is a free carboxylic acid group, $z-1$ fragments and $(M-H)^-$ ions are favored and these form at low electron energies. In the case of the esterified peptides, the formation of c type ions is favored and these are produced with low electron energies. The mechanism for the fragmentation and formation of the $z-1$ and c ions occurs by first capturing an electron at an amide site followed by peptide backbone cleavage (Fig. 102). The formation of the $z-1$

ion is then likely to involve reorganization of the carboxylate ion after backbone cleavage (Fig. 103). The alternative mechanism for cleavage involves the capture of an electron at the carboxylate to form a hydrogen atom which then attacks the amide group leading to backbone cleavage. It is unlikely that the z-1 and c backbone cleavages should be observed at the same electron energy as in the case of the z-1 ions at 1-2 eV and the pseudo c ions ≥ 5 eV from the N-acetyl amino acids. The formation of the c and z-1 ions for the N-acetyl Ala-Ala-Ala and N-acetyl Ala-Ala-Ala-OMe occurs at approximately the same energy (Fig. 104-105). The formation of the “hot band” ions of N-acetyl Ala-Ala-Ala are an artifact of the heating required to volatilize the sample and can be discounted as an important difference between the two compounds.

Combined Peptide Results

The results from the C-terminal underivatized peptides can be briefly summarized as z-1 ions are the dominant fragment negative ions as peptide size increases. C-terminal underivatized peptides also have (M-H)⁻ ions in the mass spectra. C series ions are also observed along with other fragmentation channels that are uncharacterized at present. The methyl ester peptide mass spectra show c ions but no z-Me ions, the z-1 equivalent for methyl esters. All of the aforementioned fragment negative ions have effective yield between 1 – 2 eV and are therefore associated with π^* shape resonances as previously assigned for amino acids[12, 48-50]. These results will be discussed at length below.

Phi - Psi Potential Energy Surfaces

Two ϕ - ψ potential energy surfaces were constructed. The two surfaces were performed on the D-stereoisomer of the derivatized alanine dimer rather than on the L-stereoisomer. Due to the time the complete potential energy surfaces were not recalculated for the L-stereoisomer but instead four points were calculated for the “corners” of the potential energy surface for the L-stereoisomer for comparison to the D-stereoisomer.

The model using the 6-311 **G++ basis set had a total change in energy of ~ 0.4 eV over the surface range (Fig. 106). The estimated minimum energy for the vertical electron attachment energy is ~ 3.2 eV and the maximum is ~ 3.6 eV. The ψ value has the greater effect on the VEAE potential energy surfaces. The potential energy surfaces for the vertical electron attachment energy calculated with the aug-cc-pVDZ method gave a total change in energy of ~ 0.3 eV over the range of surfaces (Fig. 107). Both the ϕ and ψ angles affect the VEAE calculated for the potential energy surface using the aug-cc-pVDZ method.

The four “corners” of the L-stereoisomer potential energy surface are very close to the values of the “corners” of the D-stereoisomer potential energy surface (Table 14). The VEAE values for the L-stereoisomer in the table must be compared with the VEAE values for the ϕ and ψ value with the opposite sign. This means that the D-stereoisomer with $\Phi = -180$ and $\Psi = 180$ must be compared to the L-stereoisomer with $\Phi = 180$ and $\Psi = -180$. When the VEAE values for the stereoisomers are compared in the manner described above, the difference between three of the calculated values is ≥ 0.02 eV; a difference too small to be of significance given that the experimental technique of

REC-MS has an error associated with the width of the electron energy beam an order of magnitude bigger (~ 0.2 eV) and the half height width for the effective yield peaks are on average 1 eV and larger. The last “corner” of $\Phi = -60$ and $\Psi = 60$ for the L-stereoisomer and $\Phi = 60$ and $\Psi = -60$ for the D-stereoisomer is an energy difference of 0.11 eV; a difference that is larger but still significantly smaller than the width of the effective yield peak. Therefore, the changes observed in between the two stereoisomers are too small to warrant calculating the potential energy surface with the L-stereoisomer and any conclusions that can be reached with the D-stereoisomer will almost certainly be valid for the L-stereoisomer.

Table 2. Relative intensities (RI) and effective yield maxima (E_m) for the specific ion types listed for amino acids and their esters.

Glycine					
ions	Gly-OH RI, %, (E_m , eV)	Gly-OMe RI, %, (E_m , eV)	Gly-OEt RI, %, (E_m , eV)	Gly-OiPr RI, %, (E_m , eV)	Gly-OtBu RI, %, (E_m , eV)
(M-X) ⁻	100 (1.28) 5.6 (5.15)	15 (1.3) 3 (8-12)	9 (1.2) 14.4 (3.6) 9 (5.6) 29.3 (9.5)	72.6 (3.6) 47.1 (8.4) 37.3 (9.3)	21.1 (3.7) 18.4 (5.51) 40.4 (9.6)
OX ⁻	4.4 (6) 1.9 (10)	100 (5.45) 47 (7) sh	64 (5.9)	68.6 (5.5)	34.5 (5.7)
(M-R) ⁻	5.6 (5.15)	4.8 (5)	4.2 (2.7) 13.8 (5.5)	11.8 (5.15)	17.0 (5.3)
R ⁻	Not Studied	Not Studied	Not Studied	Not Studied	Not Studied
NH ₂ /O ⁻	10-80 (6.7)	18 (6) 15 (9.2)	Not Observed	100 (6.5)	5.8 (0.8) 3.1 (6)

Alanine					
ions	Ala-OH RI, %, (E_m , eV)	Ala-OMe RI, %, (E_m , eV)	Ala-OEt RI, %, (E_m , eV)	Ala-OiPr RI, %, (E_m , eV)	Ala-OtBu RI, %, (E_m , eV)
(M-X) ⁻	100 (1.2)	51 (1.2) 7 (8-12)	41.4 (3.5) 70.7 (9.4)	Not Studied	74.3 (3.7) 83.5 (9.4)
OX ⁻	4.4 (6) 1.9 (10)	23 (3.1) 100 (6)	24.1 (5.8)	Not Studied	39.5 (5.7)
(M-R) ⁻	Not observed	7 (8-12)	Not observed	Not Studied	Not observed
R ⁻	Not observed	Not observed	Not observed	Not Studied	Not observed
NH ₂ /O ⁻	10 (6.6)	50 (6.6) 80 (7-11)	22.4 (6.6) 32.8 (9.5)	Not Studied	5.5 (0.8)

Table 2 continued.

Phenylalanine					
ions	Phe-OH RI, %, (E _m , eV)	Phe-OMe RI, %, (E _m , eV)	Phe-OEt RI, %, (E _m , eV)	Phe-OiPr RI, %, (E _m , eV)	Phe-OtBu RI, %, (E _m , eV)
(M-X) ⁻	100 (1.16)	13 (1.2) 2.7 (9-11)	36 (2.8) 28 (8.6)	61.9 (1.3) 73.8 (3.3) 33.3 (8.2)	4.5 (0.8) 29.5 (3.5) 38.5 (9.2)
OX ⁻	9.5 (6)	100 (6.65) 40 (9.5) sh	64 (6)	28.6 (6)	3.5 (0.7) 10 (7.9) 3.5 (8.8)
(M-R) ⁻	12 (1.45)	20 (1.7) 6 (6.8)	24 (1.5)	Not Observed	3 (1.9)
R ⁻	1.8 (1.4) 2.9 (6.4)	4 (1.55) 28 (6.3)	28 (6)	16.7 (6.3)	14.5 (6.5) 12.5 (8.4)
NH ₂ /O ⁻	49 (6.6)	12 (6.4)	100 (6.5)	100 (6.6)	2.5 (0.7) 5 (6) 4.5 (9.4)

Table 3. Relative intensities (RI) calculated from a resonance electron capture ion and effective yield maxima (E_m) for the specific ion types listed for amino acids and their esters.

Glycine					
ions	Gly-OH RI, %, (E_m , eV)	Gly-OMe RI, %, (E_m , eV)	Gly-OEt RI, %, (E_m , eV)	Gly-OiPr RI, %, (E_m , eV)	Gly-OtBu RI, %, (E_m , eV)
(M-X) ⁻	100 (1.28) 5.6 (5.15)	15 (1.3) 3 (8-12)	14 (1.2) 22.4 (3.6) 14 (5.6) 45.8 (9.5)	72.6 (3.6) 47.1 (8.4) 37.3 (9.3)	52.2 (3.7) 45.56 (5.51) 100 (9.6)
OX ⁻	4.4 (6) 1.9 (10)	100 (5.45) 47 (7) sh	100 (5.9)	68.6 (5.5)	85.6 (5.7)
(M-R) ⁻	5.6 (5.15)	4.8 (5)	6.5 (2.7) 21.5 (5.5)	11.8 (5.15)	42.2 (5.3)
R ⁻	Not Studied	Not Studied	Not Studied	Not Studied	Not Studied
NH ₂ /O ⁻	10-80 (6.7)	18 (6) 15 (9.2)	Not observed	100 (6.5)	14.4 (0.8) 7.8 (6)

Alanine					
ions	Ala-OH RI, %, (E_m , eV)	Ala-OMe RI, %, (E_m , eV)	Ala-OEt RI, %, (E_m , eV)	Ala-OiPr RI, %, (E_m , eV)	Ala-OtBu RI, %, (E_m , eV)
(M-X) ⁻	100 (1.2)	51 (1.2) 7 (8-12)	58.5 (3.5) 100 (9.4)	Not Studied	89 (3.7) 100 (9.4)
OX ⁻	4.4 (6) 1.9 (10)	23 (3.1) 100 (6)	34.2 (5.8)	Not Studied	47.3 (5.7)
(M-R) ⁻	Not observed	7 (8-12)	Not observed	Not Studied	Not observed
R ⁻	Not observed	Not observed	Not observed	Not Studied	Not observed
NH ₂ /O ⁻	10 (6.6)	50 (6.6) 80 (7-11)	31.7 (6.6) 46.4 (9.5)	Not Studied	6.6 (0.8)

Table 3 continued.

Phenylalanine					
ions	Phe-OH RI, %, (E _m , eV)	Phe-OMe RI, %, (E _m , eV)	Phe-OEt RI, %, (E _m , eV)	Phe-OiPr RI, %, (E _m , eV)	Phe-OtBu RI, %, (E _m , eV)
(M-X) ⁻	100 (1.16)	13 (1.2) 2.7 (9-11)	100 (3.3) 95.8 (9.2)	61.9 (1.3) 73.8 (3.3) 33.3 (8.2)	11 (0.8) 72 (3.5) 93.9 (9.2)
OX ⁻	9.5 (6)	100 (6.65) 40 (9.5) sh	93.8 (6)	28.6 (6)	8.5 (0.7) 24.4 (7.9) 8.5 (8.8)
(M-R) ⁻	12 (1.45)	20 (1.7) 6 (6.8)	14.6 (1.5)	Not observed	13.4 (1.9)
R ⁻	1.8 (1.4) 2.9 (6.4)	4 (1.55) 28 (6.3)	31.4 (6)	16.7 (6.3)	35.4 (6.5) 30.5 (8.4)
NH ₂ /O ⁻	49 (6.6)	12 (6.4)	27.1 (6.5)	100 (6.6)	6.1 (0.7) 12.2 (6) 11 (9.4)

Table 4. The effective yield (EY) maxima for each m/z from N-acetyl Ala, the associated intensities for each maximum, and the relative intensity (RI) as calculated compared to the most intense effective yield maximum. M/z's without EY maxima listed denote that no clear EY maxima or range that lead to the m/z were present in the effective yield curve.

	EY max 1	Intensity 1	EY max 2	Intensity 2	RI 1	RI 2
m/z	(eV)		(eV)		(%)	(%)
17					0.0	0.0
41					0.0	0.0
42	6+	4			0.9	0.0
43					0.0	0.0
44					0.0	0.0
45	6 to 7	5			1.1	0.0
46					0.0	0.0
53					0.0	0.0
58	2.0	7	9.6	8	1.5	1.7
71	9.4	18			3.9	0.0
72	1.8	237			51.7	0.0
73					0.0	0.0
74	1.3	5			1.1	0.0
88	1.1	5	5+	8	1.1	1.7
130	1.1	458			100.0	0.0

Table 5. The effective yield (EY) maxima for each m/z from N-acetyl Phe, the associated intensities for each maximum, and the relative intensity (RI) as calculated compared to the most intense effective yield maximum. M/z's without EY maxima listed denote that no clear EY maxima or range that lead to the m/z were present in the effective yield curve.

	EY max 1	Intensity 1	EY max 2	Intensity 2	RI 1	RI 2
m/z	(eV)		(eV)		(%)	(%)
16	6+	3			1.5	0.0
17	6.4	10			5.1	0.0
26	6+	10			5.1	0.0
42					0.0	0.0
43					0.0	0.0
44					0.0	0.0
45					0.0	0.0
58	6.9	9			4.6	0.0
70					0.0	0.0
72	6.4	12			6.1	0.0
74					0.0	0.0
91	6.9	13			6.6	0.0
98	0.7	23			11.7	0.0
103					0.0	0.0
115	0.8	3	7.6	7	1.5	3.6
116	1.0	189			96.4	0.0
117					0.0	0.0
129	0.3	9			4.6	0.0
147	6.4	8			4.1	0.0
148	1.0	10			5.1	0.0
161					0.0	0.0
164	1.5	2	5+	5	1.0	2.6
206	0.8	196			100.0	0.0

Table 6. The effective yield (EY) maxima for each m/z from N-acetyl Try, the associated intensities for each maximum, and the relative intensity (RI) as calculated compared to the most intense effective yield maximum. M/z's without EY maxima listed denote that no clear EY maxima or range that lead to the m/z were present in the effective yield curve.

	EY max 1	Intensity 1	EY max 2	Intensity 2	RI 1	RI 2
m/z	(eV)		(eV)		(%)	(%)
16	6.0	6			9.1	0.0
17	5 to 8	4			6.1	0.0
26					0.0	0.0
42					0.0	0.0
46					0.0	0.0
58	7.6	5			7.6	0.0
59					0.0	0.0
70					0.0	0.0
71	1.9	6			9.1	0.0
72	6.8	8			12.1	0.0
74	6 to 8	5			7.6	0.0
84					0.0	0.0
98	0.7	7	5 to 8	7	10.6	10.6
106	0.7	7			10.6	0.0
107					0.0	0.0
115					0.0	0.0
116	1.4	25	5.7	15	37.9	22.7
162					0.0	0.0
164	1.3	6			9.1	0.0
177	0.3	15			22.7	0.0
178					0.0	0.0
180					0.0	0.0
203					0.0	0.0
204					0.0	0.0
205					0.0	0.0
206	0.8	5			7.6	0.0
222	0.9	66			100.0	0.0

Table 7. The effective yield (EY) maxima for each m/z from N-acetyl Trp, the associated intensities for each maximum, and the relative intensity (RI) as calculated compared to the most intense effective yield maximum. M/z's without EY maxima listed denote that no clear EY maxima or range that lead to the m/z were present in the effective yield curve.

	EY max 1	Intensity 1	EY max 2	Intensity 2	RI 1	RI 2
m/z	(eV)		(eV)		(%)	(%)
16	6.9	7			11.5	0.0
17	5 to 7	4			6.6	0.0
26					0.0	0.0
42					0.0	0.0
46	0.0	6			9.8	0.0
58	5+	5			8.2	0.0
59	1.2	7	7+	3	11.5	4.9
71	1.5	31	5+	14	50.8	23.0
72	5+	5			8.2	0.0
74	5 to 7	6			9.8	0.0
84					0.0	0.0
98					0.0	0.0
115	0.2	41	1.3	15	67.2	24.6
116	5+	7			11.5	0.0
128					0.0	0.0
129	0.5	4			6.6	0.0
130					0.0	0.0
131	0.0	7			11.5	0.0
187	0.8	11			18.0	0.0
188					0.0	0.0
200	0.2	8			13.1	0.0
203					0.0	0.0
226	0.0	20			32.8	0.0
227	1 to 2	4	7+	3	6.6	4.9
245	0.7	61	5+	25	100.0	41.0
246					0.0	0.0

Table 8. The effective yield (EY) maxima for each m/z from Ala-Ala, the associated intensities for each maximum, and the relative intensity (RI) as calculated compared to the most intense effective yield maximum. M/z's without EY maxima listed denote that no clear EY maxima or range that lead to the m/z were present in the effective yield curve.

	EY max 1	Intensity 1	EY max 2	Intensity 2	RI 1	RI 2
m/z	(eV)		(eV)		(%)	(%)
16	6	17	9.2	12	3.5	2.5
17	5.5	8			1.7	0.0
26	1 to 2	4	6+6	7	0.8	1.5
27	8+	5			1.0	0.0
42	0.1	9			1.9	0.0
44	6.4	7	8.2	8	1.5	1.7
45	0.2	13	5.8	8	2.7	1.7
46	0.3	12			2.5	0.0
70					0.0	0.0
71	9.2	18			3.8	0.0
72	1.6	366			76.4	0.0
73					0.0	0.0
87	1.4	35	8 to 10	13	7.3	2.7
88	5.4	30	7 to 9	14	6.3	2.9
98	5+	5			1.0	0.0
109	0.3	10			2.1	0.0
115	5.2	13	8 to 9	7	2.7	1.5
124	0.3	13			2.7	0.0
125	0.4	7			1.5	0.0
126	0.2	6			1.3	0.0
141	1.7	27			5.6	0.0
142	0	6	7+	5	1.3	1.0
143	0	14			2.9	0.0
157	0.3	13			2.7	0.0
158	0.2	26			5.4	0.0
159	0.9	479			100.0	0.0

Table 9. The effective yield (EY) maxima for each m/z from N-acetyl Ala-Ala, the associated intensities for each maximum, and the relative intensity (RI) as calculated compared to the most intense effective yield maximum. M/z's without EY maxima listed denote that no clear EY maxima or range that lead to the m/z were present in the effective yield curve.

	EY max 1	Intensity 1	EY max 2	Intensity 2	RI 1	RI 2
m/z	(eV)		(eV)		(%)	(%)
16	5 to 7	6			5.3	0.0
17	6+	4			3.5	0.0
42	6+	5			4.4	0.0
58	6 to 8	4			3.5	0.0
70	0.8	34			30.1	0.0
72	1.4	69			61.1	0.0
86					0.0	0.0
88	1 to 2	6	5 to 8	5	5.3	4.4
99	1.4	25			22.1	0.0
111	0.5	7			6.2	0.0
115	1 to 2	6	5 to 8	5	5.3	4.4
117					0.0	0.0
119	1.1	9			8.0	0.0
129	1.4	25			22.1	0.0
130	0.8	29			25.7	0.0
143	1.1	57			50.4	0.0
148	0	25			22.1	0.0
156	0	35			31.0	0.0
201	0.7	113			100.0	0.0

Table 10. The effective yield (EY) maxima for each m/z from Ala-Ala-Ala, the associated intensities for each maximum, and the relative intensity (RI) as calculated compared to the most intense effective yield maximum. M/z's without EY maxima listed denote that no clear EY maxima or range that lead to the m/z were present in the effective yield curve.

	EY max 1	Intensity 1	EY max 2	Intensity 2	EY max 3	Intensity 3	RI 1	RI 2	RI 3
m/z	(eV)		(eV)		(eV)		(%)	(%)	(%)
16	6.2	74	9.2	31			15.4	6.5	
17	0.3	18					3.8	0.0	
26	2.0	5					1.0	0.0	
42	0.0	39					8.1	0.0	
45	0.0	94					19.6	0.0	
46	0.0	203					42.4	0.0	
58	0.4	8					1.7	0.0	
59	0.0	10					2.1	0.0	
70							0.0	0.0	
71	0.0	20					4.2	0.0	
72	2.0	33					6.9	0.0	
84	0.0	20					4.2	0.0	
87	0.0	14					2.9	0.0	
88	1.2	14					2.9	0.0	
96	0.0	13					2.7	0.0	
97	0.0	13					2.7	0.0	
98	0.2	26					5.4	0.0	
99	1.6	19					4.0	0.0	
114	0.0	34					7.1	0.0	
115	0.0	20					4.2	0.0	
124	0.2	16					3.3	0.0	
125	0.0	27					5.6	0.0	
126	0.0	97					20.3	0.0	
127	0.0	23					4.8	0.0	
137	1.6	10					2.1	0.0	
142	0.0	25					5.2	0.0	
143	0.0	133	1.0	91.0			27.8	19.0	
144	0.0	30					6.3	0.0	
146	0.0	82					17.1	0.0	
152	0.2	141					29.4	0.0	
158	1.6	50					10.4	0.0	
193	0.1	77					16.1	0.0	
196	0.1	50					10.4	0.0	
214	0.3	19					4.0	0.0	
229	0.0	117					24.4	0.0	
230	0.9	85					17.7	0.0	

Table 11. The effective yield (EY) maxima for each m/z from N-acetyl Ala-Ala-Ala, the associated intensities for each maximum, and the relative intensity (RI) as calculated compared to the most intense effective yield maximum. M/z's without EY maxima listed denote that no clear EY maxima or range that lead to the m/z were present in the effective yield curve.

	EY max 1	Intensity 1	EY max 2	Intensity 2	EY max 3	Intensity 3	RI 1	RI 2	RI 3
m/z	(eV)		(eV)		(eV)		(%)	(%)	(%)
16	6.5	7	9.2	11			0.2	0.4	0.0
17	5.8	14					0.5	0.0	0.0
26	1.6	14	6.7	27			0.5	0.9	0.0
40	0.0	10	6+	8			0.3	0.3	0.0
42	0.0	28	1.6	18	6.4	54	1.0	0.6	1.9
44	6.6	13					0.4	0.0	0.0
45	6.5	9					0.3	0.0	0.0
58	1.5	21	7.1	27			0.7	0.9	0.0
72	1.3	131					4.5	0.0	0.0
86	0.0	74	1.5	71			2.5	2.4	0.0
87	6.4	29					1.0	0.0	0.0
88	1.2	33	6.2	76			1.1	2.6	0.0
97	0 to 2	11	4.5+	9			0.4	0.3	0.0
98	0.0	54	1.4	30	60.0	23	1.9	1.0	0.8
99	1.4	132					4.5	0.0	0.0
109	0.0	31					1.1	0.0	0.0
110	0.0	71					2.4	0.0	0.0
111	0.0	116	0.9	1006			4.0	34.6	0.0
115	1.4	26	6.0	19			0.9	0.7	0.0
123	0.0	50	1.3	38			1.7	1.3	0.0
124	0.0	21					0.7	0.0	0.0
125	0.0	123	1.3	17			4.2	0.6	0.0
126							0.0	0.0	0.0
129	0.0	115	1.3	87	5+	33	4.0	3.0	1.1
130	0.9	39					1.3	0.0	0.0
			1 to						
137	0.0	23	2.5	23			0.8	0.8	0.0
138	0.0	44	0.7	21			1.5	0.7	0.0
141	0.0	65	1.3	20			2.2	0.7	0.0
143	0.0	2904	0.9	766			100.0	26.4	0.0
144							0.0	0.0	0.0
152	0.0	212					7.3	0.0	0.0
153							0.0	0.0	0.0
156	0.0	420					14.5	0.0	0.0

Table 11 continued.

	EY max 1	Intensity 1	EY max 2	Intensity 2	EY max 3	Intensity 3	RI 1	RI 2	RI 3
m/z	(eV)		(eV)		(eV)		(%)	(%)	(%)
178	0.0	448					15.4	0.0	0.0
179							0.0	0.0	0.0
181	0.0	98					3.4	0.0	0.0
182	0.0	491					16.9	0.0	0.0
183							0.0	0.0	0.0
186	6.9	16					0.6	0.0	0.0
196	0.0	65					2.2	0.0	0.0
197	0.0	97					3.3	0.0	0.0
200	0.0	172	1.4	186			5.9	6.4	0.0
201							0.0	0.0	0.0
214	0.0	364	0.9	115			12.5	4.0	0.0
227	0.0	1748					60.2	0.0	0.0
228	0.0	1691					58.2	0.0	0.0
253	0.0	157					5.4	0.0	0.0
254							0.0	0.0	0.0
255	0.0	70					2.4	0.0	0.0
271	0.0	77	1.0	20			2.7	0.7	0.0
272	0.0	180	1.0	139			6.2	4.8	0.0

Table 12. The effective yield (EY) maxima for each m/z from Ala-Ala-Ala-OMe, the associated intensities for each maximum, and the relative intensity (RI) as calculated compared to the most intense effective yield maximum. M/z's without EY maxima listed denote that no clear EY maxima or range that lead to the m/z were present in the effective yield curve.

	EY max 1	Intensity 1	EY max 2	Intensity 2	EY max 3	Intensity 3	RI 1	RI 2	RI 3
m/z	(eV)		(eV)		(eV)		(%)	(%)	(%)
16	6.0	6					2.1	0.0	0.0
26	0.8	7	8+	6			2.5	2.1	0.0
31							0.0	0.0	0.0
42	0.2	20	5 to 6	5	9.8	8	7.1	1.8	2.8
45	6.6	12					4.3	0.0	0.0
56							0.0	0.0	0.0
59							0.0	0.0	0.0
72							0.0	0.0	0.0
73							0.0	0.0	0.0
75	0.4	6					2.1	0.0	0.0
84	4.8	18					6.4	0.0	0.0
86	0.1	9					3.2	0.0	0.0
87	1.2	4	6+	6			1.4	2.1	0.0
88	1.2	20					7.1	0.0	0.0
113	0 to 2	12					4.3	0.0	0.0
123	0.9	10					3.5	0.0	0.0
141	1.9	17					6.0	0.0	0.0
157	1.6	29					10.3	0.0	0.0
158	1 to 2	8					2.8	0.0	0.0
164	1.2	7	2.5 to 4	4	8+	7	2.5	1.4	2.5
192	0.1	282					100.0	0.0	0.0
242	0 to 1	5					1.8	0.0	0.0
244							0.0	0.0	0.0

Table 13. The effective yield (EY) maxima for each m/z from N-acetyl Ala-Ala-Ala-OMe, the associated intensities for each maximum, and the relative intensity (RI) as calculated compared to the most intense effective yield maximum. M/z's without EY maxima listed denote that no clear EY maxima or range that lead to the m/z were present in the effective yield curve.

m/z	EY max 1 (eV)	Intensity 1	EY max 2 (eV)	Intensity 2	EY max 3 (eV)	Intensity 3	RI 1 (%)	RI 2 (%)	RI 3 (%)
16	6+	6					1.3	0.0	0.0
26	7.3	20	9 to 11	13			4.3	2.8	0.0
31	6.8	27					5.8	0.0	0.0
42	1.6	36	6.8	57	9 to 11	36	7.7	12.2	7.7
45							0.0	0.0	0.0
58	1.5 to 2.5	7	6.8	18			1.5	3.9	0.0
59							0.0	0.0	0.0
87	6.7	36					7.7	0.0	0.0
98	6.8	15	9 to 11	15			3.2	3.2	0.0
111	1.3	24	5+	9			5.1	1.9	0.0
113	7.4	13	9 to 11	8			2.8	1.7	0.0
125	0.1	42	1 to 2	4			9.0	0.9	0.0
126	1 to 2	7	6 to 8	5			1.5	1.1	0.0
129	1.4	467	9.3	134			100.0	28.7	0.0
130							0.0	0.0	0.0
141	0.1	24	6.1	21			5.1	4.5	0.0
156	0.1	53					11.3	0.0	0.0
157	1.4	15					3.2	0.0	0.0
182	0.0	28	1.6	16			6.0	3.4	0.0
186	7.6	15					3.2	0.0	0.0
200	1.2	190					40.7	0.0	0.0
201							0.0	0.0	0.0
227	0.0	176	1.2	22			37.7	4.7	0.0
228	1.2	52					11.1	0.0	0.0
272	1 to 2	6					1.3	0.0	0.0
286	1.6	58					12.4	0.0	0.0

Table 14. Comparison of the “corners” of the Φ and Ψ potential energy surfaces for the L- and D-stereoisomers of the N-methyl alanine dimer. The VEAE values are given in eV for each Φ and Ψ combination where Φ and Ψ are given in degrees. The VEAE values are compared between the inverse Φ and Ψ angles for the stereoisomers so that $\Phi = -180$ and $\Psi = 180$ of the L-stereoisomer is compared with the $\Phi = 180$ and $\Psi = -180$ of the D-stereoisomer. All other comparisons are made in the same manner.

L-stereoisomer		Φ	
Ψ		-180	-60
	180	0.62	0.51
	60	0.52	0.36
D-stereoisomer		Φ	
Ψ		180	60
	-180	0.62	0.51
	-60	0.50	0.47

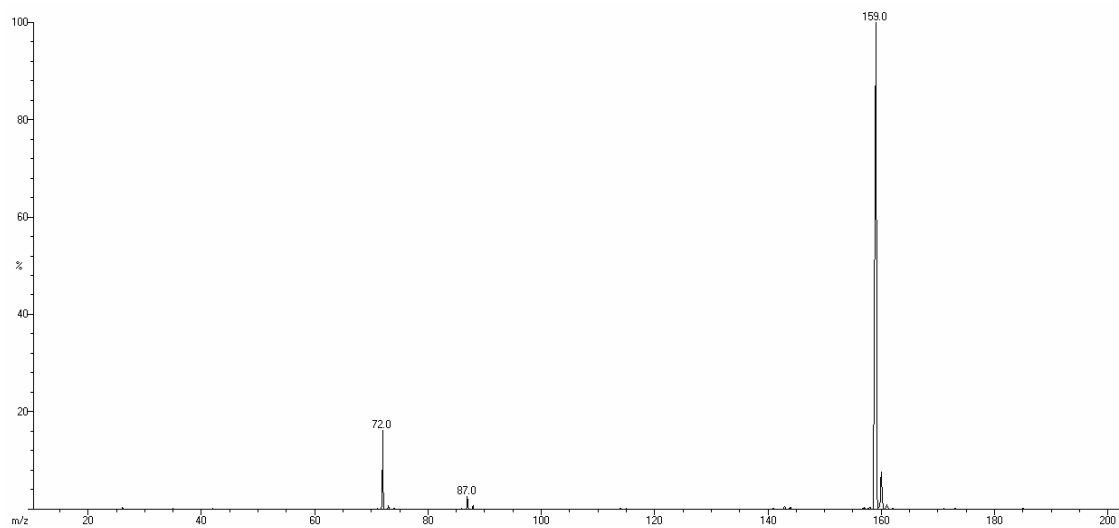


Figure 26. Resonant electron capture spectrum produced from alanine dimer with electron energy of ~ 1 eV. The samples were introduced into the JEOL 600H – MS as a dry solid on the in-beam probe and were loaded on the in-beam probe as a solution or suspension in volatile solvent and dried by evaporation or heating before introduction to the instrument vacuum system. The ion source temperature was between 200 and 240 °C.

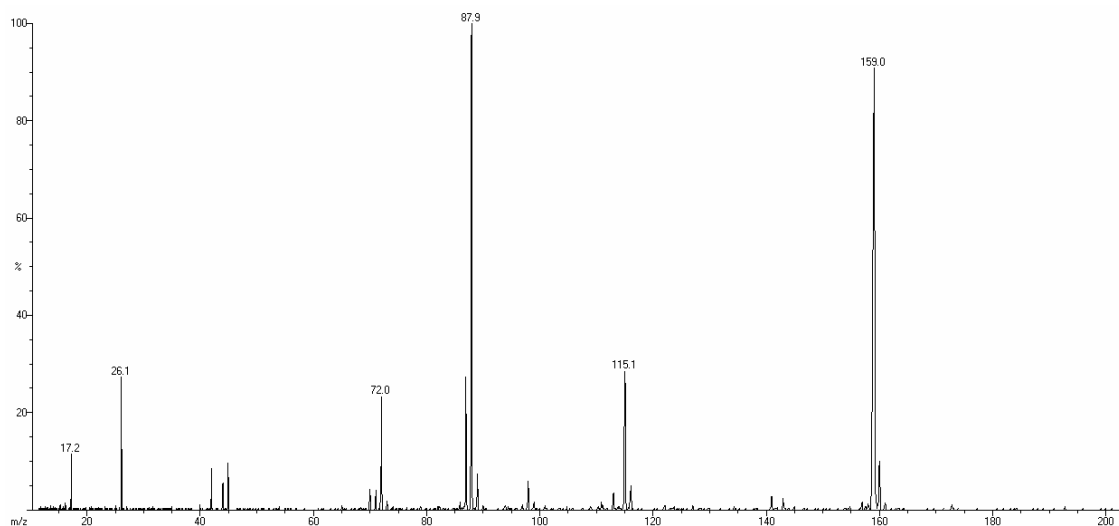


Figure 27. Resonant electron capture spectrum produced from alanine dimer with electron energy of ~ 6 eV. The samples were introduced into the JEOL 600H – MS as a dry solid on the in-beam probe and were loaded on the in-beam probe as a solution or suspension in volatile solvent and dried by evaporation or heating before introduction to the instrument vacuum system. The ion source temperature was between 200 and 240 °C.

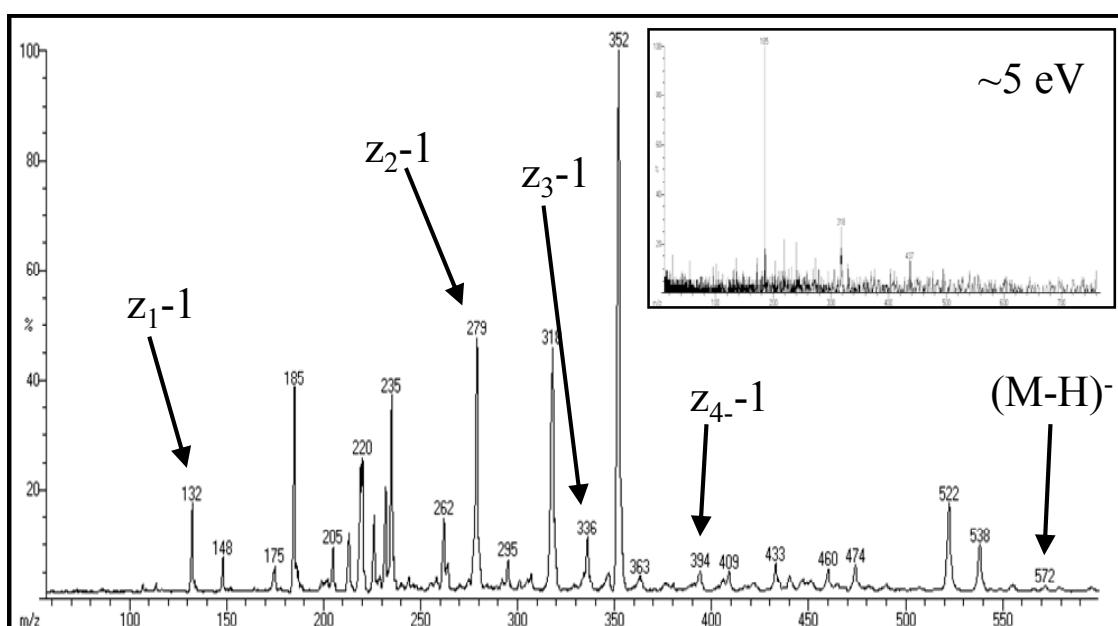


Figure 28. The resonance electron capture mass spectrum from methionine enkephalin shows all four possible z-1 type and (M-H)⁻ ions. The ions were observed at electron energies ~1 -1.5 eV. The inset spectrum was produced under the same experimental conditions except the electron energy was set at ~5-6 eV. The samples were introduced into the JEOL 600H – MS as a dry solid on the in-beam probe and were loaded on the in-beam probe as a solution or suspension in volatile solvent and dried by evaporation or heating before introduction to the instrument vacuum system. The ion source temperature was between 200 and 240 °C.

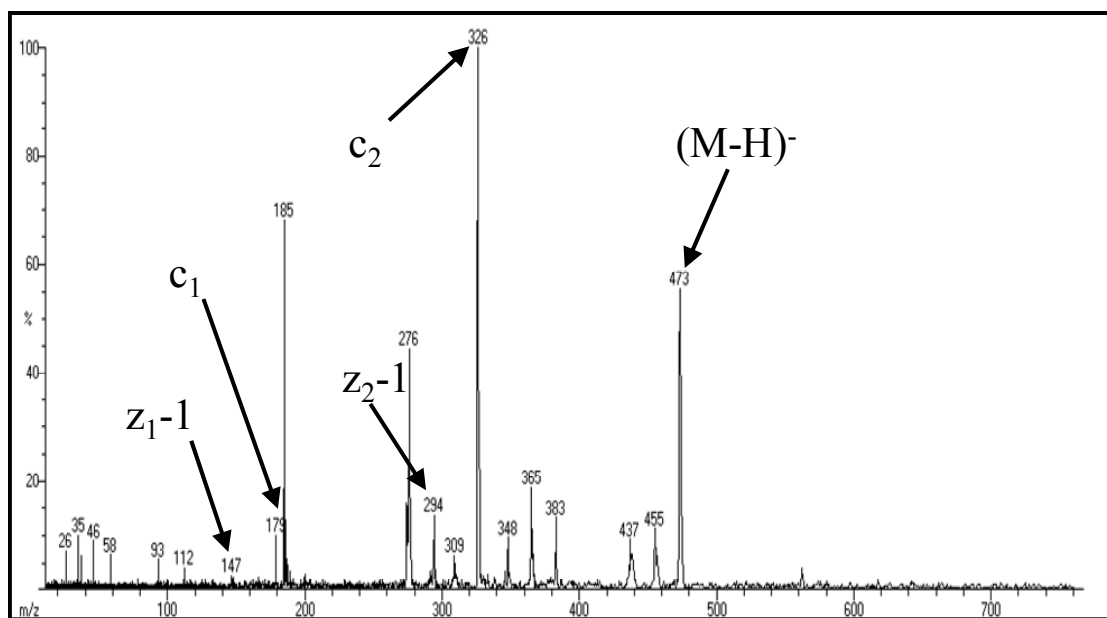


Figure 29. The resonance electron capture mass spectrum of YFF amide shows peaks for c_1 , c_2 , z_1-1 , z_2-1 , and $(M-H)^-$ ions at electron energies between ~ 0.5 - 1.5 eV. The samples were introduced into the JEOL 600H – MS as a dry solid on the in-beam probe and were loaded on the in-beam probe as a solution or suspension in volatile solvent and dried by evaporation or heating before introduction to the instrument vacuum system. The ion source temperature was between 200 and 240 °C.

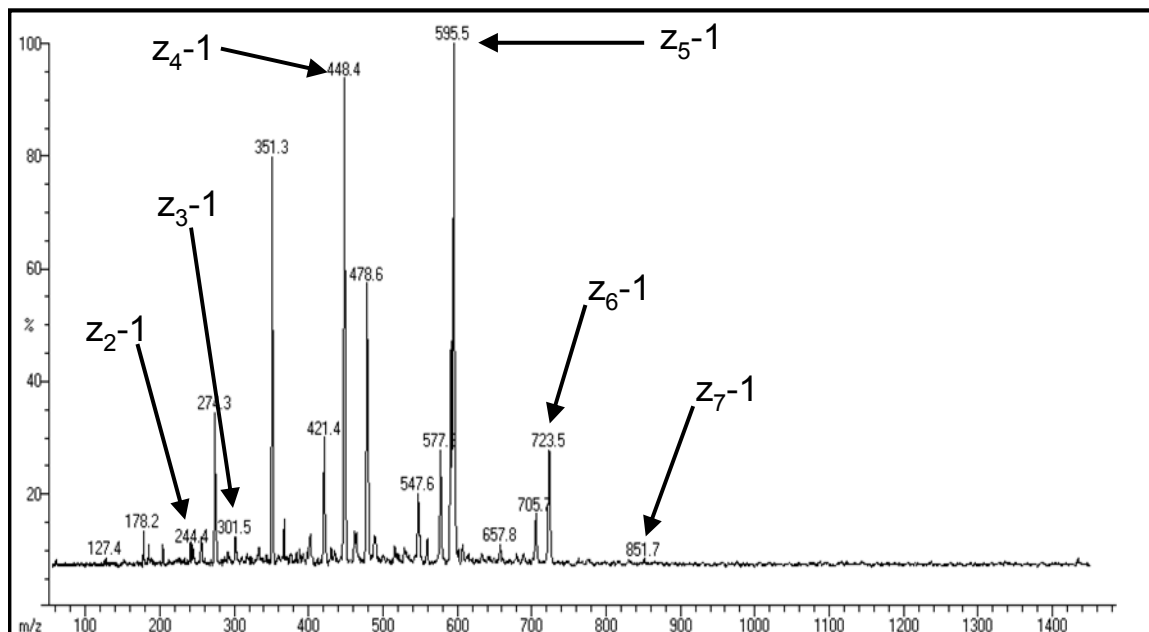


Figure 30. The resonance electron capture mass spectrum of substance p shows prominent peaks for the z_n-1 series ($n = 2-7$) with the most abundant peaks of z_4-1 and z_5-1 . Not surprisingly, no z_8-1 or $z_{10}-1$ ions are observed as these species would result from cleavage at proline residues. The samples were introduced into the JEOL 600H – MS as a dry solid on the in-beam probe and were loaded on the in-beam probe as a solution or suspension in volatile solvent and dried by evaporation or heating before introduction to the instrument vacuum system. The ion source temperature was between 200 and 240 °C.

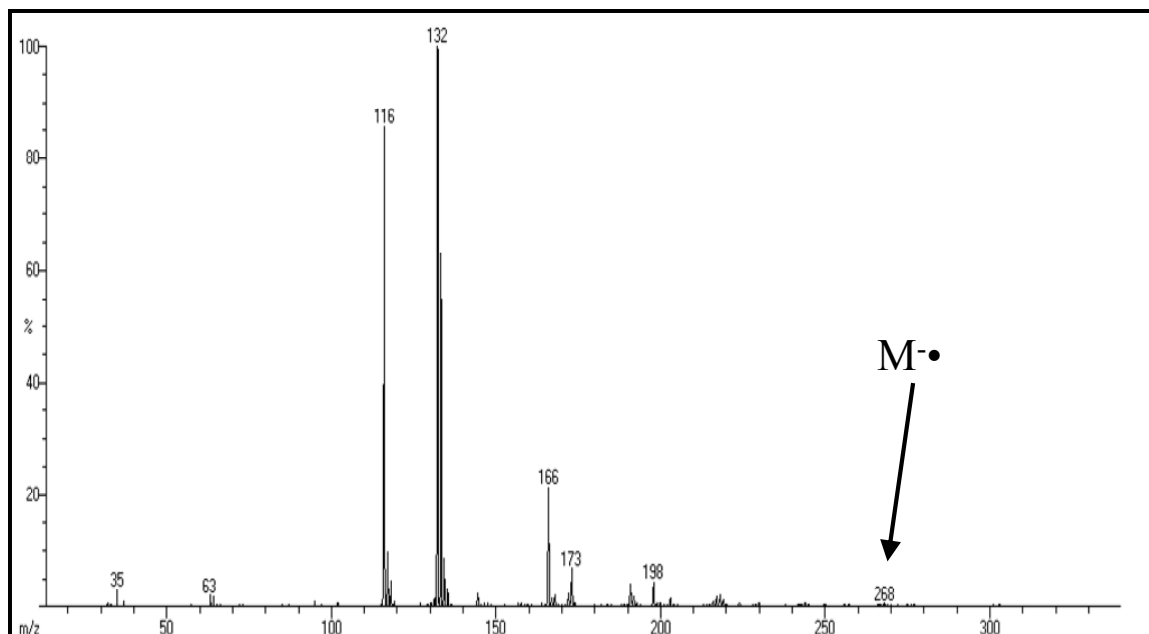


Figure 31. The resonance electron capture mass spectrum of cystine dimethyl ester diHCl shows the M^{\bullet} ion and other ions from the interaction of electrons with energies $\sim 1 - 1.5$ eV. The samples were introduced into the JEOL 600H – MS as a dry solid on the in-beam probe and were loaded on the in-beam probe as a solution or suspension in volatile solvent and dried by evaporation or heating before introduction to the instrument vacuum system. The ion source temperature was between 200 and 240 °C.

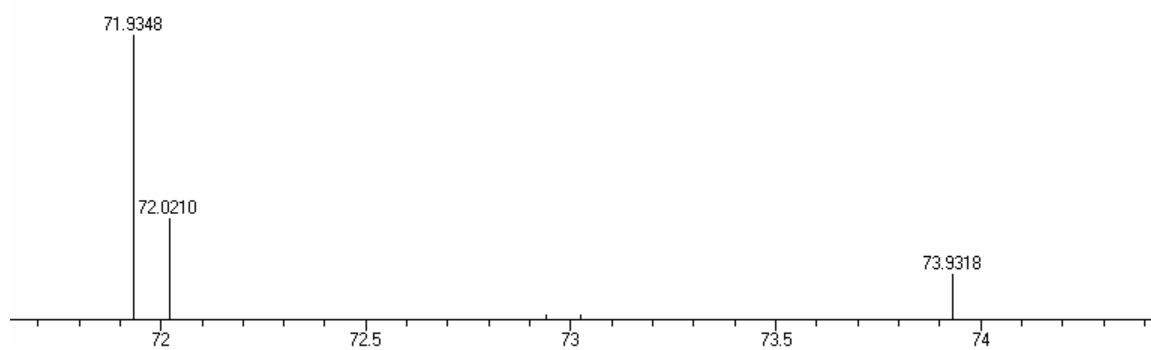


Figure 32. High resolution negative ion mass spectrum of the alanine dimer fragment ion m/z 72, $C_3H_4O_2$, or $(z-1)$ ion at ~ 1 eV electron energy with the $^{35}Cl^{37}Cl^-$ and $^{37}Cl_2^-$ ions as internal reference ions. The samples were introduced into the JEOL 600H – MS as a dry solid on the in-beam probe and were loaded on the in-beam probe as a solution or suspension in volatile solvent and dried by evaporation or heating before introduction to the instrument vacuum system. The ion source temperature was between 200 and 240 °C.

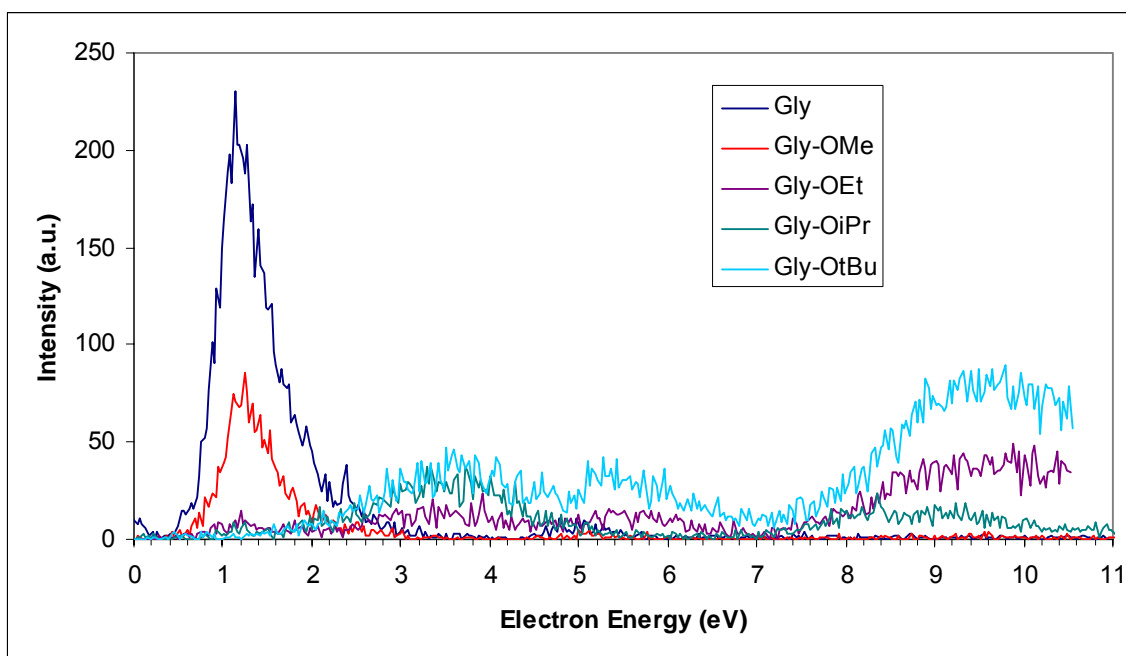


Figure 33. Effective yield curves for the formation of the carboxylate anion, (M-X)-, from glycine (blue) and its esters, methyl (red), ethyl (purple), isopropyl (green), and t-butyl (aqua). The samples were introduced into the instrument by heating dry solid loaded in a capillary in the direct insertion probe.

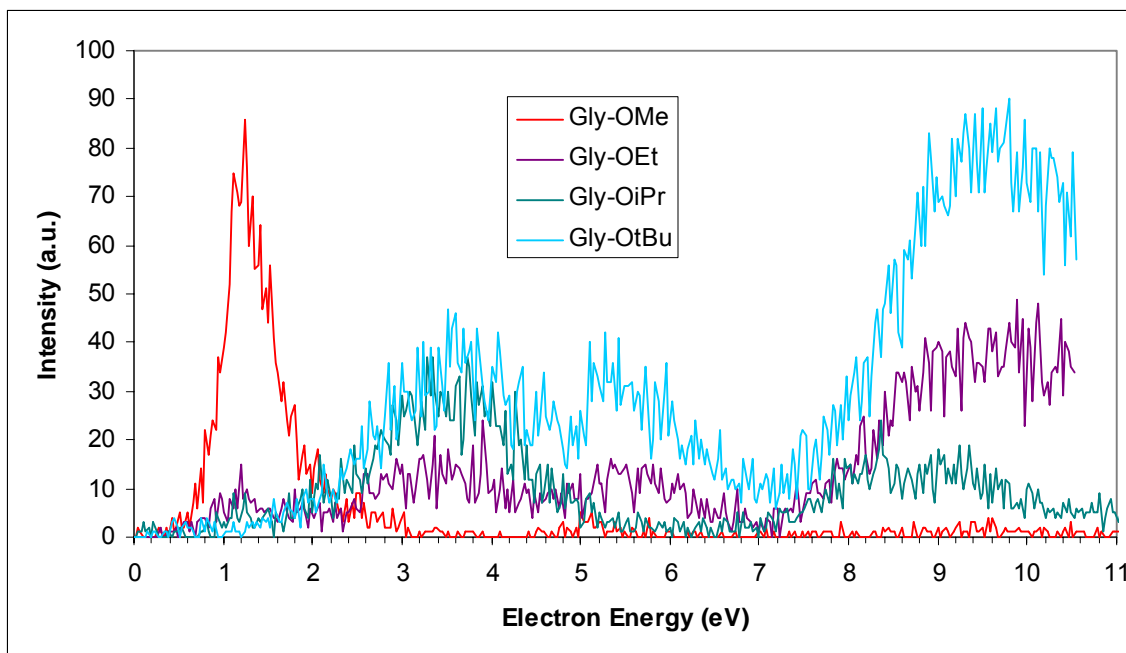


Figure 34. Effective yield curves for the formation of the carboxylate anion, (M-X)-, from the esters of glycine, methyl (red), ethyl (purple), isopropyl (green), and t-butyl (aqua). The samples were introduced into the instrument by heating dry solid loaded in a capillary in the direct insertion probe.

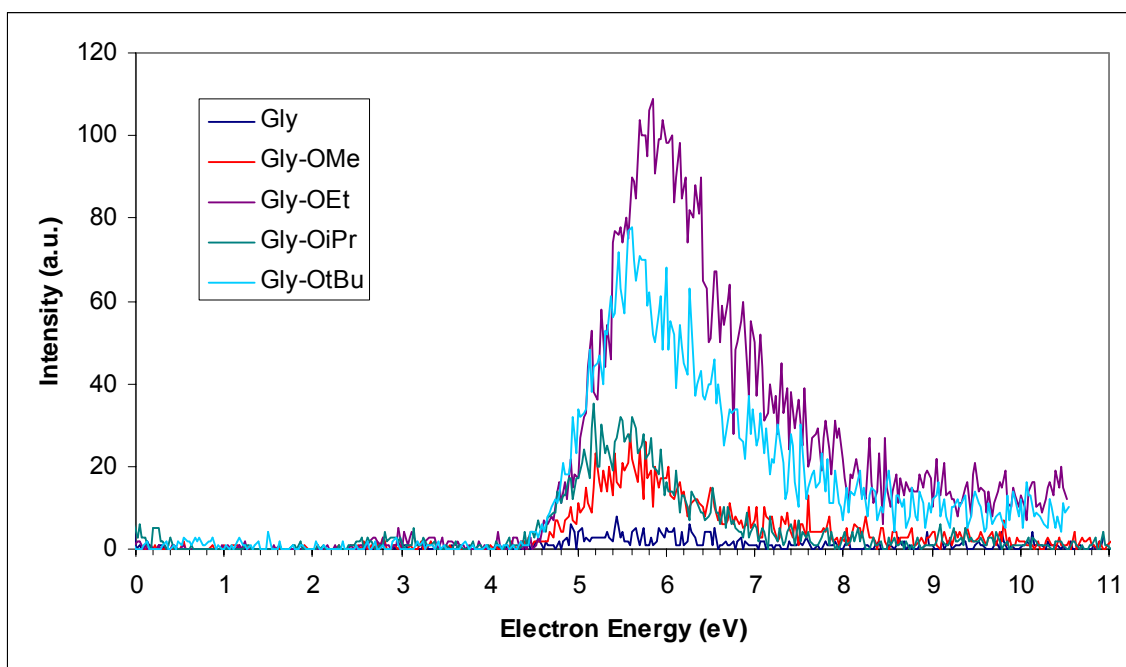


Figure 35. Effective yield curves for the formation of the -OX anion from glycine (blue) and its esters; methyl (red), ethyl (purple), isopropyl (green), and t-butyl (aqua). OX is the dehydrogenated alcohol of the ester, i.e. -OMe from the glycine methyl ester, and -OH in the case of the underivatized glycine. The samples were introduced into the instrument by heating dry solid loaded in a capillary in the direct insertion probe.

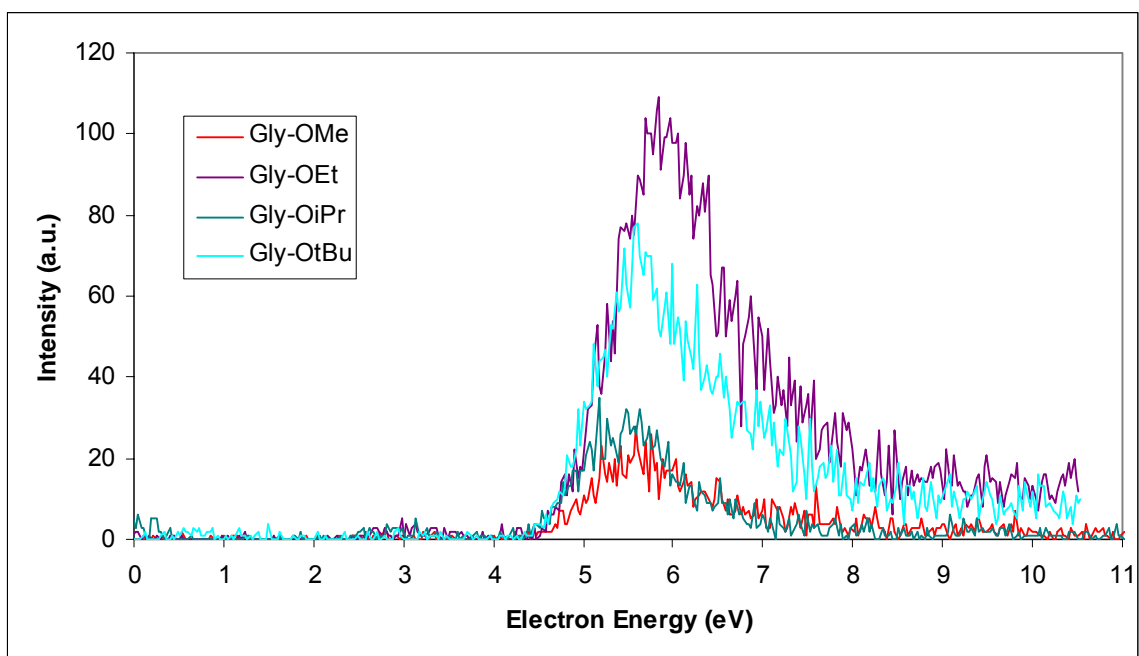


Figure 36. Effective yield curves for the formation of the -OX anion from the esters of glycine; methyl (red), ethyl (purple), isopropyl (green), and t-butyl (aqua). OX is the dehydrogenated alcohol of the ester, i.e. -OMe from the glycine methyl ester, and -OH in the case of the underivatized glycine. The samples were introduced into the instrument by heating dry solid loaded in a capillary in the direct insertion probe.

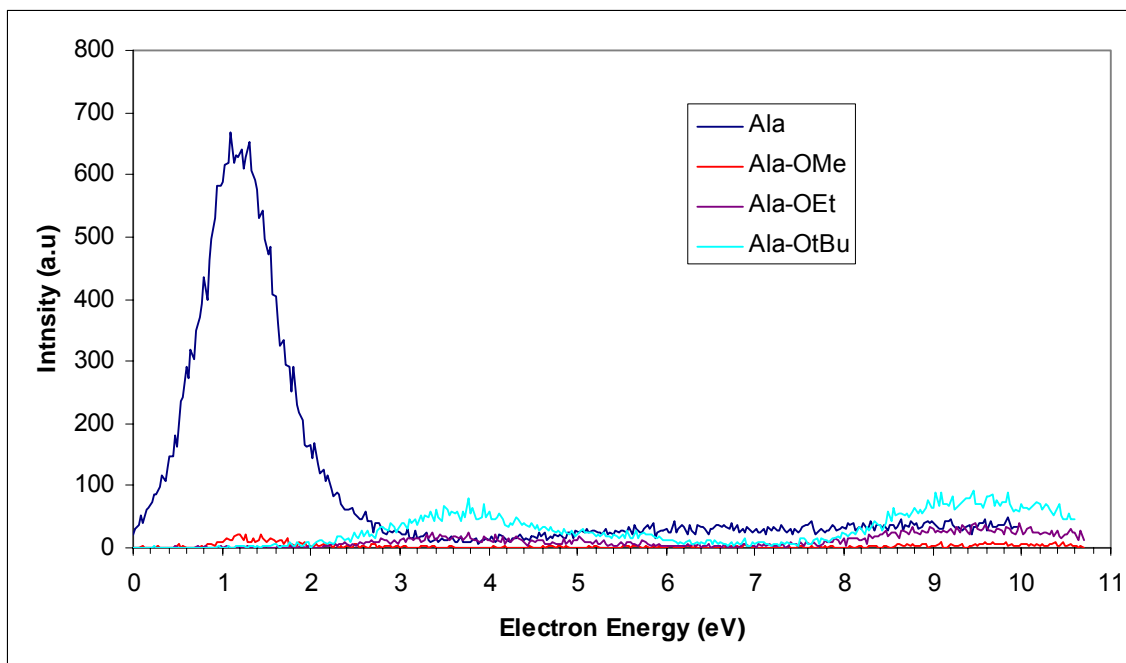


Figure 37. Effective yield curves for the formation of the carboxylate anion, (M-X)-, from alanine (blue) and its esters; methyl (red), ethyl (purple), and t-butyl (aqua). The samples were introduced into the instrument by heating dry solid loaded in a capillary in the direct insertion probe.

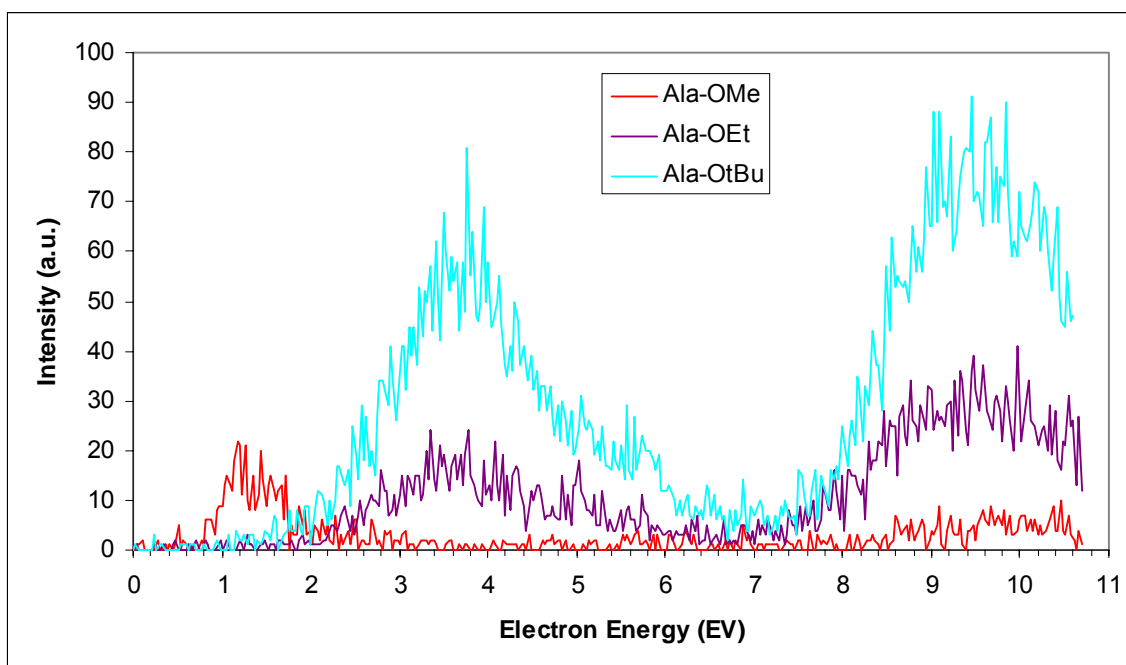


Figure 38. Effective yield curves for the formation of the carboxylate anion, (M-X)-, from the esters of alanine; methyl (red), ethyl (purple), and t-butyl (aqua). The samples were introduced into the instrument by heating dry solid loaded in a capillary in the direct insertion probe.

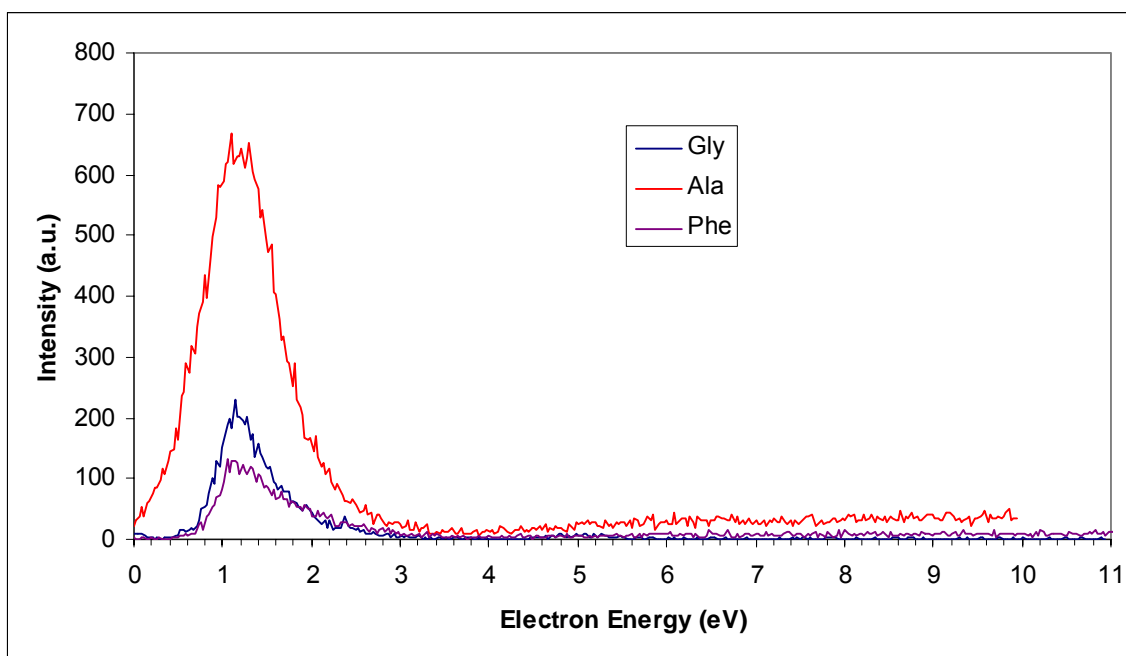


Figure 39. Effective yield curves for the formation of the carboxylate anion, (M-H)-, from glycine (blue), alanine (red), and phenylalanine (purple). The samples were introduced into the instrument by heating dry solid loaded in a capillary in the direct insertion probe.

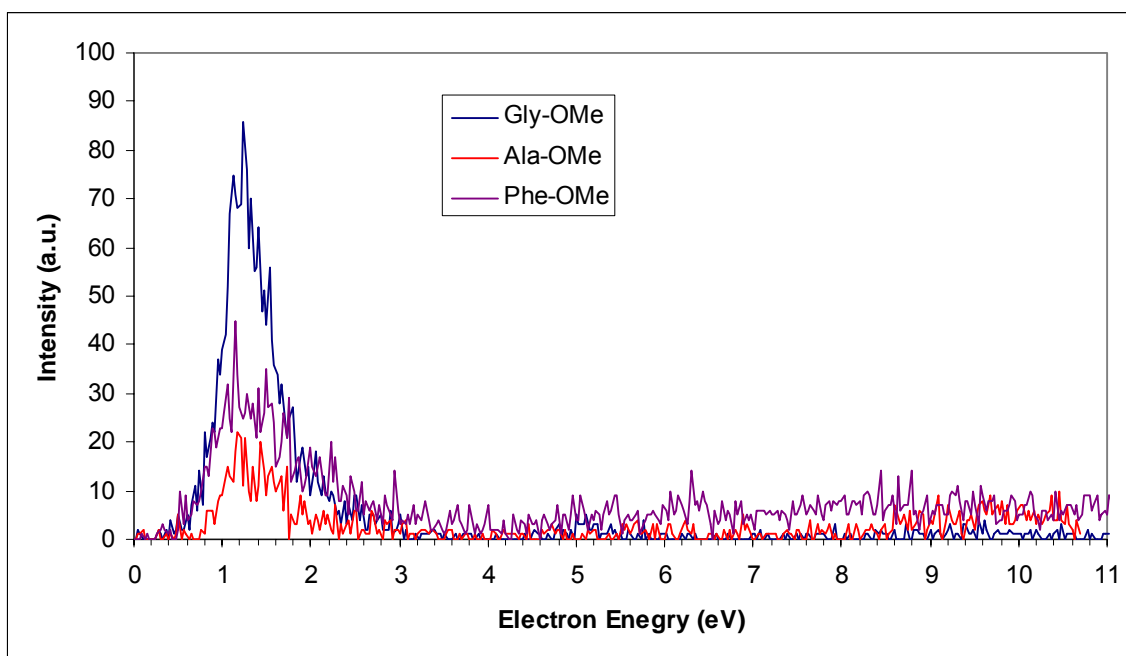


Figure 40. Effective yield curves for the formation of the carboxylate anion, (M-Me)-, from the methyl esters of glycine (blue), alanine (red), and phenylalanine (purple). The samples were introduced into the instrument by heating dry solid loaded in a capillary in the direct insertion probe.

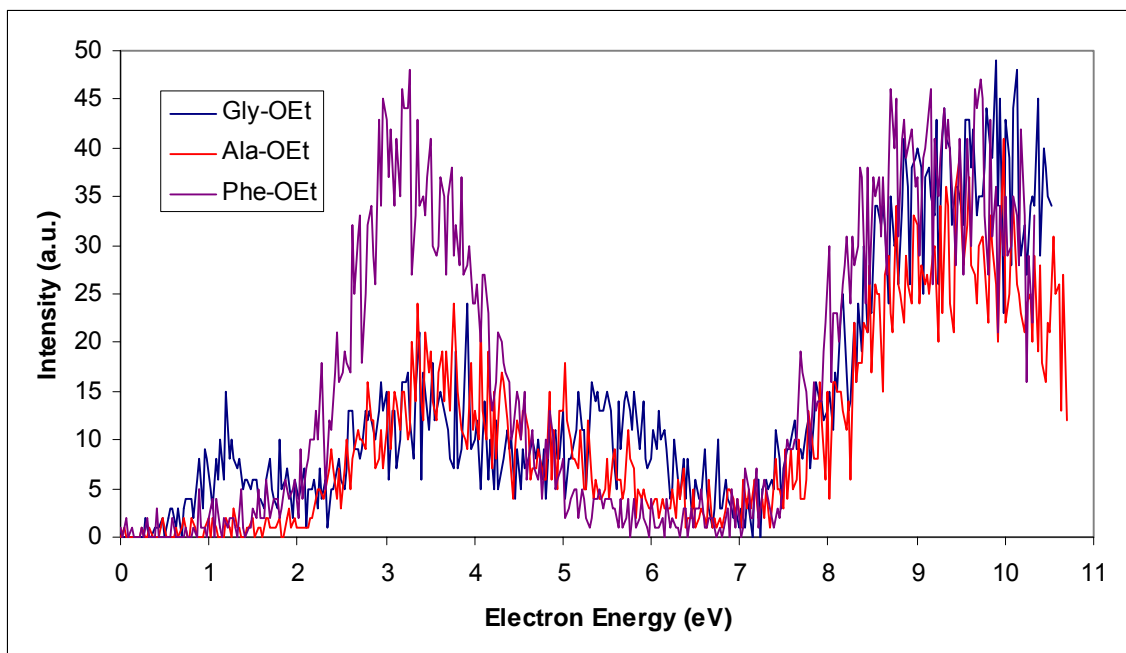


Figure 41. Effective yield curves for the formation of the carboxylate anion, (M-Et)-, from the ethyl esters of glycine (blue), alanine (red), and phenylalanine (purple). The samples were introduced into the instrument by heating dry solid loaded in a capillary in the direct insertion probe.

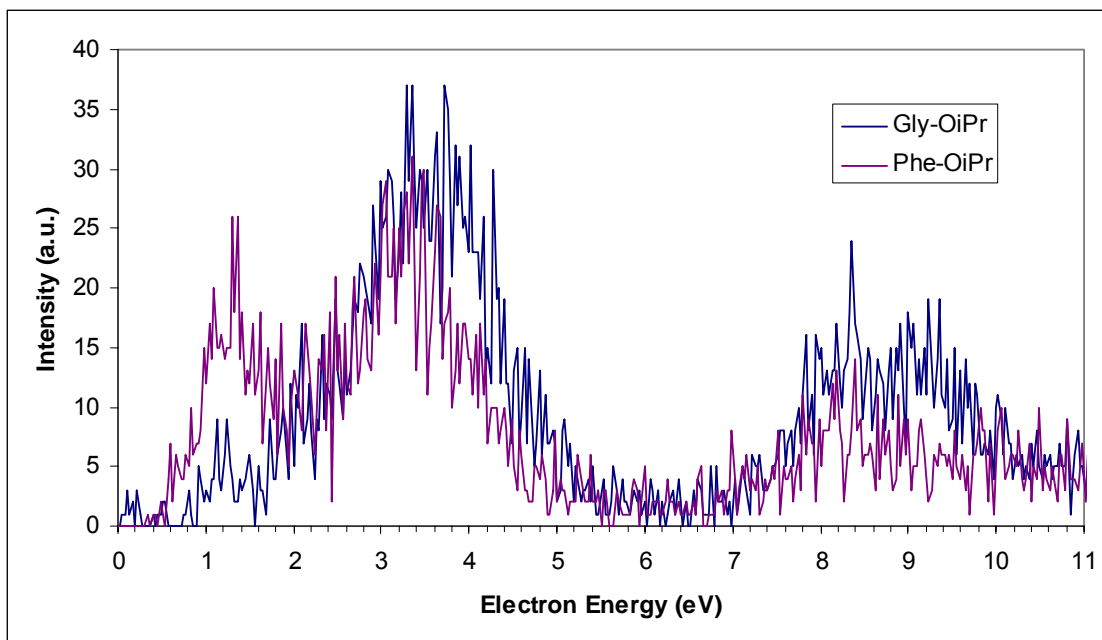


Figure 42. Effective yield curves for the formation of the carboxylate anion, (M-iPr)-, from the isopropyl esters of glycine (blue) and phenylalanine (purple). The samples were introduced into the instrument by heating dry solid loaded in a capillary in the direct insertion probe.

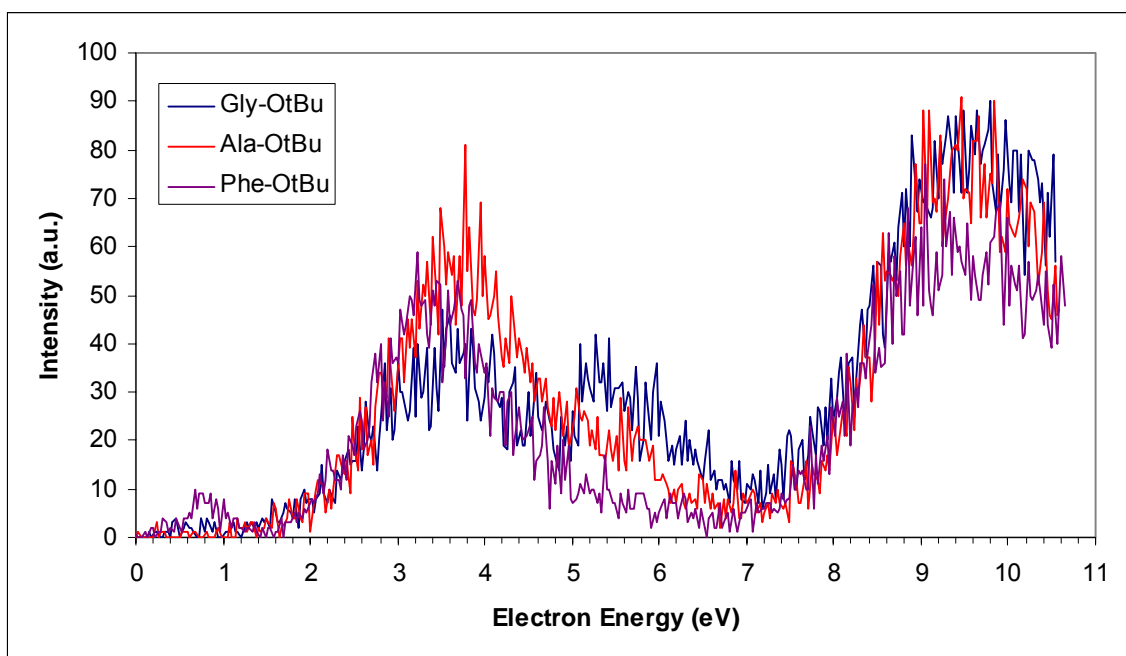


Figure 43. Effective yield curves for the formation of the carboxylate anion, (M-tBu)-, from the t-butyl esters of glycine (blue), alanine (red), and phenylalanine (purple). The samples were introduced into the instrument by heating dry solid loaded in a capillary in the direct insertion probe.

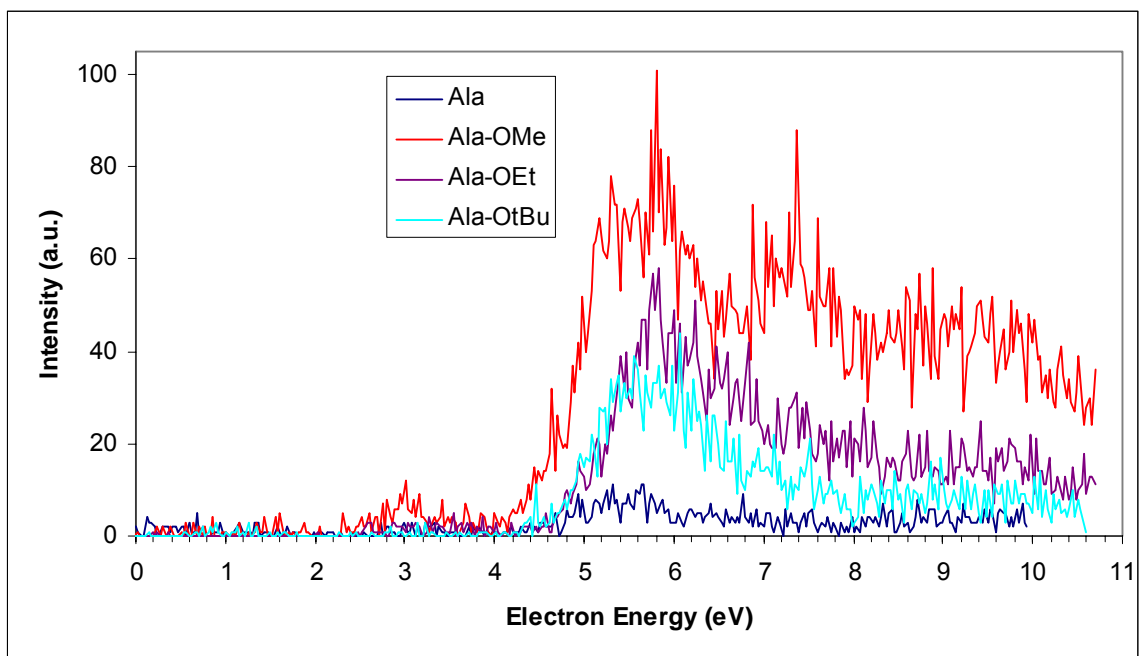


Figure 44. Effective yield curves for the formation of the -OX anion from glycine (blue) and its esters; methyl (red), ethyl (purple), and t-butyl (aqua). -OX is the dehydrogenated alcohol of the ester, i.e. -OMe from the alanine methyl ester, and -OH in the case of the underivatized glycine. The samples were introduced into the instrument by heating dry solid loaded in a capillary in the direct insertion probe.

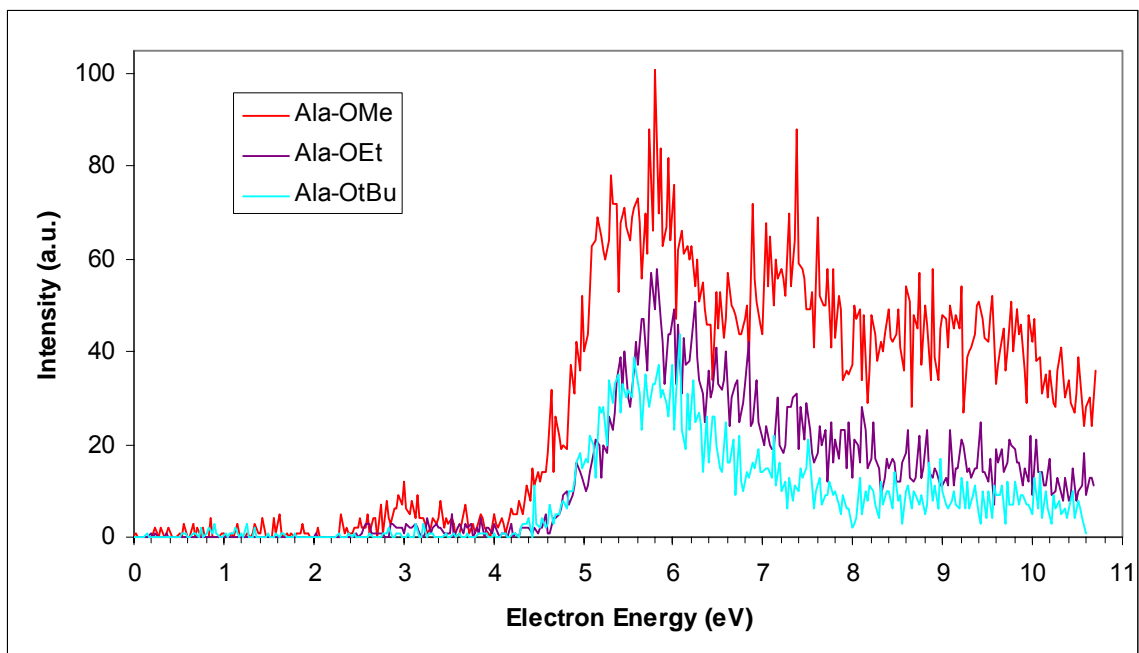


Figure 45. Effective yield curves for the formation of the -OX anion from the esters of alanine; methyl (red), ethyl (purple), and t-butyl (aqua). -OX is the dehydrogenated alcohol of the ester, i.e. -OMe from the glycine methyl ester. The samples were introduced into the instrument by heating dry solid loaded in a capillary in the direct insertion probe.

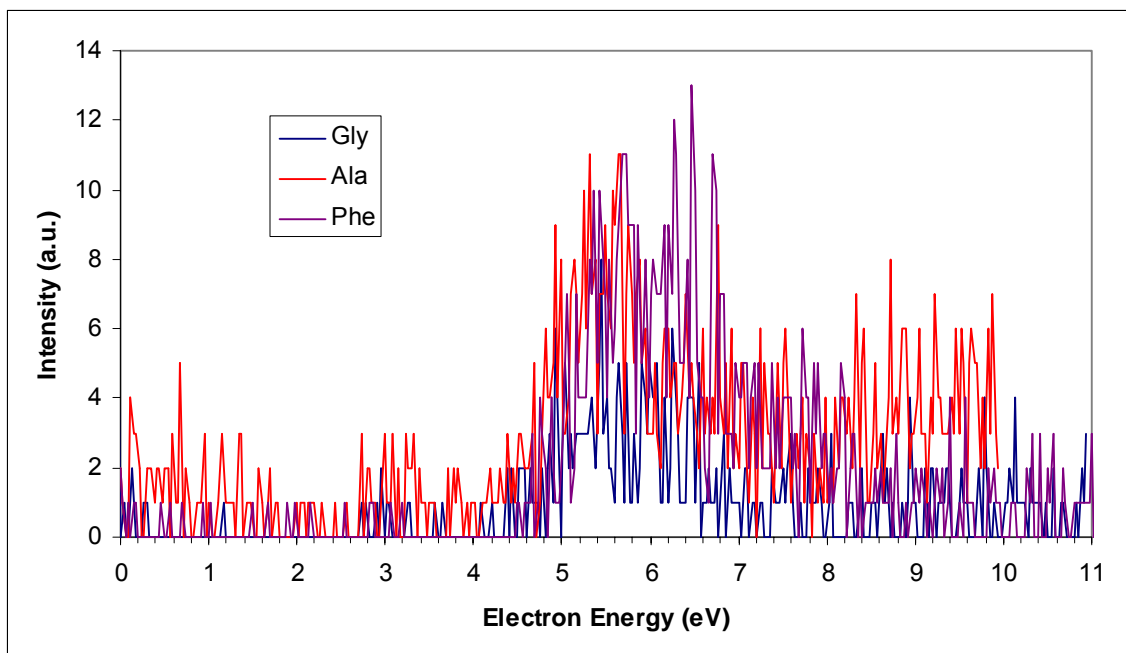


Figure 46. Effective yield curves for the formation of the hydroxyl anion, $-\text{OH}$, from glycine (blue), alanine (red), and phenylalanine (purple). The samples were introduced into the instrument by heating dry solid loaded in a capillary in the direct insertion probe.

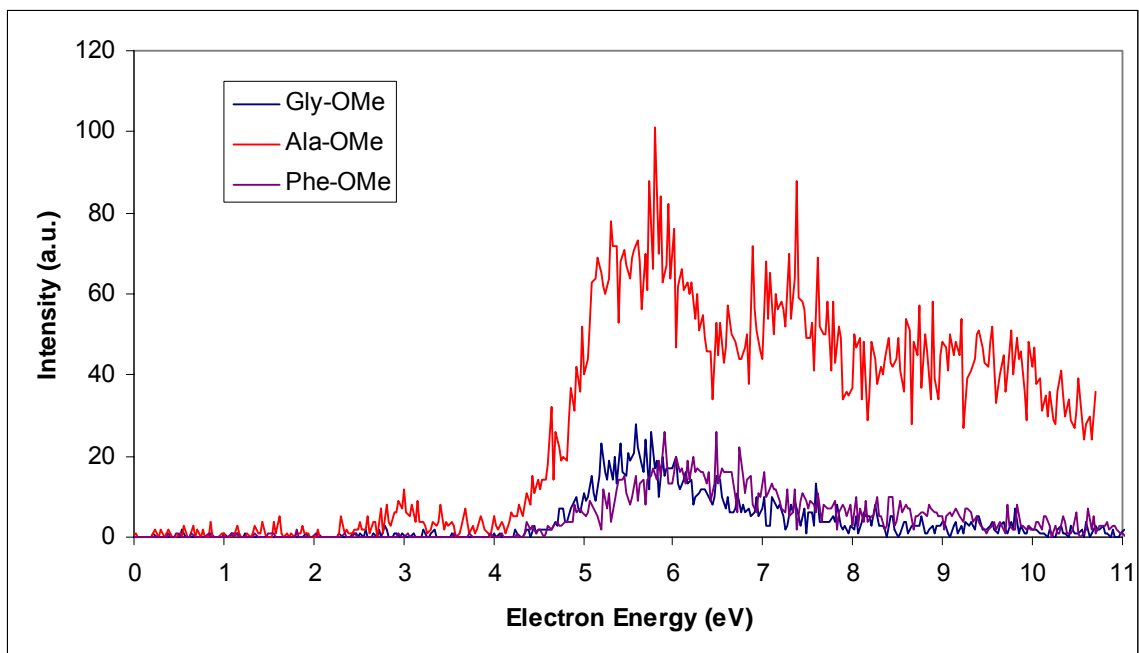


Figure 47. Effective yield curves for the formation of the methoxy anion, -OMe, from the methyl esters of glycine (blue), alanine (red), and phenylalanine (purple). The samples were introduced into the instrument by heating dry solid loaded in a capillary in the direct insertion probe.

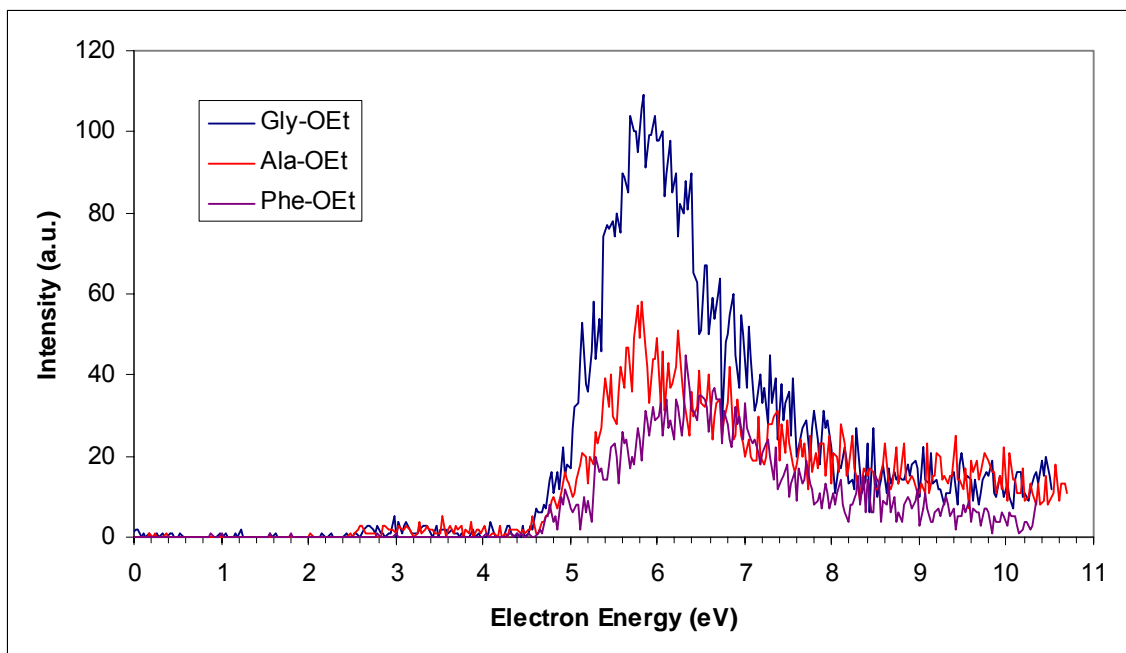


Figure 48. Effective yield curves for the formation of the ethoxy anion, -OEt, from the ethyl esters of glycine (blue), alanine (red), and phenylalanine (purple). The samples were introduced into the instrument by heating dry solid loaded in a capillary in the direct insertion probe.

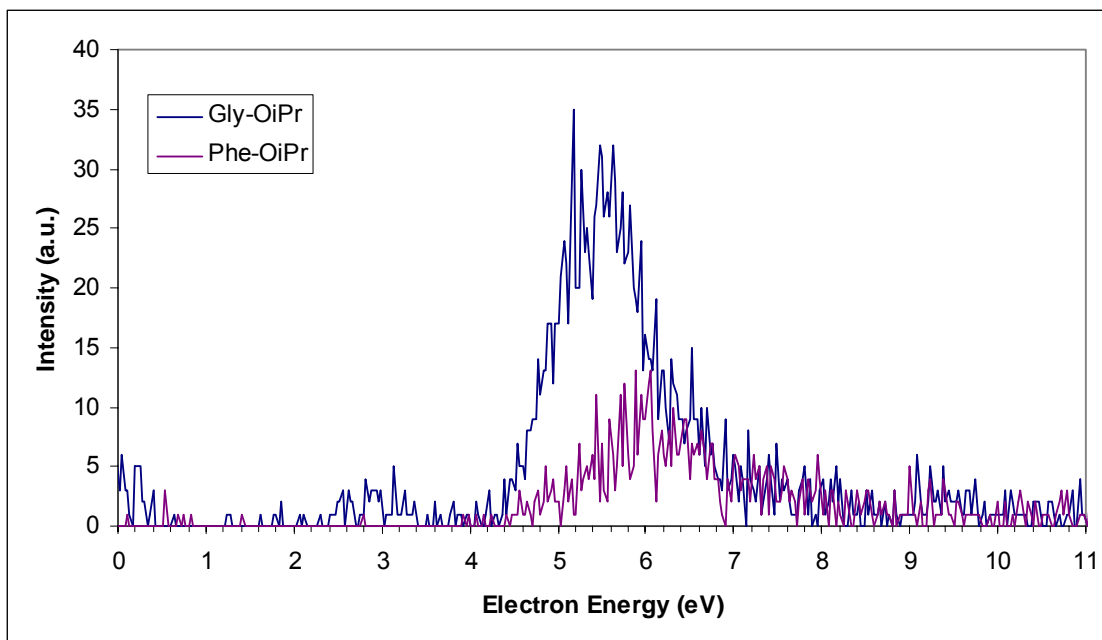


Figure 49. Effective yield curves for the formation of the iso-propyl anion, -OiPr, from the isopropyl esters of glycine (blue) and phenylalanine (purple). The samples were introduced into the instrument by heating dry solid loaded in a capillary in the direct insertion probe.

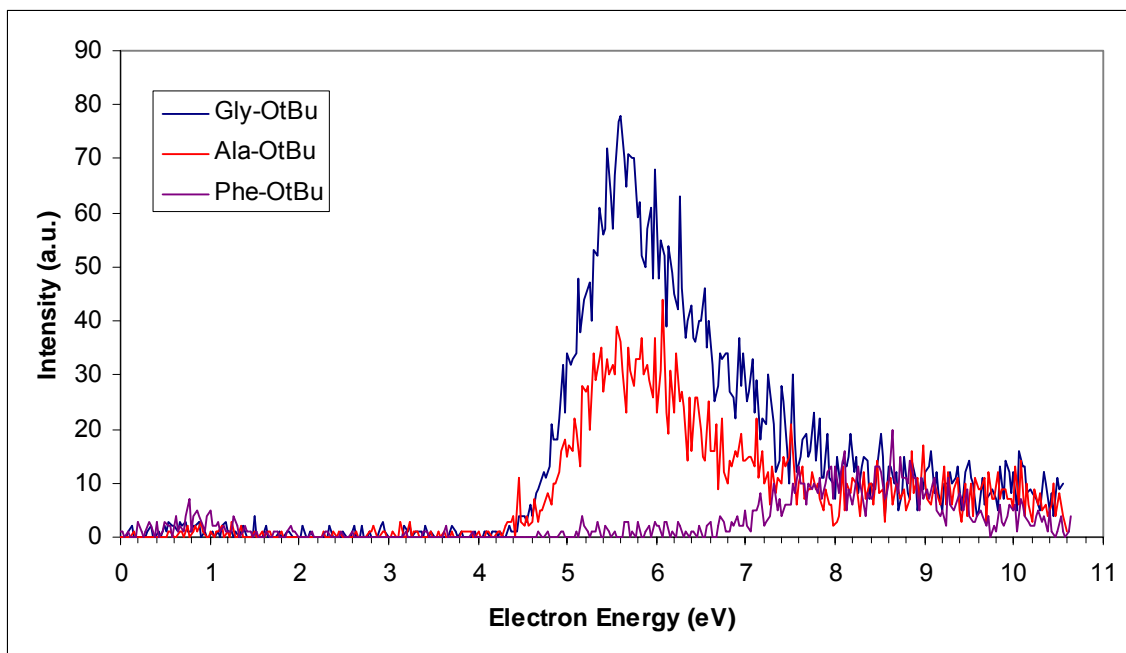


Figure 50. Effective yield curves for the formation of the t-butoxy anion, $-\text{OtBu}$, from the t-butyl esters of glycine (blue), alanine (red), and phenylalanine (purple). The samples were introduced into the instrument by heating dry solid loaded in a capillary in the direct insertion probe.

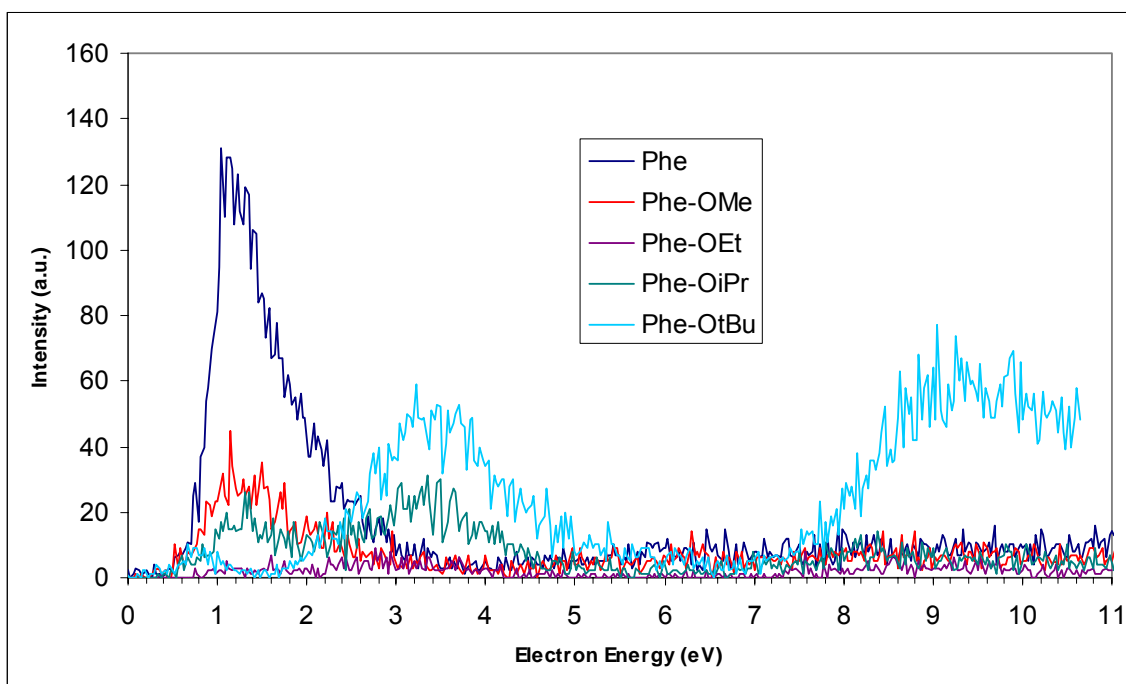


Figure 51. Effective yield curves for the formation of the carboxylate anion, (M-X)-, from phenylalanine (blue) and its esters; methyl (red), ethyl (purple), isopropyl (green), and t-butyl (aqua). The samples were introduced into the instrument by heating dry solid loaded in a capillary in the direct insertion probe.

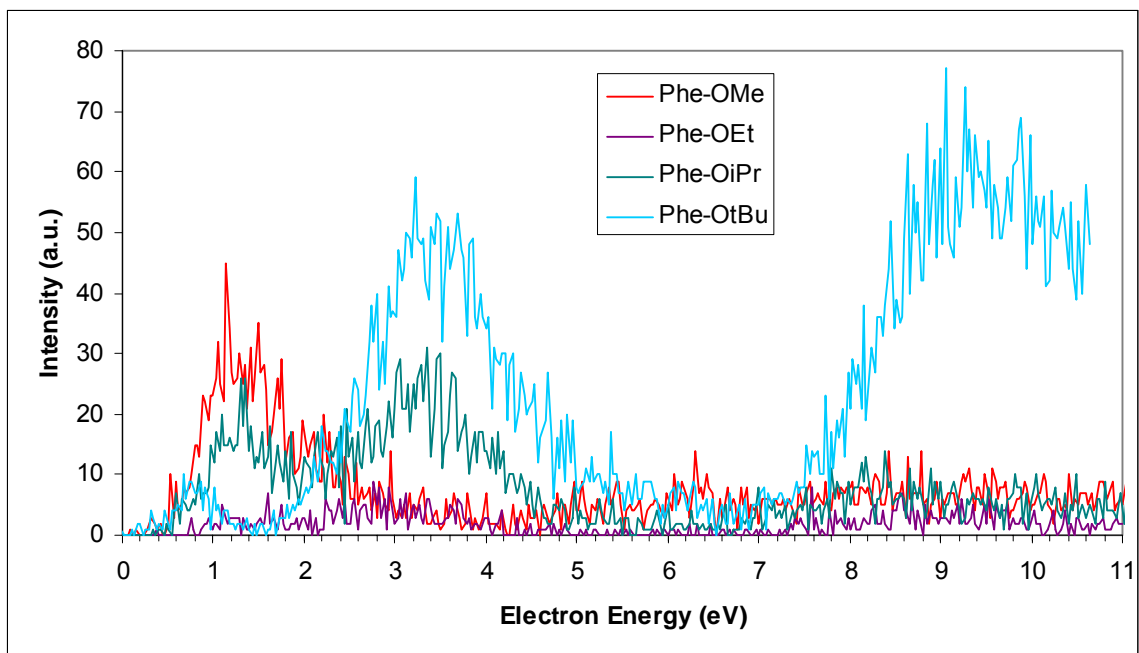


Figure 52. Effective yield curves for the formation of the carboxylate anion, (M-X)-, from the esters of phenylalanine; methyl (red), ethyl (purple), isopropyl (green), and t-butyl (aqua). The samples were introduced into the instrument by heating dry solid loaded in a capillary in the direct insertion probe.

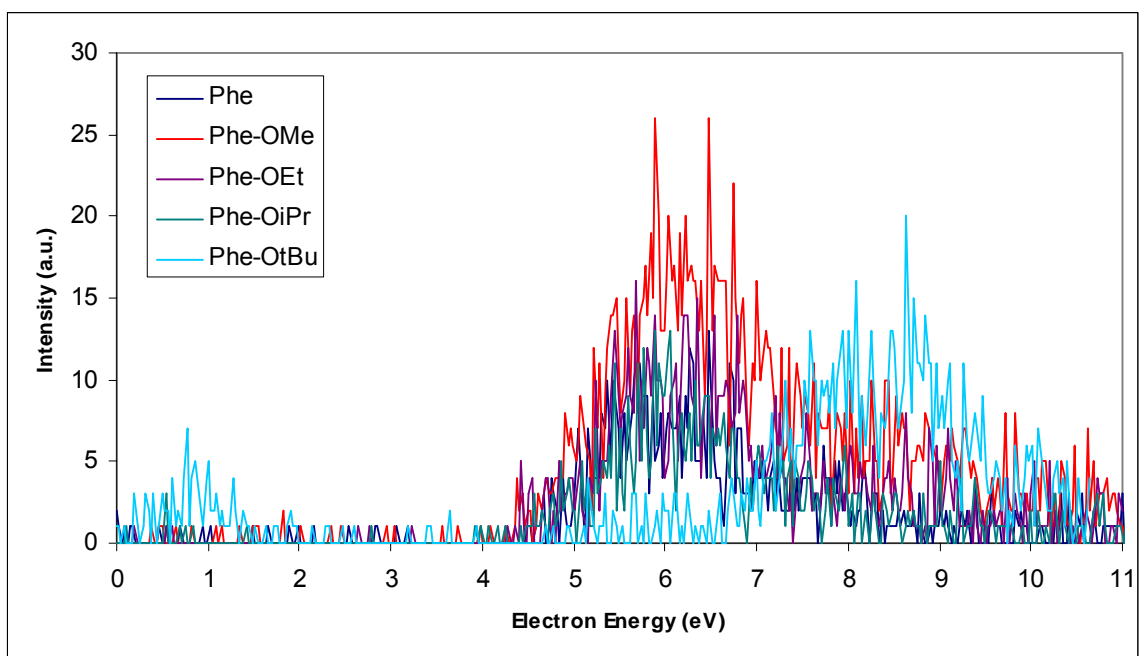


Figure 53. Effective yield curves for the formation of the -OX anion from phenylalanine (blue) and its esters; methyl (red), ethyl (purple), isopropyl (green), and t-butyl (aqua). -OX is the dehydrogenated alcohol of the ester, i.e. -OMe from the phenylalanine methyl ester, and -OH in the case of the underivatized glycine. The samples were introduced into the instrument by heating dry solid loaded in a capillary in the direct insertion probe.

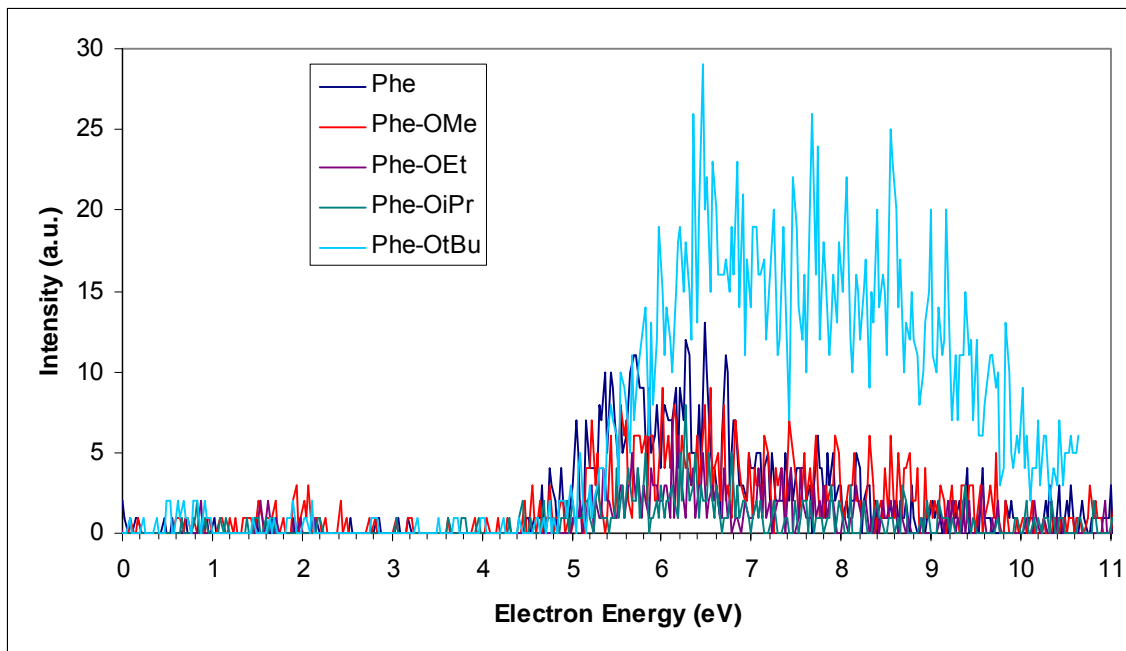


Figure 54. Effective yield curves for the formation of the $-R$ anion from phenylalanine (blue) and its esters; methyl (red), ethyl (purple), isopropyl (green), and t-butyl (aqua). The samples were introduced into the instrument by heating dry solid loaded in a capillary in the direct insertion probe.

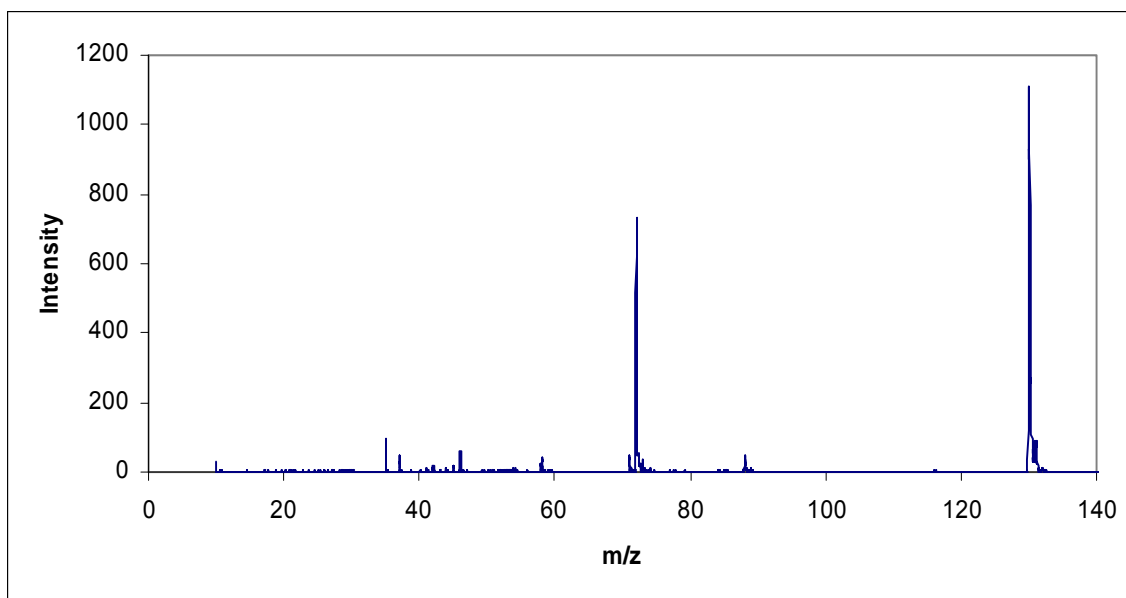


Figure. 55. The REC-MS of N-Acetyl Alanine for ions generated by scanning electron energies from 0 - ~10 eV. The sample was introduced into the instrument by heating dry solid loaded in a capillary in the direct insertion probe. The ion source temperature was 52 °C and the direct insertion probe temperature was 90 °C.

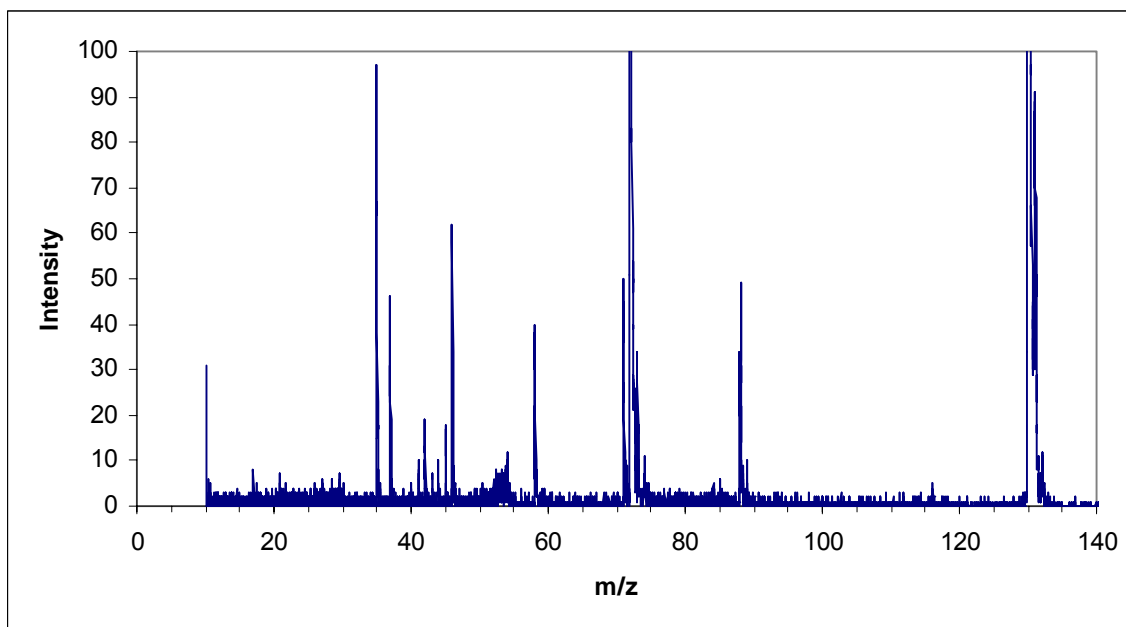


Figure 56. The REC-MS of N-Acetyl Alanine for ions generated by scanning electron energies from 0 - ~10 eV. The sample was introduced into the instrument by heating dry solid loaded in a capillary in the direct insertion probe. The ion source temperature was 52 °C and the direct insertion probe temperature was 90 °C.

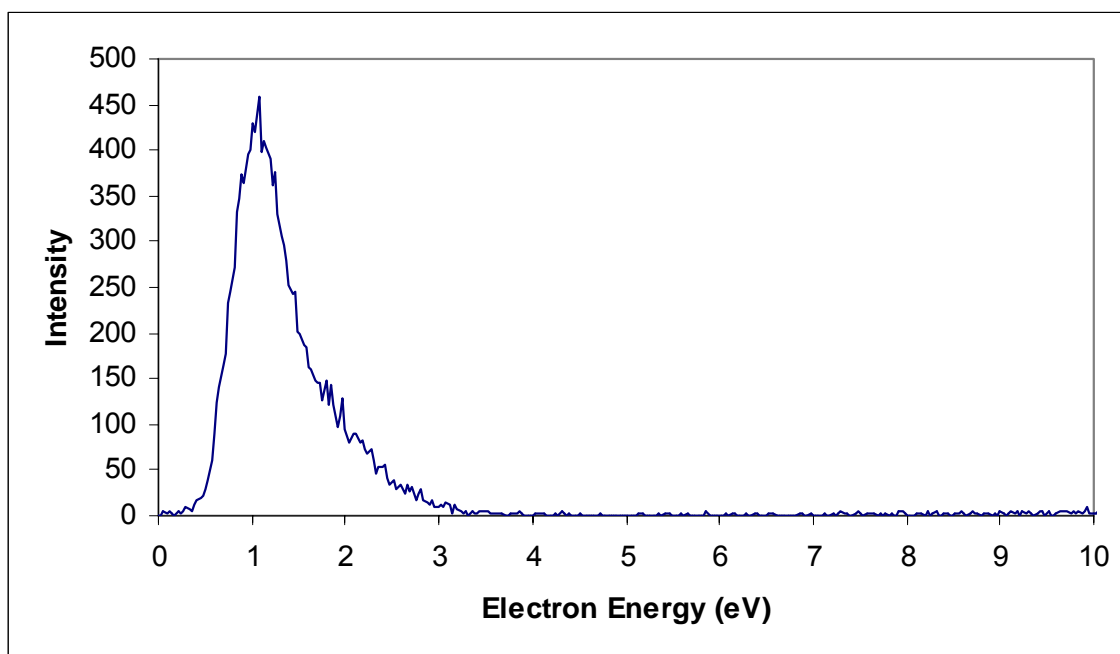


Figure 57. Effective yield curve for the (M-H)⁻ ion with m/z 130 from N-Acetyl Alanine. The sample was introduced into the instrument by heating dry solid loaded in a capillary in the direct insertion probe. The ion source temperature was 52 °C and the direct insertion probe temperature was 90 °C.

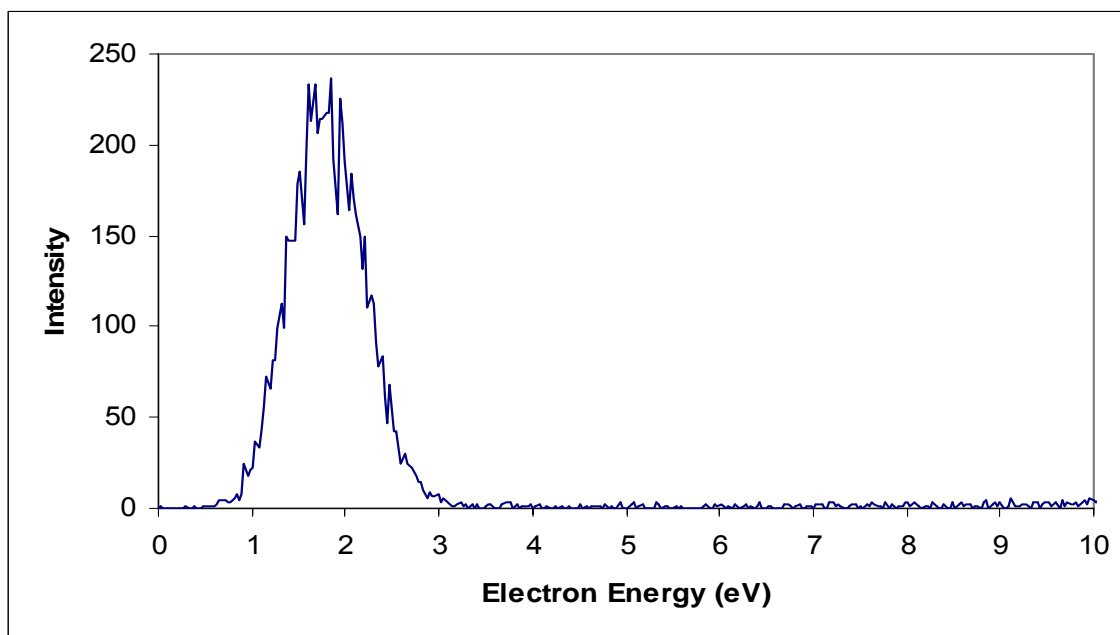


Figure 58. Effective yield curve for pseudo z-1 ion with m/z 72 from N-Acetyl Alanine. The sample was introduced into the instrument by heating dry solid loaded in a capillary in the direct insertion probe. The ion source temperature was 52 °C and the direct insertion probe temperature was 90 °C.

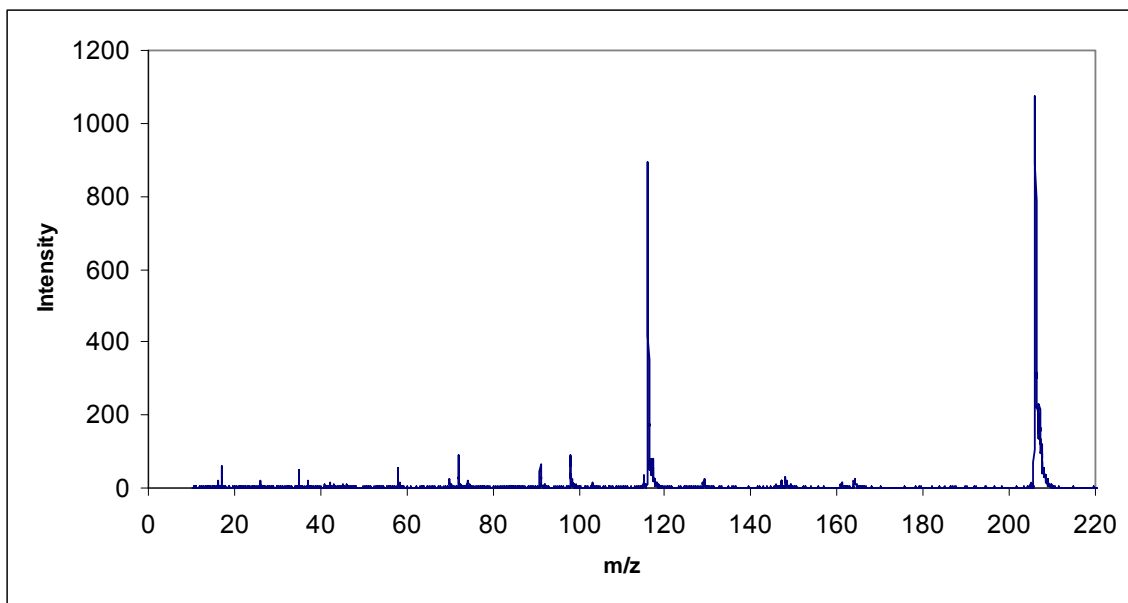


Figure. 59. The REC-MS of N-Acetyl Phenylalanine for ions generated by scanning electron energies from 0 - ~10 eV. The sample was introduced into the instrument by heating dry solid loaded in a capillary in the direct insertion probe. The ion source temperature was 151 °C and the direct insertion probe temperature was 160 °C.

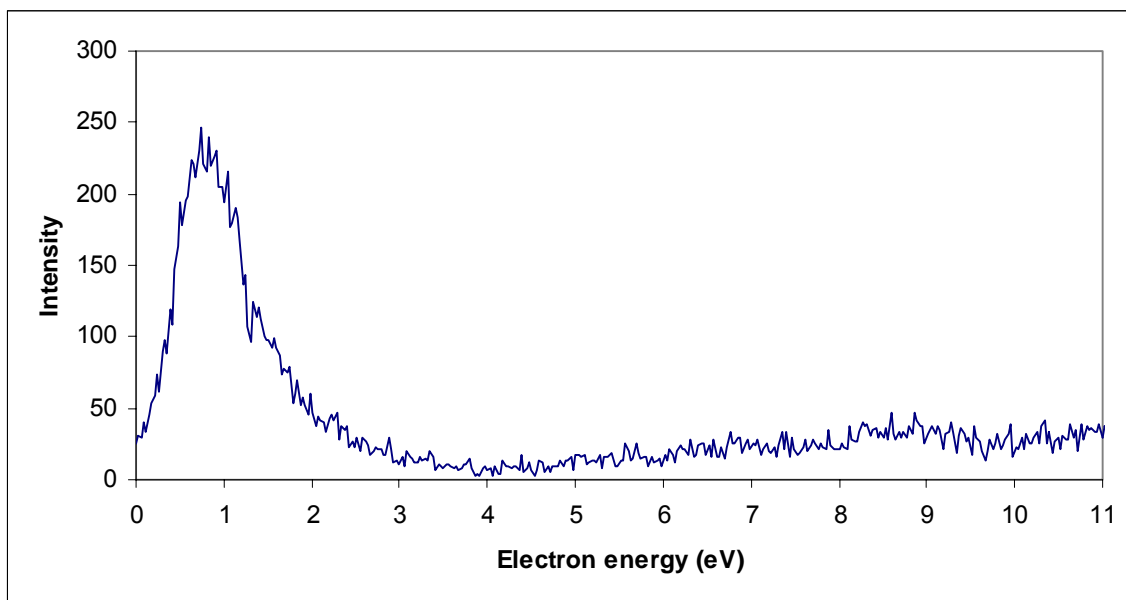


Figure. 60. Effective yield curve for the (M-H)⁻ ion with m/z 206 from N-Acetyl Phenylalanine. The samples were introduced into the instrument by heating dry solid loaded in a capillary in the direct insertion probe. The ion source temperature was 151 °C and the direct insertion probe temperature was 160 °C.

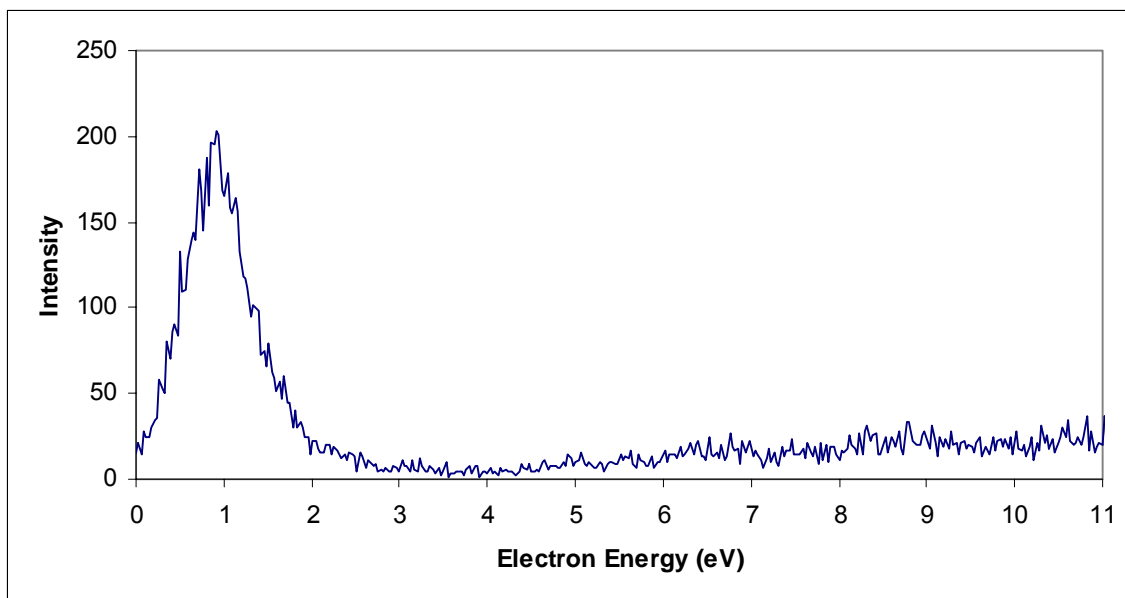


Figure. 61. Effective yield curve for the (M-R)⁻ ion with m/z 116 from N-Acetyl Phenylalanine. The samples were introduced into the instrument by heating dry solid loaded in a capillary in the direct insertion probe. The ion source temperature was 151 °C and the direct insertion probe temperature was 160 °C.

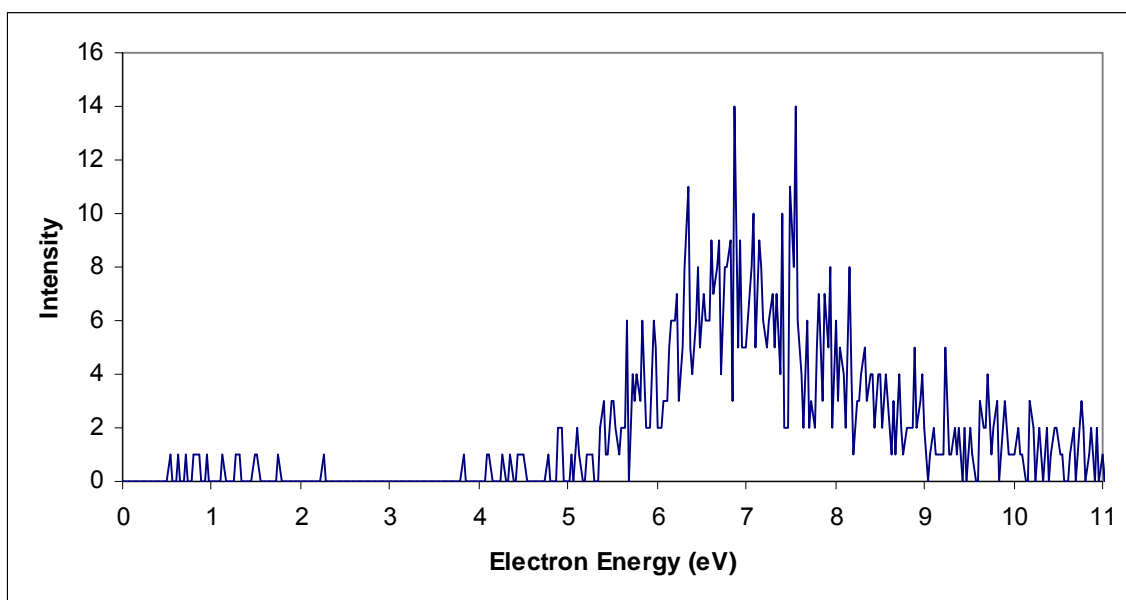


Figure. 62. Effective yield curve for the R^- ion with m/z 91 from N-Acetyl Phenylalanine. The samples were introduced into the instrument by heating dry solid loaded in a capillary in the direct insertion probe. The ion source temperature was 151 °C and the direct insertion probe temperature was 160 °C.

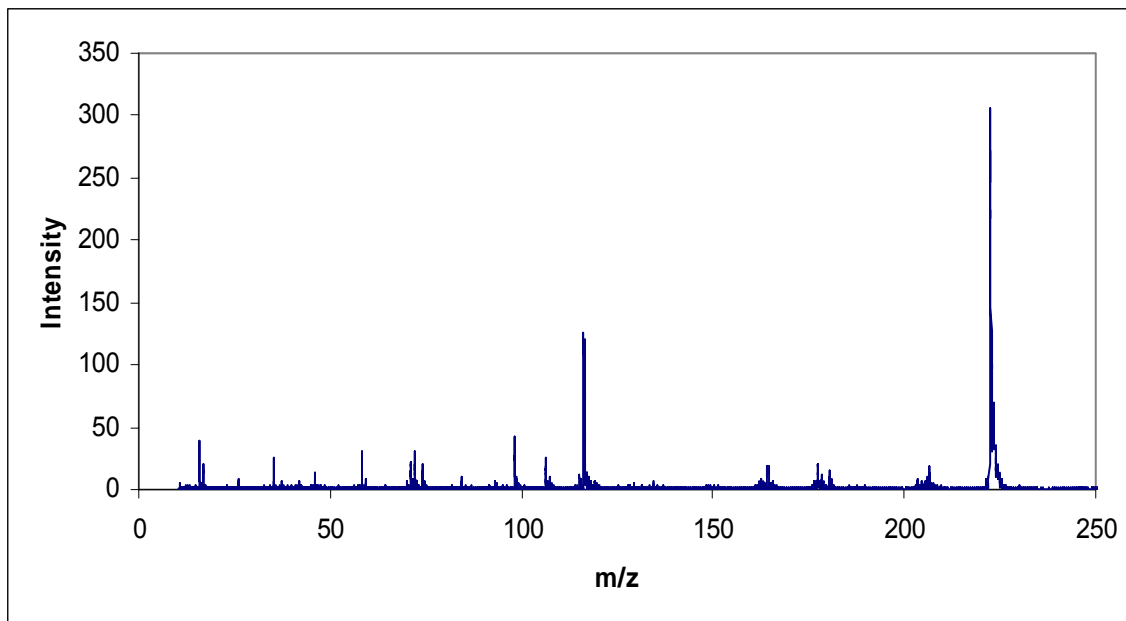


Figure. 63. The REC-MS of N-Acetyl Tyrosine for ions generated by scanning electron energies from 0 - ~10 eV. The sample was introduced into the instrument by heating dry solid loaded in a capillary in the direct insertion probe. The ion source temperature was 151 °C and the direct insertion probe temperature was 160 °C.

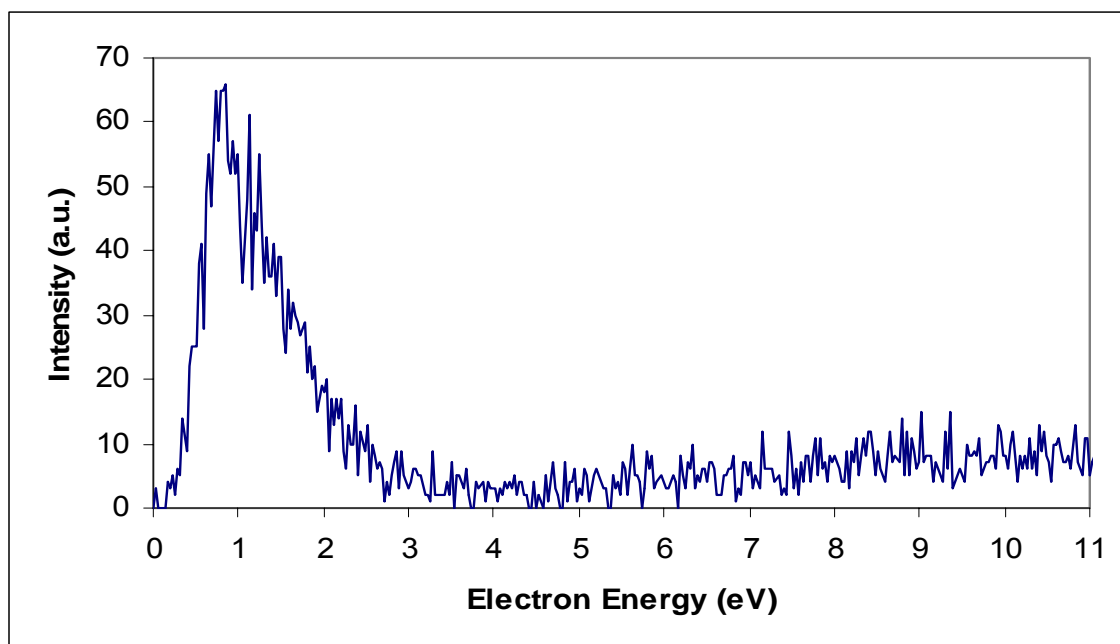


Figure. 64. Effective yield curve for the (M-H)⁻ ion with m/z 222 from N-Acetyl Tyrosine. The samples were introduced into the instrument by heating dry solid loaded in a capillary in the direct insertion probe. The ion source temperature was 151 °C and the direct insertion probe temperature was 160 °C.

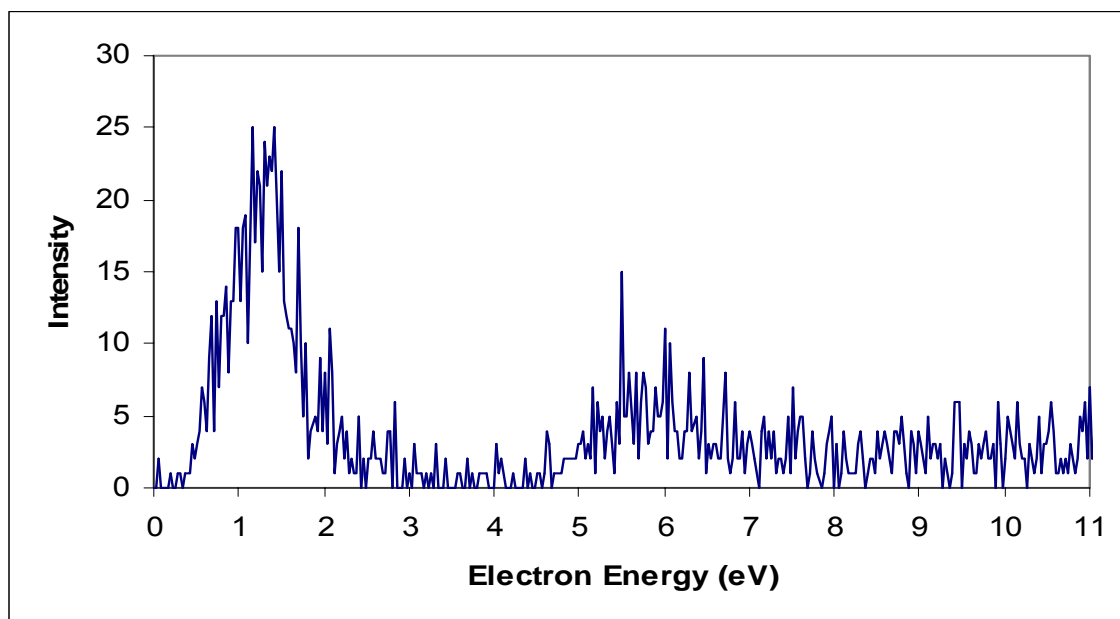


Figure. 65. Effective yield curve for the (M-R)⁻ ion with m/z 116 from N-Acetyl Tyrosine. The samples were introduced into the instrument by heating dry solid loaded in a capillary in the direct insertion probe. The ion source temperature was 151 °C and the direct insertion probe temperature was 160 °C.

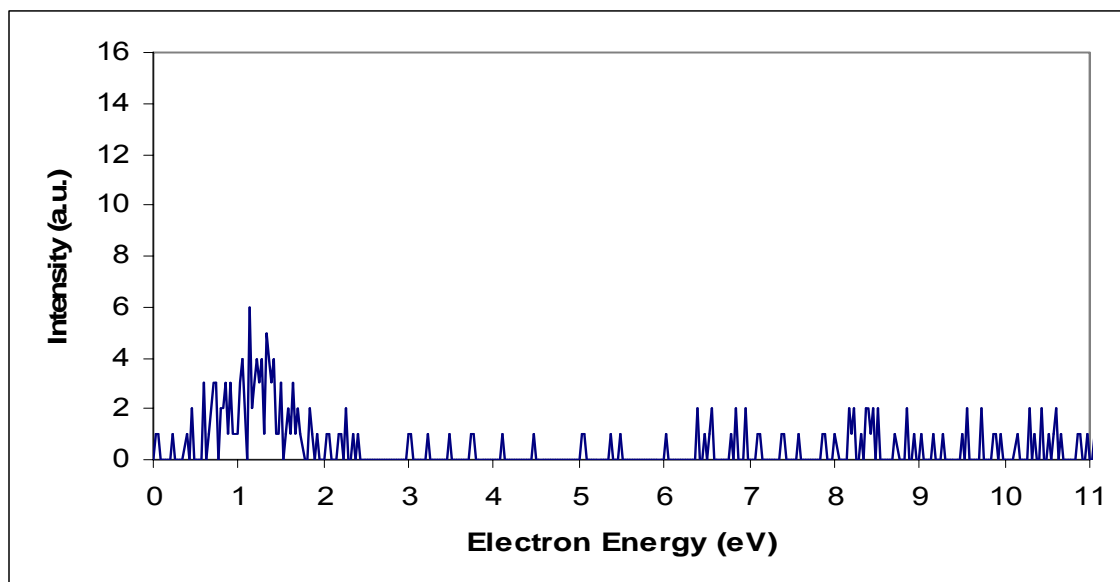


Figure. 66. Effective yield curve for the pseudo z-1 ion with m/z 164 from N-Acetyl Tyrosine. The samples were introduced into the instrument by heating dry solid loaded in a capillary in the direct insertion probe. The ion source temperature was 151 °C and the direct insertion probe temperature was 160 °C.

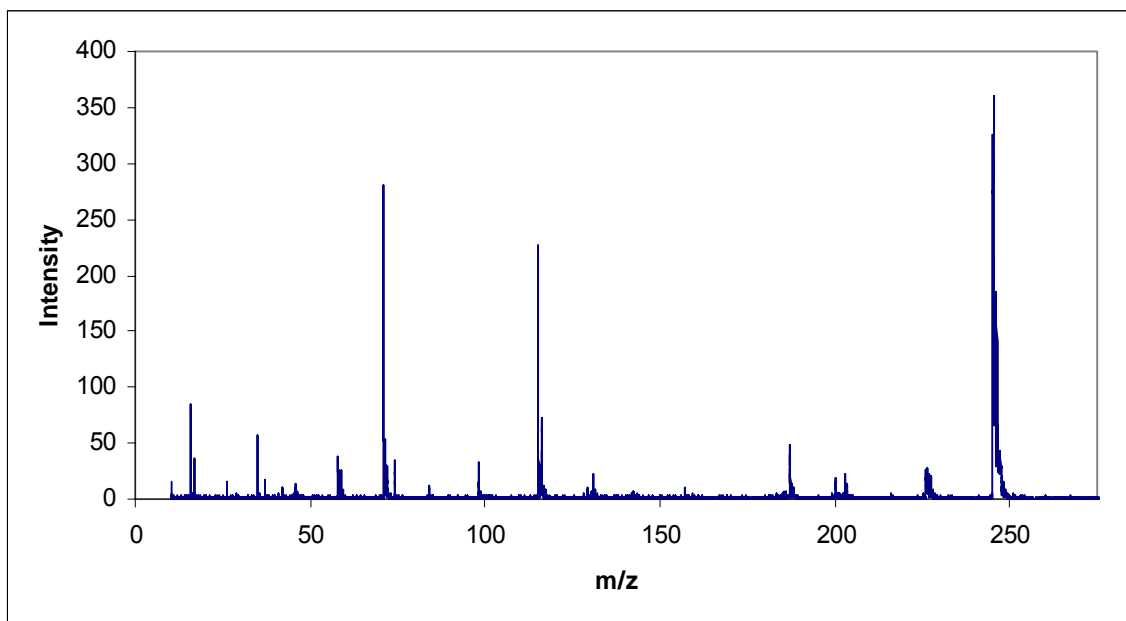


Figure. 67. The REC-MS of N-Acetyl Tryptophan for ions generated by scanning electron energies from 0 - ~10 eV. The sample was introduced into the instrument by heating dry solid loaded in a capillary in the direct insertion probe. The ion source temperature was 150 °C and the direct insertion probe temperature was 165 °C.

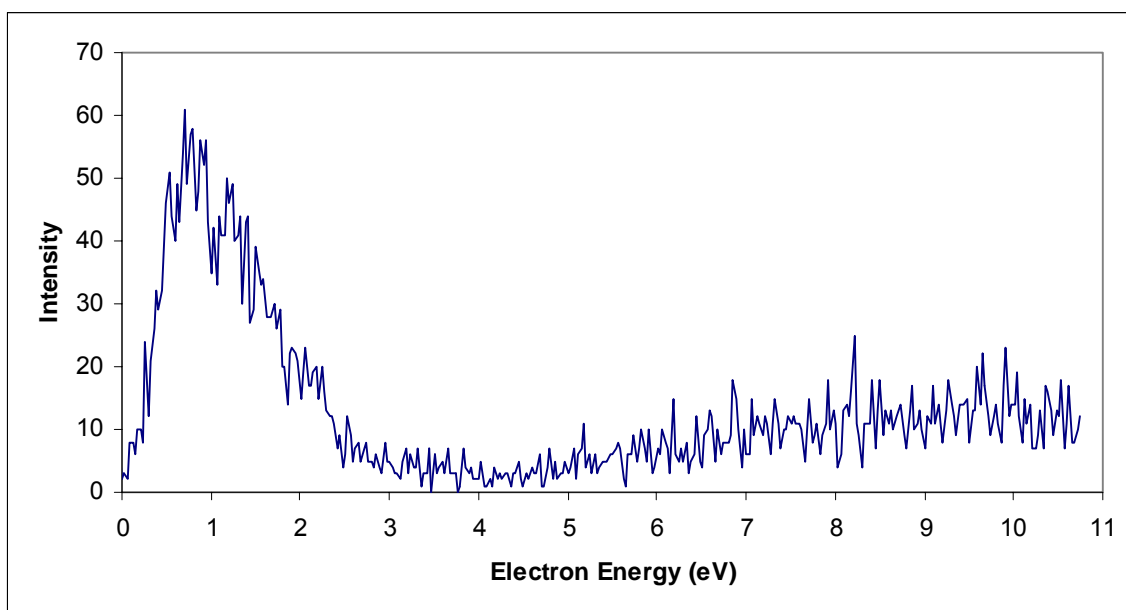


Figure. 68. Effective yield curve for the (M-H)⁻ ion with m/z 245 from N-Acetyl Tyrosine. The sample was introduced into the instrument by heating dry solid loaded in a capillary in the direct insertion probe. The ion source temperature was 150 °C and the direct insertion probe temperature was 165 °C.

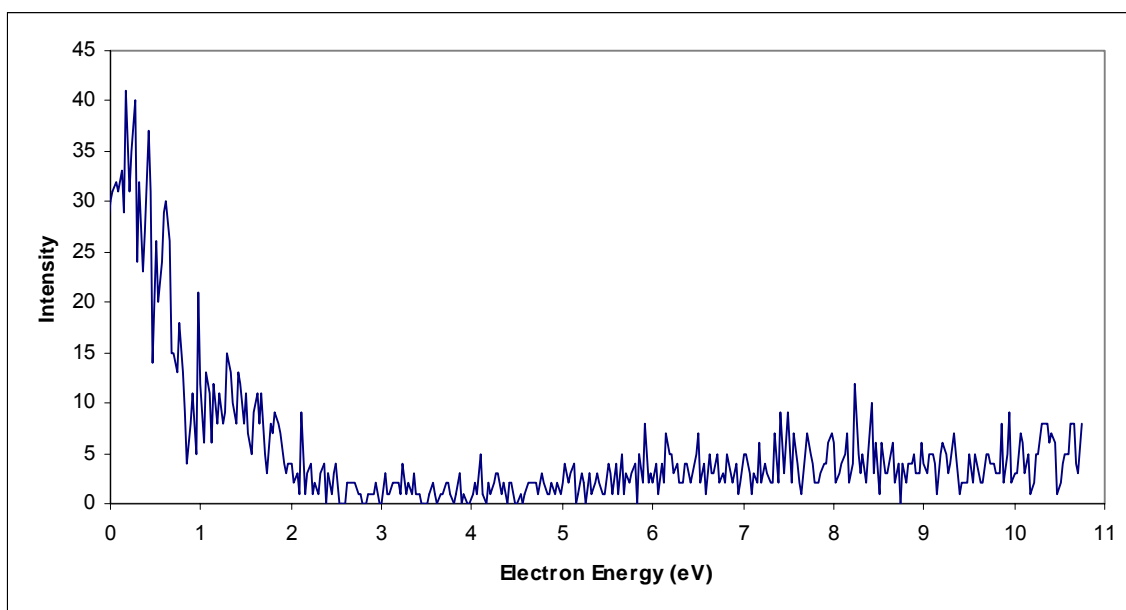


Figure. 69. Effective yield curve for the (M-R-H)⁻ ion with m/z 115 from N-Acetyl Tyrosine. The sample was introduced into the instrument by heating dry solid loaded in a capillary in the direct insertion probe. The ion source temperature was 150 °C and the direct insertion probe temperature was 165 °C.

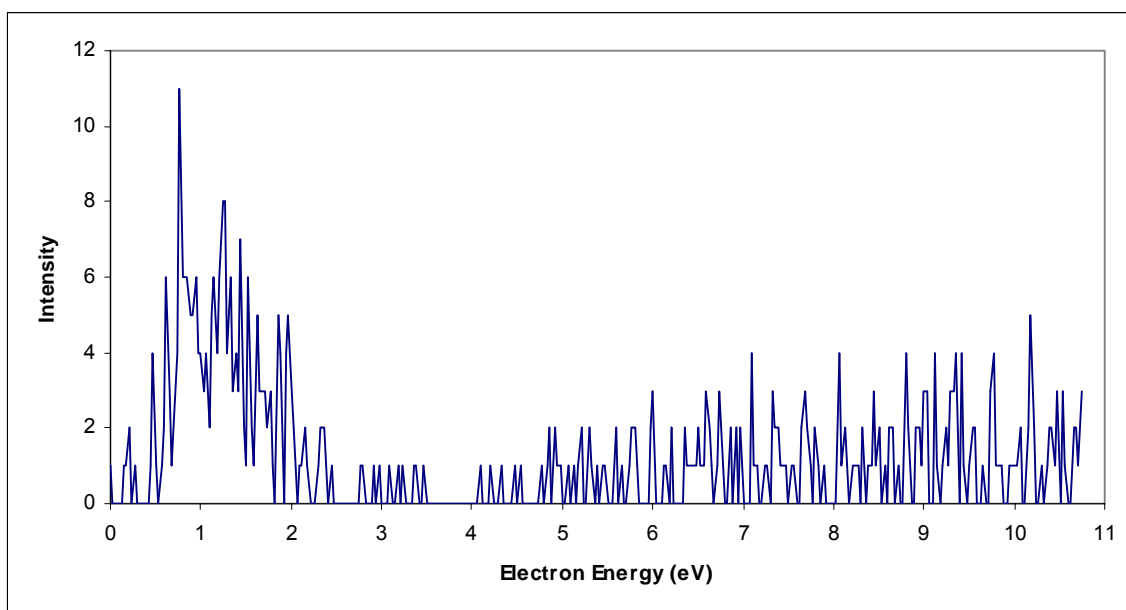


Figure. 70. Effective yield curve for the pseudo z-1 ion with m/z 187 from N-Acetyl Tyrosine. The sample was introduced into the instrument by heating dry solid loaded in a capillary in the direct insertion probe. The ion source temperature was 150 °C and the direct insertion probe temperature was 165 °C.

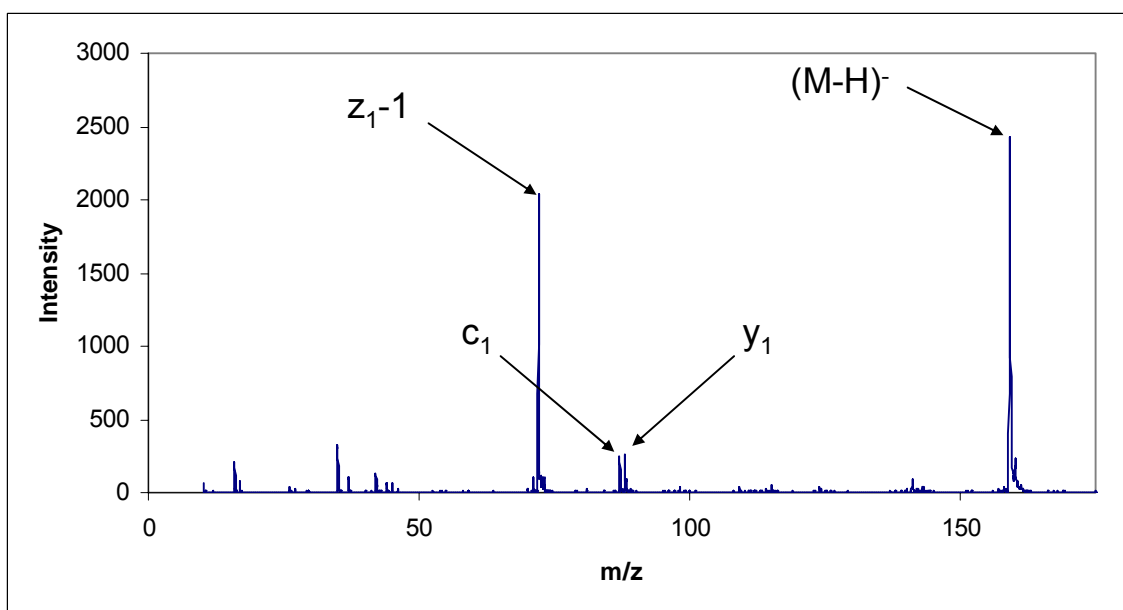
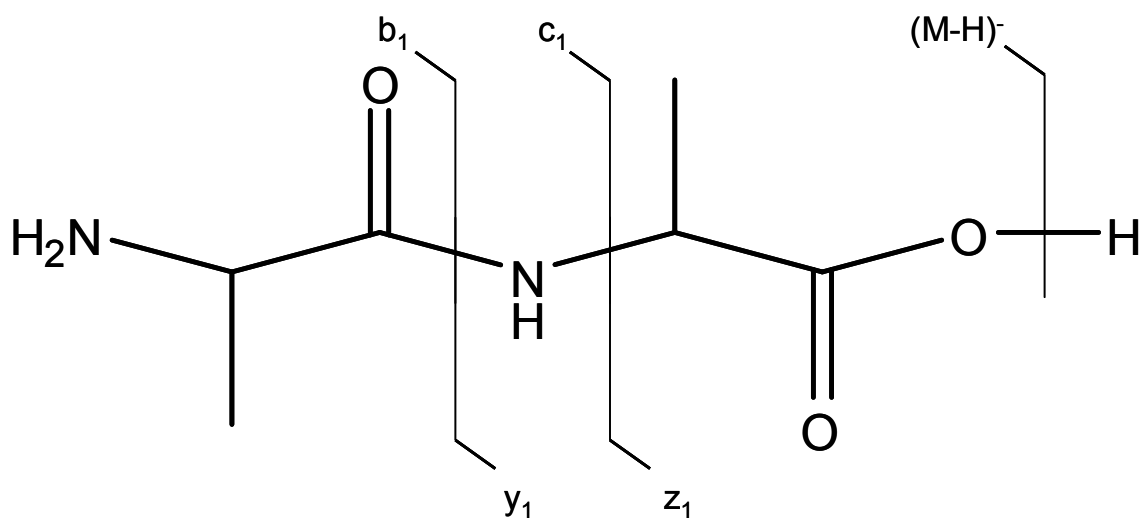


Figure. 71. The REC-MS of Ala₂ for ions generated by scanning electron energies from 0 - ~10 eV. The sample was introduced into the instrument by heating dry solid loaded in a capillary in the direct insertion probe. The ion source temperature was 125 °C and the direct insertion probe temperature was 150 °C.

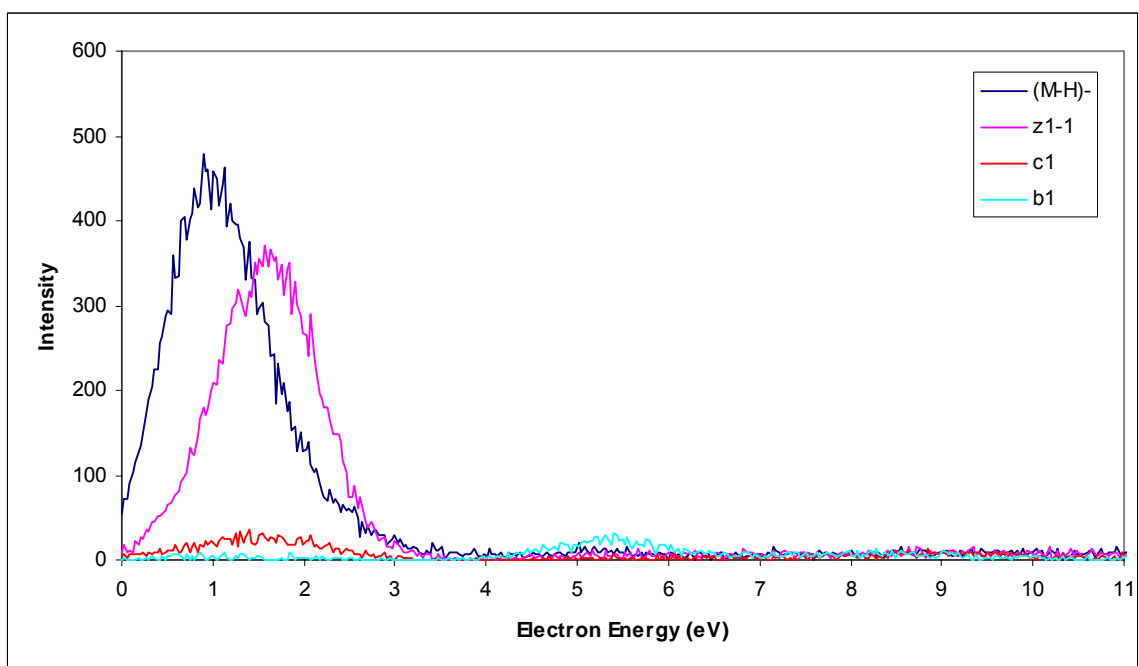
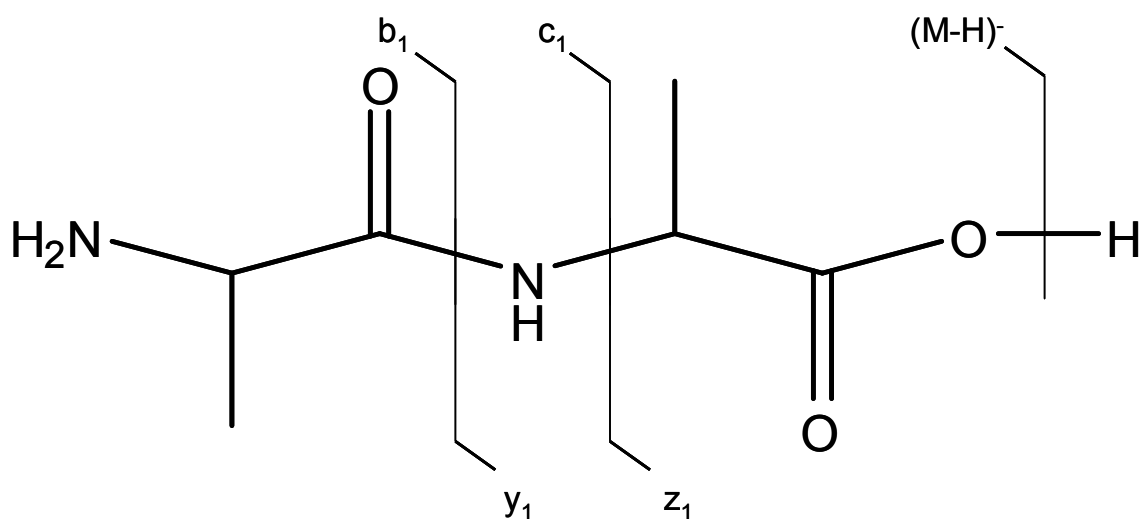


Figure. 72. Effective yield curves for the formation of the four most intense ions from the REC-MS of Ala₂; (M-H)⁻ (blue), z₁-1 (pink), c₁ (red), and b₁ (aqua). The samples were introduced into the instrument by heating dry solid loaded in a capillary in the direct insertion probe. The ion source temperature was 125 °C and the direct insertion probe temperature was 150 °C.

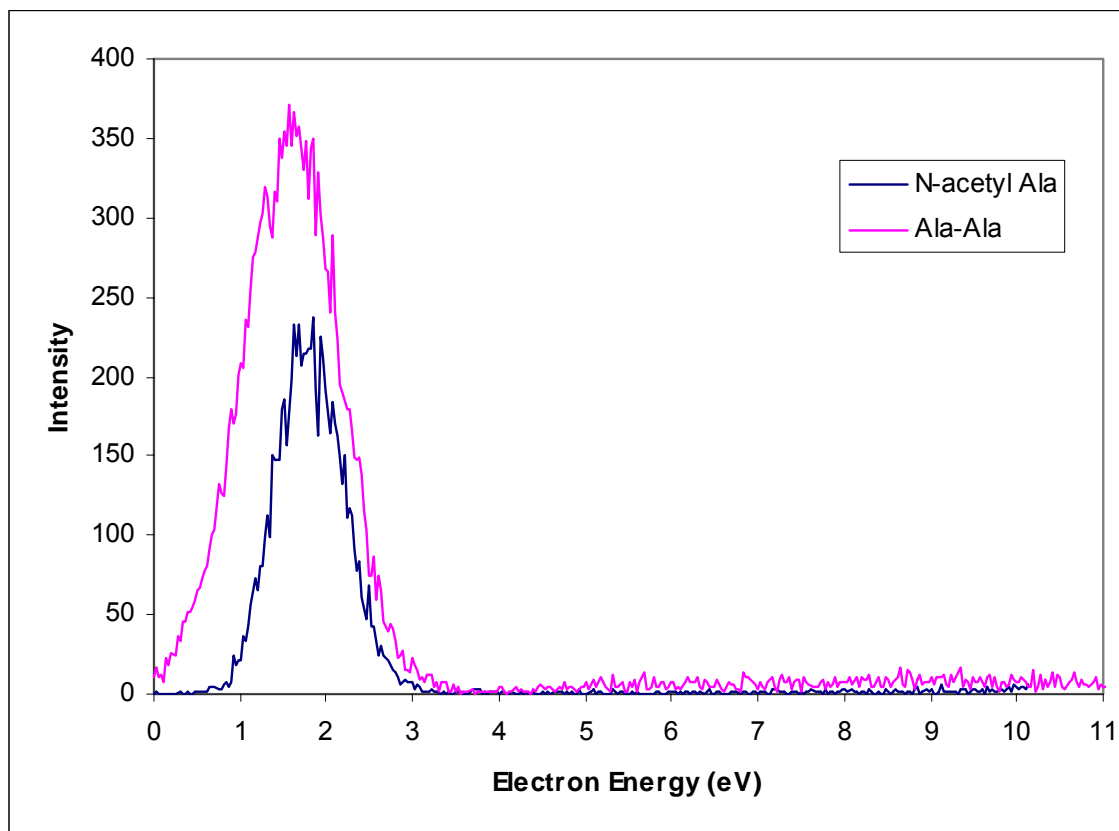


Figure 73. The effective yield curves for the $(M-H)^-$ ions from N-acetyl alanine (blue) and the alanine dimer (pink). The samples were introduced into the instrument by heating dry solid loaded in a capillary in the direct insertion probe.

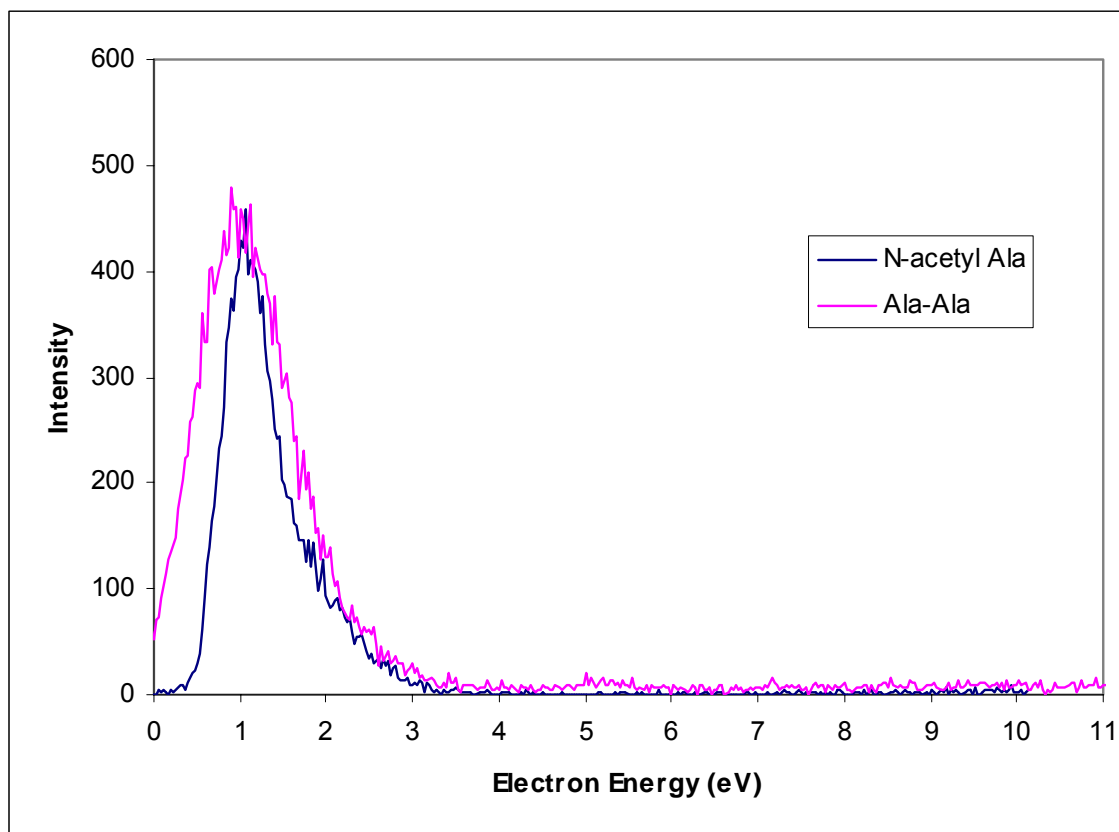


Figure 74. The effective yield curves for the pseudo $z-1$ ion from N-acetyl alanine (blue) and z_1-1 ion from the alanine dimer (pink). The samples were introduced into the instrument by heating dry solid loaded in a capillary in the direct insertion probe.

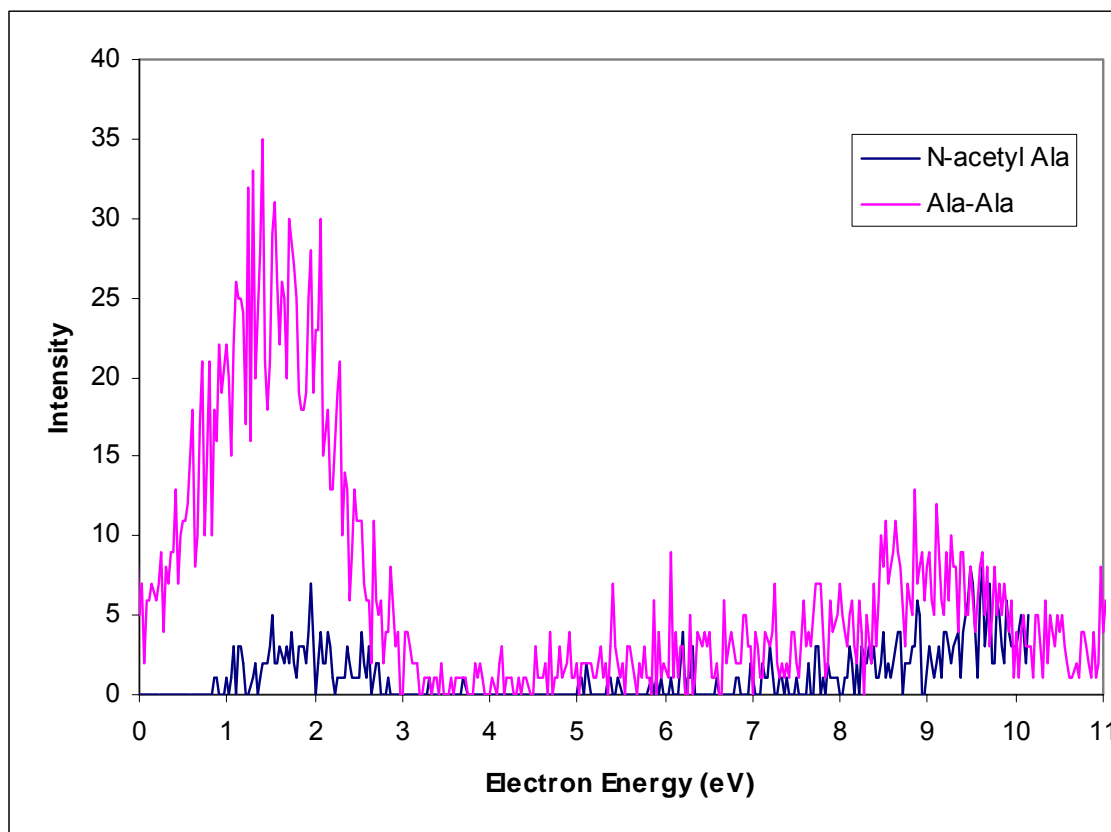


Figure 75. The effective yield curves for the pseudo c ion from N-acetyl alanine (blue) and c_1 ion from the alanine dimer (pink). The samples were introduced into the instrument by heating dry solid loaded in a capillary in the direct insertion probe.

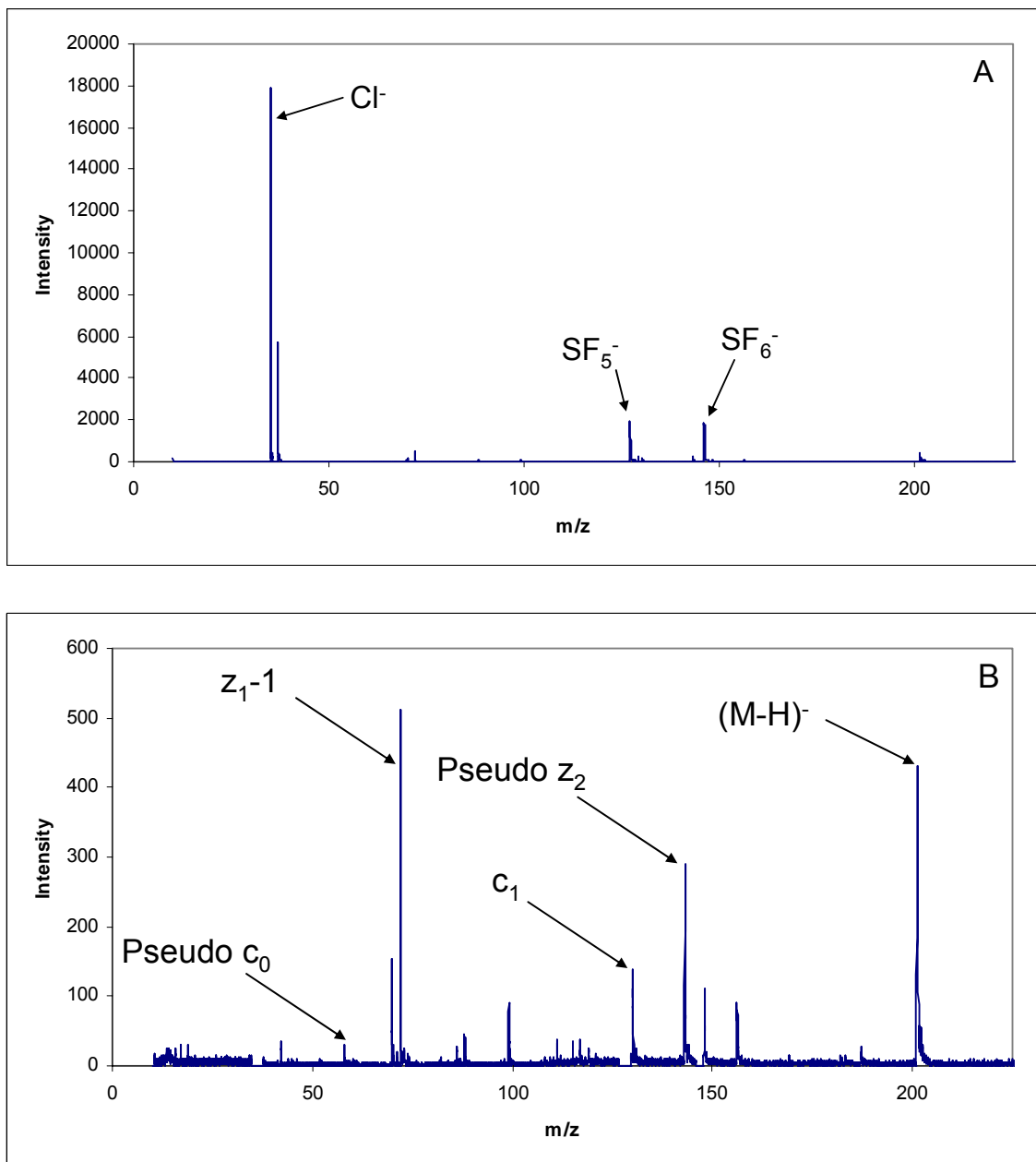


Figure. 76. (A) The raw REC-MS of N-Acetyl Ala₂ generated by scanning electron energies from 0 - ~10 eV. (B) The REC-MS of N-Acetyl Ala₂ with overwhelming Cl⁻ from CCl₄ and ions with m/z 127 and m/z 146 from SF₆ removed and the z-1 series, c series, and (M-H)⁻ ions generated by scanning electron energies from 0 - ~10 eV. The sample was introduced into the instrument by heating dry solid loaded in a capillary in the direct insertion probe. The ion source temperature was 106 °C and the direct insertion probe temperature was 150 °C.

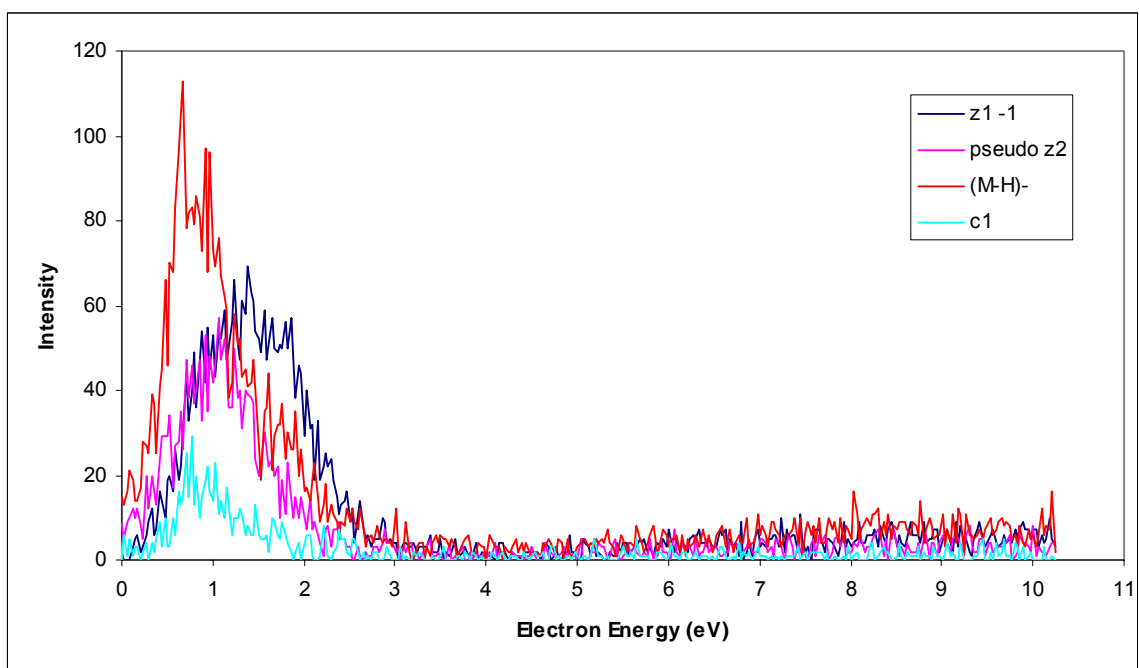
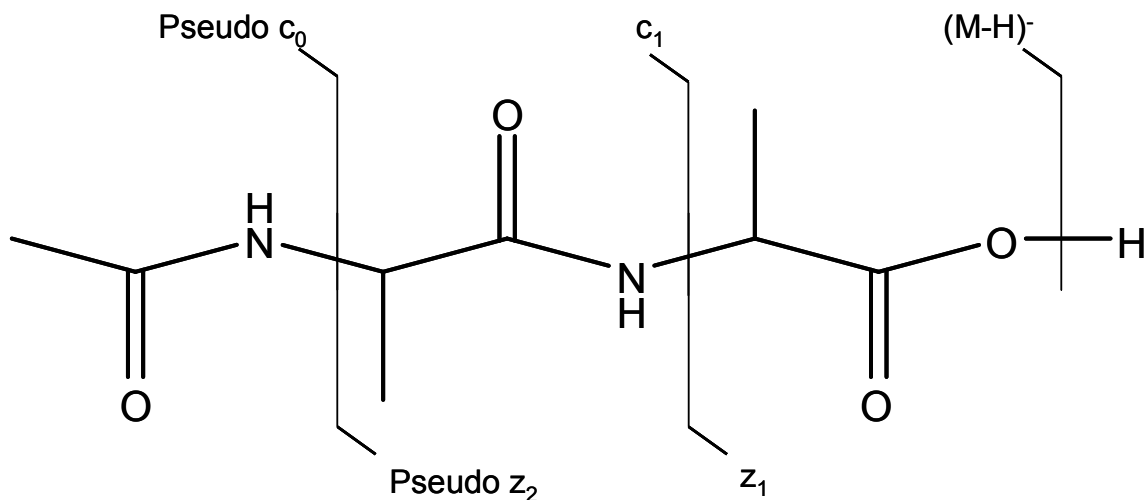


Figure. 77. Effective yield curves for the formation of the four most intense ions from the REC-MS of Acetyl-Ala₂; (M-H)⁻ (red), z₁-1 (blue), pseudo z₂-1 (pink), and c₁ (aqua). The samples were introduced into the instrument by heating dry solid loaded in a capillary in the direct insertion probe. The ion source temperature was 106 °C and the direct insertion probe temperature was 150 °C.

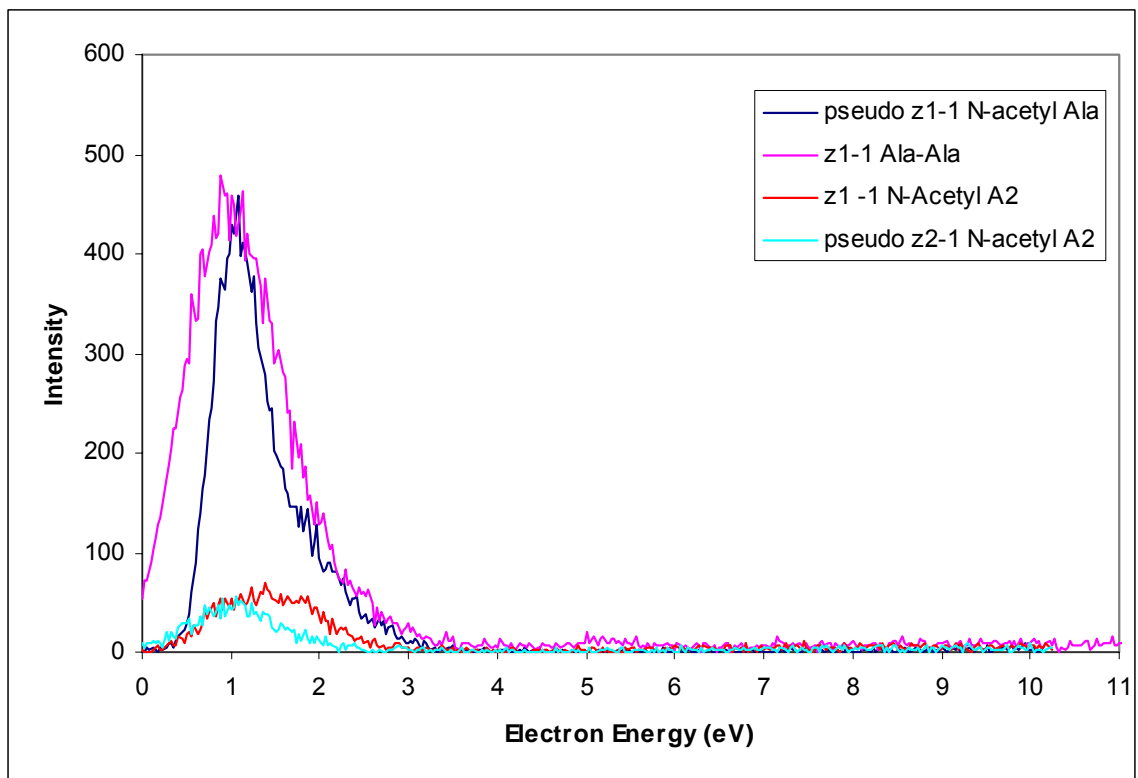


Figure 78. Effective yield curves for pseudo z-1 (blue) from the N-Acetyl Ala, z_1 -1 (red) ion from Ala-Ala, and the z_1 -1 (red) ion and pseudo z_2 -1 (aqua) from N-Acetyl Ala-Ala. The samples were introduced into the instrument by heating dry solid loaded in a capillary in the direct insertion probe.

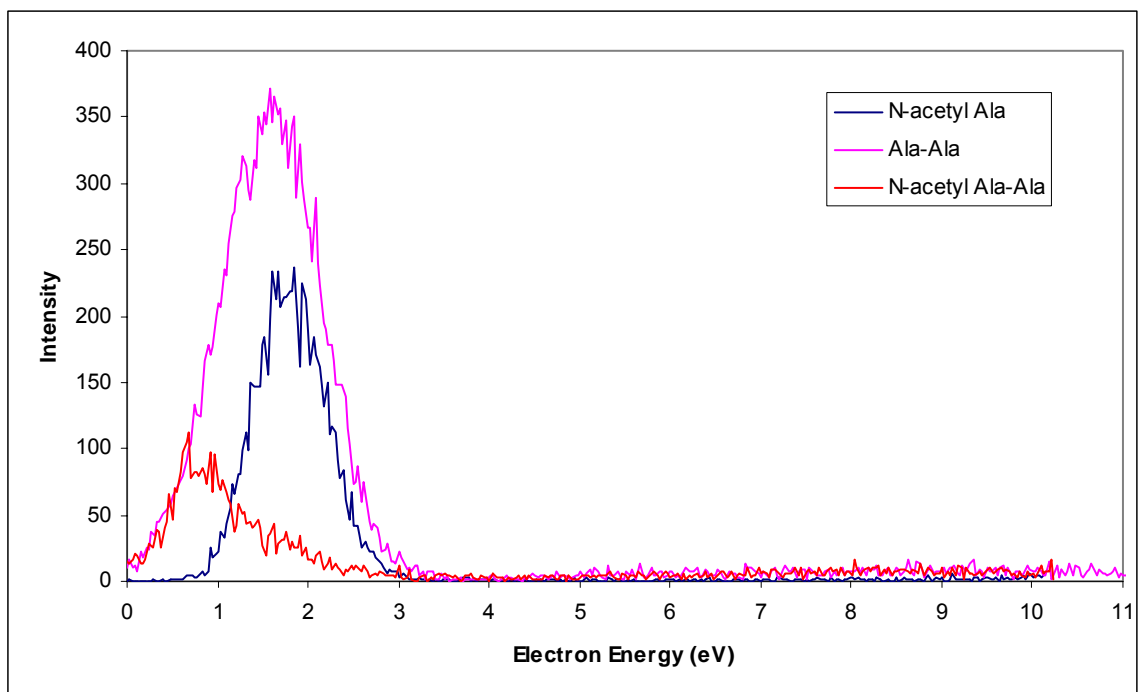


Figure 79. Effective yield curves of the (M-H)⁻ ions for N-acetyl Ala (blue), Ala-Ala (pink), and N-acetyl Ala-Ala (red). The samples were introduced into the instrument by heating dry solid loaded in a capillary in the direct insertion probe.

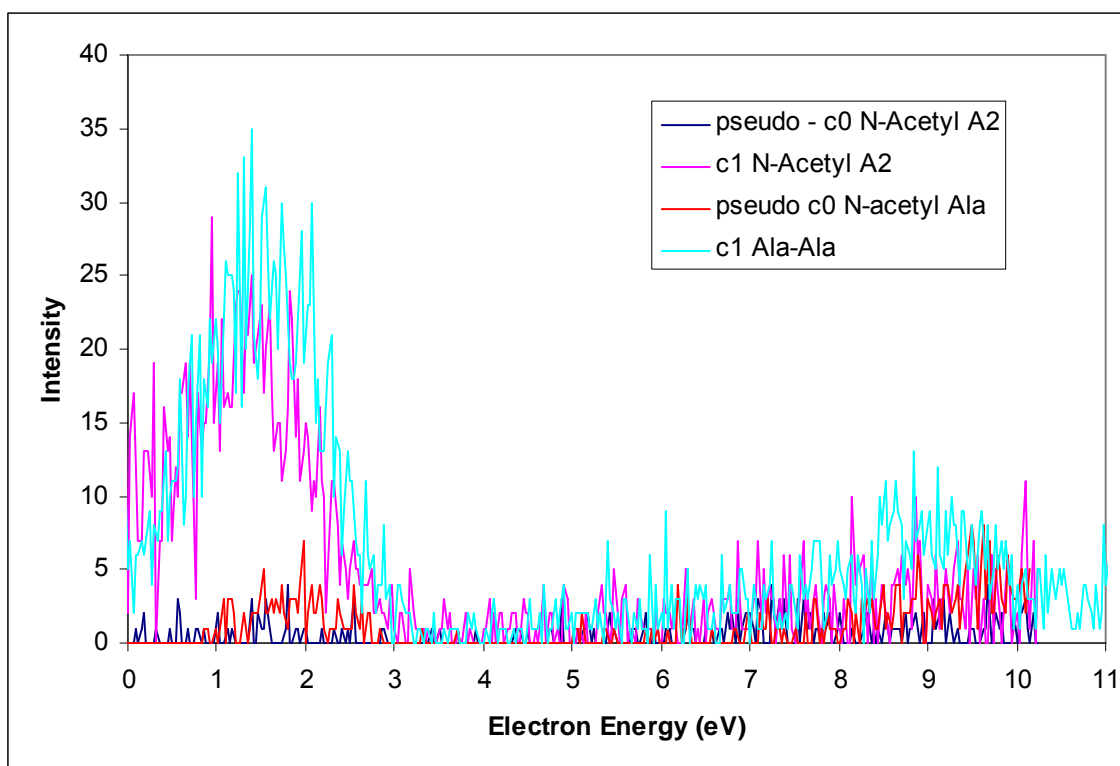


Figure 80. Effective yield curves for the pseudo c_0 ion (blue) and c_1 ion (pink) from the N-Acetyl Ala-Ala, pseudo c_0 ion (red) from the N-Acetyl Ala, and the c_1 ion (aqua) from the Ala-Ala. The samples were introduced into the instrument by heating dry solid loaded in a capillary in the direct insertion probe.

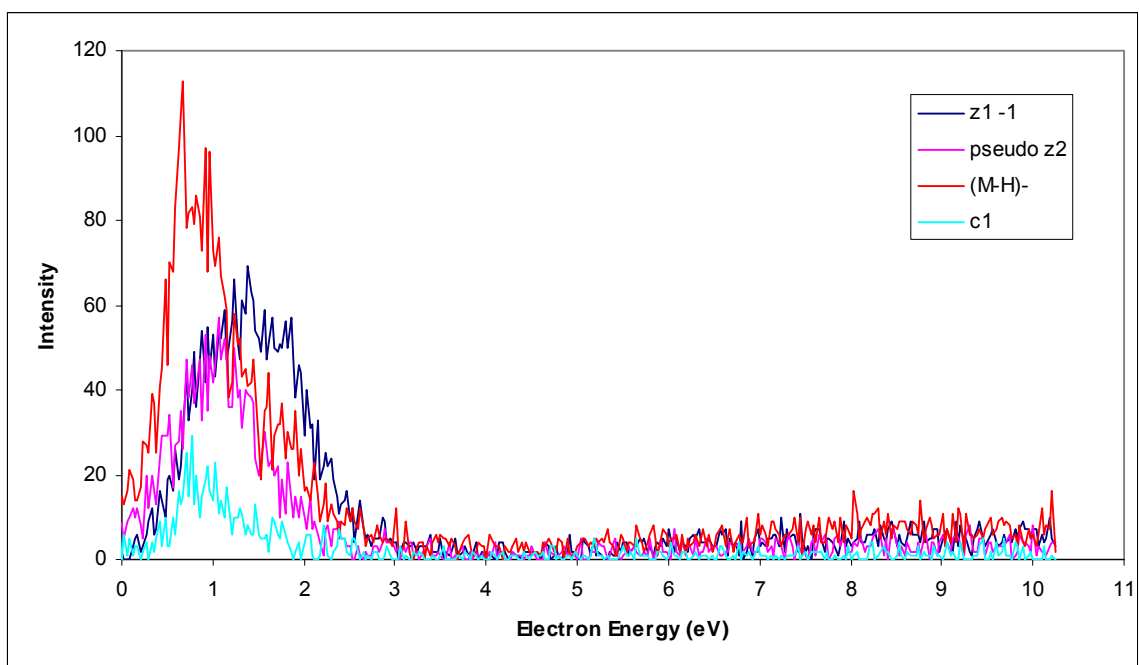


Figure 81. The effective yield curves of (M-H)⁻ (red), pseudo z₂-1 (pink), z₁-1 (blue), and c₁ (aqua) ions from N-Acetyl Ala-Ala. The samples were introduced into the instrument by heating dry solid loaded in a capillary in the direct insertion probe.

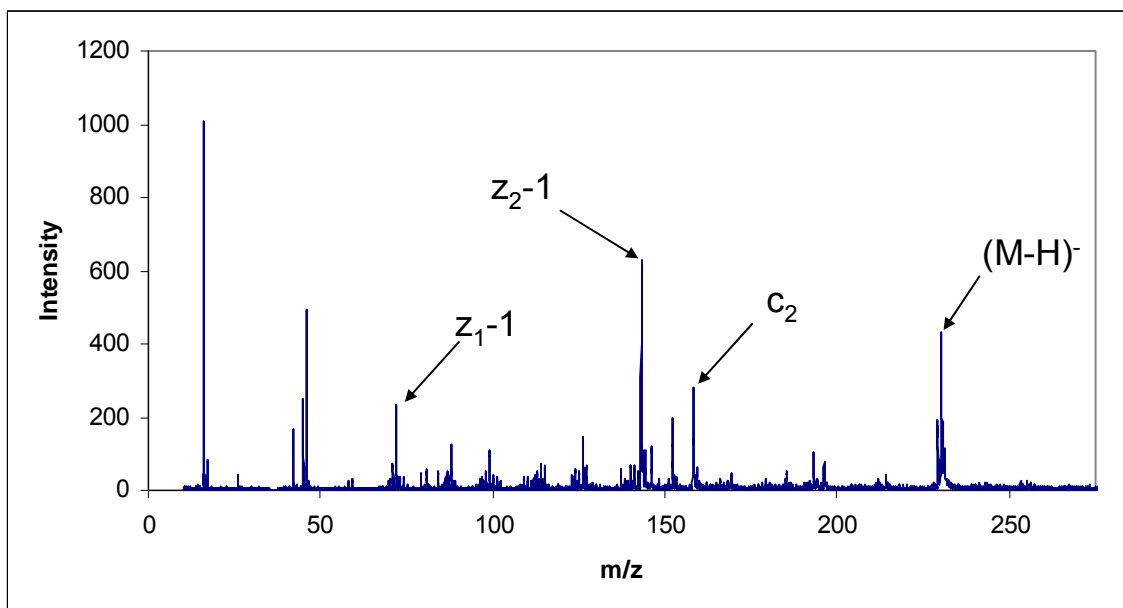
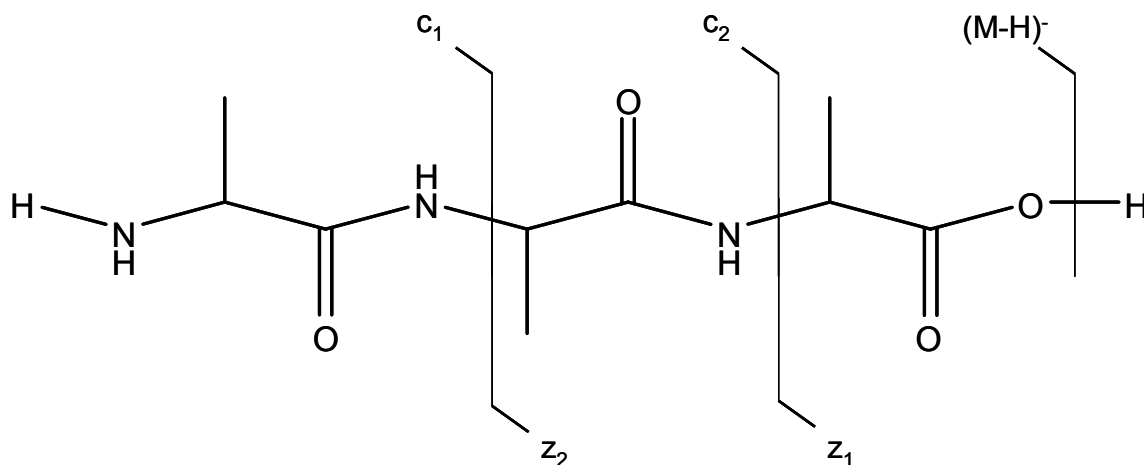


Figure. 82. The REC-MS of Al₃ with Cl⁻ removed with z-1 series, c₂, and (M-H)⁻ ions generated by scanning electron energies from 0 - ~10 eV. The sample was introduced into the instrument by heating dry solid loaded in a capillary in the direct insertion probe. The ion source temperature was 125 °C and the direct insertion probe temperature was 120 °C.

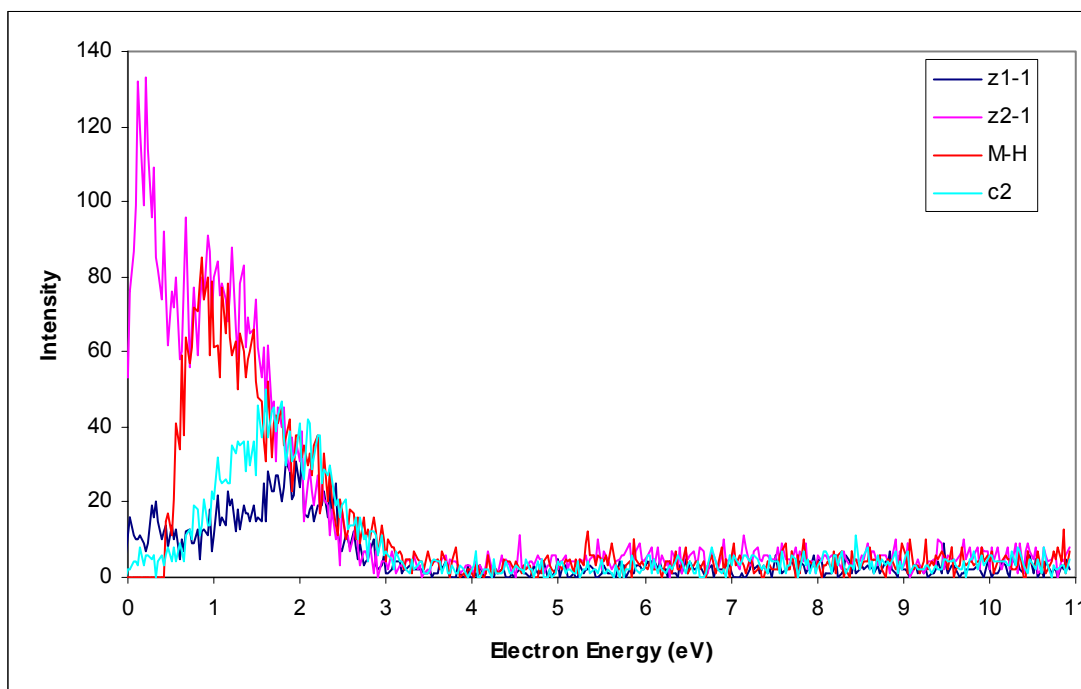
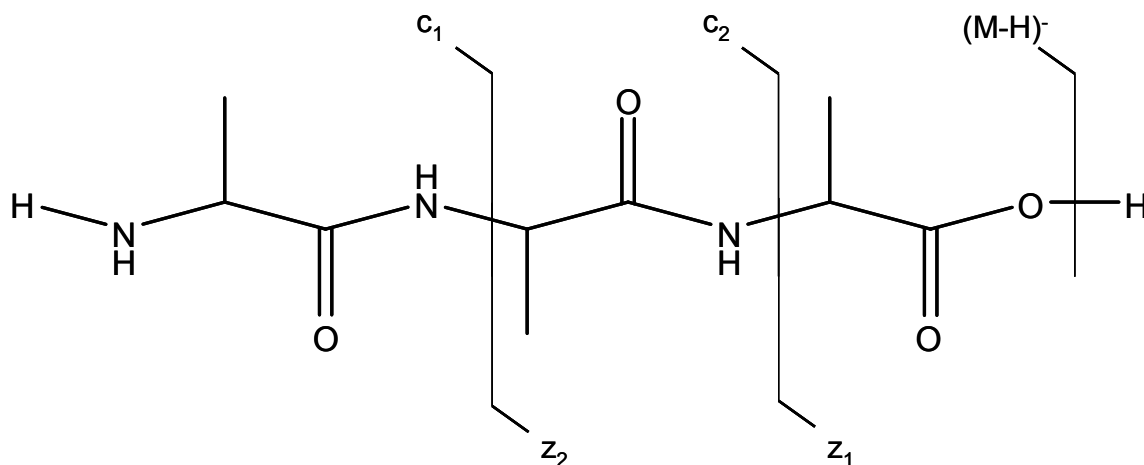


Figure. 83. Effective yield curves for the formation of the four intense ions from the REC-MS of Ala_3 ; $(\text{M}-\text{H})^-$ (red), z_1-1 (blue), pseudo z_2-1 (pink), and c_2 (aqua). The samples were introduced into the instrument by heating dry solid loaded in a capillary in the direct insertion probe. The ion source temperature was 125°C and the direct insertion probe temperature was 120°C .

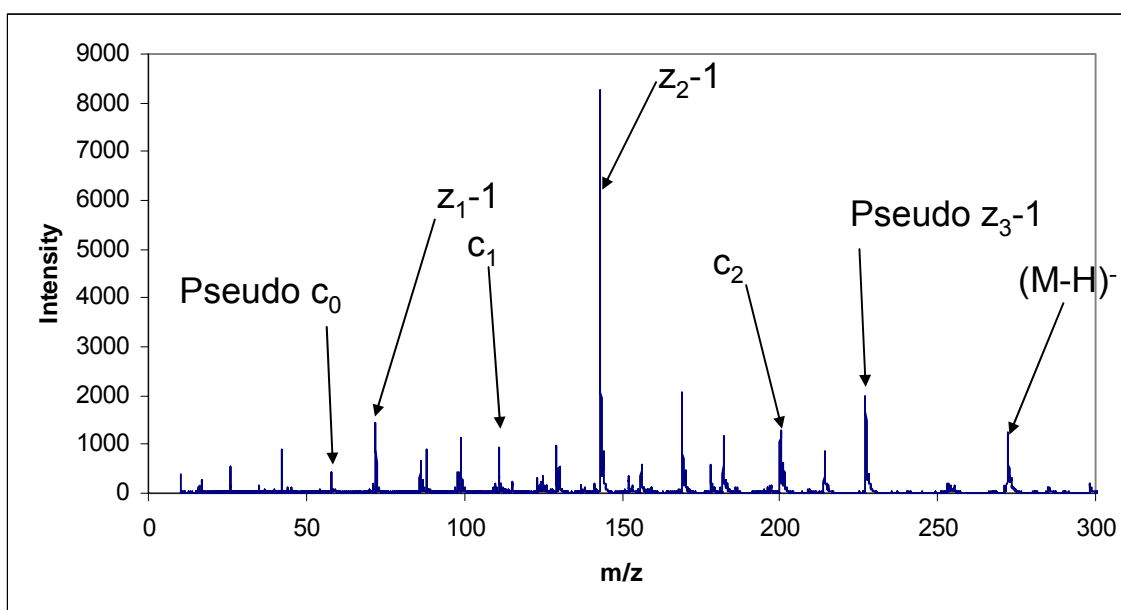
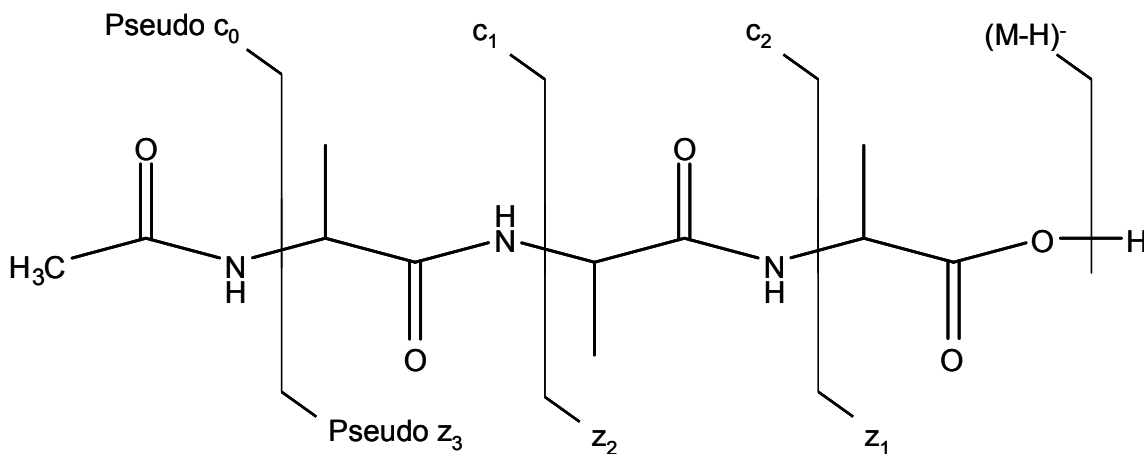


Figure. 84. The REC-MS of N-Acetyl Ala₃ with Cl⁻ removed with the c series, z-1 series, and (M-H)⁻ ions generated by scanning electron energies from 0 - ~10 eV. The sample was introduced into the instrument by heating dry solid loaded in a capillary in the direct insertion probe. The ion source temperature was 169 °C and the direct insertion probe temperature was 170 °C.

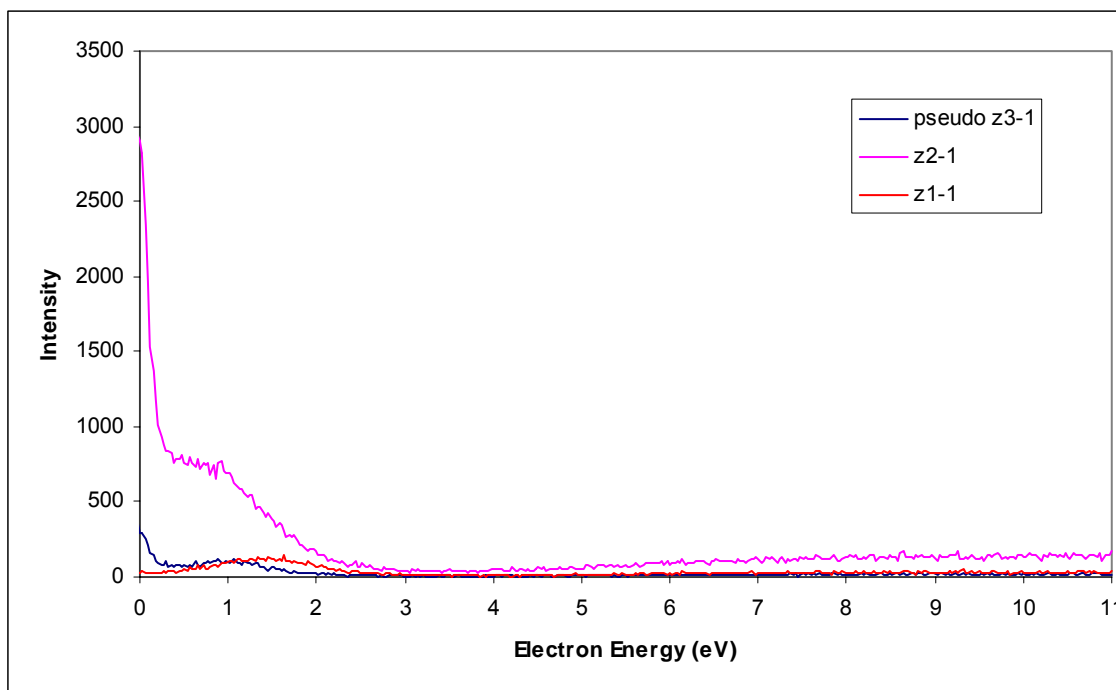


Figure 85. Effective yield curves for the formation of the three z- 1 ions from the REC-MS of N-acetyl Ala₃. The sample was introduced into the instrument by heating dry solid loaded in a capillary in the direct insertion probe. The ion source temperature was 169 °C and the direct insertion probe temperature was 170 °C.

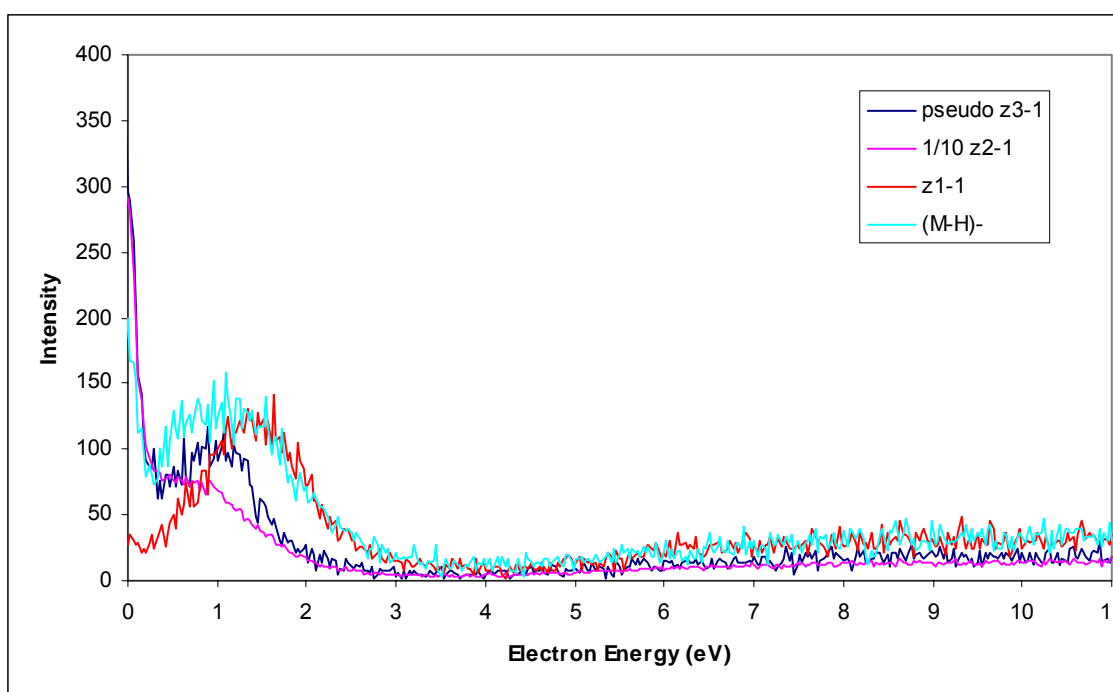
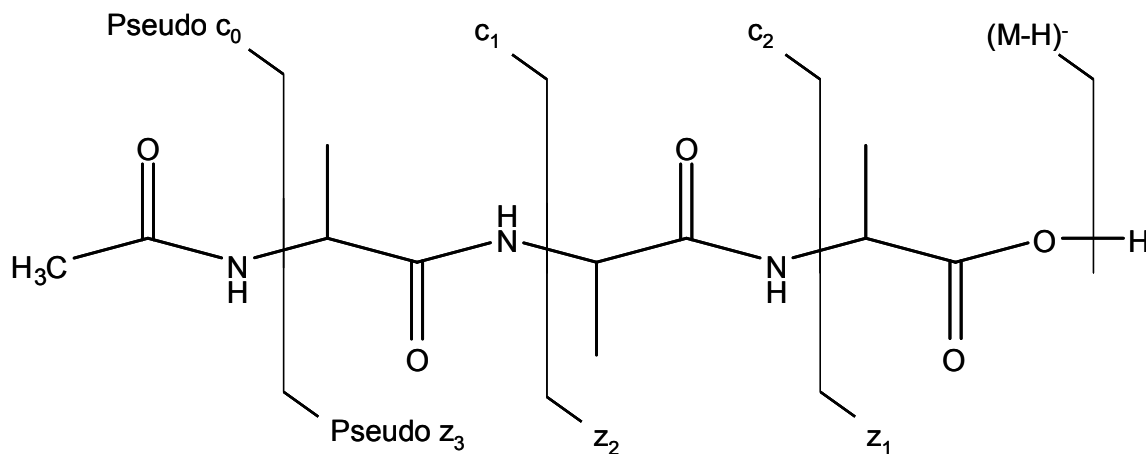


Figure 86. Effective yield curves for the formation of the four intense ions from the RECM-MS of N-acetyl Ala₃; pseudo z₃-1 (blue), z₂-1 scaled by 1/10 (pink), z₁-1 (red), and (M-H)⁻ (cyan). The sample was introduced into the instrument by heating dry solid loaded in a capillary in the direct insertion probe. The ion source temperature was 169 °C and the direct insertion probe temperature was 170 °C.

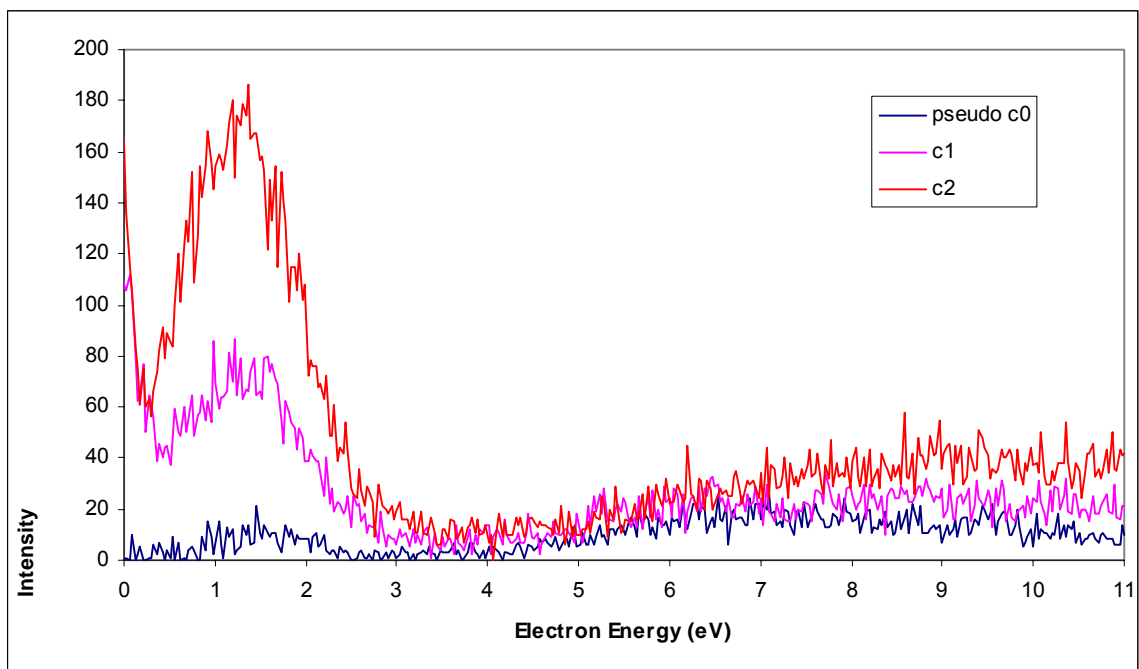


Figure 87. Effective yield curves of three intense ions from the REC-MS of N-acetyl Ala₃; pseudo c₀ (blue), c₁ (pink), and c₂ (red). The sample was introduced into the instrument by heating dry solid loaded in a capillary in the direct insertion probe. The ion source temperature was 169 °C and the direct insertion probe temperature was 170 °C.

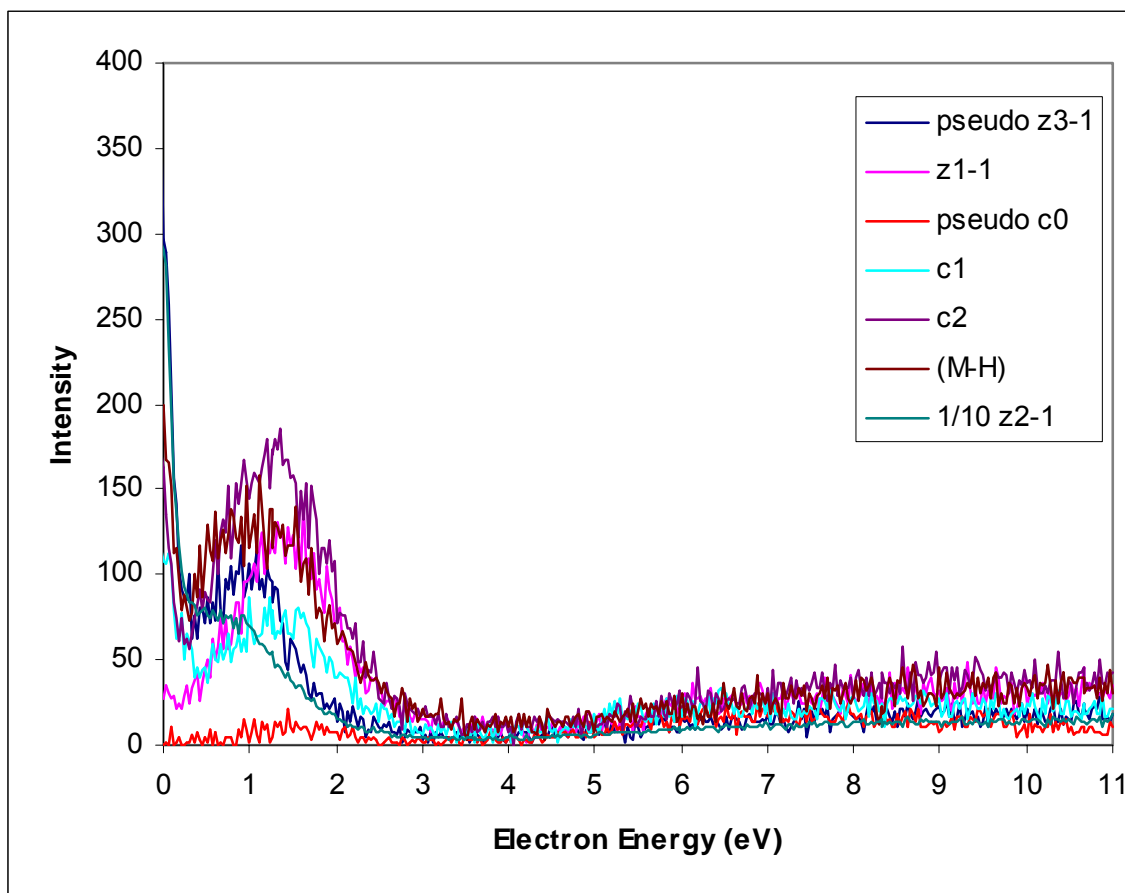


Figure 88. The effective yield curves of the z-1 ion series (pseudo z₃-1, blue, z₁-1, pink, and 1/10 z₂-1, green), c ion series (pseudo-c₀, red, c₁, aqua, and c₂, purple), and the (M-H)⁻ ion (brown) from N-Acetyl Ala-Ala-Ala. The samples were introduced into the instrument by heating dry solid loaded in a capillary in the direct insertion probe.

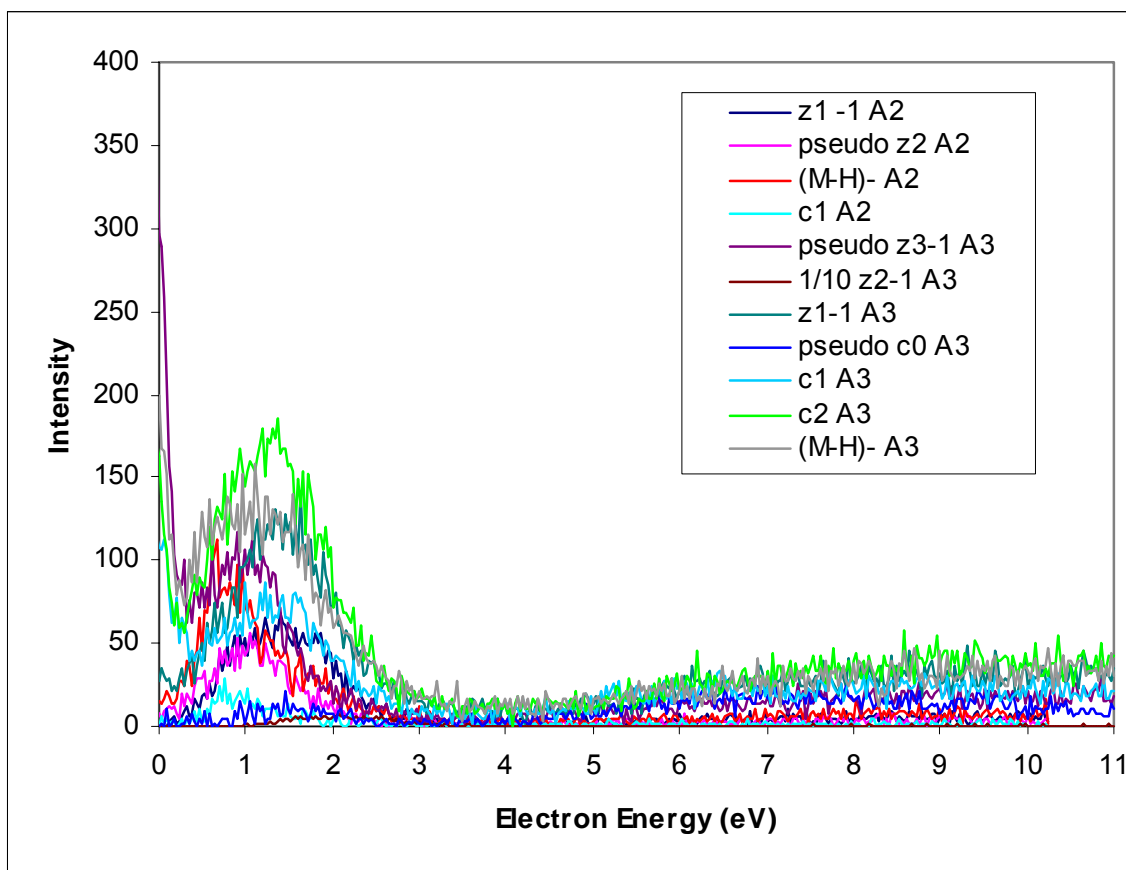


Figure 89. The effective yield curves for the z-1 ions (z_1 -1, blue, pseudo z_2 -1, pink), c ions (c_1 , aqua), and (M-H)⁻ (red) ions from N-acetyl Ala-Ala and for the z-1 ions (z_1 -1, green, 1/10 z_2 -1, brown, pseudo z_3 -1, purple), c ions (pseudo c_0 , light blue, c_1 , light aqua, c_2 , neon green), and (M-H)⁻ (grey) ions from N-acetyl Ala-Ala-Ala. The samples were introduced into the instrument by heating dry solid loaded in a capillary in the direct insertion probe.

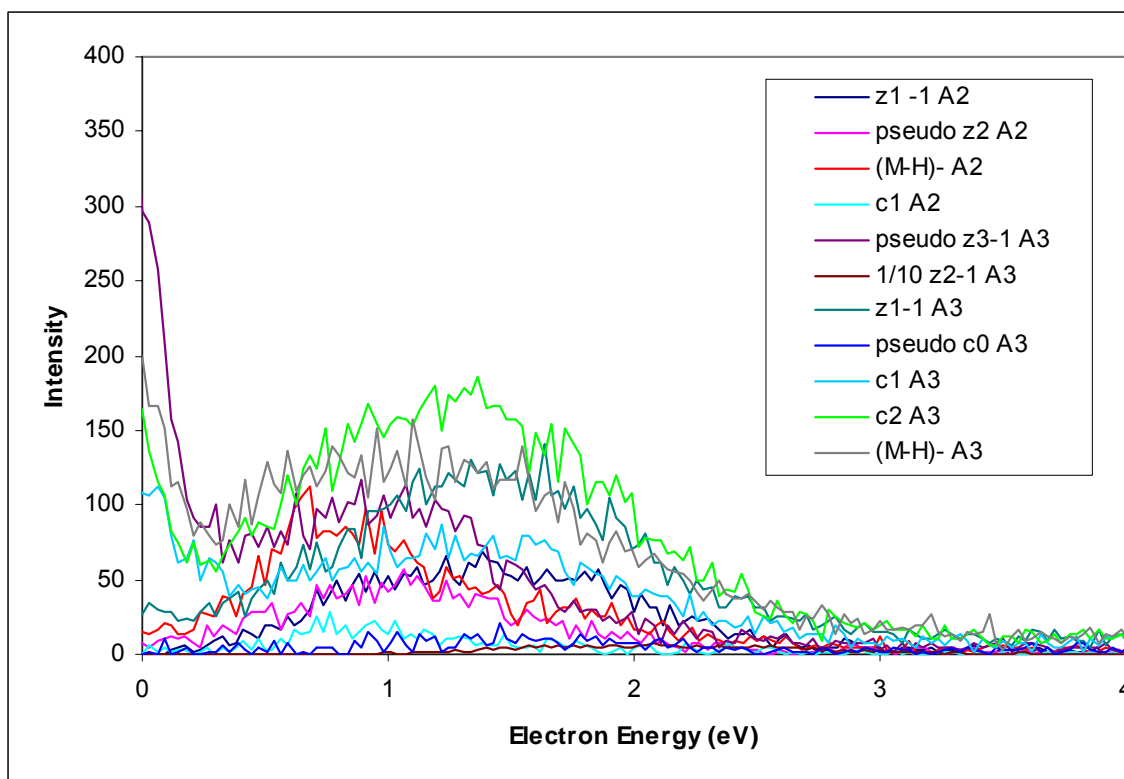


Figure 90. The effective yield curves for the z-1 ions (z_1-1 , blue, pseudo z_2-1 , pink), c ions (c_1 , aqua), and $(M-H)^-$ (red) ions from N-acetyl Ala-Ala and for the z-1 ions (z_1-1 , green, $1/10 z_2-1$, brown, pseudo z_3-1 , purple), c ions (pseudo c_0 , light blue, c_1 , light aqua, c_2 , neon green), and $(M-H)^-$ (grey) ions from N-acetyl Ala-Ala-Ala. The samples were introduced into the instrument by heating dry solid loaded in a capillary in the direct insertion probe.

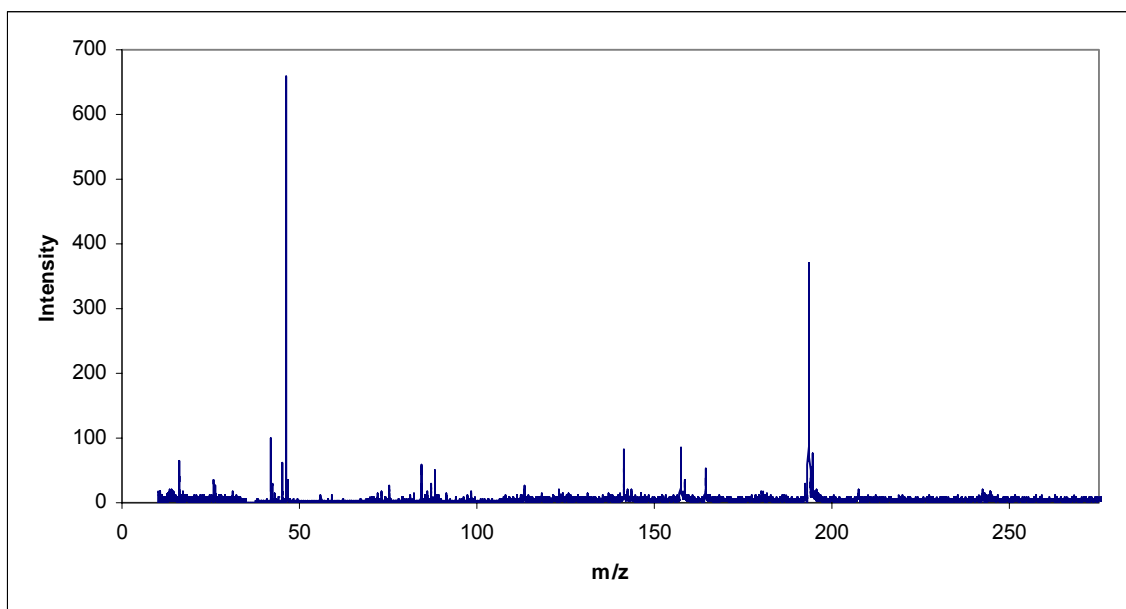
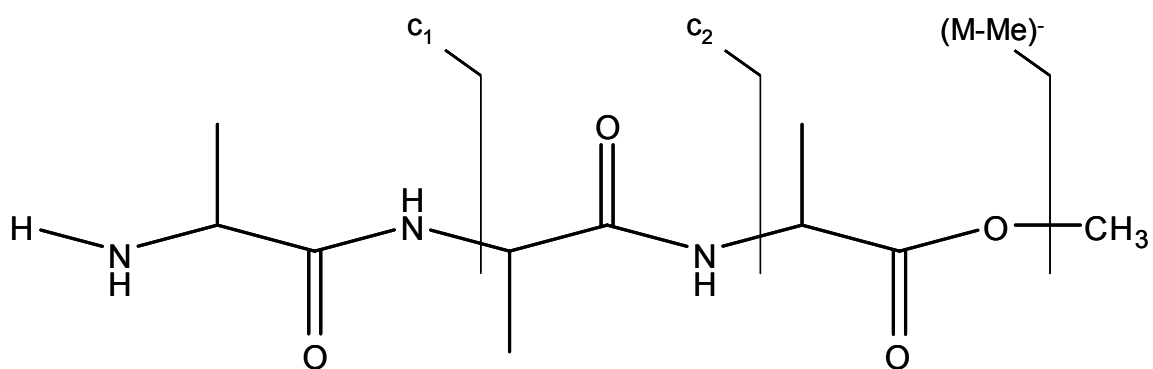


Figure 91. The REC-MS of $\text{Ala}_3\text{-OMe}$ with Cl^- from CCl_4 removed with ions generated by scanning electron energies from 0 - ~10 eV. The sample was introduced into the instrument by heating dry solid loaded in a capillary in the direct insertion probe. The ion source temperature was 67 °C and the direct insertion probe temperature was 160 °C.

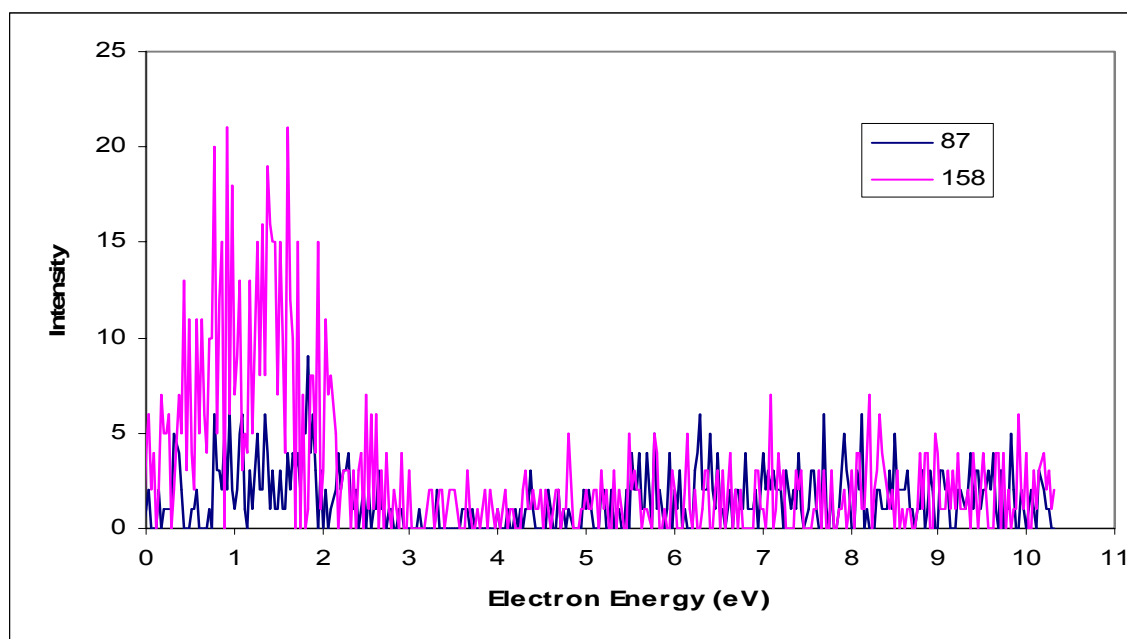
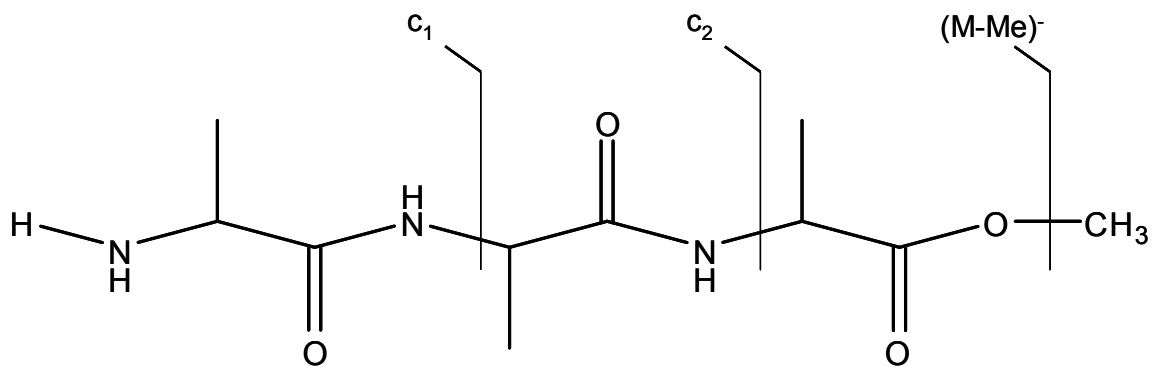


Figure 92. Effective yield curves for the formation of the ions c_1 with m/z 87 and c_2 with 158 from the REC-MS of Ala₃-OMe. The sample was introduced into the instrument by heating dry solid loaded in a capillary in the direct insertion probe. The ion source temperature was 67 °C and the direct insertion probe temperature was 160 °C.

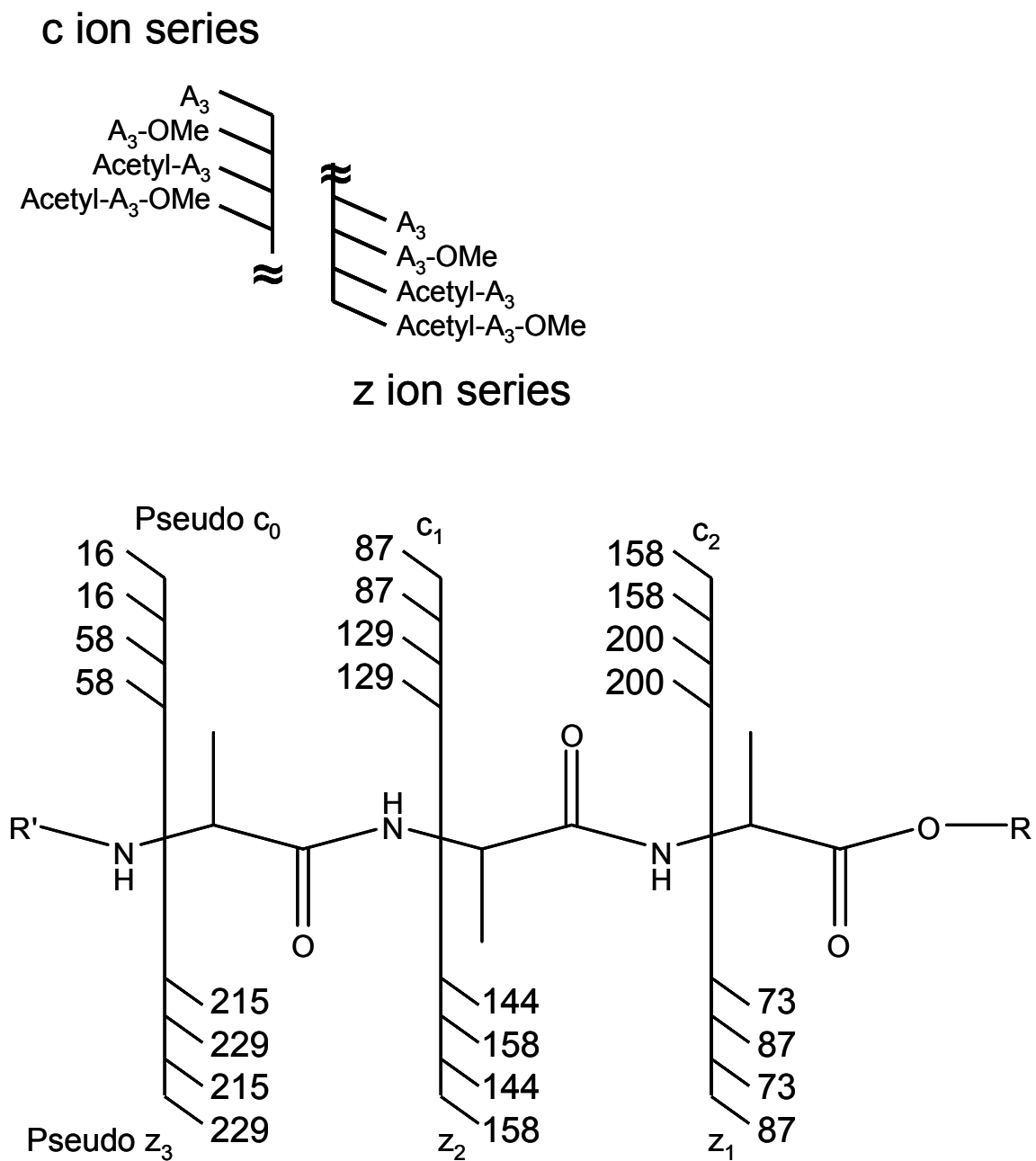


Figure 93. The m/z for the c and z ion series of alanine trimer compounds.

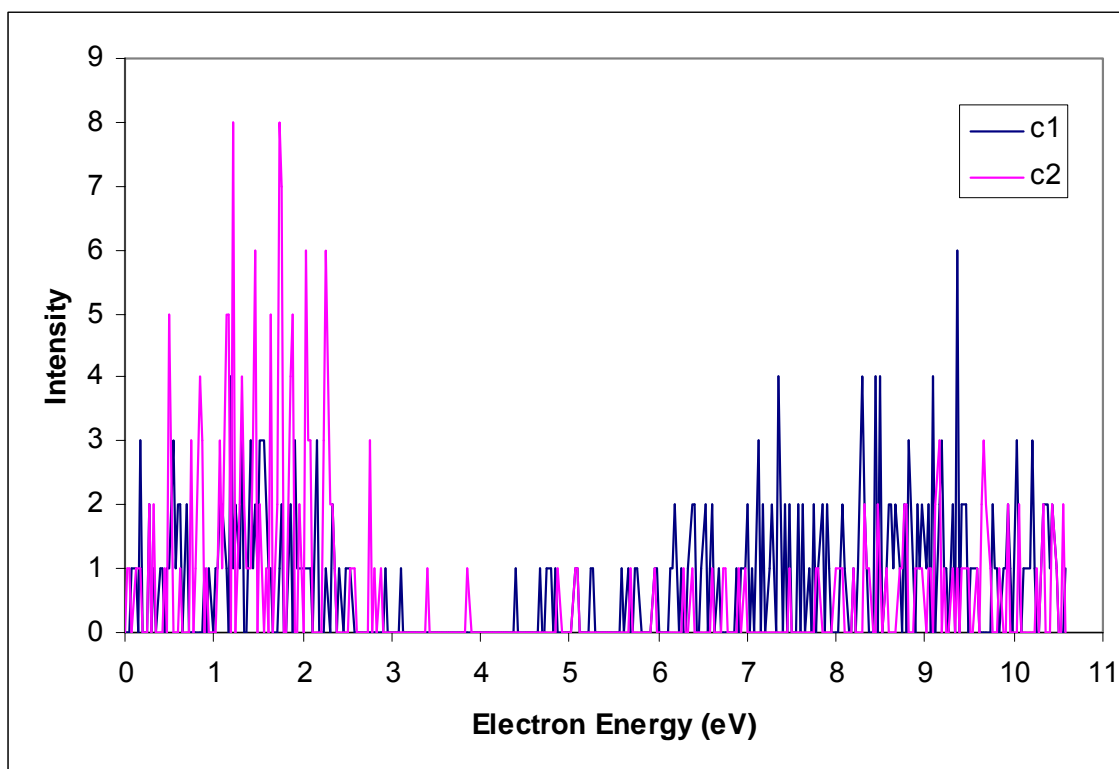


Figure 94. Effective yield curves for c_1 (blue) and c_2 (pink) ions from Ala-Ala-Ala-OMe. The samples were introduced into the instrument by heating dry solid loaded in a capillary in the direct insertion probe.

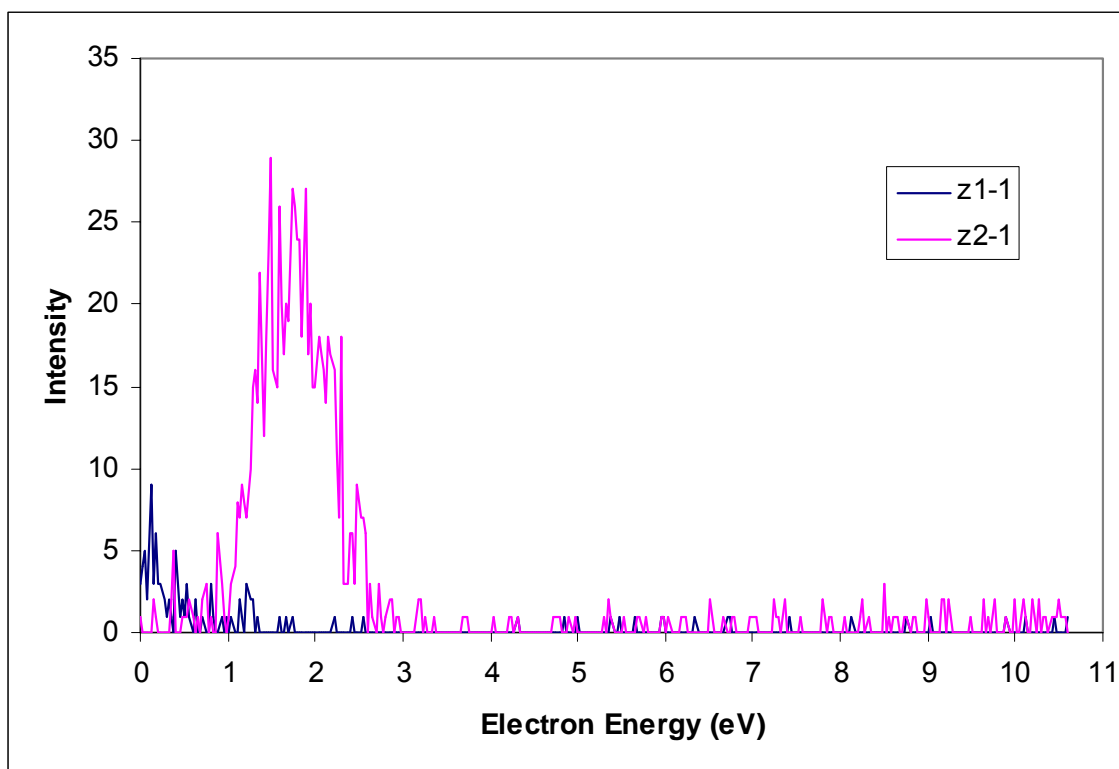


Figure 95. Effective yield curves for z_1-1 and z_2-1 ions from Ala-Ala-Ala-OMe. The samples were introduced into the instrument by heating dry solid loaded in a capillary in the direct insertion probe.

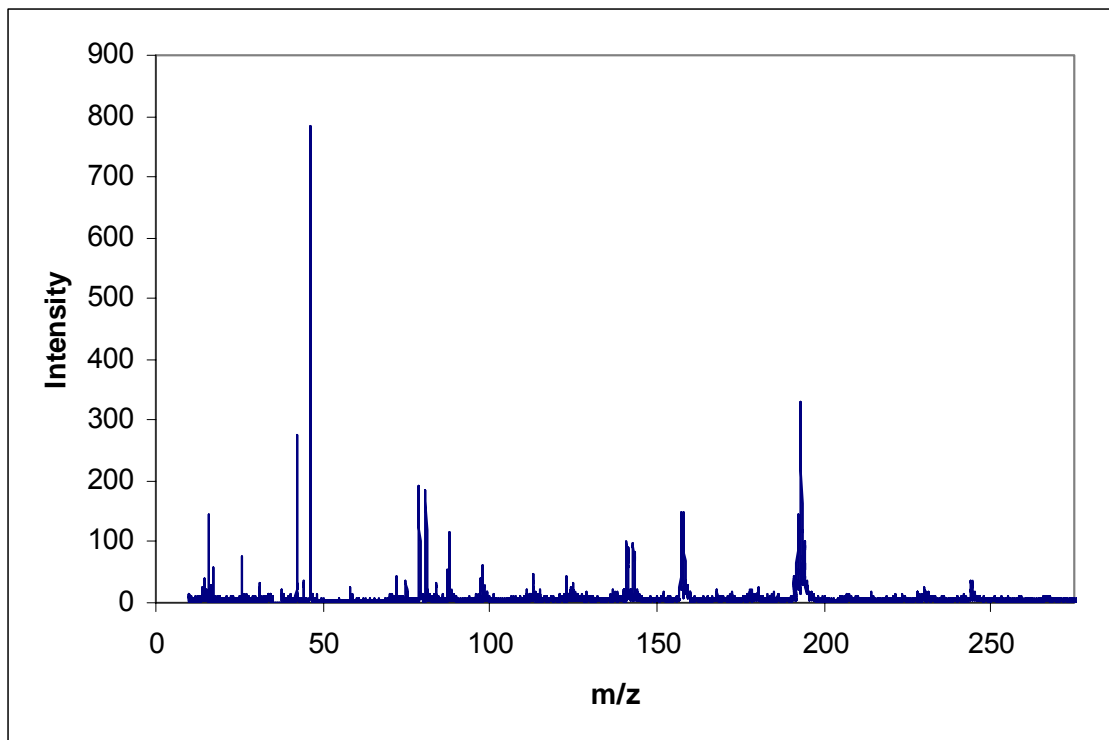


Figure 96. REC-MS of a less purified Ala-Ala-Ala-OMe product with the Cl^- ion removed. The samples were introduced into the instrument by heating dry solid loaded in a capillary in the direct insertion probe.

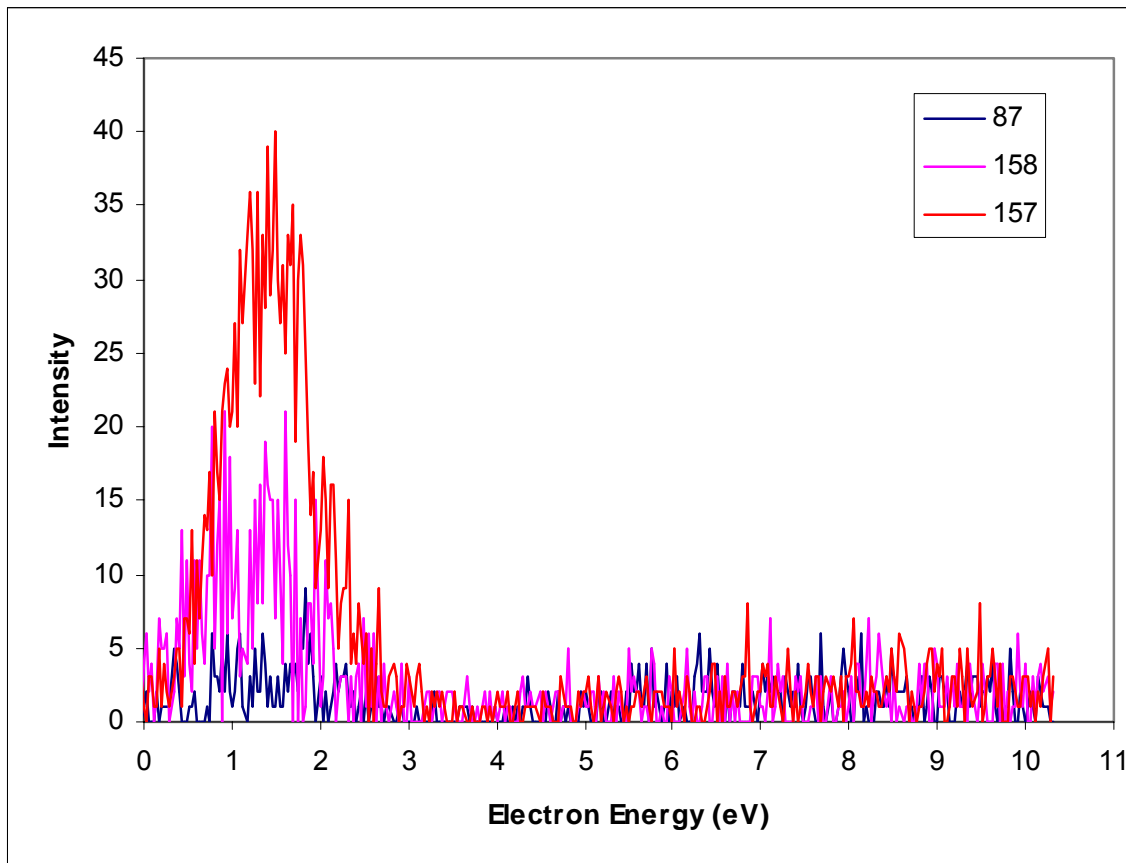


Figure 97. Effective yield curves from c_1 (m/z 87), c_2 (m/z 158), and z_2-1 (m/z 157) ions from A_3 -OMe. The samples were introduced into the instrument by heating dry solid loaded in a capillary in the direct insertion probe.

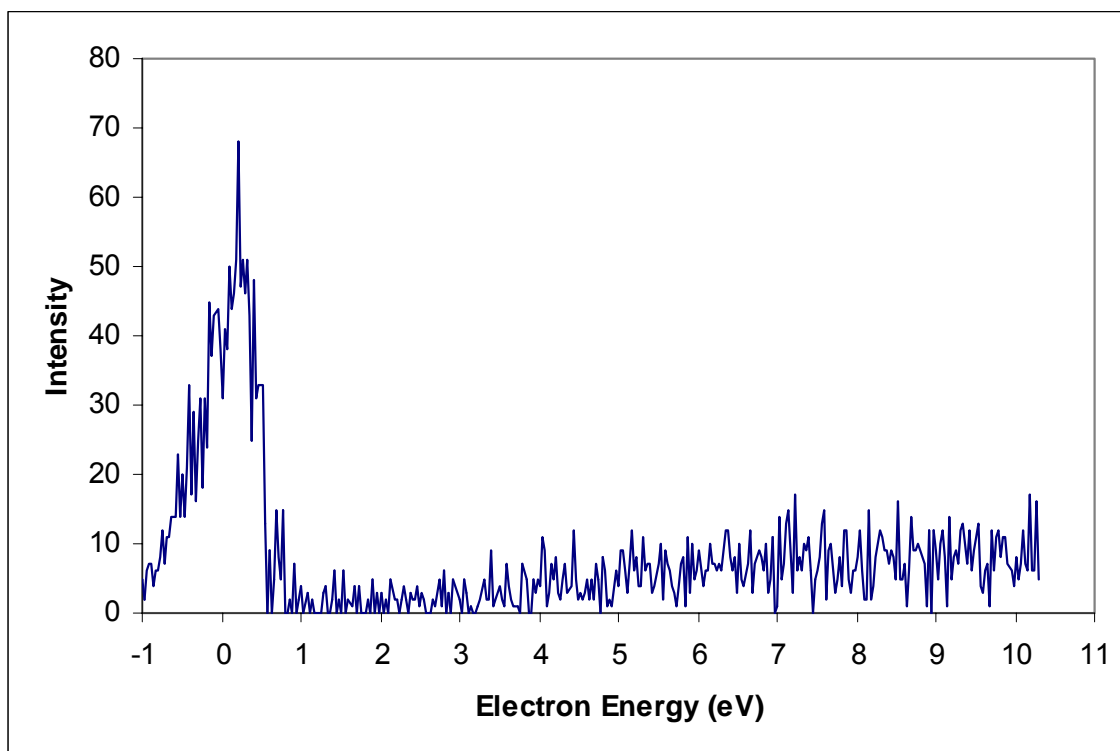


Figure 98. Effective yield curve for m/z 193 for the ion of the Fmoc side product from Ala-Ala-Ala-OMe. The samples were introduced into the instrument by heating dry solid loaded in a capillary in the direct insertion probe.

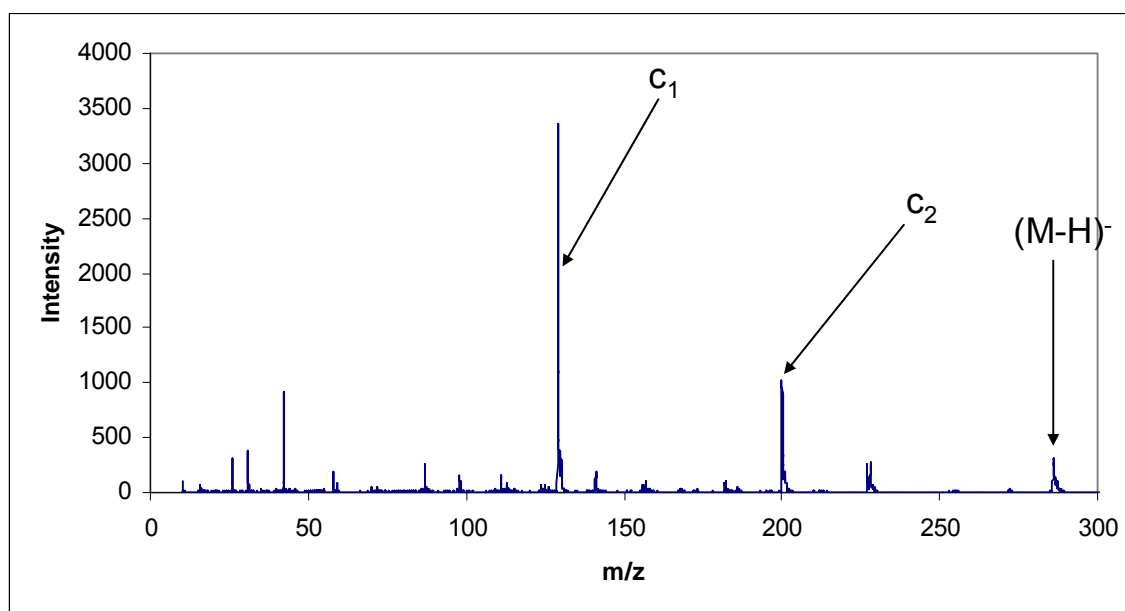
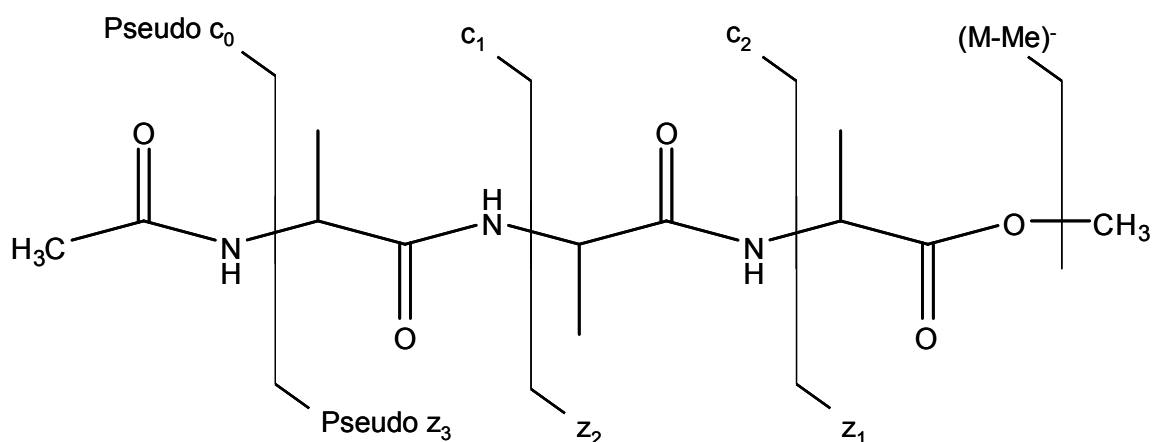


Figure 99. The REC-MS of N-Acetyl Ala₃-OMe with the c₁, c₂, (M-H)⁻ ions labeled and with ions generated by scanning electron energies from 0 - ~10 eV. The sample was introduced into the instrument by heating dry solid loaded in a capillary in the direct insertion probe. The ion source temperature was 153 °C and the direct insertion probe temperature was 170 °C.

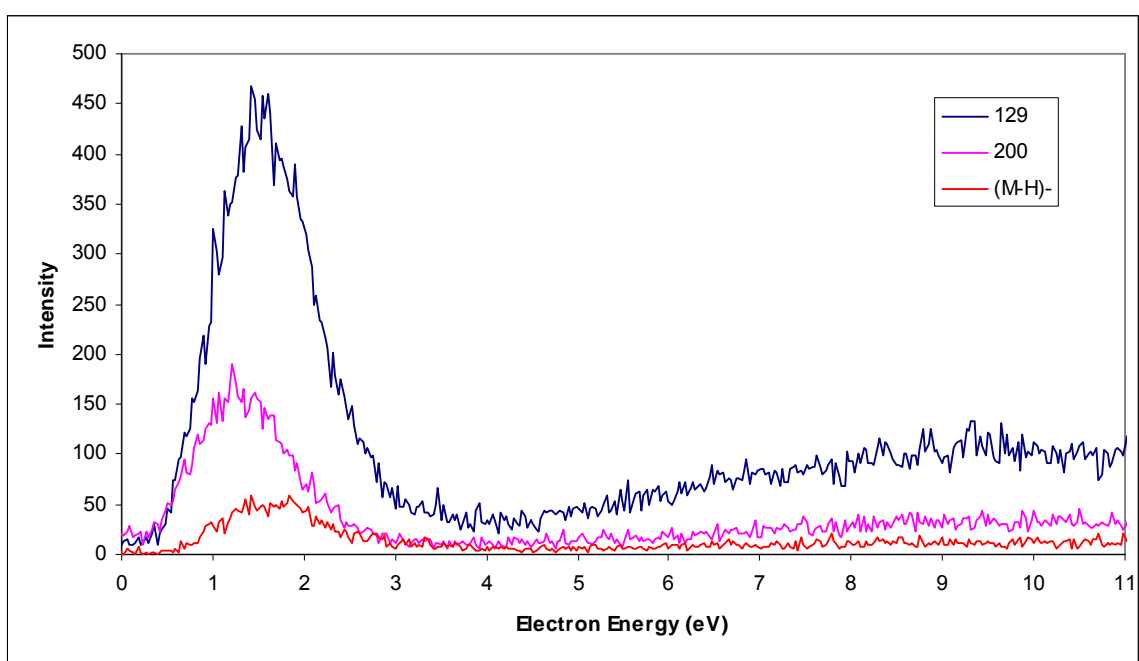
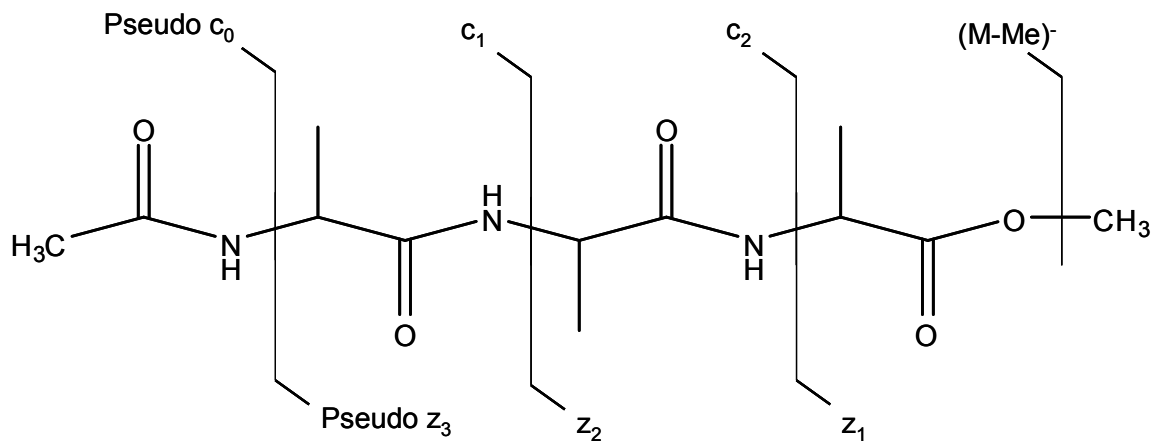


Figure 100. Effective yield curves for the formation of the ions c_1 , c_2 , and $(M-H)^-$ with m/z 's 129, 200, and 286 from the REC-MS of N-acetyl Ala₃-OMe. The sample was introduced into the instrument by heating dry solid loaded in a capillary in the direct insertion probe. The ion source temperature was 153 °C and the direct insertion probe temperature was 170 °C.

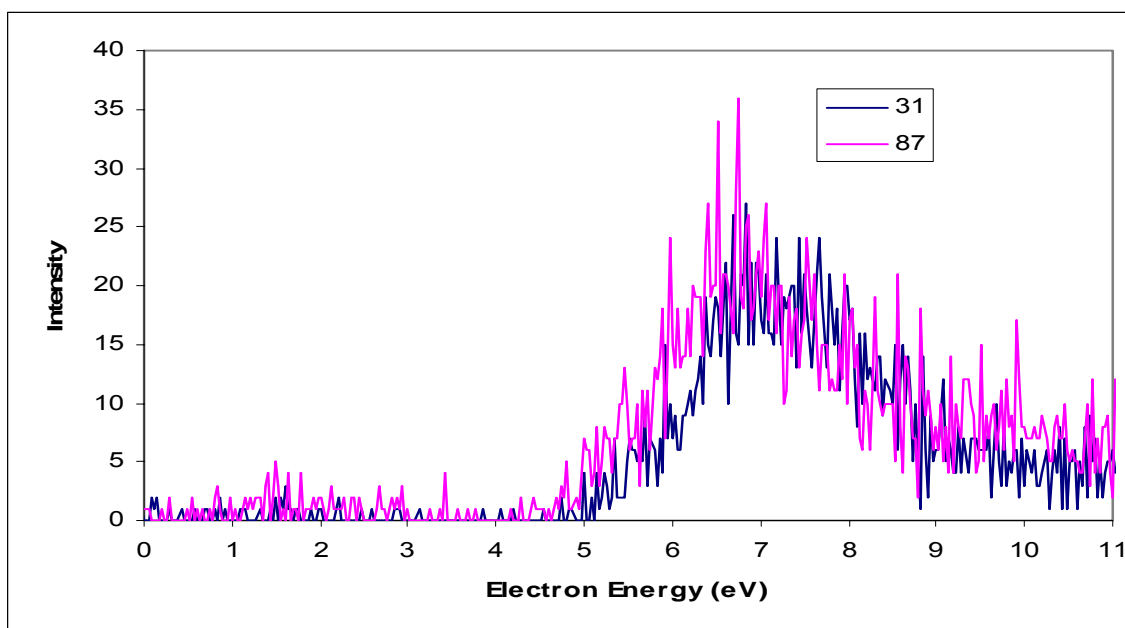
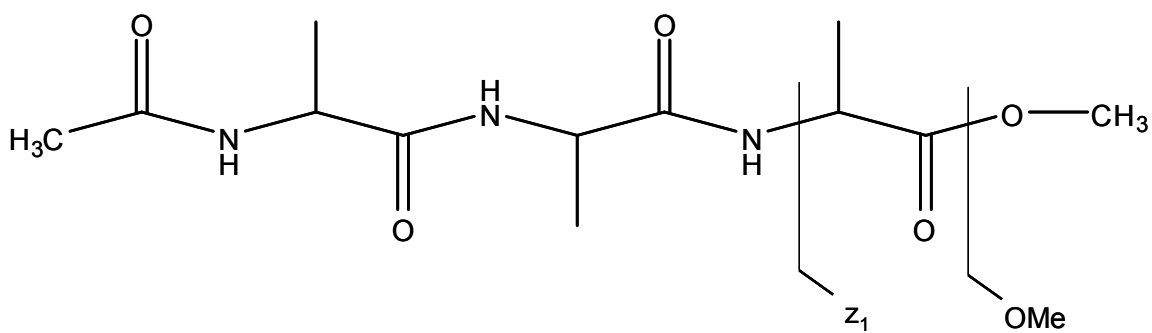


Figure 101. Effective yield curves for the formation of the ion OMe^- with m/z 31 and z_1^- with m/z 87 from the REC-MS of N-acetyl Ala₃-OMe. The sample was introduced into the instrument by heating dry solid loaded in a capillary in the direct insertion probe. The ion source temperature was 153 °C and the direct insertion probe temperature was 170 °C.

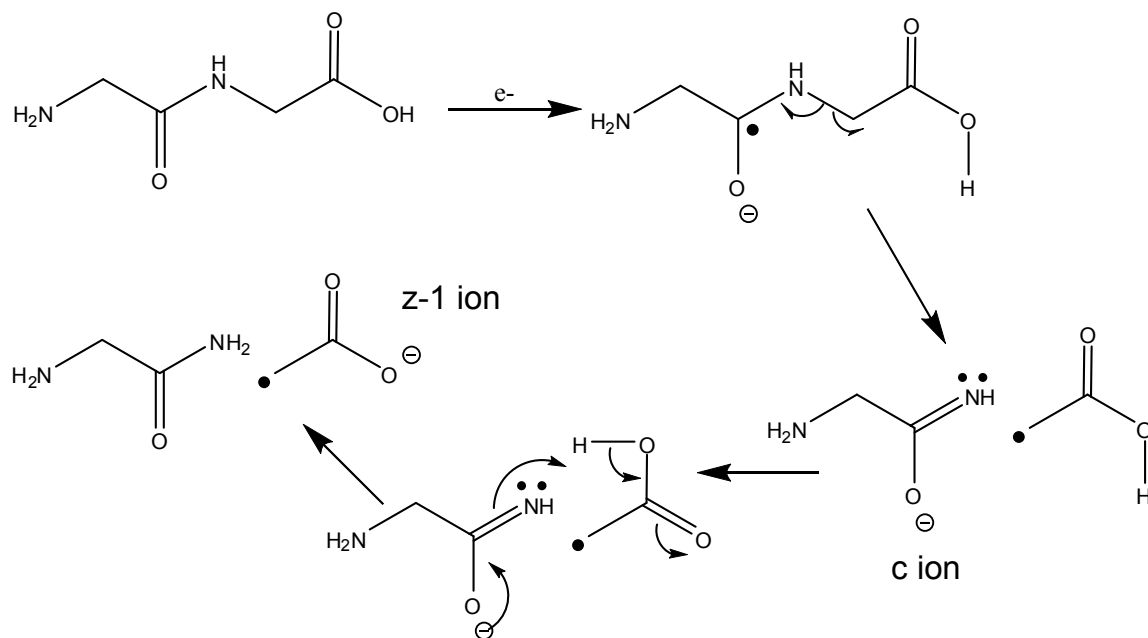


Figure 102. Scheme for capture of an electron at the amide group and peptide backbone cleavage to form c and z-1 ions.

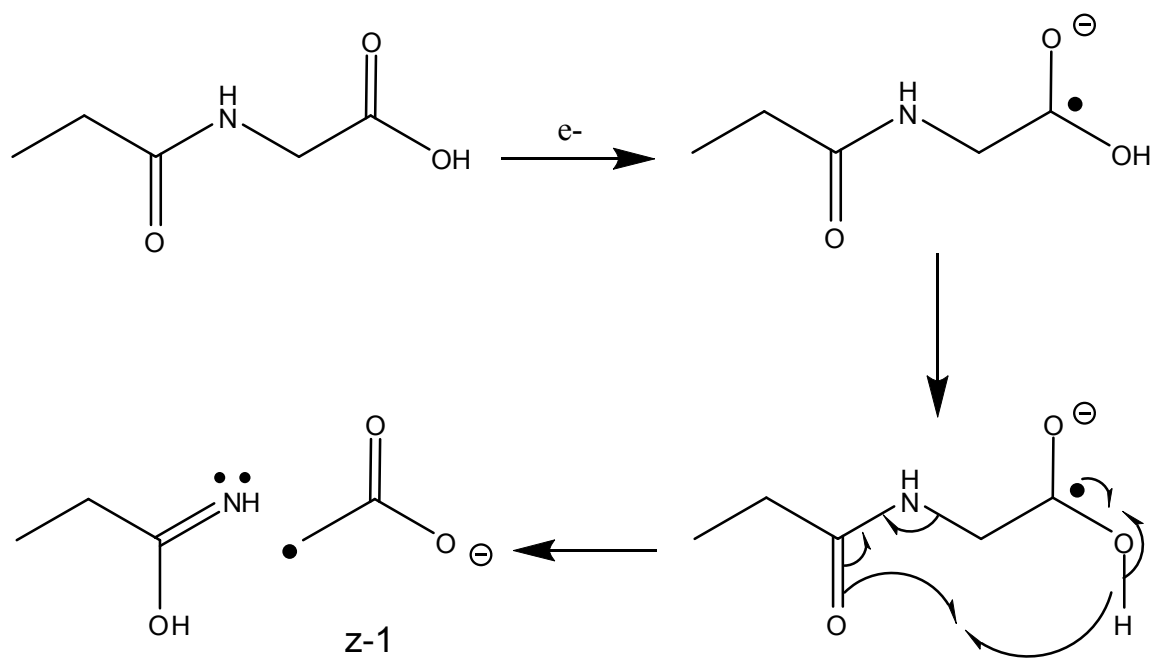


Figure 103. Scheme for capture of an electron at the carboxylic acid group and peptide backbone cleavage to form z-1 ions.

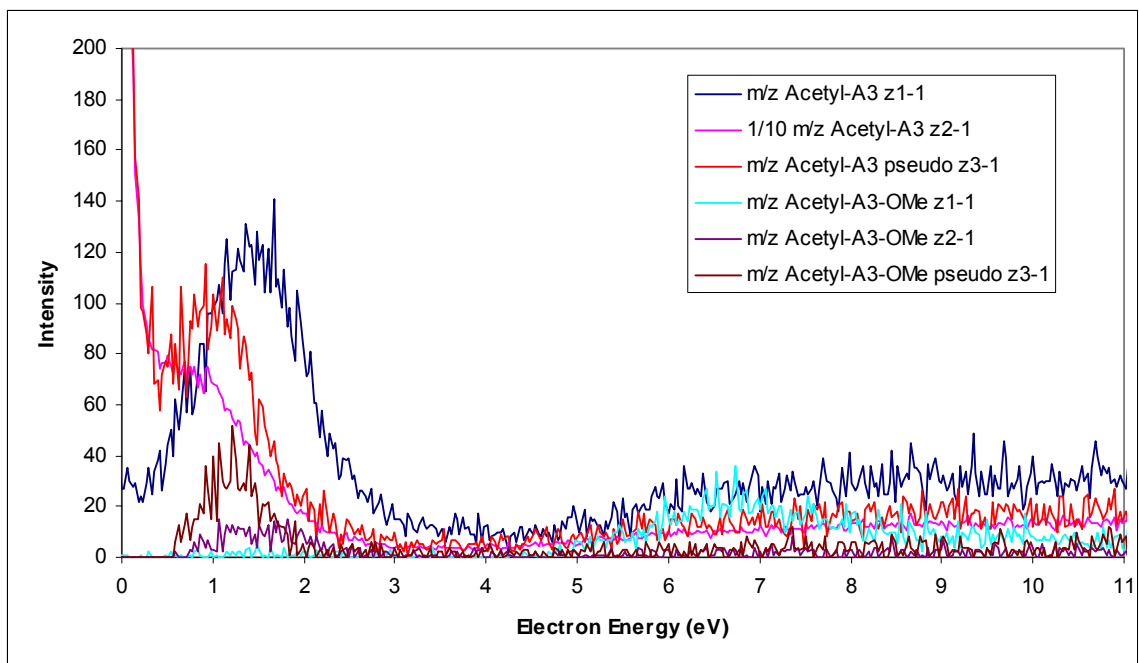


Figure 104. Effective yield curves from z-1 ion series: z₁-1 (blue), z₂-1 (pink), and pseudo z₃-1 (red), for N-acetyl-A₃ and z-1 ion series: z₁-1 (aqua), z₂-1 (purple), and pseudo z₃-1 (brown), for N-acetyl-A₃-OMe. The samples were introduced into the instrument by heating dry solid loaded in a capillary in the direct insertion probe.

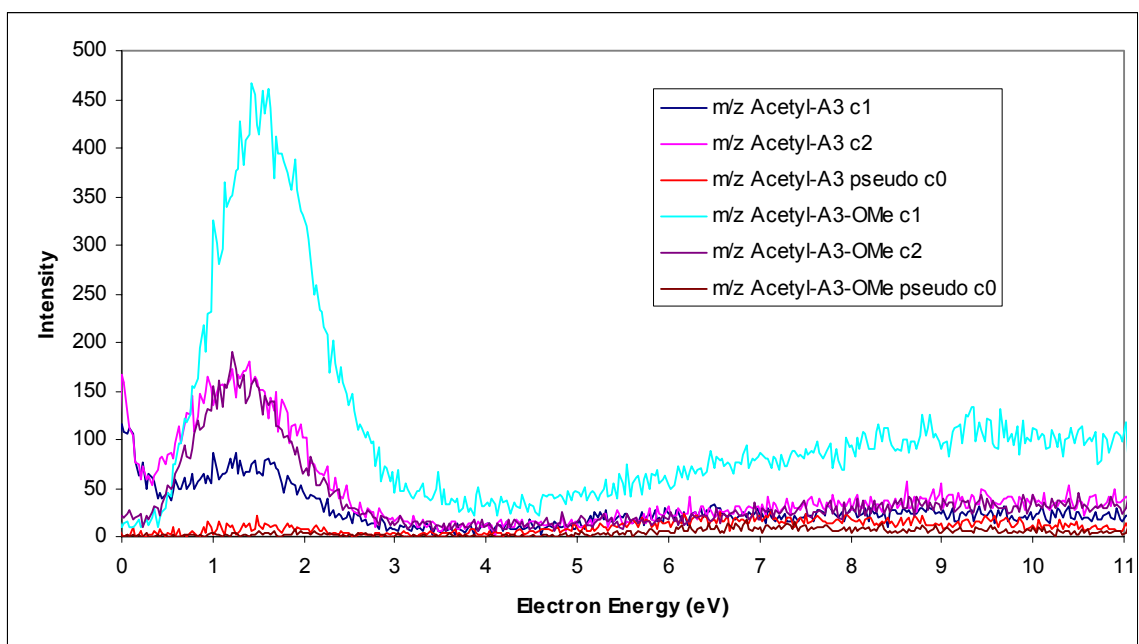


Figure 105. Effective yield curves from the c ion series: pseudo c₀ (red), c₁ (pink), and c₂ (blue), for N-acetyl-A₃ and c ion series: pseudo c₀ (aqua), c₁ (purple), and c₂ (brown), for N-acetyl-A₃-OMe. The samples were introduced into the instrument by heating dry solid loaded in a capillary in the direct insertion probe.

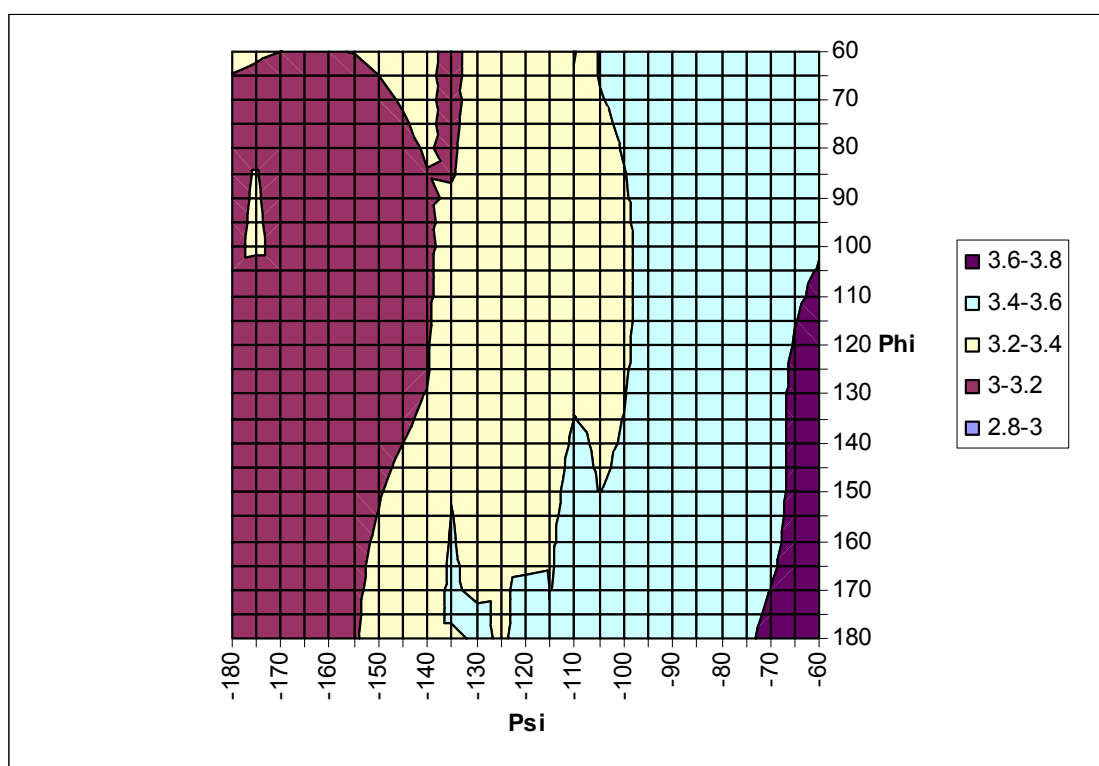
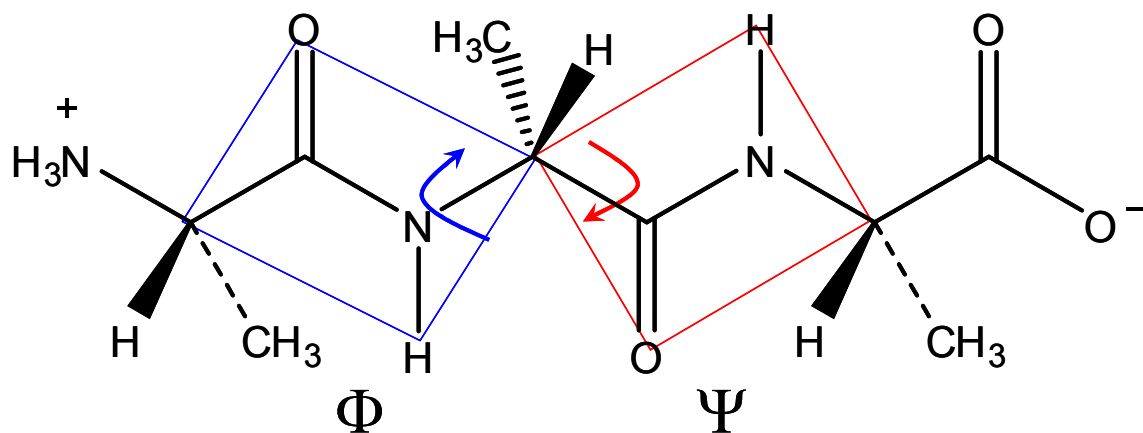


Figure 106. Potential energy surface in relation to the phi-psi angles for alanine dimer using the UHF/6-31 **G++ method to calculate the vertical electron attachment energy. The VEAES are shown by the different colors given in the legend in eV. By definition the trans extended conformation is defined as 180 degrees for phi (ϕ) and psi (Ψ) angles. The angle is varied based upon clockwise rotation of the plane as viewed from the C_{α} to the first atom of the plane. For phi this is the N and psi it is the C of the carboxylate. The dihedral angle between the plane of the amide bond and the C_{α} carbon is used as the angle varied experimentally. The model to demonstrate phi and psi angles was not the one used to calculate the potential energy surface.

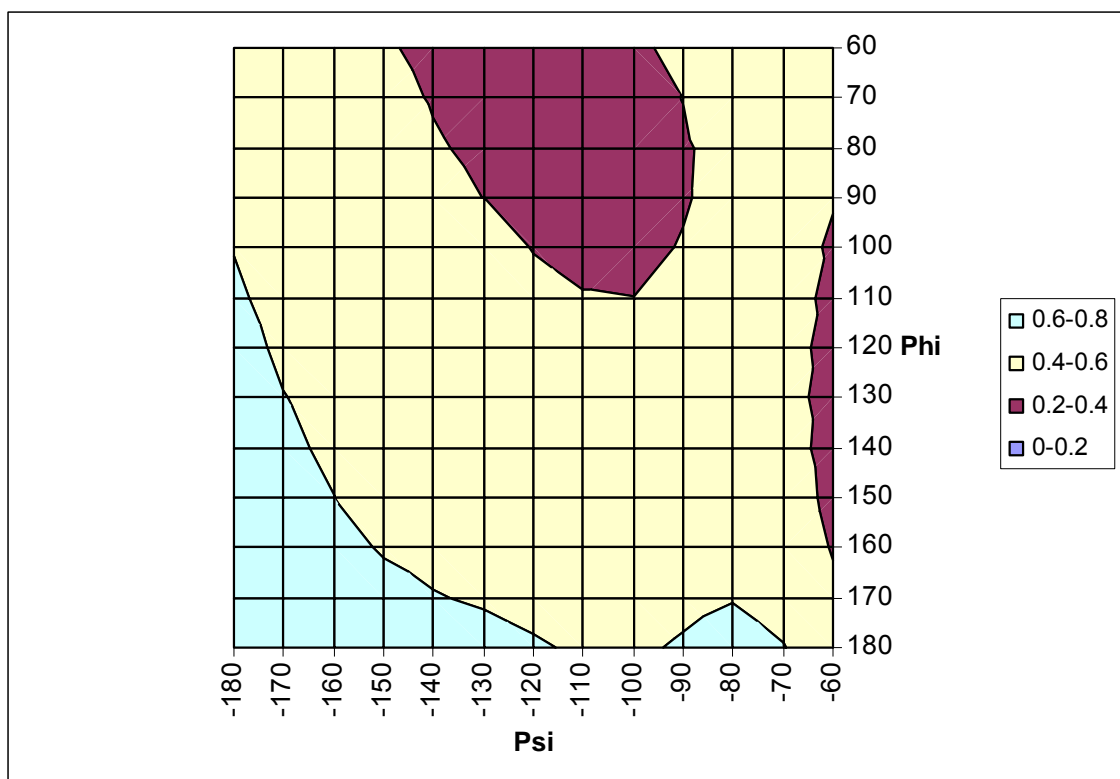


Figure 107. Potential energy surface in relation to the phi-psi angles for alanine dimer using the UHF/aug-cc-pVDZ method to calculate the vertical electron attachment energy. The VEAE's are shown by the different colors given in the legend in eV.

Discussion

In-beam 2D Mass Spectroscopy

The in-beam mass spectra of the peptides studied show proof of principle that low energy electron - peptide interactions can produce REC-MS negative fragment ions even when the peptides are non-volatile. In the mass spectra, fragment ions from the peptide backbone were observed for b and y series as well as for c and z-1 ion series, i.e. typical ions that are seen in REC-MS, ECD, EDD, and ETD. Furthermore, these experiments show that larger peptides, with molecular weights greater than 300 amu, can be studied by resonance electron capture. This is truly impressive and has not been achieved before. The largest peptide fragment observed was an ion with m/z 851 from substance P which has a MW of 1347 Da. The mass of the fragment ion with m/z 851 matches that for the z_{7-1} ion (Fig. 30). Aside from cystine dimethyl ester, all peptides showed backbone cleavages. $(M-H)^-$ ions were observed for smaller linear peptides up to a hexamer regardless of the C-terminal modifications. The energy calibrated in-beam results are proof that resonant electron capture results in fragment negative ions that are also seen in ECD experiments and that provide a preliminary estimate of the electron energy, i.e. ~ 1 eV that leads to the aforementioned fragment negative ions.

Negative Ion High Resolution Energy Calibrated Mass Spectrometry

The high resolution experiments on the alanine dimer were required to resolve whether fragmentation of the alanine dimer led to z-1 or b ions. It was assumed that if the ion with m/z 72 is a b ion then the fragmentation observed would have been unlikely to be due to resonance electron capture. The observation of an ion with the exact mass of 72.02100 Th lead to the assignment of the ion with m/z 72 as the z-1 ion. The error from the calculated mass is -1.8 ppm which is well within the limit of 5 ppm for reporting exact mass measurements in publications. The experimental conditions for high resolution mass spectrometry with electron energy at ~1 eV are similar to the experimental conditions in REC-MS obtained with the EM-rToF-MS. The energy spread of the electron beam of the JEOL 600 MS is estimated to be ~1 eV which therefore will generate electrons within the energy range necessary to form the m/z 72 ion as determined in the REC-MS. The energy calibrated mass spectrum (Fig. 26) for alanine dimer and the mass spectrum from the REC-MS (Fig. 71) are found to be nearly identical and therefore the conditions used in the energy calibrated negative ion experiments and the high resolution energy calibrated negative ion experiments performed on the JEOL instrument, provide the groundwork for studying the ions formed by REC as in the EM-rToF-MS. Because of these results, the ions with m/z 72 in the REC-MS for Ala-Ala were assigned to z-1 ions and similar ones in other peptides can be reasonably assigned as z-1 ions based on these high mass resolution results.

In addition, the ion recorded with m/z of 87.05613 Th is within an error of 3.3 ppm of the theoretical mass value of the c ion (Fig. 71). The data show that cleavage of the C_α-N bond is possible at the low electron energy of ~1 eV. The capture of an electron with energy of ~1 eV by the alanine dimer likely results in a π* state as mentioned before

but this energy of ~ 1 eV is less than the calculated vertical electron attachment energy of 2.5 – 2.8 eV for the π^* state of the neutral molecule [42]. Studies by Simons et al suggest coupling of π^* - σ^* orbitals of the alanine dimer for cleaving the C_α -N bond. The discrepancy between the experimental data and the calculated vertical electron attachment energy, does not invalidate this mechanism and thus the origin of the ions through π^* - σ^* coupling appears reasonable. Electron attachment directly into a σ orbital is estimated to be ~ 6 eV which is still considerably higher in energy than the experimental data leading to these fragments even when corrected by the energy difference between the experimental data and the calculated π^* orbital energy of 1.5 to 1.8 eV.

Resonance Electron Capture – Mass Spectrometry

Amino Acid Esters

The effective yield peaks of the amino acids and their methyl esters involve two types of resonances that produce fragment ions [50]. The low energy resonances at 1-2 eV are shape resonances associated with the π^* orbital of the carboxylic acid. Resonances leading to the effective yield maxima at 5 eV and greater are Feshbach resonances. Because the effective yield maxima overall remain unchanged for all fragmentations except for those that form the carboxylate anions, it can be concluded that the shape resonances involving π^* orbitals and the higher energy Feshbach resonances, i.e. ≥ 5 eV, are still contributors for fragmentation of amino acids and their esters. Therefore the

discussion of results for the amino acid ethyl, isopropyl, and t-butyl esters will be limited to the effective yield curves of the carboxylate anions. These results that have lead to re-evaluation of previous conclusions, and anomalies.

Fragmentation of ethyl, isopropyl, and t-butyl esters of the amino acids, glycine, alanine, and phenylalanine by low energy resonance electron capture involve interactions between low energy electrons and the amino acids and their esters which occur through three types of resonances. Specifically, electrons interacting with these compounds have energies 1.2 - 1.9 eV. They result in shape resonances thereby creating π^* states localized through either the carboxylate group or the aromatic side chain when present. The fragments arising from attachment of electrons of energies 3.3 - 3.7 eV are not unequivocally assigned but are proposed to involve triplet electronic transition Feshbach resonances. The experimental observation of fragment ions arising through this type of resonance, is a new result and unique to the ethyl, isopropyl, and t-butyl esters. The possibility remains that this resonance leads to fragmentation in the underivatized amino acids as well as the methyl esters, but it is unresolved from the effective yield maxima at 1.2 - 1.3 eV. The fragment ions resulting from capture of electrons with energies of ~ 5.5 eV and higher involve $\pi \rightarrow \pi^*$ and $n \rightarrow \pi^*$ singlet state Feshbach resonances as assigned previously[50].

Furthermore, as was determined in the case of the methyl esters the fragmentation pathways are not affected by the presence of additional carbon atoms but the relative intensities of the carboxylate anions vary considerably. The ethyl, isopropyl, and t-butyl esters all have effective yield maxima at ~ 3.5 eV and ~ 9.4 eV for production of the carboxylate anion which is in contrast to that observed for the underivatized amino acids

whose effective yield maxima are ~ 1.2 eV and in the case of methyl esters at ~ 1.25 eV and ≥ 8 eV. All other ions remain fundamentally the same with respect to their effective yield maxima.

N-Acetyl Amino Acids

The N-Acetyl compounds represent a bridge between amino acids and peptides. The addition of an amide bond formed by the acetylation of the N-terminal amine adds a new site for electron capture that mimics the formation of a dimer without the additional problem of the polar primary amine group that decreases the compound's volatility.

The overall trends of the N-acetyl amino acids can be summarized. First, the most intense peaks in the mass spectra are low electron energy peaks 0.7 eV to 1.5 eV and are associated with the π^* states as previously observed in amino acids and other derivatives and the most intense ion is invariably the $(M-H)^-$ ion. Second, the z-1 ions are higher in energy than the effective yield maxima for the $(M-H)^-$ ion by 0.7 eV for N-acetyl alanine, 0.3 eV for N-acetyl tyrosine, and 0.4 eV for N-acetyl tryptophan. In the case of N-acetyl phenylalanine, the z ion with m/z 148 shows a 0.2 eV energy difference between its formation and that of the $(M-H)^-$ ion. Third, the c type ions with m/z 58, produced from N-acetyl amino acids, have effective yield maxima at high energies, i.e. ≥ 5 eV, and only N-acetyl alanine has an effective yield maximum at low electron energy, specifically at 2 eV. The higher energy maximum at ~ 5 eV is similar in energy to that for the fragment ion with m/z 16 from the amino acids. This fragmentation may be associated with electron capture at the carboxylic acid that cleaves the C_α -N bond in a manner consistent with the

loss of m/z 16 from amino acids without N-terminal derivatization. Fourth, the N-acetyl aromatic amino acids have lower effective yield maxima for the $(M-H)^-$ and $z-1$ ions compared to those for N-acetyl alanine. The observation of lower effective yield maxima for aromatic N-acetyl amino acids is consistent with those reported for underivatized amino acids and the methyl esters[50]. Lastly, the N-acetyl aromatic amino acids do not favor backbone cleavages. The $(M-R)^-$ ions are the second most intense ions arising from N-acetyl phenylalanine and N-acetyl tyrosine and these are potentially the ions analogous to the ion with m/z 115 from N-acetyl tryptophan. The previously reported data for N-acetyl tryptophan shows $(M-R)^-$ as the most intense fragment ion. Overall, the negative fragment ions can be assigned as arising from either low energy (1 – 2 eV) π^* shape resonances or higher energy (> 5 eV) Feshbach resonances, specifically electronically excited Feshbach resonances of 5 – 7 eV and core excited resonances of ≥ 8 eV.

Peptides

The dominant ions formed by interactions of low energy electrons with peptides are due to π^* state resonances. The formation of these ions cannot be unequivocally assigned to orbitals localized at either the amide or carboxylic acid groups except in the case of $(M-H)^-$ ion, which matches almost identically the effective yield maxima of the underivatized and N-acetylated amino acids and therefore is associated with the π^* orbital of the carboxylic acid. It must be concluded that $\pi^* - \sigma^*$ orbital mixing precedes cleavage of the sigma bonds in the peptide backbone, specifically in the case of the $C_\alpha-N$ bond as predicted by Simons et al[42], because direct electron attachment to the σ^*

orbital requires more energy than is observed experimentally for formation of these fragment negative ions. Furthermore, the presence of the N-acetyl group has a limited effect on the formation of the ions compared to the underivatized peptide. As noted with the acetylated amino acids the N-acetyl group provides improved volatility and may also be considered an extension of the peptide sequence as it mimics an amino acid. The same type cleavages are seen as those observed for peptides and at the same electron energies.

Increasing the peptide chain length leads to a change in fragmentation from the (M-H)⁻ dominant ion to peptide backbone cleavages. The shift in dominant fragmentation occurs with the trimer, where the dominant ion is due to backbone cleavage at the second amino acid residue. The electron energy required for peptide backbone cleavage appears to be fairly insensitive to the chain length of the peptide. The alanine dimer and the N-acetyl alanine dimer have slightly higher effective yield maxima for the z₁-1 ion than for the (M-H)⁻ ion. The mechanistic implication of the results for the alanine dimer and the N-acetyl alanine dimer is that there is an additional energy requirement for the formation of the z-1 ion as described before. This difference in energy was not observed in the larger unesterified peptides. The reason the energy difference was not observed is that the “hot band” capture at ~0 eV obscured the effective yield peaks at 1-2 eV.

The most important result from the studies with peptide ions has been the change in fragment ions observed between the N-acetyl Ala-Ala-Ala and the N-acetyl Ala-Ala-Ala methyl ester. The formation of c ions from the methyl ester suggests that the capture of the electron occurs to give the π* state involving the amide group in a manner consistent with the mechanism proposed for amide electron capture in ECD. If the formation of the c ions occurs via the capture of the electron at the amide group then the

formation of the z-1 ion likely goes through the same mechanism with an additional transfer of a hydrogen atom to the c fragment to form the negative ion (Fig. 103).

The presence of “hot bands” in the compounds suggests that the capture of a near to zero energy electron can lead to fragments of the peptide backbone. Given the energy of FT-ICR ions - the exact determination of this energy is outside the scope of this study - the possibility of energetically excited ions occurring may be extremely important to the mechanism of ECD and related techniques.

Combined REC-MS Discussion

The presence of neither N-acetyl groups nor methyl esters dramatically change the resonances states of the amino acids or peptides. The methyl esters do affect the fragment negative ions observed from peptide backbone cleavage. Put another way, the orbital energies of electron-capturing amino acids derivatives are relatively unaffected by the derivatization but the selection of the fragmentation channels from the resonances is effected by the presence of methyl esters but not by N-acetyl groups. Second, the dominant fragment ions observed result from by π^* shape resonance whose energies are in the range 1-2 eV and localized on the carboxylic acid, amide, or aromatic side chain moieties. Third, in addition to the π^* shape resonances, three other trapping interactions lead to fragment negative ions observed in these experiments. The effective yield peaks between 3 – 4 eV are possibly associated with singlet – triplet electronically excited Feshbach resonances. The peaks between 5 - 7 eV are associated with singlet – singlet electronically excited Feshbach resonances as assigned previously [50]. The effective

yield peaks observed at ≥ 8 eV are likely associated with the core-excited resonances. Lastly, from a comparison of the fragment ions and effective yield maxima observed in the alanine trimers, the likely mechanism for forming c and z-1 ions involves capture of the electron to create a π^* state with the electron density associated with the amide, followed by $\pi^* - \sigma^*$ orbital mixing that results in C_α -N bond cleavage. It is postulated that the formation of the z-1 ion involves reorganization of the neutral radical fragment with z structure to form the z-1 ion.

Potential Energy Surfaces

The most important conclusion that can be reached from calculations on the impact of phi psi angles with vertical electron attachment energy is that the change is minimal. In the aug-cc-pVDZ calculation the change in VEAE is on the order of the energy spread of the electron beam in an electron monochromator, i.e. ~ 0.2 eV. Secondly, even if the larger VEAE difference of ~ 0.4 eV from the 6-31 **G++ calculation is used, the width of the majority of the effective yield peaks is sufficiently greater than the variation in the calculated VEAE. An additional important result from this investigation is that the compounds studied are too small to allow for a conformational preference in the REC-MS and the results from the “average” of REC from the different structures. A secondary conclusion is that by using the aug-cc-pVDZ method, a more reasonable model results because of the smooth nature of the potential energy surfaces calculated. The 6-31 **G++ calculations show greater discontinuities in the potential energy surface suggesting that, the “scf=qc” command is required to lead to

a smooth energy surface with the UHF/ 6-31 **G++ basis set and that even with high level calculations the results show “ripples.”

Conclusion

In-beam

The in-beam experiments performed on the JEOL 600H – MS provide proof of principle that larger peptides can be studied by electron capture and that these non-volatile species will produce fragment ions that result from peptide backbone cleavages. Furthermore, the possibility of calibrating the electron energy to study the relative fragmentations of peptides at high (~5-6 eV) and low (~0-1 eV) energies also has been demonstrated. The z_{7-1} ion with m/z 851 from substance P is the largest ion that was observed using the in-beam experimental technique. However, the in-beam analysis of peptides also shows prominent y ions in the mass spectrum which become more intense with increasing numbers of residues in the peptide. The y ions are due to thermal breakdown of the peptides because the temperature of the source in the in-beam experiments is still too high.

High Resolution

The determination of the exact masses of the z_{-1} ion with -1.8 ppm error and the c ion with 3.3 ppm error unambiguously assigns these fragments from the alanine dimer. Proving that the ions observed with low electron energies are z_{-1} and c type allows for assignment of the fragment ions observed in the EM-rToF-MS. Furthermore, the assignment of z_{-1} and c type ions proves that resonance electron capture leads to

cleavages of the peptide backbone at the same position, i.e. at the C $_{\alpha}$ -N bond, as is observed in electron capture dissociation.

Amino Acid Esters

Fragmentation of esters of the amino acids, glycine, alanine, and phenylalanine and ionization by low energy resonance electron capture involves the interaction between the low energy electrons and the amino acids and their esters and occurs through three types of resonances. Specifically, the electrons interact with these compounds with energies 1.2 - 1.9 eV through shape resonances involving π^* states of either the carboxylate group or the aromatic side chain when present. The fragments arising with electron energies 3.3 - 3.7 eV are not unequivocally assigned but are proposed to involve singlet to triple electronic transition Feshbach resonances. The experimental observation of fragment ions due to these resonances is a new result and unique to the ethyl, isopropyl, and t-butyl esters. The possibility remains that this resonance leads to fragmentation in the underivatized amino acids and the methyl esters but is unresolved from the effective yield maxima at 1.2 - 1.3 eV. The fragment ions due to the electron energies at ~ 5.5 eV and higher are due to $\pi \rightarrow \pi^*$, $n \rightarrow \pi^*$ singlet state Feshbach resonances, and core excited resonances as assigned previously[50].

As was determined in the case of methyl esters the fragmentation pathways are not affected by the presence of additional carbon atoms, but the relative intensities of the carboxylate anion produced by resonant capture vary considerably. The ethyl, isopropyl, and t-butyl esters all have effective yield maxima at ~ 3.5 eV and ~ 9.4 eV for formation

of the carboxylate anion which contrasts with the results observed for the underivatized amino acids with their effective yield maxima at ~ 1.2 eV and the methyl esters at ~ 1.25 eV and ≥ 8 eV. All other ions remain fundamentally the same with respect to effective yield maxima.

The results reported here show that esters can be used to study the gas phase interactions between low energy electrons and derivatized amino acids. The esters of amino acids serve as representatives of the amino acids themselves because the effect of different esterifying groups is limited to changes in ion intensity and effective yield maxima for carboxylate anion formation.

N-acetyl Amino Acids

The $(M-H)^-$ ions are observed for the N-acetyl amino acids at similar electron energies to that of the underivatized amino acids. For N-acetyl alanine, the ions were observed at 1.8 eV for the $z-1$ and at 2.0 eV and 9.8 eV for the c ions. The c ion from N-acetyl amino acids is similar in energy to the formation of the ion with m/z 16 in peptides with underivatized N- termini. The site of electron capture may be the carboxylic acid group in a manner similar to the formation of the ion with m/z 16 from underivatized amino acids which therefore would arise from a Feshbach resonance of electronic transitions. The $z-1$ ion is clearly a shape resonance associated with the π^* state but whether the orbital is associated with the amide or carboxylic acid groups cannot be determined.

The aromatic N-acetyl amino acids show formation of the (M-H)⁻ and (M-R)⁻ ions as the primary fragmentation pathways. The fragment ions are generated by electron energies 1.0 – 1.4 eV and are again shape resonances involving the π^* states but whether they are associated with the side chain group or with the amide or carboxylic acid groups cannot be determined. Furthermore, the pseudo z-1 and c ions are observed at higher energies, i.e. ≥ 6 eV, suggesting that the capture of low energy electrons is into unoccupied orbitals that do not favor backbone fragmentation in aromatic amino acids.

N-acetylation of amino acids appears to have a limited effect on the electron energy requirement for formation of ions, but derivatization of this type has a high impact on their volatility. The formation of the (M-R)⁻ ion from aromatic amino acids is favored as seen by the increased relative intensity but the peak maxima remain unchanged between the underivatized aromatic amino acids and the esters.

Peptides

Peptides show cleavages of the backbone to form z-1 and c ions at electron energies from 1-2 eV. The formation of the z-1 and c ions most likely involves π^* shape resonances of the carboxylic acid and amide groups but these cannot be unequivocally assigned. However, the ETS and REC –MS data for amino acids leads to the proposal that low energy effective yield peaks are due to the π^* states. The computational work of Simons et al on the alanine dimer predicts that vertical electron attachment energy to create a π^* state at 2.5-2.8 eV which is only slightly higher than the experimentally observed effective yield peaks for z-1 and c ions from peptides. The comparison of peak

maxima for the $(M-H)^-$ and z-1 ions suggest that there may be an additional energy requirement to form the z-1 ions at 0.3 – 0.7 eV on top of the energy required for formation of the $(M-H)^-$ ion.

The presence of an easily lost hydrogen atom from the carboxylic acid leads to the formation of z-1 ions, but esters of peptides predominantly produce c ions. The electron energies that lead to the z-1 and c ions suggest a common parent negative ion state. The observation of c ions in methyl esters suggests that the capture of electrons that leads to backbone cleavage involves the amide groups. The ester functionality is too remote from c_1 and the pseudo c_0 ions to be the site of capture leading to cleavage in the trimers. Therefore the mechanism for fragmentation of the peptide backbone is proposed to be capture of low energy electrons to produce a shape resonance associated with the π^* state of an amide group which proceeds through $\pi^* - \sigma^*$ mixing and cleavage of the $C_\alpha-N$ bond. The formation of z-1 ions in unesterified compounds involves rearrangement of the c-terminal fragment by loss of the hydrogen atom on the carboxylic acid group to produce a stable negative ion.

Overall Summary

The interactions of low energy electrons and amino acids, peptides, and their N-acetyl and ester derivatives occur through three resonances. First, is the π^* shape resonances of the carboxylic acid or ester, the amide, and aromatic side chains. The cleavage of the peptide backbone most likely occurs via the capture of an electron by an unoccupied π orbital of the amide and leads to c ions or z-1 ions by rearrangement. The

z-1 ion is favored in the underivatized c-terminal peptides due the more stable carboxylate negative ion. Second, the resonances observed (3.3 - 3.8 eV) in larger esters (ethyl, isopropyl, and t-butyl) of amino acids are attributed to Feshbach resonances of singlet – triplet electronic transitions and are not observed in N-acetyl amino acids and peptides. Third, the Feshbach resonances associated with higher energy, ≥ 5 eV were observed for amino acids and their methyl esters.

Finally, the primary conclusion of this thesis is that mechanism of peptide backbone cleavages that form negative ions is proposed to occur by capture of an electron to produce a shape resonance π^* state at the amide group. Through $\pi^* - \sigma^*$ orbital mixing the cleavage of the adjacent C_α -N sigma bond occurs, producing negative fragment ions. The formation of these negative ions from C_α -N sigma bond cleavage is consistent with the fragmentation types seen in ECD and suggests that there is a similar mechanism involved in both REC and ECD fragmentation even though the charge states of the target molecules are different.

The study of low energy electron interactions with biomolecules is important for explaining possible biochemical damage and physiological consequences from radiation as well as for providing understanding of electron leakage from mitochondrial process. These data provide a foundation for further studies to provide more exact electron energies for the cleavage of the peptide backbone by ECD and other electron capture mediated fragmentation techniques.

Bibliography

1. Zubarev, R.A., *Reactions of polypeptide ions with electrons in the gas phase.* Mass spectrometry reviews 2003. **22**(1): p. 57-77. .
2. Zubarev, R.A., N.L. Kelleher, and F.W. McLafferty, *Electron Capture Dissociation of Multiply Charged Protein Cations. A Nonergodic Process.* Journal of the American Chemical Society, 1998. **120**(13): p. 3265-3266.
3. Zubarev, R.A., et al., *Electron Capture Dissociation of Gaseous Multiply-Charged Proteins Is Favored at Disulfide Bonds and Other Sites of High Hydrogen Atom Affinity.* Journal of the American Chemical Society, 1999. **121**(12): p. 2857-2862.
4. Syrstad, E.A., D.D. Stephens, and F. Turecek, *Hydrogen Atom Adducts to the Amide Bond. Generation and Energetics of Amide Radicals in the Gas Phase.* Journal of Physical Chemistry A, 2003. **107**(1): p. 115-126.
5. Syrstad, E.A. and F. Turecek, *Toward a general mechanism of electron capture dissociation.* Journal of the American Society for Mass Spectrometry, 2005. **16**(2): p. 208-224.
6. Turecek, F., *N-Ca Bond Dissociation Energies and Kinetics in Amide and Peptide Radicals. Is the Dissociation a Non-ergodic Process?* Journal of the American Chemical Society, 2003. **125**(19): p. 5954-5963.
7. Turecek, F., et al., *Peptide cation-radicals. A computational study of the competition between peptide N-Ca bond cleavage and loss of the side chain in the*

- [GlyPhe-NH₂ + 2H]⁺. cation-radical*. Journal of Mass Spectrometry, 2003. **38**(10): p. 1093-1104.
8. Turecek, F. and A. Syrstad Erik, *Mechanism and energetics of intramolecular hydrogen transfer in amide and peptide radicals and cation-radicals*. Journal of the American Chemical Society, 2003. **125**(11): p. 3353-69.
 9. Uggerud, E., *Electron Capture Dissociation of the disulfide bond - a quantum chemical model study*. Inter. J. Mass Spectrom., 2004. **234**: p. 45-50.
 10. Abdoul-Carime, H., S. Gohlke, and E. Illenberger, *Conversion of amino-acids by electrons at subexcitation energies*. Phys. Chem. Chem. Phys., 2004. **6**(1): p. 161-164.
 11. Abdoul-Carime, H., S. Gohlke, and E. Illenberger, *Fragmentation of tryptophan by low-energy electrons*. Chemical Physics Letters, 2005. **402**(4-6): p. 497-502.
 12. Aflatooni, K., et al., *Temporary anion states of selected amino acids*. Journal of Chemical Physics, 2001. **115**(14): p. 6489-6494.
 13. Aflatooni, K., G.A. Gallup, and P.D. Burrow, *Electron Attachment Energies of the DNA Bases*. Journal of Physical Chemistry A, 1998. **102**(31): p. 6205-6207.
 14. Aflatooni, K., A.M. Scheer, and P.D. Burrow, *Dissociative electron attachment in uracil: Total anion yield*. Chemical Physics Letters, 2005. **408**(4-6): p. 426-428.
 15. Aflatooni, K., A.M. Scheer, and P.D. Burrow, *Total dissociative electron attachment cross sections for molecular constituents of DNA*. Journal of Chemical Physics, 2006. **125**(5): p. 054301/1-054301/5.
 16. Martin, F., et al., *DNA Strand Breaks Induced by 0-4 eV Electrons: The Role of Shape Resonances*. Physical Review Letters, 2004. **93**(6): p. 068101/1-068101/4.

17. Zumwalt, R.W., K. Kuo, and C.W. Gehrke, *A nanogram and picogram method for amino acid analysis by gas phase-liquid chromatography*. J. Chromatogr., 1971. **57**: p. 193-208.
18. Illenberger, E. and P. Swiderek, *Electron-driven molecular processes: A general introduction*. European Physical Journal D: Atomic, Molecular and Optical Physics, 2005. **35**(2): p. 173-176.
19. Christophorou, L.G., D.L. McCorkle, and A.A. Christodoulides, *Electron-Molecule Interactions and their applications*, ed. L.G. Christophorou. Vol. 1. 1984, Orlando, FL: Academic Press.
20. Ingolfsson, O., F. Weik, and E. Illenberger, *The reactivity of slow electrons with molecules at different degrees of aggregation: gas phase, clusters and condensed phase*. Int. J. Mass Spectrom., 1996. **155**: p. 1-68.
21. Vasil'ev, Y. 2006.
22. Oster, T., A. Kuhn, and E. Illenberger, *Gas Phase Negative Ion Chemistry*. Int. J. Mass Spectrom., 1989. **89**: p. 1-72.
23. Balog, R., et al., *Low Energy Electron Driven Reactions in Free and Bound Molecules: from Unimolecular processes in the Gas Phase to Complex Reactions in a Condensed Environment*. Int. J. Mass. Spec, 2003. **233**: p. 267-291.
24. Christophorou, L.G., D.L. McCorkle, and A.A. Christodoulides, *Electron Attachment Processes, in Electron-Molecule Interactions and Their APPLICATIONS*, L.G. Christophorou, Editor. 1984, Academic Press: Orlando, FL. p. 477-617.

25. Mazurkiewicz, P., *Analysis of Electrophilic Compounds Using an Electron Monochromator-Mass Spectrometer System*, in *Organic Chemistry*. 1998, Oregon State University: Corvallis, OR. p. 263.
26. Muftakhov, M.V., Y.V. Vasil'ev, and V.A. Mazunov, *Determination of electron affinity of carbonyl radicals by means of negative ion mass spectrometry*. *Rapid Commun. Mass Spectrom.*, 1999. **13**(12): p. 1104-1108.
27. Jordan, K.D. and P.D. Burrow, *Studies of the Temporary Anion States of Unsaturated Hydrocarbons by Electron Transmission Spectroscopy*. *Acc. Chem. Res.*, 1978. **11**: p. 341-348.
28. Figard, B.J., *The Analysis of Haloethylenes Using Resonance Electron Capture – Mass Spectrometry and Data Analysis Software.*, in *Dept. of Chemistry*. 2004, Oregon State University: Corvallis, OR.
29. Vasil'ev, Y.V., et al., *Resonant electron capture by some amino acids and their methyl esters*. *JACS*, 2005. **resubmitted**.
30. Stamatovic, A. and G.J. Schultz, *Characteristics of the Trochoidal Electron Monochromator*. *Rev. Sci. Instr.*, 1970. **41**(3): p. 423-7.
31. Stamatovic, A. and G.J. Schulz, *Trochoidal electron monochromator*. *Rev. Sci. Instrum.*, 1968. **39**(11): p. 1752-1753.
32. Aflatooni, K. and P.D. Burrow, *Dissociative electron attachment in chlorofluoromethanes and the correlation with vertical attachment energies*. *International Journal of Mass Spectrometry*, 2001. **205**(1-3): p. 149-161.

33. Baldwin, M.A. and F.W. McLafferty, *Direct chemical ionization of relatively involatile samples. Application to underivatized oligopeptides*. *Org. Mass Spectrom.*, 1973. **7**: p. 1353-1356.
34. Dell, A., et al., *JACS*, 1975. **97**(9): p. 2497-2502.
35. Anderson, W.R.J., et al., *Mass spectra of underivatized peptide amides related to substance P*. *Biochemical and Biophysical Research Communications*, 1977. **78**(1): p. 372-376.
36. Beuhler, R.J., et al., *Proton transfer mass spectrometry of peptides. A rapid heating technique for underivatized peptides containing arginine*. *J. Am. Chem. Soc.*, 1974. **96**(12): p. 3990-3999.
37. Hunt, D.F., J. Shabanowitz, and F.K. Botz, *Chemical ionization mass spectrometry of salts and thermally labile organics with field desorption emitters as solids probes*. *Analytical Chemistry*, 1977. **49**(8): p. 1160-1163.
38. Cooper, H., J., K. Hakansson, and A.G. Marshall, *The role of electron capture dissociation in biomolecular analysis*. *Mass spectrometry reviews* 2005. **24**(2): p. 201-22. .
39. Hakansson, K., et al., *Electron capture dissociation and infrared multiphoton dissociation MS/MS of an N-glycosylated tryptic peptide to yield complementary sequence information*. *Analytical Chemistry*, 2001. **73**(18): p. 4530-4536.
40. Adams, C.M., et al., *Probing solution- and gas-phase structures of Trp-cage cations by chiral substitution and spectroscopic techniques*. *International Journal of Mass Spectrometry*, 2006. **253**(3): p. 263-273.

41. Adams, C.M. and R.A. Zubarev, *Distinguishing and Quantifying Peptides and Proteins Containing D-Amino Acids by Tandem Mass Spectrometry*. Analytical Chemistry, 2005. **77**(14): p. 4571-4580.
42. Sobczyk, M., et al., *Coulomb-Assisted Dissociative Electron Attachment: Application to a Model Peptide*. Journal of Physical Chemistry A, 2005. **109**(1): p. 250-258.
43. Anusiewicz, I., et al., *A Theoretical Model for Indirect Dissociative Electron Attachment*. Journal of Physical Chemistry A, 2005. **109**(3): p. 484-492.
44. Sawicka, A., et al., *Model calculations relevant to disulfide bond cleavage via electron capture influenced by positively charged groups*. J. Phys. Chem. B., 2003. **107**(13): p. 505-511.
45. Gohlke, S., et al., *Formation of anion fragments from gas phase glycine by low energy (0-15 eV) electron impact*. J. Chem. Phys., 2002. **116**: p. 10164-10169.
46. Ptasinska, S., et al., *Dissociative electron attachment to gas-phase glycine*. Analytical and Bioanalytical Chemistry, 2003. **377**(7-8): p. 1115-1119.
47. Ptasinska, S., et al., *Dissociative electron attachment to gas phase alanine*. Chem. Phys. Lett., 2005. **403**(1-3): p. 107-112.
48. Abdoul-Carime, H. and E. Illenberger, *Fragmentation of proline induced by slow electrons*. Chem. Phys. Lett., 2004. **397**(4-6): p. 309-313.
49. Abdoul-Carime, H., S. Gohlke, and E. Illenberger, *Degradation of N-Acetyl Tryptophan by Low-Energy (<12 eV) Electrons*. J. Am. Chem. Soc., 2004. **126**(38): p. 12158-12161.

50. Vasil'ev, Y.V., et al., *Resonant electron capture by some amino acids and their methyl esters*. J. Am. Chem. Soc., 2006. **128**(16): p. 5506-5515.
51. Aflatooni, K., et al., *Temporary anion states of selected amino acids*. Journal of Chemical Physics, 2001. **115**(14): p. 6489-6494.
52. O'Malley, T.F., *Theory of Dissociative Attachment*. Physical Review, 1966. **150**(1): p. 14-29.
53. Heni, M., G. Kwiatkowski, and E. Illenberger, *Negative Ions in the Gas Phase Observed in Electron Transmission and Electron Attachment Spectroscopy*. Ber. Bunsenges. Phys. Chem., 1984. **88**: p. 670-75.
54. Vasil'ev, Y., B. Figard, and M. Deinzer, *Resonance Electron Capture Mass Spectrometry*, in *The Encyclopedia of Mass Spectrometry*, M. Gross and R. Caprioli, Editors. 2007, Elsevier: Amsterdam. p. 295 - 305.
55. Voinov, V.G., et al., *A Gas Chromatograph/Resonant Electron Capture-TOF Mass Spectrometer for Four Dimensions of Negative Ion Analytical Information*. Analytical Chemistry, 2004. **76**(10): p. 2951-2957.
56. Voinov, V.G., et al., *A Resonant Electron Capture Time-of-Flight MS with Trochoidal Electron Monochromator*. Anal. Chem., 2003. **75**(13): p. 3001-3009.
57. JEOL, *JEOL corporate site*. 2007.
58. Carey, F.A. and R.J. Sundberg, *Advanced Organic Chemistry*. 3rd ed. Vol. 1. 1990, New York: Plenum Publishing corporation. 802.
59. Jones, J., *Amino Acid and Peptide Synthesis*. 2 ed. Oxford Chemistry Primers, ed. S.G. Davies. 2002, Oxford, UK: Oxford University Press.
60. *Novabiochem Catalog 2006/2007*. 2006, EMD Biosciences: Germany.

61. Silicycle, *Silicycle catalog*. 2005.
62. Foresman, J.B. and A. Frisch, *Exploring Chemistry with Electronic Structure Methods*. 2 ed. 1996, Pittsburgh, PA: Gaussian, Inc. 302.
63. Laramee, J.A., C.A. Kocher, and M.L. Deinzer, *Application of a trochoidal electron monochromator/mass spectrometer system to the study of environmental chemicals*. *Analytical Chemistry*, 1992. **64**(20): p. 2316-22.